R-08-23

Hydrogeological conceptual model development and numerical modelling using CONNECTFLOW, Forsmark modelling stage 2.3

Sven Follin, SF GeoLogic AB

Lee Hartley, Peter Jackson, David Roberts
Serco TAP

Niko Marsic, Kemakta Konsult AB

May 2008

Svensk Kärnbränslehantering AB
Swedish Nuclear Fuel
and Waste Management Co
Box 250, SE-101 24 Stockholm
Tel +46 8 459 84 00

SKB

ISSN 1402-3091
SKB Rapport R-08-23
ID 1203451
Updated 2013-08

Hydrogeological conceptual model development and numerical modelling using CONNECTFLOW, Forsmark modelling stage 2.3

Sven Follin, SF GeoLogic AB

Lee Hartley, Peter Jackson, David Roberts
Serco TAP

Niko Marsic, Kemakta Konsult AB

May 2008

Keywords: Forsmark, Hydrogeology, Modelling, Calibration, Sensitivity.

Update notice

The original report, dated May 2008, was found to contain both factual and editorial errors which have been corrected in this updated version. The corrected factual errors are presented below.

Updated 2013-08

Location	Original text	Corrected text
Page 45, Table 3-10, last column, last row	(–8.3, 1.0)	(–8.8, 1.0)
Page 118, Table 7-4, column 1	$K_h = K_v$/...	$K_v = K_h$/...

The updated tables show what was actually used in the groundwater flow modelling for SDM-Site Forsmark.

Abstract

Three versions of a site descriptive model (SDM) have been completed for the Forsmark area. Version 0 established the state of knowledge prior to the start of the site investigation programme. Version 1.1 was essentially a training exercise and was completed during 2004. Version 1.2 was a preliminary site description and concluded the initial site investigation work (ISI) in June 2005. Three modelling stages are planned for the complete site investigation work (CSI). These are labelled stage 2.1, 2.2 and 2.3, respectively. An important component of each of these stages is to address and continuously try to resolve discipline-specific uncertainties of importance for repository engineering and safety assessment. Stage 2.1 included an updated geological model for Forsmark and aimed to provide a feedback from the modelling working group to the site investigation team to enable completion of the site investigation work. Stage 2.2 described the conceptual understanding and the numerical modelling of the bedrock hydrogeology in the Forsmark area based on data freeze 2.2. The present report describes the modelling based on data freeze 2.3, which is the final data freeze in Forsmark. In comparison, data freeze 2.3 is considerably smaller than data freeze 2.2. Therefore, stage 2.3 deals primarily with model confirmation and uncertainty analysis, e.g. verification of important hypotheses made in stage 2.2 and the role of parameter uncertainty in the numerical modelling. On the whole, the work reported here constitutes an addendum to the work reported in stage 2.2.

Two changes were made to the CONNECTFLOW code in stage 2.3. These serve to: 1) improve the representation of the hydraulic properties of the regolith, and 2) improve the conditioning of transmissivity of the deformation zones against single-hole hydraulic tests. The changes to the modelling of the regolith were made to improve the consistency with models made with the MIKE SHE code, which involved the introduction of spatial variability of the hydraulic properties within soil layers and horizontal versus vertical anisotropy in the hydraulic conductivity of soils. For the deformation zones, the same prescription for assigning transmissivities was followed as for stage 2.2, but a new method for automating the local conditioning of the deformation zone transmissivity in the vicinity of a measurement interval was used.

The numerical simulations carried out in stage 2.2 demonstrated that the three geological units: deformation zones, fracture domains and regolith, can be parameterised by means of single-hole hydraulic tests and satisfactorily transformed into heterogeneous hydraulic conductor domains (HCD), hydraulic rock mass domains (HRD) and hydraulic soil domains (HSD). This means that the conceptual model developed from the interpretation of Forsmark data in stage 2.2 can be used to predict a wide range of different types of data and processes such as 1) large-scale cross-hole test responses, 2) natural point-water heads in the bedrock and the regolith, and 3) hydrochemistry profiles along the many cored boreholes drilled in close proximity to the so-called target area. It is noted that a primary idea of the confirmatory testing applied in stage 2.2 is that the same groundwater flow and solute transport model is used for each type of simulation to make it transparent that a single implementation of the conceptual model could be calibrated against all three types of field observations, although it may have been possible to improve the modelling of a particular data type by refining the model around a relevant observation borehole, for example.

The *conceptual modelling* in stage 2.2 invoked a number of hypotheses, three of which that were addressed in stage 2.3 by means of complementary field investigations (hydraulic tests). The results from these investigations do not falsify (contradict) any of the three hypotheses, hence none of them should be rejected. In fact, the three hypotheses are supported by new evidence, which strengthens the overall credibility in the conceptual model presented in stage 2.2.

The sensitivity of the calibrated groundwater flow and solute transport model developed in stage 2.2 to parameter uncertainty was addressed in stage 2.3 by means of *numerical modelling*. A comprehensive set of uncertainties have been quantified to each of the model elements: HCD, HRD and HSD as well as boundary conditions both in terms of their effects on the model calibration processes and in predictions of discharge areas for groundwater flow through the repository candidate volume. The results from the sensitivity tests carried out confirm that high degrees of anisotropy in the regolith and/or the uppermost bedrock seem to characterise the near-surface hydrogeological conditions of the site. Furthermore, the envelope of realisations used to simulate the structural-hydraulic heterogeneity of the deeper parts of bedrock captures much of the sampled hydrochemical data and shows that the few shortcomings in the predictions of using a calibrated single realisation (here called the *base model simulation*) may be explained by the heterogeneity in the structural-hydraulic properties.

Sensitivities studies considering the role of structural-hydraulic heterogeneity on discharge locations for the repository target area by means of particle tracking corroborate that the *base model simulation* gives a consistent prediction of the main discharge areas, confirming that the geometry of deterministically modelled structures (larger deformation zones and sheet joints) are the dominant control on groundwater pathways, and that hydraulic heterogeneity does not disperse the exit locations to any radical degree. Exploratory simulations considering the Singö deformation zone as potential barrier to flow emphasise the importance of this zone for controlling the ultimate fate of any release.

Sammanfattning

Tre versioner av den platsbeskrivande modellen för Forsmark har färdigställts. Version 0 beskrev kunskapsläget innan platsundersökningarna påbörjades. Version 1.1, som var en övningsversion, färdigställdes år 2004 och version 1.2 färdigställdes i juni år 2005. Version 1.2 utgör den preliminära platsbeskrivningen för Forsmark och beskriver kunskapsläget efter det inledande platsundersökningsskedet. Det avslutande platsundersökningsskedet består av tre steg, vilka betecknas 2.1, 2.2 och 2.3. En viktig uppgift för arbetet inom var och ett av dessa steg är att tydligt redovisa kunskapsläget samt osäkerheter av betydelse för projektering och säkerhetsanalys.

Steg 2.1 syftade till att ge feedback till genomförandet av de återstående platsundersökningarna och innehåller dessutom en uppdaterad geologisk modell över Forsmark. Steg 2.2 och 2.3 karaktäriseras av ett stort antal ämnesspecifika underlagsrapporter. Den föreliggande rapporten ingår i steg 2.3 och beskriver det hydrogeologiska kunskapsläget i Forsmark och den numeriska modellering som utförts baserat på datafrys 2.3, som är den sista datafrysen inom ramen för platsundersökningarna i Forsmark. I jämförelse med datafrys 2.2 är datafrys 2.3 betydligt mindre rik på data. Syftet med steg 2.2 var att redovisa en konceptuell modell baserat på datafrys 2.2 och pröva densamma medelst numerisk modellering. Syftet med steg 2.3 är att verifiera de olika hypoteser som ställdes i steg 2.2 och demonstera beräkningsresultatens känslighet för olika typer av osäkerheter inkl parameterheterogenitet. På det hela taget är arbetet i steg 2.3 att betrakta som ett komplement till arbetet i steg 2.2, där tonvikten ligger på verifiering och osäkerhetsanalys.

De numeriska simuleringarna i steg 2.2 visar att hydrauliska egenskaper som tilldelats jordlager, sprickor och deformationszoner kan användas för att prediktera olika datatyper och processer som 1) responser vid storskaliga mellanhålstester, 2) naturliga grundvattennivåer i berggrunden och i det kvartära jordtäcket och 3) hydrokemiska profiler längs med ett stort antal kärnborrhål borrade i närheten av det potentiella förvarsområdet. Det bör påpekas att en huvudtanke i steg 2.2 har varit att använda en och samma grundvattenflödes- och transporttmodell för de olika simuleringarna, dvs skapa transparens och konsistens i modelleringen. Två mindre ändringar har utförts i steg 2.3 i beräkningsmodellen som utvecklades i steg 2.2. Ändringarna syftar till att förbättra beskrivningen av det kvartära jordtäcket och att automatisera konditioneringen av deformationszonernas hydrauliska egenskaper. I övrigt är beräkningsmodellen som utvecklades i steg 2.2 oförändrad.

Arbetet i steg 2.3 har dels prövat tre hypoteser från steg 2.2 genom att ställa dessa mot nya data från datafrys 2.3, dels prövat olika typer av osäkerheter med hjälp av den grundvattenmodell som utvecklades i steg 2.2. Data visar att ställda hypoteserna inte kan förkastas med den nya informationen som grund. Faktum är att den nya informationen stödjer de tre hypoteserna, vilket i sin tur stärker tilltron till den konceptuella modellen. Omfattande känslighetstester har utförts och resultaten visar att de hydrogeologiska förhållandena i Forsmarksområdet är mycket heterogena och anisotropa. I huvudsak styrs flödesvägarna av två typer av geologiska strukturer – deformationszoner och bankningsplan. Den hydrauliska heterogeniteten hos dessa strukturer innebär inga stora variationer i vare sig flöden eller utsläppsområden.

Contents

1 Introduction

1.1 Model development

Three versions of a site descriptive model (SDM) have been completed for the Forsmark area (Appendix A). Version 0 established the state of knowledge prior to the start of the site investigation programme. Version 1.1was essentially a training exercise and was completed during 2004. Version 1.2 was a preliminary site description and concluded the initial site investigation work (ISI) in June 2005. Three modelling stages are planned for the complete site investigation work (CSI). These are labelled stage 2.1, 2.2 and 2.3, respectively. An important component of each of these stages is to address and continuously try to resolve discipline-specific uncertainties of importance for repository engineering and safety assessment. Stage 2.1 included an updated geological model for Forsmark and aimed to provide a feedback from the modelling working group to the site investigation team to enable completion of the site investigation work. Stage 2.2 described the conceptual understanding and the numerical modelling of the bedrock hydrogeology in the Forsmark area based on data freeze 2.2. The present report describes the modelling based on data freeze 2.3, which is the final data freeze.

Table 1-1 shows the cumulative number of boreholes providing hydraulic information about the bedrock in the Forsmark area. (Appendix A shows the location of the boreholes.) The number of boreholes is shown in relation to the two investigation stages (ISI and CSI), the three versions (0, 1.1 and 1.2) and the three stages (2.1, 2.2 and 2.3) carried out during the period 2002–2007. Table 1-1 also shows the reference numbers of the major background reports in relation to each version/stage.

Table 1-1. The cumulative number of boreholes providing hydraulic information about the bedrock in the Forsmark candidate area at the end of each of the three versions and three stages carried out during the period 2002–2007. KFM = core-drilled boreholes, HFM = percussion-drilled boreholes. The reports with reference numbers typed in *italics* describe the hydraulic data gathered and/or the hydrogeological modelling undertaken. The reports with underlined reference numbers summarise the development of the hydrogeological modelling along with the developments achieved within the other disciplines.

	Initial site investigation (ISI)			**Complete site investigation (CSI)**	
Desk top exercise Version 0	**Training exercise Version 1.1**	**Preliminary SDM Version 1.2**	**Feedback and strategy Stage 2.1**	**Hydrogeological model stage 2.2**	**Model verification and uncertainty assessment stage 2.3**
0 KFM (0%)	1 KFM (4%)	5 KFM (21%)	9 KFM (38%)	20 KFM (83%)	25 KFM (100%)
0 HFM (0%)	8 HFM (21%)	19 HFM (50%)	22 HFM(58%)	32 HFM (84%)	38 HFM (100%)
R-02-32	R-04-15	R-05-18	R-06-38	*R-07-48*	*R-08-23*
		R-05-32	*R-07-20*	*R-07-49*	
		R-05-60			

1.2 Scope and objectives

As shown in Table 1-1, stage 2.3 deals primarily with model verification and uncertainty assessment. On the whole, stage 2.3 constitutes an addendum to the work reported in stage 2.2 and the primary objectives of the work reported here are therefore the same as those of stage 2.2 /Follin et al. 2007bc/:

- to assess and illustrate the hydrogeological conceptual understanding of the Forsmark area, in particular the target area and its boundaries (cf. Appendix A), and
- to build a numerical groundwater flow and solute transport model using the CONNECTFLOW code and test its representation of the site against field data as a means of approaching Step 4 in Figure 1-1.

A numerical demonstration of the conceptual model is necessary in order to gain credibility for the SDM in general and the site hydrogeological description in particular. This is important since the numerical models developed are to serve as a basis for describing the present hydrogeological conditions as well as for forthcoming predictions of future hydrogeological conditions and transport pathways. Equally important is a need to illustrate the role of field data in reducing uncertainty.

In addition to the primary objectives listed above, two particular objectives of the work conducted in stage 2.3 are:

- to verify three important hypotheses invoked in the conceptual modelling in stage 2.2, and
- to assess the sensitivity of the calibrated groundwater flow and solute transport model developed in stage 2.2 to parameter uncertainty.

These particular objectives were addressed here by means of complementary field investigations (hydraulic tests) and additional numerical modelling.

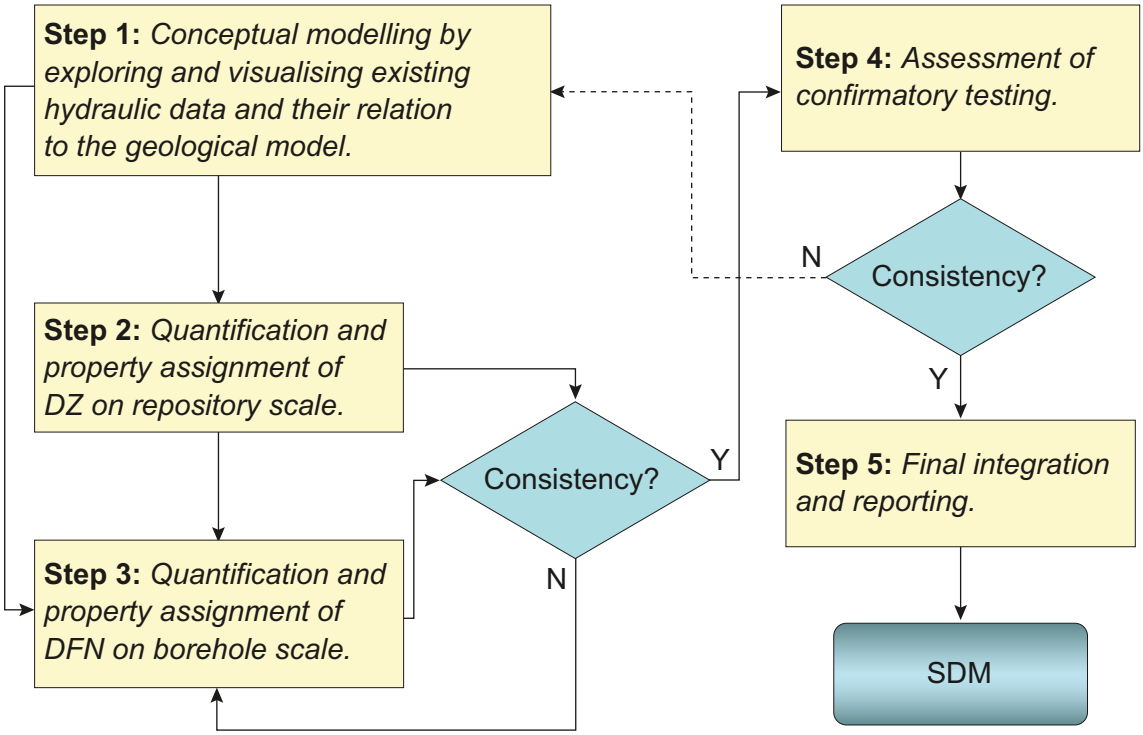

Figure 1-1. *Flow chart of the five steps suggested for the hydrogeological modelling during the complete site investigation (CSI) phase. DZ = deformation zone, DFN = discrete fracture network.*

1.3 This report

The present work is divided into eight sections:

- Chapter 2 provides an overview of SKB's systems approach to hydrogeological modelling in the SDM.
- Chapter 3 presents a summary of conceptual and numerical modelling carried out in stage 2.2.
- Chapter 4 handles three major hypotheses established in stage 2.2 and attempts to falsify them with new data belonging to data freeze 2.3.
- Chapter 5 presents the derivation of the *stage 2.3 base model simulation*.
- Chapter 6 presents exploration simulations using the *stage 2.3 base model simulation*.
- Chapter 7 deals with model uncertainties, in particular parameter heterogeneity.
- Chapter 8 presents the conclusions drawn and the primary unresolved issues identified.

2 Hydrogeological modelling in the SDM

2.1 Bedrock hydrogeological model

Figure 2-1 illustrates schematically the division of the groundwater system into hydraulic domains as used in the *bedrock hydrogeological model* for Forsmark. The groundwater system in the bedrock hydrogeological model consists of three hydraulic domains, HSD, HCD and HRD, where:

- HSD represents the regolith,
- HCD represents deformation zones, and
- HRD represents the fracture domains between the deformation zones.

The division into hydraulic domains constitutes the basis for the conceptual modelling, the planning of the site investigations and the numerical modelling carried out with the CONNECTFLOW code in support of the SDM. The variable-density flow models used in the SDM simulate the shore level displacement in the Fennoscandian Shield during Holocene time, i.e. between 8000 BC and 2000 AD.

2.1.1 Groundwater flow and solute transport modelling

Besides the three hydraulic domains shown in Figure 2-1, the groundwater flow and solute transport modelling with the CONNECTFLOW code consists of three additional elements:

- A solute (salt) transport model for the modelling of matrix diffusion.
- Initial conditions for groundwater flow and hydrochemistry.
- Boundary conditions for groundwater flow and hydrochemistry.

The parameterisation of the six elements is based on of altogether 13 different submodels, see Table 2-1. /Follin et al. 2007c/ provide a detailed description of the 13 submodels and how they merged in the numerical modelling.

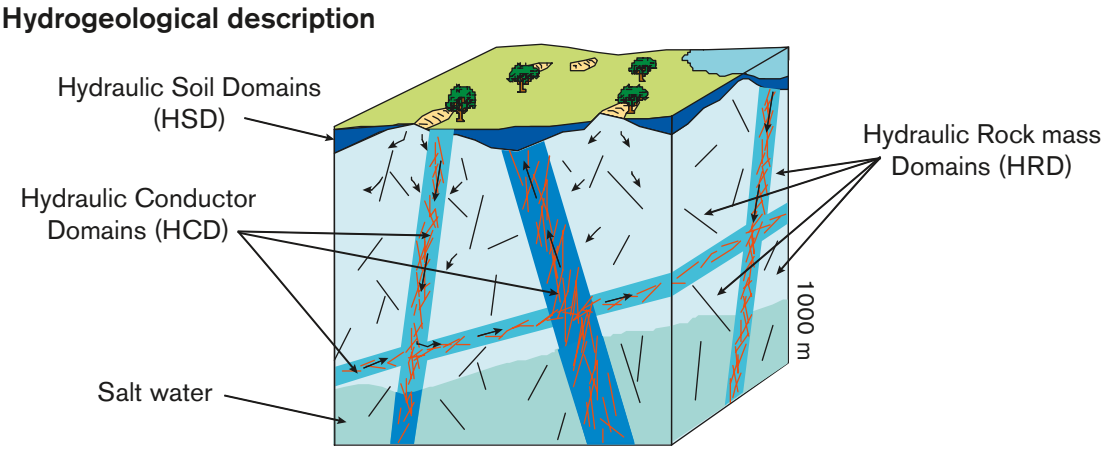

Figure 2-1. *Cartoon showing the division of the crystalline bedrock and the regolith above it (Quaternary deposits mainly) into three hydraulic domains. Reproduced from /Rhén et al. 2003/.*

Table 2-1. The groundwater flow and solute transport modelling with the CONNECTFLOW code is based on altogether 13 different submodels. The shaded fields show the key field/ laboratory data used to conceptualise and parameterise the six elements listed in the top row.

HCD, Hydraulic conductor domain model	HRD, Hydraulic rock mass domain model	HSD, Hydraulic soil domain model	Solute (salt) transport model	Initial conditions	Boundary conditions
2. Deformation zone model	1. Rock domain model	8. Regolith model	7. Hydro-DFN model	10. Palaeo-hydrological model	3. Digital elevation model
5. Bedrock hydrogeological model	4. Fracture domain model	3. Digital elevation model	13. Bedrock transport properties model		11. Shore level displacement model
	5. Bedrock hydrogeological model	9. Quaternary deposits hydrogeological model			12. Baltic Sea salinity model
	6. Geo-DFN model				
	7. Hydro-DFN model				
Single-hole hydraulic tests (PSS and PFL)	Single-hole hydraulic tests (PFL)	Slug-tests BAT tests	Single-hole hydraulic tests (PFL)	Hydrochemical database	Hydrochemical database
Borehole core description	Borehole fracture data		Dilution tests SWIW tests Tracer tests Laboratory tests		Hydrological monitoring data

2.1.2 Confirmatory testing

The implementation of the HSD, HCD and HRD elements in CONNECTFLOW is based on the geological models of the regolith and the bedrock, respectively, and the hydraulic investigations conducted in the KFM, HFM and SFM boreholes. That is, the geometries of the hydraulic domains are coherent with the geometries of the geological features, and their hydraulic properties reflect the anisotropy and spatial variability observed in the hydraulic investigations. Table 1-1 shows the cumulative number of boreholes providing hydraulic information about the bedrock in the Forsmark area.

As a means of approaching the issue of confirmatory testing, a strategy was developed after version 1.2 /Follin et al. 2007a/, see Figure 1-1. In practice, four kinds of data were treated during stage 2.2 (Figure 2-2) /Follin et al. 2007bc/:

A. Hydraulic properties deduced from single-hole hydraulic tests (double-packer injection tests, PSS, difference flow logging pumping tests, PFL-f, and open-hole pumping tests combined with impeller flow logging, HTHB) /Follin et al. 2007b/.

B. Groundwater level responses (point-water head drawdowns) in the bedrock in the depth interval 0 to c. 700 m observed during large-scale interference (cross-hole) tests /Follin et al. 2007c/.

C. Present-day mean groundwater levels (point-water heads) observed in the Quaternary deposits and the uppermost (c. 150 m) part of the bedrock /Follin et al. 2007c/.

D. Hydrochemical data (fracture water and matrix pore water) gathered from the bedrock investigations (primarily the core-drilled boreholes) /Follin et al. 2007c/.

The general approach applied in the numerical modelling in stage 2.2 was to first parameterise the deformation zones and fracture domains hydraulically using fracture and inflow data from individual boreholes (A). Second, the confirmatory step relies on using essentially the same groundwater flow and solute transport model in terms of grid discretisation and parameter settings for matching three types of independent field data (B-D). Using the three types of data, a unified conceptual description of the groundwater system has been attempted.

It is noted that a primary idea of the confirmatory testing is that the same groundwater flow and solute transport model is used for each type of simulation to make it transparent that a single implementation of the conceptual model could be calibrated against all four types of field observations, although it may have been possible to improve the modelling of a particular data type by refining the model around a relevant observation borehole, for example.

2.2 Hydrologic cycle

Figure 2-3 shows a cartoon of how the modelling of the hydrologic cycle is handled in the SDM. Two codes are used in parallel, the CONNECTFLOW code /Hartley and Holton 2004, Hartley et al. 2004ab, Hoch and Jackson 2004/ and the MIKE SHE code /DHI 2004/.

As explained above, numerical modelling with the CONNECTFLOW code has been performed as part of the modelling of the bedrock hydrogeology at Forsmark. This modelling has been made with an emphasis on (*i*) the assignment of hydraulic properties to the identified deformation zones and the fracture domains in between /Follin et al. 2007b/, and (*ii*) variable-density flow and solute transport in an equivalent continuous porous medium (ECPM) model of the fracture system and in the bedrock matrix over long time periods (thousands of years) /Follin et al. 2007c/. The analysis of open fractures vis-à-vis flowing fractures and the upscaling of discrete fracture network (DFN) models to an ECPM are two examples of key assignments of the bedrock hydrogeological modelling.

Numerical modelling with the MIKE SHE code /DHI 2004/ has been performed as a part of the modelling of surface hydrology and near-surface hydrogeology at Forsmark /Johansson 2008, Bosson et al. 2008/. This modelling has been made on a diurnal basis and includes evapotranspiration processes, surface water flow and groundwater flow in the regolith and the superficial parts of the bedrock. In contrast to the bedrock hydrogeological modelling, the modelling with MIKE SHE has been performed for the present-day conditions only. It is noted that variable-density and solute transport is not modelled has not been modelled with MIKE SHE.

In summary, the focus and objectives of the two model applications are somewhat different. However, the integration of the different works carried out is essential to the site description in general and to the description of the recharge-discharge conditions in particular. The origins of the suggested strategy for integrated numerical modelling outlined in /Follin et al. 2007a/ are found in /Follin et al. 2005, Hartley et al. 2005, Werner et al. 2006, Bosson and Berglund 2006, Werner et al. 2007/. The data support for analysing recharge-discharge conditions in the Forsmark area are discussed and analysed analytically in several reports, see in particular /Tröjbom et al. 2007/ and /Johansson 2008/. The works by /Follin et al. 2007c/ and /Bosson et al. 2008/ deal with recharge and discharge in terms of numerical modelling.

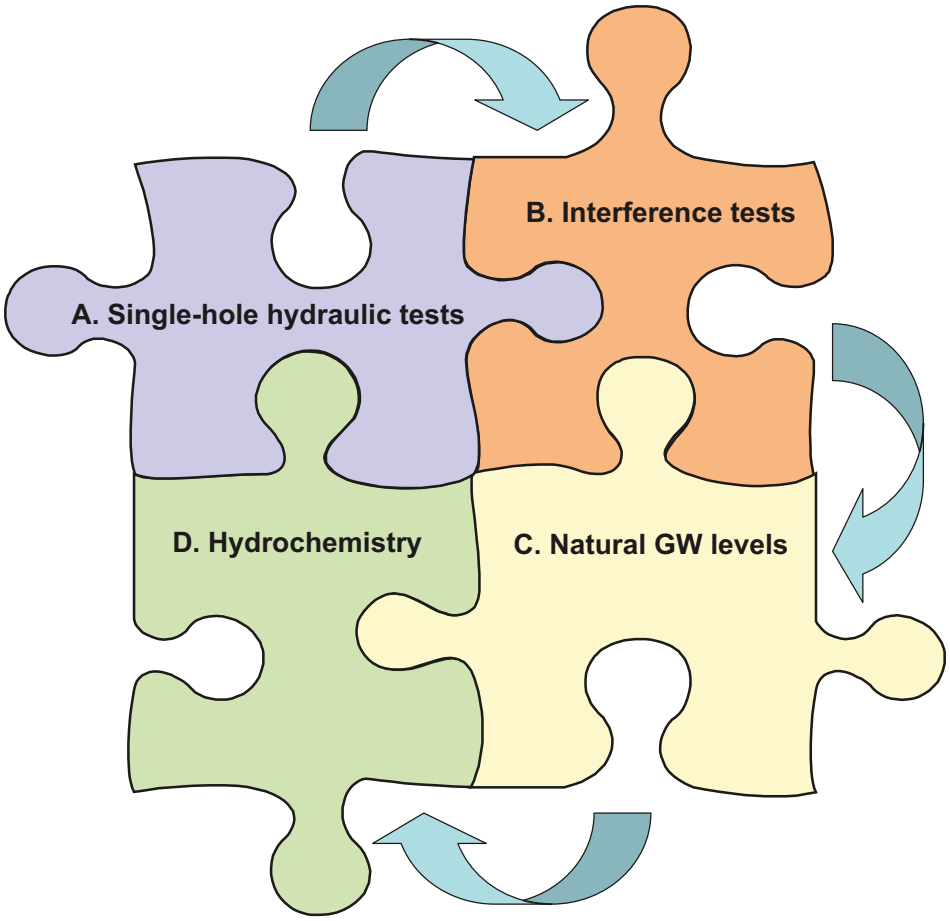

Figure 2-2. *Four kinds of data are used in the calibration of a numerical model a means of approaching the issue of confirmatory testing: A) Hydraulic properties of deformation zones and fracture domains as deduced from single-hole tests; B) Interference (cross-hole) tests; C) Natural groundwater levels; D) Hydrochemistry. Reproduced from /Follin et al. 2007c/.*

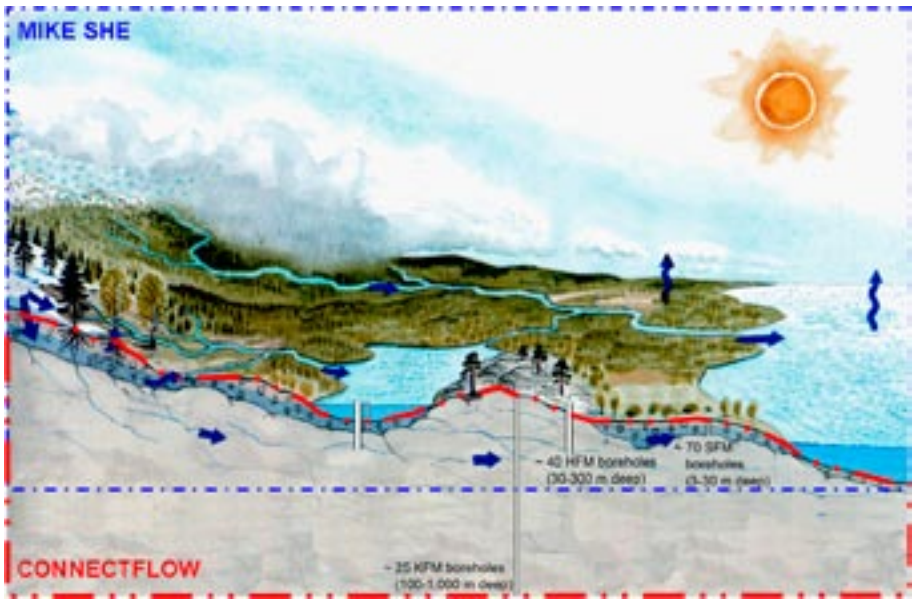

Figure 2-3. *Cartoon showing how the modelling of the hydrologic cycle is divided into a surface-based system and a bedrock-based system. The former is modelled with the MIKE SHE code and the latter with the CONNECTFLOW code. Reproduced from /Follin et al. 2007c/.*

3 Summary of the modelling in stage 2.2

3.1 Regolith geology

In the Forsmark area, all known regolith was deposited during the Quaternary period, thus generally referred to as Quaternary deposits. In addition, most of the Quaternary deposits at Forsmark were probably deposited during or after the latest deglaciation (Weichsel). Figure 3-1 shows the conceptual model of the stratigraphical distribution of the Quaternary deposits at Forsmark. The model consists of nine layers (L1-L3, Z1-Z6). Not all layers exist everywhere, and the thickness of individual layers varies significantly. The overall thickness of the Quaternary deposits varies from less than a decimetre to a maximum of 42 m /Hedenström et al. 2008/. The definition of the nine layers is shown in Table 3-1.

Table 3-1. Names and definition of Quaternary deposits layers /Hedenström et al. 2008/.

Layer	Description and comments
L1	Layer consisting of different kinds of gyttja/mud/clay or peat. Is interpolated from input data, thickness will therefore vary.
L2	Layer consisting of sand and gravel. Is interpolated from input data, thickness will therefore vary.
L3	Layer consisting of different clay (glacial and postglacial). Is interpolated from input data, thickness will therefore vary.
Z1	Surface affected layer present all over the model, except where peat is found and under lakes with lenses. Thickness is 0.10 m on bedrock outcrops, 0.60 m elsewhere. If total regolith thickness is less than 0.60 m, Z1 will have the same thickness as the total, i.e. in those areas only Z1 will exist.
Z2	Surface layer consisting of peat. Zero thickness in the sea. Always followed by Z3.
Z3	Middle layer of sediments. Only found where surface layers are other than till, clay or peat.
Z4a	Middle layer consisting of postglacial clay. Always followed by Z4b.
Z4b	Middle layer of glacial clay.
Z5	Corresponds to a layer of till. No min or max range. The bottom of layer Z5 corresponds to the bedrock surface.
Z6	Upper part of the bedrock. Fractured rock. Constant thickness of 0.5 m. Calculated as an offset from Z5.

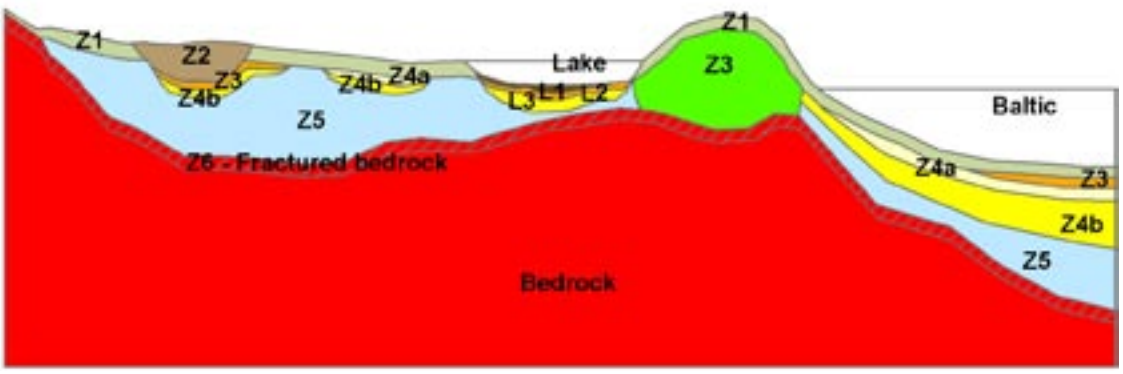

Figure 3-1. *Conceptual model for the layering of Quaternary deposits at Forsmark in stage 2.2 /Hedenström et al. 2008/. The different layers are explained in Table 3-1.*

The conceptual model was developed for the area shown in Figure 3-2, which covers most of the site descriptive regional model area. The model was truncated in the south slightly more than in the regional-scale hydrogeological model. The interpreted thicknesses of the QD are also shown in Figure 3-2. The compilation of different kinds of data obtained from several types of investigations has produced this model. The accuracy of the map varies therefore and the most detailed information was obtained from the central part of the model area and in the near shore coastal area. The profile in Figure 3-2 shows the stratification of the Quaternary deposits layers beneath Lake Bolundsfjärden for an example.

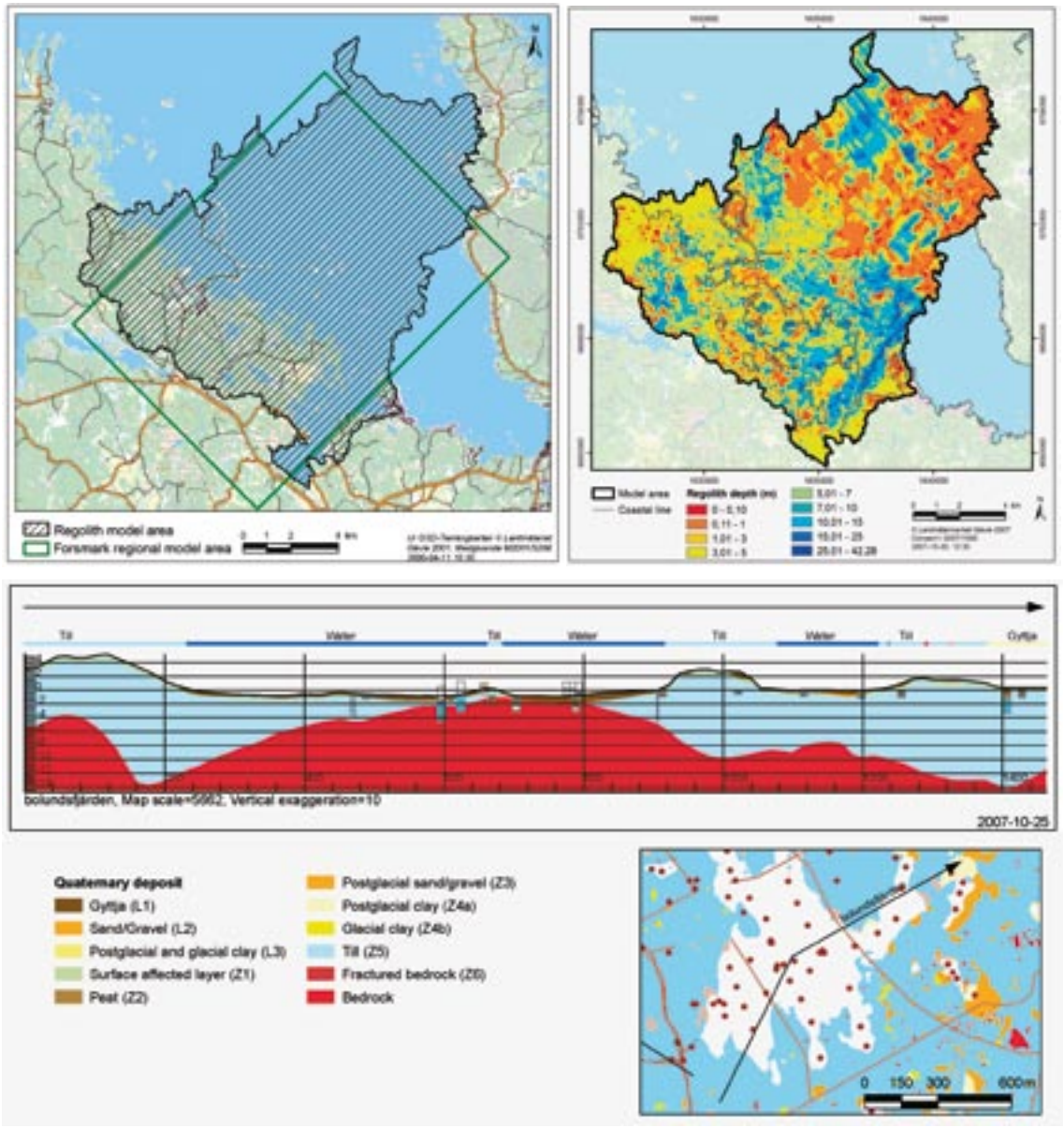

Figure 3-2. *Top left: Extent of the model of the Quaternary deposits in stage 2.2. Top right: Interpreted total thickness of the Quaternary deposits. Bottom: Example cross-section showing the interpreted stratification and thicknesses of the Quaternary deposits layers beneath Lake Bolundsfjärden. Reproduced from Appendix 2 in /Hedenström et al. 2008/.*

3.2 Bedrock geology

3.2.1 Rock domain model

The bedrock in the Forsmark area is divided into rock domains. A rock domain refers to a rock volume in which rock units that show similar composition, grain size, degree of bedrock homogeneity, and degree and style of ductile deformation have been combined and distinguished from each other. Rock volumes that show early-stage alteration (albitisation) are also distinguished as separate rock domains. The modelling of the rock domains and their petrophysical properties, e.g. the porosity of fresh bedrock samples without visible fractures, are described in detail in /Stephens et al. 2007/.

The different rock domains at Forsmark are referred to as RFM in SKB's 3D geometric modelling work and rock visualisation system (RVS). The dominant rock domains within the local model area are referred to as RFM029 and RFM045 (see Appendix B). The extent in 3D of these two rock domains defines by and large the repository target area at Forsmark shown in Appendix A.

3.2.2 Deformation zone model

A deformation zone is a general term referring to an essentially 2D structure along which there is a concentration of brittle, ductile or combined brittle and ductile deformation. The term fracture zone is used to denote a brittle deformation zone without any specification whether there has or has not been a shear sense of movement along the zone. A fracture zone that shows a shear sense of movement is referred to as a fault zone. Table 3-2 presents the terminology for brittle structures based on trace length and thickness as presented in /Andersson et al. 2000/.

The borderlines between the different structures are approximate. The so-called 3D DZ block model for Forsmark described in /Stephens et al. 2007/ contains 103 deterministically modelled deformation zones. These are referred to as ZFMxxxx, where xxxx is an identification label. All but 11 of the 103 deformation zones have trace lengths longer than one kilometre, which implies that the 3D DZ block model, in principle, consists of regional or local major deformation zones, cf. Table 3-2. The eleven deformation zones with trace lengths shorter than one kilometre are either a part (splay) of a nearby deformation zone longer than one kilometre, or gently dipping.

In addition to the 103 deterministically modelled deformation zones, /Stephens et al. 2007/ describe 28 minor deformation zones deterministically, i.e. deformation zones with trace lengths shorter than one kilometre. These are also referred to as ZFM, but *not* part of the 3D DZ block model. Finally, /Stephens et al. 2007/ discuss 43 so-called "possible deformation zones", i.e. borehole intervals with "deformation zone type properties". These are probably shorter than one kilometre, hence judged to be minor deformation zones, and not modelled deterministically.

Table 3-2. Terminology and general description (length and width are approximate) of brittle structures /Andersson et al. 2000/.

Terminology	Length	Width	Geometrical description
Regional deformation zone	> 10 km	> 100 m	Deterministic
Local major deformation zone	1 km–10 km	5 m–100 m	Deterministic (with scale-dependent description of uncertainty
Local minor deformation zone	10 m–1 km	0.1–5 m	Statistical (if possible, deterministic)
Fracture	< 10 m	< 0.1 m	Statistical

Conceptually, the 28 minor deformation zones are no different than the possible deformation zones not modelled deterministically. Despite the conceptual inconsistency created, it was decided by the hydrogeological modelling group to incorporate the 28 deterministically modelled minor deformation zones in the deformation zone model used in the hydrogeological SDM. The motive for this decision is purely pragmatic; that is, it is better to use the geometrical data available than having them modelled as stochastic features. In effect, the deformation zone model for the hydrogeological SDM contains 131 deterministically modelled deformation zones.

Figure 3-3 shows a 3D visualisation of the 131 deformation zones modelled deterministically in the hydrogeological SDM for Forsmark stage 2.2. The steeply dipping deformation zones (107) are shaded in different colours and labelled with regard to their principle direction of strike. The gently dipping zones (24) are shaded in pale grey and denoted by a G. The inset shows the direction of the main principal stress, cf. /Stephens et al. 2007/. All of the 28 minor deformation zones modelled deterministically by /Stephens et al. 2007/, but not included in the 3D DZ block model, occur inside the local model domain (cf. Figure 3-9 in /Follin et al. 2007c/). The local model domain encompasses the target volume defined in stage 2.1 /SKB 2006a/, hence investigated to a greater extent than the regional model domain. The bottom of the local model ends at elevation –1,100 m, which means that it matches fairly well the maximum penetration depths of the deepest cored boreholes.

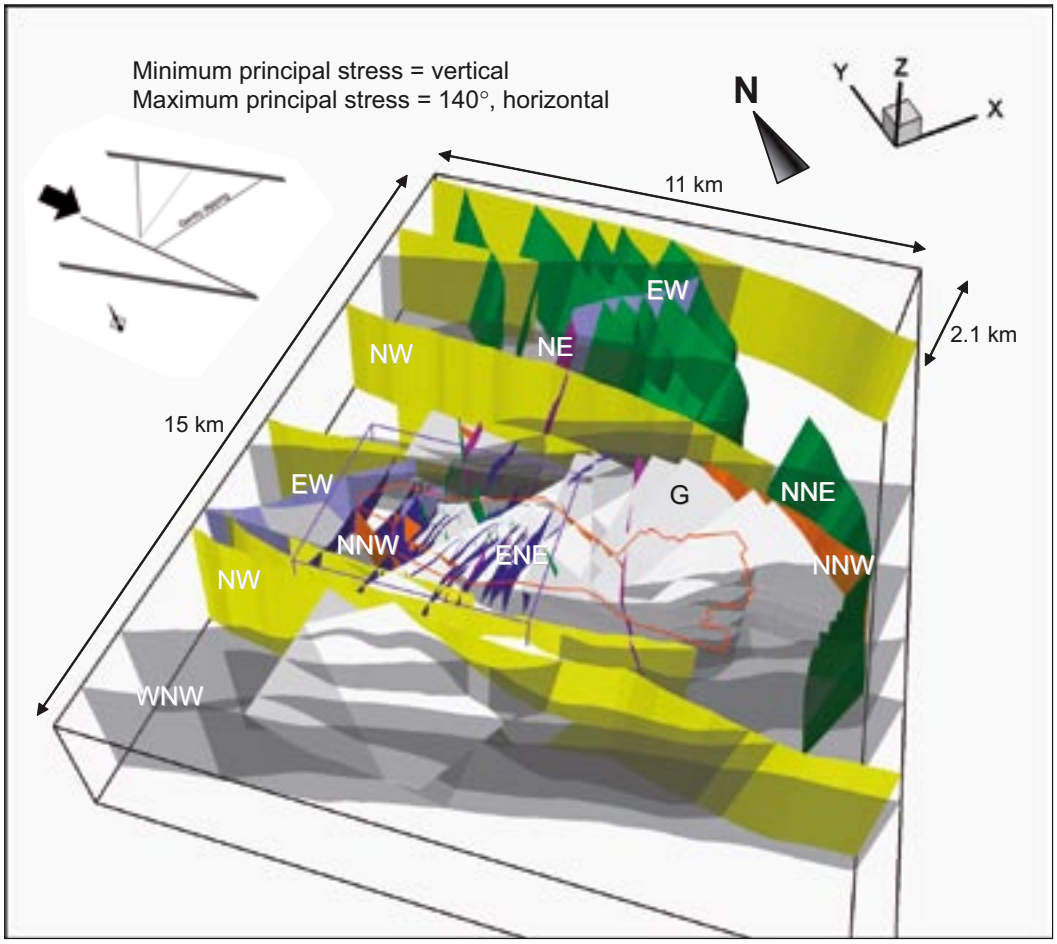

Figure 3-3. *3D visualisation of the regional model domain and the 131 deformation zones modelled deterministically for Forsmark stage 2.2 /Stephens et al. 2007/. The steeply dipping deformation zones (107) are shaded in different colours and labelled with regard to their principle direction of strike. The gently dipping zones (24) are shaded in pale grey and denoted by a G. The border of the candidate area is shown in red and regional and local model domains in black and purple, respectively. The inset in the upper left corner of the figure shows the direction of the main principal stress. Reproduced from /Follin et al. 2007b/.*

Table 3-3 shows a summary of the information presented above. We note in particular:

- 39 (28+11) deformation zones have trace lengths shorter than one kilometre and 45 deformation zones have trace lengths longer than three kilometres.
- 31 of the 103 deformation zones contained by the 3D deformation zone model occur inside the local model domain solely, 43 major deformation zones occur outside the local model domain solely and 29 major deformation zones occur both inside and outside. All of the 28 minor deformation zones modelled deterministically in the hydrogeological SDM are steeply dipping and occur inside the local model domain.
- There are 43 possible deformation zones identified in the geological single-hole interpretation but not modelled deterministically for Forsmark in stage 2.2; 34 of these intersect cored boreholes and nine the percussion-drilled holes.

The orientations of the 43 possible deformation zones not modelled deterministically may be tentatively estimated from the fracture poles. However, the lack of other strands of evidence to support a more deterministic interpretation implies that they, in theory at least, should be treated stochastically, i.e. as discrete fracture network (DFN) features, cf. Figure 3-6.

Figure 3-4 shows three profile planes (cross-sections); one WNW-ESE cross-section along the central part of the candidate volume, and two parallel WSW-ENE cross-sections in the eastern and central parts of the local model volume, respectively. Profile plane (c) in Figure 3-4 is shown in Figure 3-5. It is located 1,255 m north-west of cross-section (b) in Figure 3-4 and parallel.

The WNW-ESE cross-section demonstrates the significant structural difference in the deformation zone pattern on both sides of the gently dipping and sub-horizontal deformation zones A2 and F1, respectively. The bedrock above these zones is here referred to as the *hanging wall* and the bedrock below as the *footwall*. The hanging wall bedrock contains a number of gently dipping deformation zones, many of which extend down to one kilometre depth, or more. In contrast, there are very few gently dipping zones in the footwall bedrock. The difference in the deformation pattern between the hanging wall and the footwall is steered by, among other things, the older anisotropy at the site, with gently dipping ductile structures and rock contacts

Table 3-3. Summary of trace length data (L) for the deterministically modelled deformation zones tabulated with regard to orientation. Note that ten of the 24 gently dipping deformation zones do not outcrop. The two numbers separated by a slash in the second and fifth columns show the number of major and minor deformations zones, respectively. All minor deformation zones are steeply dipping and shorter than 1 km. The colours shown in the table correspond to the colours used in Figure 3-3.

Orientation category	No. of DZ major/minor	No. of DZ L ≥ 3 km	No. of DZ 3 km > L ≥ 1 km	No. of DZ L < 1 km major/minor	No. Of DZ Possible
G	24/–	6	6	2/–	17
WNW	23/1	15	7	1/1	3
NW	9/–	9	0	0/–	0
NNW	4/3	1	2	1/3	7
NNE	13/10	8	4	1/10	6
NE	4/6	2	1	1/6	0
ENE	24/7	2	17	5/7	9
EW	2/1	2	0	0/1	0
Total	103/28	45	37	11/28	42[1]

[1] One of the 43 possible deformation zones interpreted has no orientation data.

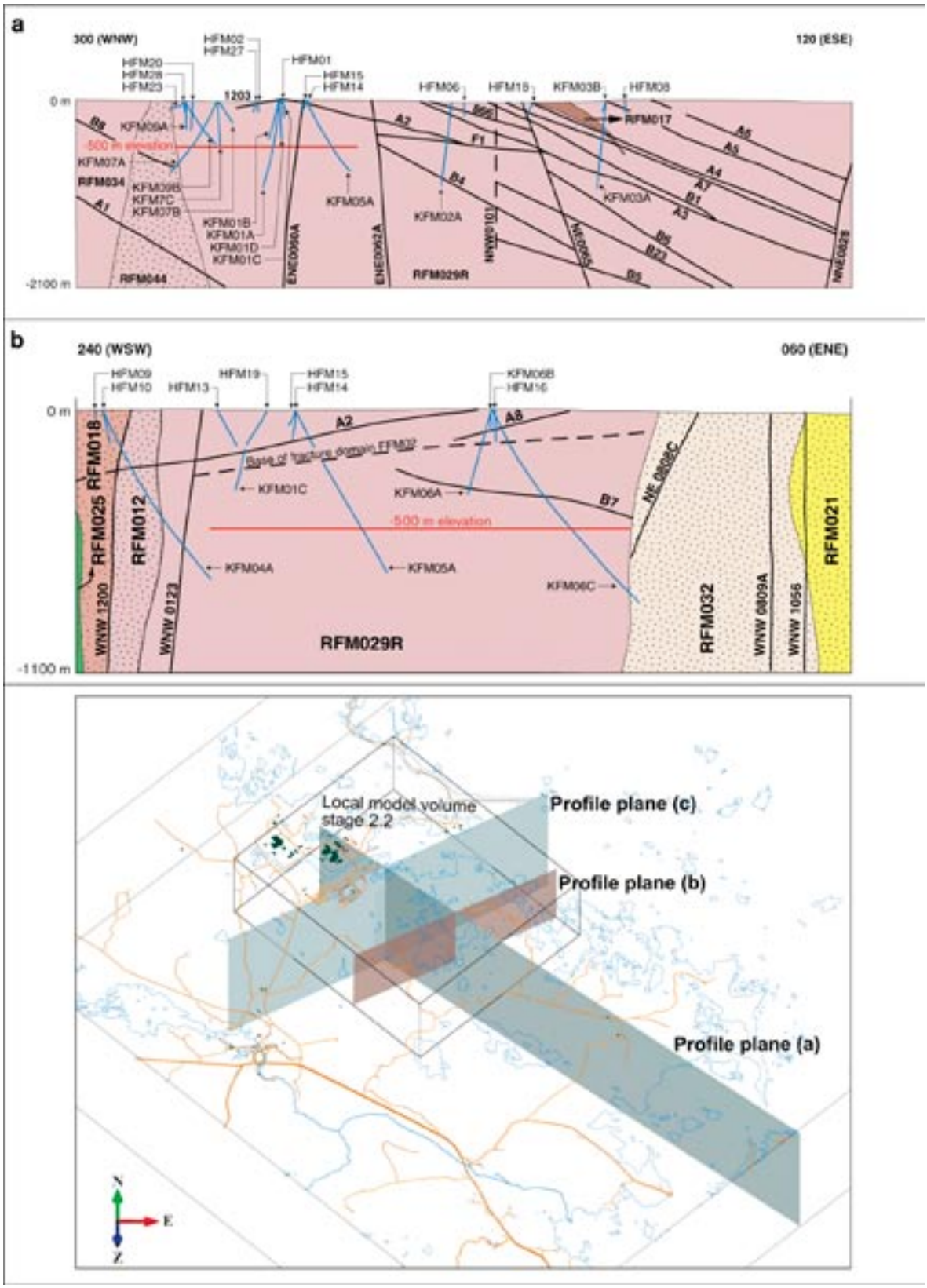

Figure 3-4. *(a) A c. 7 km long WNW-ESE cross-section along the central part of the candidate volume and (b) A c. 3 km long WSW-ENE cross-section along the south-eastern part of the local model volume. The important gently dipping deformation zones identified with reflection seismics are highlighted in these cross-sections. The bedrock above and below deformation zones A2 and F1 are referred to here as the hanging wall and the footwall, respectively. RFM029R is a regional rock domain. On a local scale RFM029R is split into the local rock domains RFM029 and RFM045 (see Appendix B). Modified after /Stephens et al. 2007/.*

in the south-eastern part of the candidate volume and more steeply dipping structures and contacts in the north-western part, in different parts of a major, sheath fold structure /Stephens et al. 2007/. It should be noted that the bedrock to the north-west of the steeply dipping deformation zone referred to as NE0065, both above and below zones A2 and F1, is intersected by a number of steeply dipping brittle deformation zones (fracture zones), many of which strike NNE and ENE. For purposes of simplicity, however, only the two zones that are included in the regional model are shown in Figure 3-4, i.e. ENE0060A and ENE0062A.

The cross-section in Figure 3-5 is closer the north-west boundary of the tectonic lens and visualises how the thickness and width of rock domain RFM029R narrow as the sheath fold structure gets steeper and the major Eckarfjärden and Singö deformation zones come closer to each other. The only major gently dipping deformation zone detected with reflection seismics in this part of the candidate volume is A1 (cf. profile plane (a) in Figure 3-4).

3.2.3 Fracture domain model

The fractured bedrock between the deterministically modelled deformation zones was divided with regard to the fracture frequency of *all* fractures, $P_{10,all}$ into six fracture domains, FFM01–06. The geological modelling of the fracture frequency analysed several types of discrete fracture network (DFN) models /Fox et al. 2007/. Key in the geological DFN modelling is the assumption of a power-law size distribution, see Figure 3-6. The key parameters of a power-law size distribution are the shape parameter, k_r, and the location parameter, r_0.

Four of the six fracture domains outcrop, FFM02–05, see Figure 3-7. The key fracture domains in the target area, FFM01 and FFM06 occur below fracture domain FFM02, see Figure 3-8. Figure 3-9 and Figure 3-10 visualise the geometry of fracture domains FFM01–03 and FFM06. Fracture domain FFM01 dominates in the lowermost part of the target volume. The darker grey volume shows the position of fracture domain FFM06. The uppermost part of the bedrock, in the north-western part of the model, is fracture domain FFM02. This domain dips gently towards the south. Fracture domain FFM03 is situated directly above the gently dipping and sub-horizontal zones A2 and F1 at depth, and above domain FFM02 close to the surface. Fracture domains FFM04–05 are not visualised in Figure 3-9 and Figure 3-10. FFM04–05 occur in the bedrock bordering the target volume.

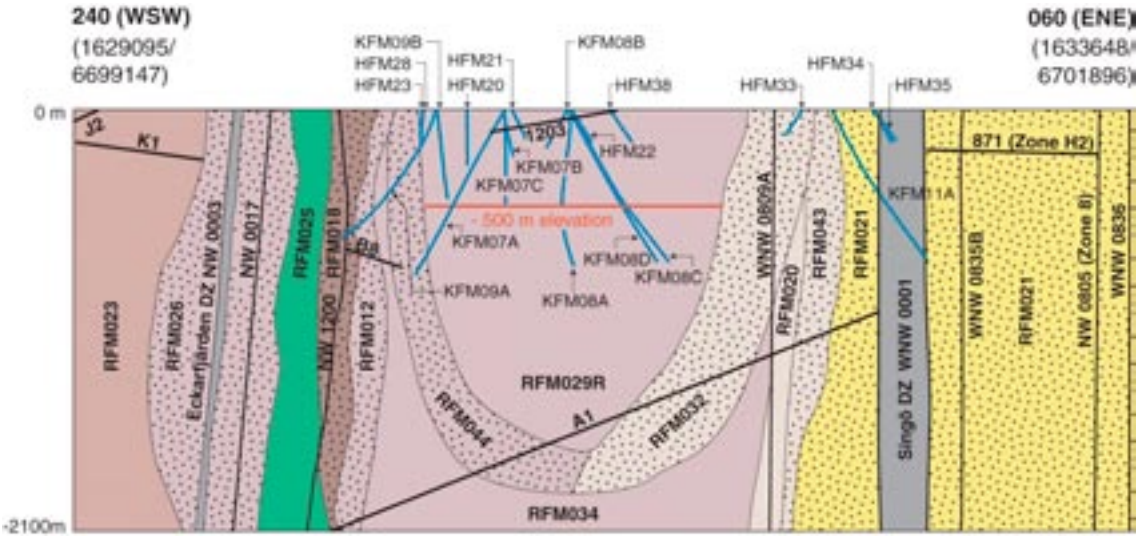

Figure 3-5. *A c. 5 km long WSW-ENE cross-section along the north-western part of the local model volume corresponding profile plane (c) in Figure 3-5. Reproduced from /Stephens et al. 2007/.*

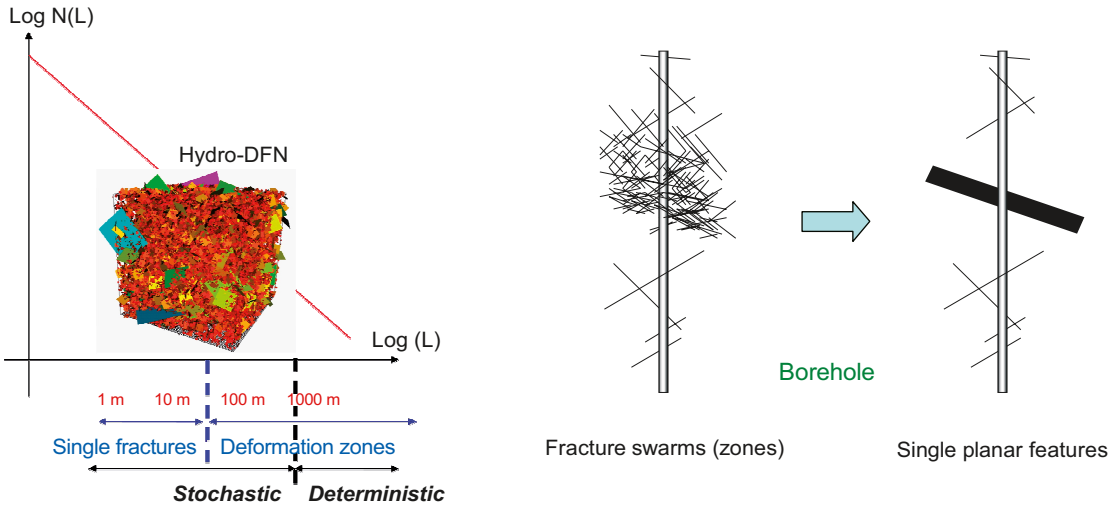

Figure 3-6. *Left: Cartoon showing the approach used for the treatment of single fractures and deformation zones in the geological DFN modelling. The number of features of different sizes is assumed to follow a power-law relationship. All features up to L = 1,000 m (r ≈ 564 m) are regarded as uncertain and treated stochastically using the DFN concept, cf. Table 3-2. Right: The fracture data gathered between the upper and lower bounds of a deformation zone interval are lumped together to form a single planar feature. (In the same fashion, all hydraulic data in the interval are also lumped together, to form a single transmissivity value.) Reproduced from /Follin et al. 2007b/.*

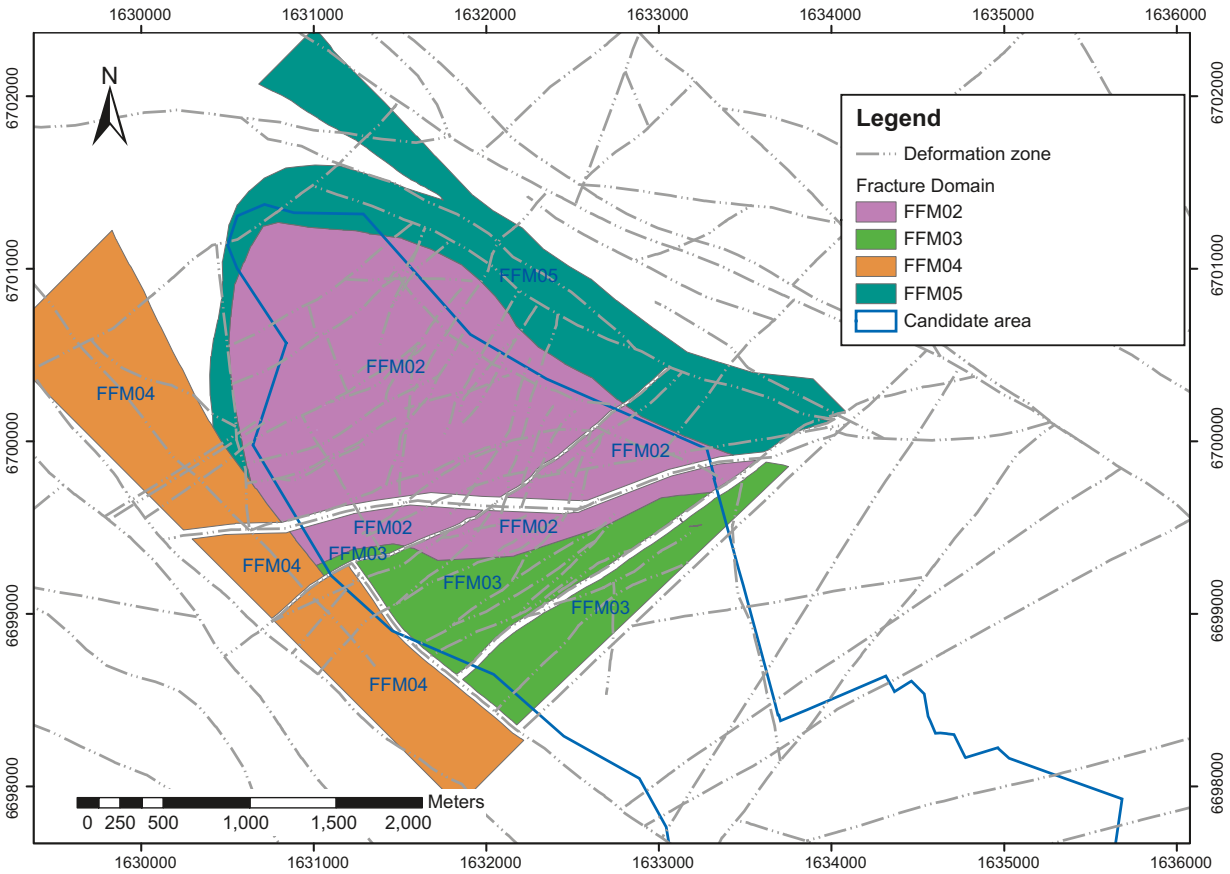

Figure 3-7. *Simplified horizontal slice at the surface showing outcropping fracture domains within the local model area for Forsmark stage 2.2. Modified after /Fox et al. 2007/.*

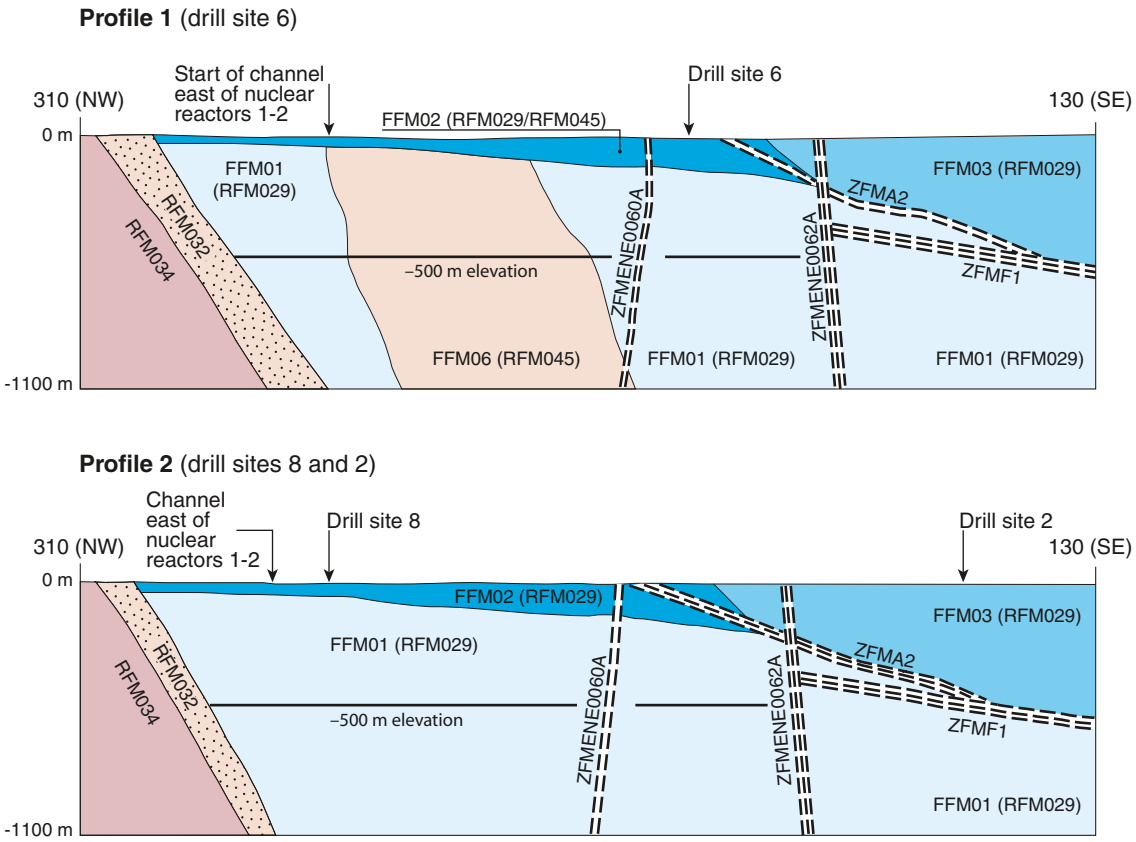

Figure 3-8. *Simplified profiles in a NW-SE direction that pass through drill sites 2 and 8 (lower profile) and drill site 6 (upper profile). The key fracture domains FFM01,- 02 and -06 occur in the footwall of zones A2 (gently dipping) and F1 (sub-horizontal). The major steeply dipping zones ENE0060A and ENE0062A are also included in the profiles. Reproduced from /Olofsson et al. 2007/.*

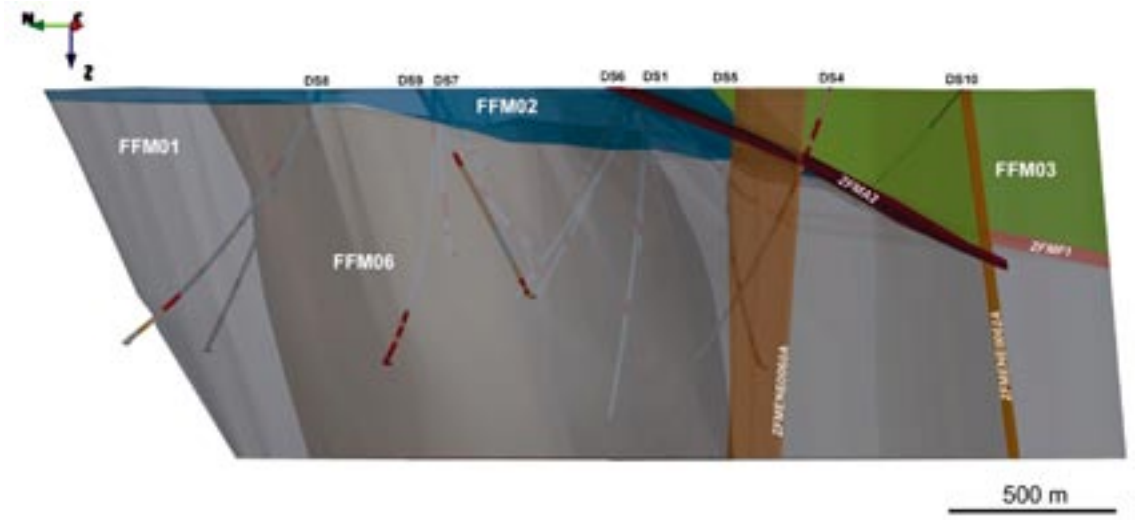

Figure 3-9. *Three-dimensional view of the fraction domain model, viewed towards the east-north-east. Fracture domains FFM01, FFM02, FFM03 and FFM06 are coloured grey, dark grey, blue and green, respectively. The gently dipping and sub-horizontal zones A2 and F1 as well as the steeply dipping deformation zones ENE0060A and ENE0062A are also shown. Reproduced from /Olofsson et al. 2007/.*

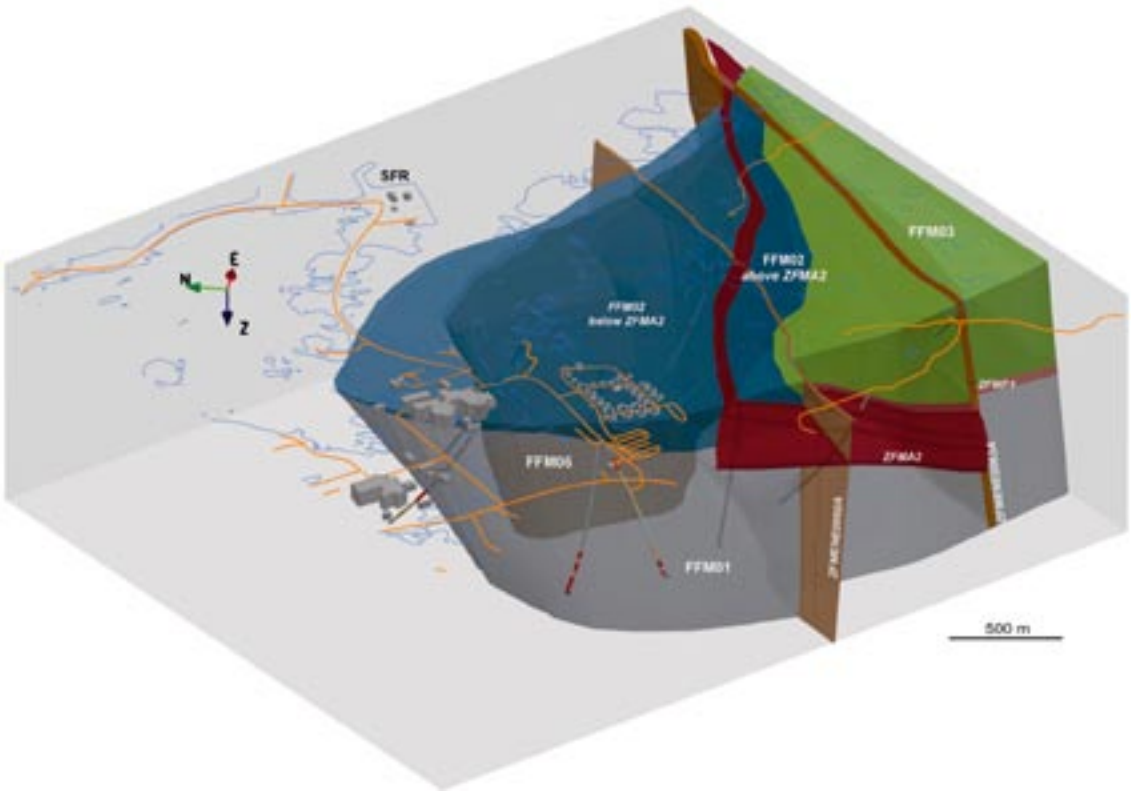

Figure 3-10. *Three-dimensional view to the east-north-east showing the relationship between deformation zone A2 (red) and fracture domain FFM02 (blue). Reproduced from /Olofsson et al. 2007/.*

3.3 Hydrogeology

The *bedrock hydrogeological model* consists of three structural elements: HSD, HCD, and HRD, cf. Figure 2-1. The conceptual modelling focussed on:

1. The difference between the groundwater levels in the Quaternary deposits and in the uppermost c. 150 m of bedrock, predominantly within the target.
2. The deterministically modelled deformation zones within the candidate area.
3. The bedrock bordering the target area.
4. The superficial bedrock above repository depth.
5. The bedrock in between deformation zones at repository depth.

3.3.1 The Quaternary deposits

The surface runoff, the surface water levels and the groundwater levels in the Quaternary deposits and in the bedrock have been monitored using SKB's hydrological monitoring system (HMS). The time series are analysed by /Juston and Johansson 2005, Johansson et al. 2005, Juston et al. 2007, Johansson and Juston 2007, Johansson 2008/ and modelled in MIKE SHE by /Bosson and Berglund 2006, Bosson et al. 2008/. The findings are analysed in /Johansson 2008/. The hydraulic measurements carried out in the Quaternary deposits are described in /Johansson et al. 2005/ and /Johansson 2008/.

The groundwater levels in the boreholes drilled in the Quaternary deposits (SFM) are strongly correlated to the topography, see Figure 3-11. In contrast, the groundwater levels in boreholes drilled the superficial bedrock (HFM) are generally low and the hydraulic gradient between adjacent boreholes is fairly flat, particularly inside the tectonic lens, see Figure 3-12. Here, the average groundwater levels range between 0.0 and +1.14 m RHB 70 with the exception of three monitoring sections with very little water, see Figure 3-12.

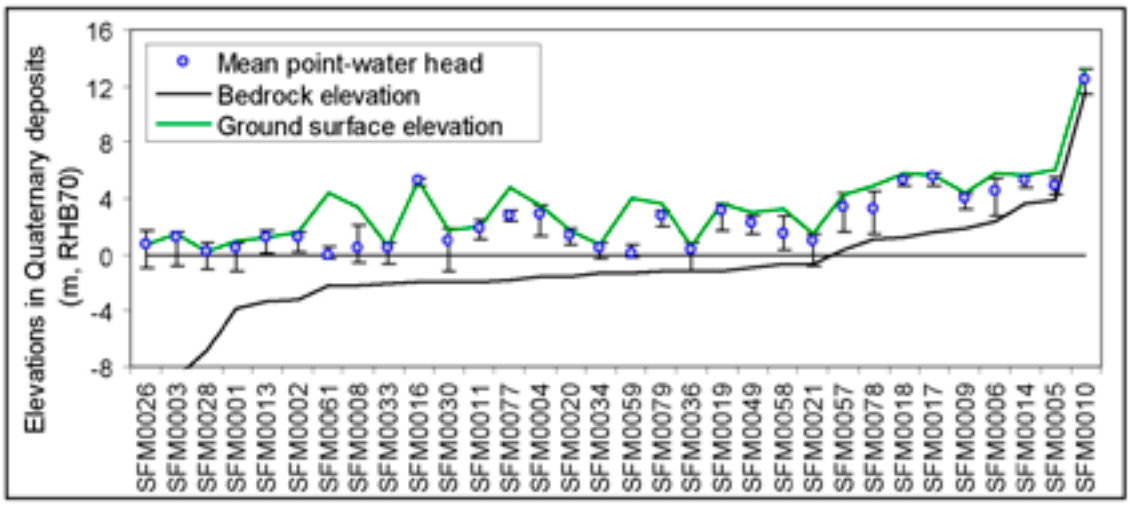

Figure 3-11. *Mean groundwater levels in boreholes drilled in the Quaternary deposits (SFM). Only boreholes with more than 150 days of level data are included. The close correlation between groundwater levels and ground levels is clear. The only exceptions are SFM0059 and SFM0061, which are located in a glaciofluvial deposit, Börstilåsen. Modified after /Werner et al. 2007/.*

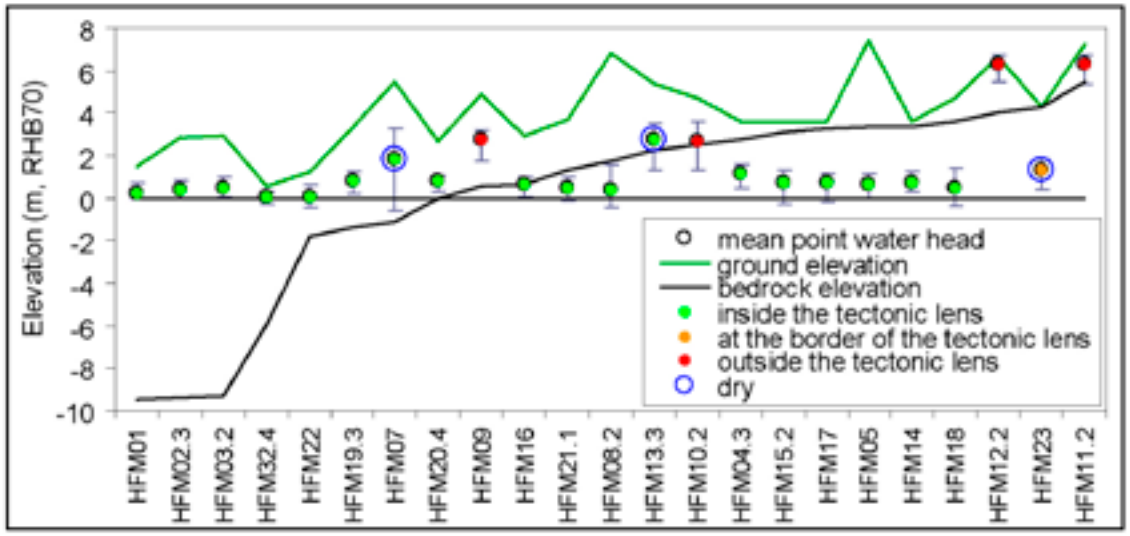

Figure 3-12. *Mean groundwater levels in the monitored sections in the boreholes drilled in the uppermost c. 150 m of bedrock (HFM). With exception for two "dry" monitoring sections, HFM07 (dry hole) and HFM13:3 (no fractures), the groundwater levels within the tectonic lens vary very little, from 0.0 to +1.14 m RHB 70. Only monitoring sections with more than 150 days of level data are included. Modified after /Werner et al. 2007/.*

The SFM and HFM boreholes shown in Figure 3-11 and Figure 3-12, respectively, are not drilled at the same locations, but the differences shown are observed also where the two types of boreholes are nearby. That is, at locations where the boreholes for groundwater level measurements in the Quaternary deposits are close to the boreholes groundwater level measurements in the bedrock, the levels in the bedrock are often considerably lower than in the Quaternary deposits. This feature is most pronounced within the target area. There are no examples within the target area of a situation where the groundwater level in the Quaternary deposits is constantly below the groundwater level in the bedrock for nearby boreholes /Johansson 2008/.

Figure 3-13 shows mean groundwater levels of 28 SFM boreholes in the Quaternary deposits and 28 monitoring sections in the HFM boreholes in the uppermost c. 150 m of the bedrock. The error bars show the 95% confidence intervals for the mean groundwater levels inside and outside the target area (TA), respectively. The mean values of the SFM boreholes (+0.89 and +3.45 m RHB 70) are calculated from the arithmetic means of 9 time series inside the target area and 19 outside the target area. The mean values of the HFM boreholes (+0.52 and +2.81 m RHB 70) are calculated from the arithmetic means of 37 time series inside the target area and 16 outside the target area, respectively. The mean sea water level during the monitoring period was –0.04 m RHB 70.

The general situation with lower groundwater levels in superficial bedrock than in the Quaternary deposits has been observed even below the middle of Lake Bolundsfjärden, which is located in the major topographical depression in the centre of the target area in Forsmark, see Appendix A. Since the water level in the lake is generally higher than in the Quaternary deposits beneath the lake, the two observations combined suggest that the lake may be a potential source for groundwater recharge rather than a discharge area.

3.3.2 The determinsitically modelled deformation zones

The role of the deterministically modelled deformation zones for regional groundwater flow and solute (salt) transport modelling was a key aspect of stage 1.2, which studied, among other things, the need for far-field realism by means of three regional deformation zone models. It was concluded by means of numerical simulations that detailed geometrical and hydraulic information about the deformation zones within the tectonic lens are much more important for the bedrock hydrogeological description within the target volume than the positions and hydraulic properties of deformation zones outside the tectonic lens /Follin et al. 2005/.

In stage 1.2, 44 deformation zone intercepts representing 28 different deformation zones were investigated hydraulically. In stage 2.2 these numbers have increased to 116 and 57, respectively, which implies a more or less doubled information density. Figure 3-14 shows a plot of transmissivity versus depth for the 57 deformation zones investigated hydraulically in stage 2.2. The colour legend used is the same as the ones used in Figure 3-3 and Table 3-3. Figure 3-14 shows that, at each elevation, the gently dipping deformation zones that occur predominantly in the

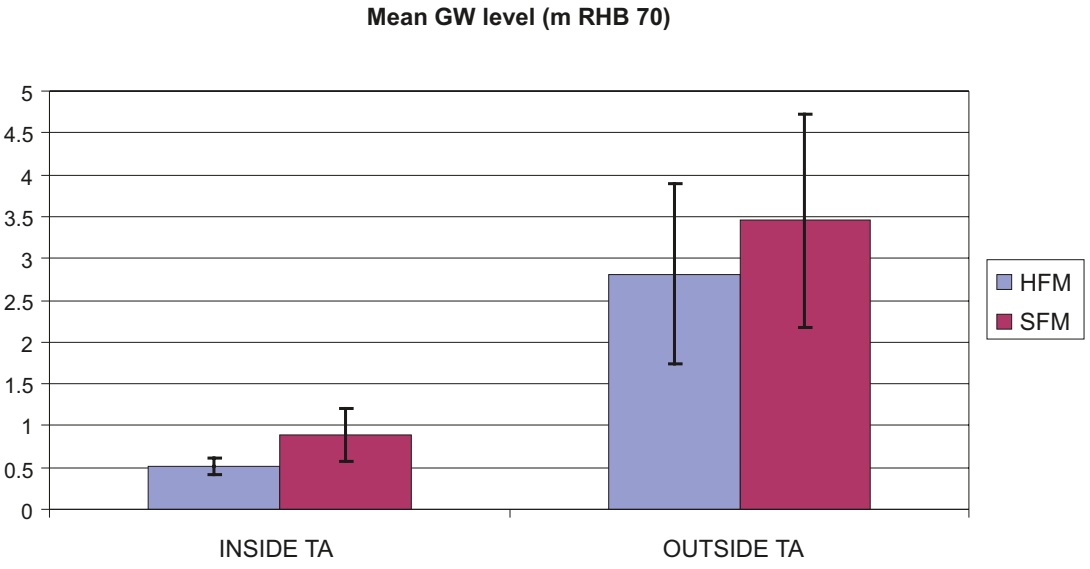

Figure 3-13. *Diagram showing mean groundwater levels of 28 boreholes in the Quaternary deposits (SFM) and 28 boreholes in the uppermost c. 150 m of the bedrock (HFM). The error bars show the 95% confidence intervals for the mean groundwater levels inside and outside the target area (TA), respectively.*

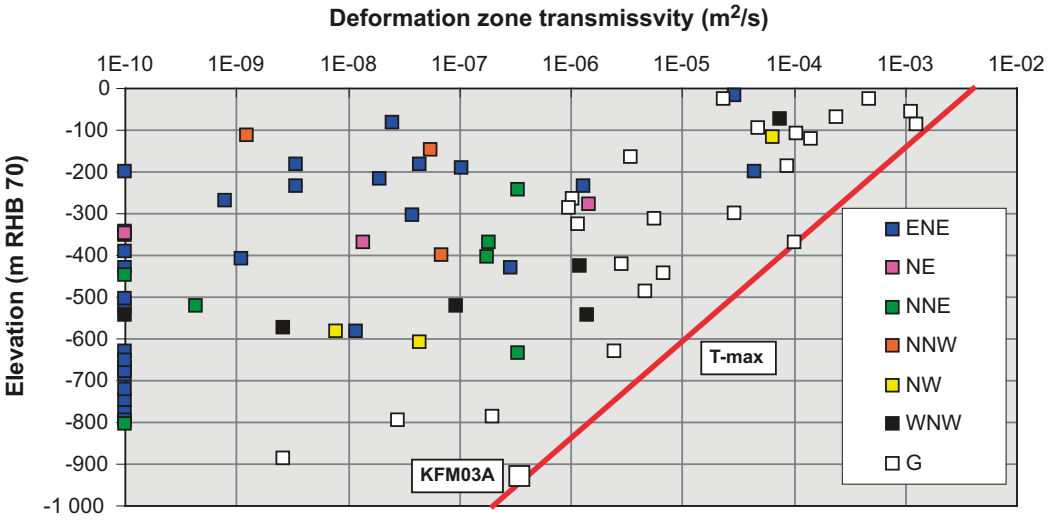

Figure 3-14. *Transmissivity versus depth for the deterministically modelled deformation zones observed in cored boreholes. The transmissivities are coloured with regard to the orientations of the deformation zones. For the purpose of this plot, deformation zones with little or no flow are assigned arbitrary low transmissivity value of 10^{-10} m^2/s in order to make them visible on the log scale. The red line is inserted to indicate a possible depth variation of the maximum transmissivity observed at each elevation. Reproduced from /Follin et al. 2007b/.*

hanging wall bedrock of zones A2 and F1 are the most transmissive. The steeply dipping deformation zones that strike WNW and NW appear to come in second place as far as transmissivity is concerned. The steeply dipping deformation zones that strike ENE and NNE occur in the footwall bedrock mainly. These zones can occasionally also be fairly transmissive, but a main characteristic, as it appears from Figure 3-14, is that they are on the average the least transmissive but at the same time significantly more heterogeneous laterally than the other categories of deformation zones.

The depth trend in the mean transmissivity of the gently dipping zones spans four to six orders of magnitude, from 10^{-4}–10^{-3} m^2/s near the bedrock surface to 10^{-9}–10^{-8} m^2/s at c. 1,000 m depth. The lateral heterogeneity in transmissivity varies also several orders of magnitude, in particular for the steeply dipping zones. The conclusion drawn from these findings is that the previously described structural anisotropy is not only accompanied by a significant hydraulic anisotropy, but also a substantial vertical and lateral hydraulic heterogeneity. This observation suggests a strongly channelised flow field within the planes of the deformation zones.

3.3.3 The bedrock bordering the target area

Hydrogeological observations in the bedrock bordering the target volume are made in boreholes KFM04A, KFM06C, KFM07A, KFM08A and KFM09A. For an illustration, the findings in the three boreholes KFM04A, KFM09A and KFM07A, cf. Appendix A, are commented upon here. The hydraulic data acquired with the PSS method in these three boreholes are shown in Figure 3-15. The hydraulic differences between the bedrock inside the target volume and the bordering bedrock are obvious. The hydraulic differences with depth within the target volume are also very clear.

KFM04A is located in the intensely fractured bedrock bordering the lens (FFM04). It is inclined 60° towards the lens and enters the sparsely fractured bedrock in the target volume (FFM01) as it reaches 400 m depth (500 m borehole length).

KFM09A is located on the border of the lens and is inclined 60° away from the lens. It investigates at first the intensely fractured superficial bedrock in the lens (FFM02 and FFM01) and secondly the intensely fractured bedrock bordering it (FFM05 and FFM04) beginning at 230 m depth (280 m borehole length).

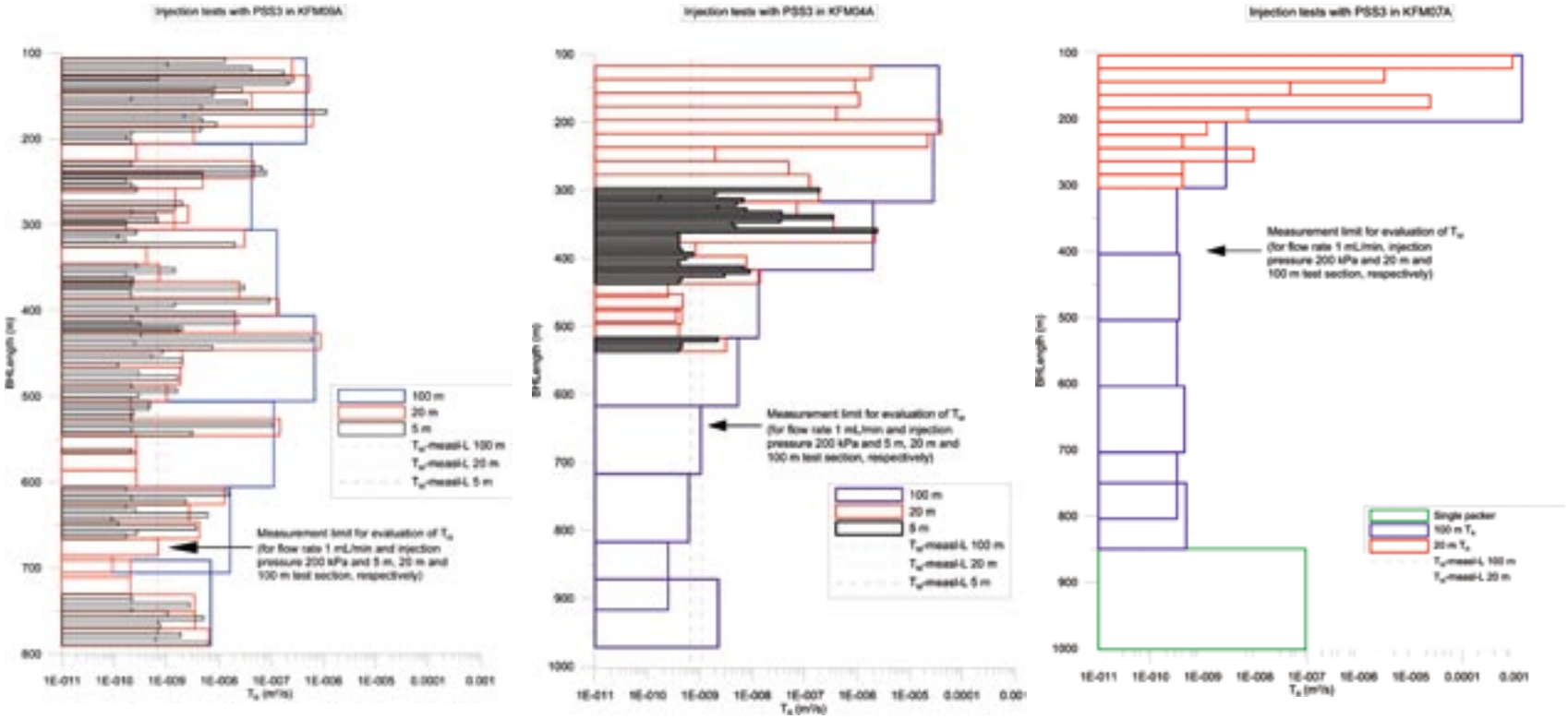

Figure 3-15. *Comparison of PSS transmissivity data gathered in the bedrock with relatively low ductile strain inside the tectonic lens, and in the bedrock with high, ductile strain both on the south-western margin of the tectonic lens and in the folded unit inside the lens. Left: KFM09A; Middle: KFM04A; Right: KFM07A. The PSS measurements are carried out with three different packer spacings, 100 m, 20 m and 5 m, depending on the results. Note that the nominal lower measurement limit of the PSS method varies slightly with the packer spacing and the ordinate axes show borehole length and not elevation. Reproduced from /Follin et al. 2007c/.*

KFM07A is located in the lens. It investigates the intensely fractured superficial bedrock in the lens (FFM02) and the very sparsely fractured bedrock in the target volume below (FFM01). KFM07A also enters the folded, ductile, high-strain and strongly fractured rock unit inside the lens (FFM05) at 665 m depth (793 m borehole length).

It is noted that the highest salinities during the site investigations are recorded at c. 700 m depth in boreholes KFM07A and KFM09A, about 15,000 mg/L Cl. However, it is unclear whether the observations are typical for the intensely fractured bedrock bordering the target volume or if the high salinities are due to upconing of more saline water during the drilling and flushing of the two boreholes /Follin et al. 2007c/.

3.3.4 The superficial bedrock above repository depth

The uppermost part of the bedrock in the Forsmark area is recognised for its large horizontal fractures/sheet joints; see Figure 3-16 for an example. Besides this structural evidence, there are three pieces of hydrogeological evidence that support the hydraulic importance of these structures:

1. Exceptionally high water yields. The median yield of the first 22 percussion-drilled boreholes is c. 12,000 L/h. This is c. 20 times higher than the median yield of the domestic water wells drilled outside the candidate area, which is no different from the median yield of all bedrock wells (c. 200,000) registered at the Geological Survey of Sweden /Berggren 1998/.
2. The near uniform groundwater level in the uppermost c. 150 m of bedrock observed among the percussion-drilled boreholes within the target area. This is on the average c. +0.5 m above the datum plane (RHB 70). In contrast, the average groundwater level among the percussion-drilled boreholes outside the candidate area is c. +2.8 m above the datum plane, see Figure 3-13. The mean gradient between the Quaternary deposits and the uppermost part of the bedrock is downwards (cf. section 3.3.1).
3. The extensive and rapid transmission of fluid pressure changes (drawdown) during the large-scale interference test that was run over three weeks during the summer of year 2006 in borehole HFM14, which is located in the centre of the target area, see Figure 3-17 and Figure 3-18.

In conclusion, geological and hydrogeological observations indicate a well-connected network of structures of high transmissivity in the uppermost c. 150 m of the bedrock in the target area. The network is thought to consist of extensive sheet joints, outcropping deformation zones and increased, though structurally anisotropic, fracture intensity in the bedrock in between the outcropping deformation zones. The groundwater levels monitored in the Quaternary deposits and in the bedrock suggest that the network catches the recharge from above as well as the discharge from below. It is recognised that the hydraulic cage analogue tentatively suggested in /Follin et al. 2007ac/ is misleading as there is no hydraulic cage at Forsmark *sensu strictu*. A more appropriate hydrogeological description of the hydraulic phenomenon is a shallow, anisotropic, bedrock aquifer on top of thicker segment of bedrock with aquitard type properties. The shallow bedrock aquifer has little or no storage, hence it has a high hydraulic diffusivity. The cartoon shown in Figure 3-19 illustrates the concept.

The sheet joints are not mapped to a very large detail in the site investigations, hence they are difficult to implement in a numerical model due to uncertainties in their spatial extent. Based on the results obtained from the interference test that was run in HFM14 for three weeks during the summer of 2006 (see Figure 3-17), the lateral extent of the horizontal fractures/sheet joints was hypothesised to correspond approximately to fracture domain FFM02, but stretching north all the way to the Singö deformation zone (WNW001) as shown in Figure 3-20. The other hypothesised physical boundaries are deformation zone ENE0062A to the south-east and the border of fracture domain FFM02 to the south-west and west, with the modification that the boundary passes between boreholes HFM20 and HFM28. The crosses in Figure 3-20 mark the positions of the percussion-drilled and core-drilled boreholes for which transmissivity measurements were available for parameterisation of the shallow bedrock aquifer.

Figure 3-16. *Picture from the construction of the 13 m deep and more than one kilometre long canal between the Baltic Sea and the nuclear power reactors in Forsmark. Horizontal fractures/sheet joints are encountered along the entire excavation. The sheet joints follow the undulations of the bedrock surface. There are probably several "horizons" of extensive sheet joints on top of each other according to the hydraulic interference tests. /Photograph by G Hansson/.*

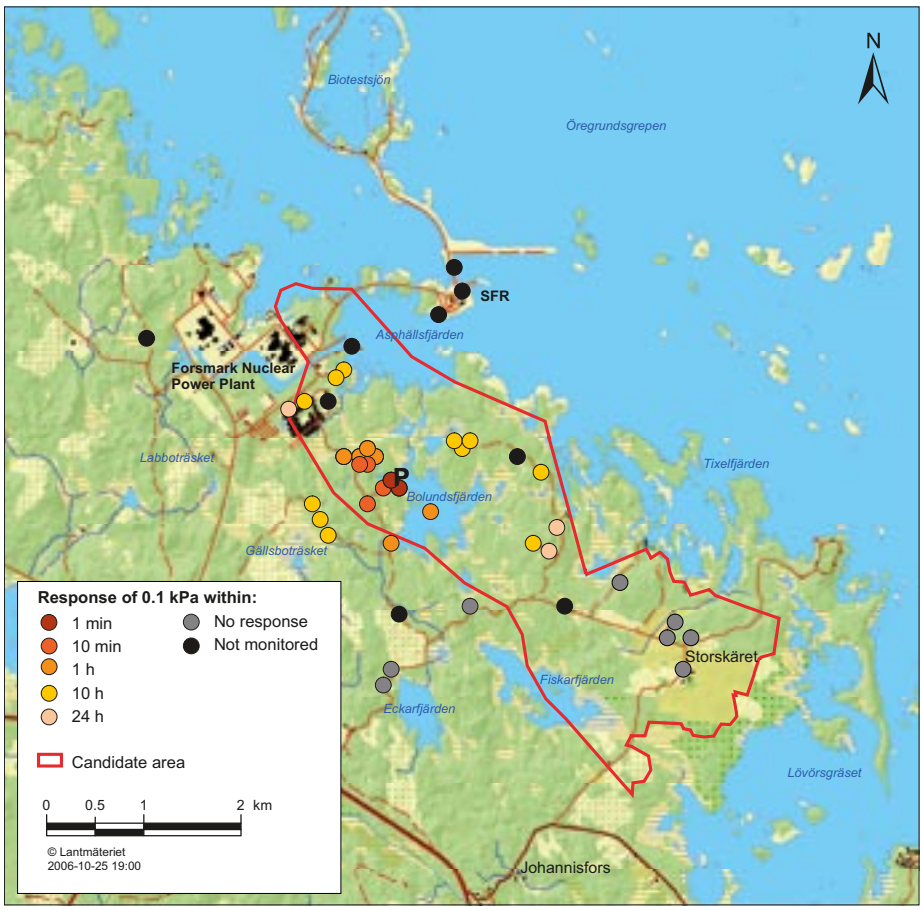

Figure 3-17. *Map showing response times in the bedrock to the three-weeks long interference test conducted in HFM14 (P) at drill site 5 during the dry summer of 2006. Clear test responses were observed in 71 out of a total of 110 monitoring sections. The maximum radius of influence was about 1.8 km. Reproduced from /Follin et al. 2007c./*

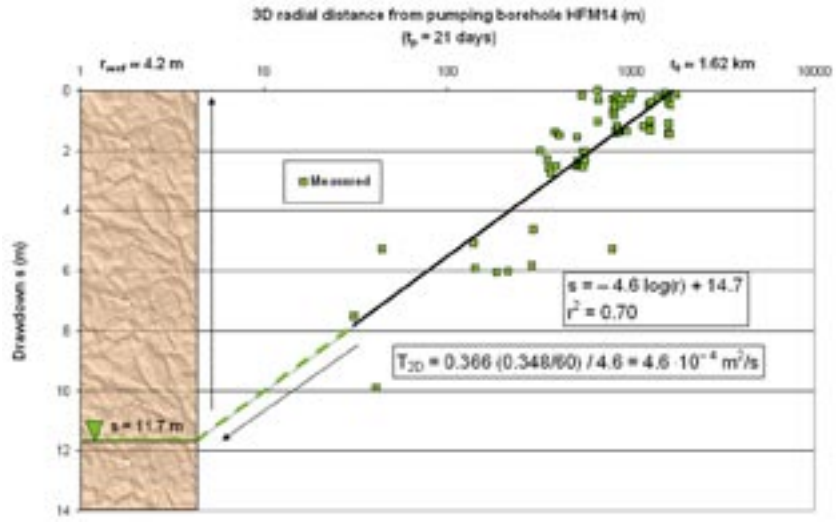

Figure 3-18. *Plot of measured drawdowns vs. log(3D radial distance) at the end of the 21-day long interference test in HFM14. The drawdown in HFM14 was 11.7 m and the flow rate was 348 L/min implying a specific capacity of approximately $5 \cdot 10^{-4}$ m²/s. The black line shows least-squares fit to the measurements. The value of the correlation coefficient ($r^2 = 0.70$) indicates a heterogeneous system. A steady-state, radial flow approximation using the slope of the least-squares fit for an estimate of Δs (difference in drawdown per log cycle of distance) renders a large-scale effective transmissivity of $5 \cdot 10^{-4}$ m²/s. An extrapolation of the regression model to 11.7 suggests an effective radius of HFM14 of about 4 m, which corresponds to a negative skin of about –4.1. Reproduced from /Follin et al. 2007c/..*

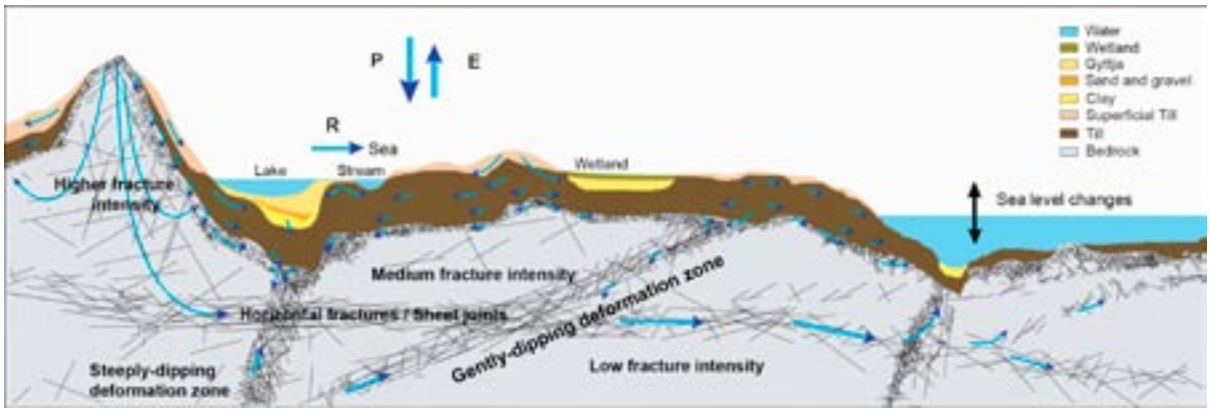

Figure 3-19. *Cross-section cartoon visualising the notion of a shallow bedrock aquifer and its envisaged impact on the groundwater flow system in the uppermost part of the bedrock within the target area. The shallow bedrock aquifer is probably hydraulically heterogeneous but at many places it is found to short circuit the recharge from above as well as the anticipated discharge from below. P = precipitation, E= evapotranspiration, R = runoff. Reproduced from /Follin et al. 2007c/.*

Figure 3-20. *The hypothesised lateral extent of the sheet joints in the shallow bedrock aquifer. The crosses mark the positions of percussion- and core-drilled boreholes for which transmissivity measurements were available. The bluish area represents fracture domain FFM02 and the pinkish area represents fracture domain FFM03. Reproduced from /Follin et al. 2007c/.*

3.3.5 The bedrock in between deformation zones at repository depth

Several boreholes penetrate fracture domain FFM01, e.g. KFM01D, -05A–07A. The plots in Figure 3-21 and Figure 3-22 show that FFM01 is very sparsely fractured with flowing fractures at repository depth, i.e. elevation –450 m RHB 70.

The four plots shown in Figure 3-23 and Figure 3-24 suggest that about 60% of the Terzaghi corrected PFL-f data in the footwall has a dip angle of less 25° regardless of fracture domain and elevation. Table 3-4 and Table 3-5 summarise the change in Terzaghi corrected linear fracture intensities, $P_{10,corr}$ of *open* fractures vis-à-vis *flowing* (PFL-f) fractures in fracture domains FFM01 and FFM02 with regard to depth and the five principal fracture set orientations, see section 3.2.3.

Above c. 400 m depth, three fracture sets dominate the flowing fractures: HZ, NS and NE with HZ very dominant. Below c. 400 m depth, the few flowing fractures observed occur in the HZ and NE sets with an average “true spacing” of about 200 m. In conclusion, below c. 400 m depth the flowing fractures in FFM01 are almost exclusively restricted to deformation zones, symptomatic of a very sparse and poorly connected network of fracture that does not reach a threshold for percolation of water into the deep rock.

Figure 3-21 and Figure 3-22 suggest that it is predominantly the significant decrease with depth in the observed intensity of flowing fractures that governs the groundwater flow at repository depth. A decreasing trend in fracture transmissivity is difficult to substantiate based on this information. Table 3-6 summarises the statistics of *open* fractures and *flowing* (PFL-f) fractures deduced in stage 2.2 for FFM01–FFM03. The cross-section cartoon in Figure 3-25 summarises the key components of the conceptual model of the different bedrock segments in the target volume at Forsmark.

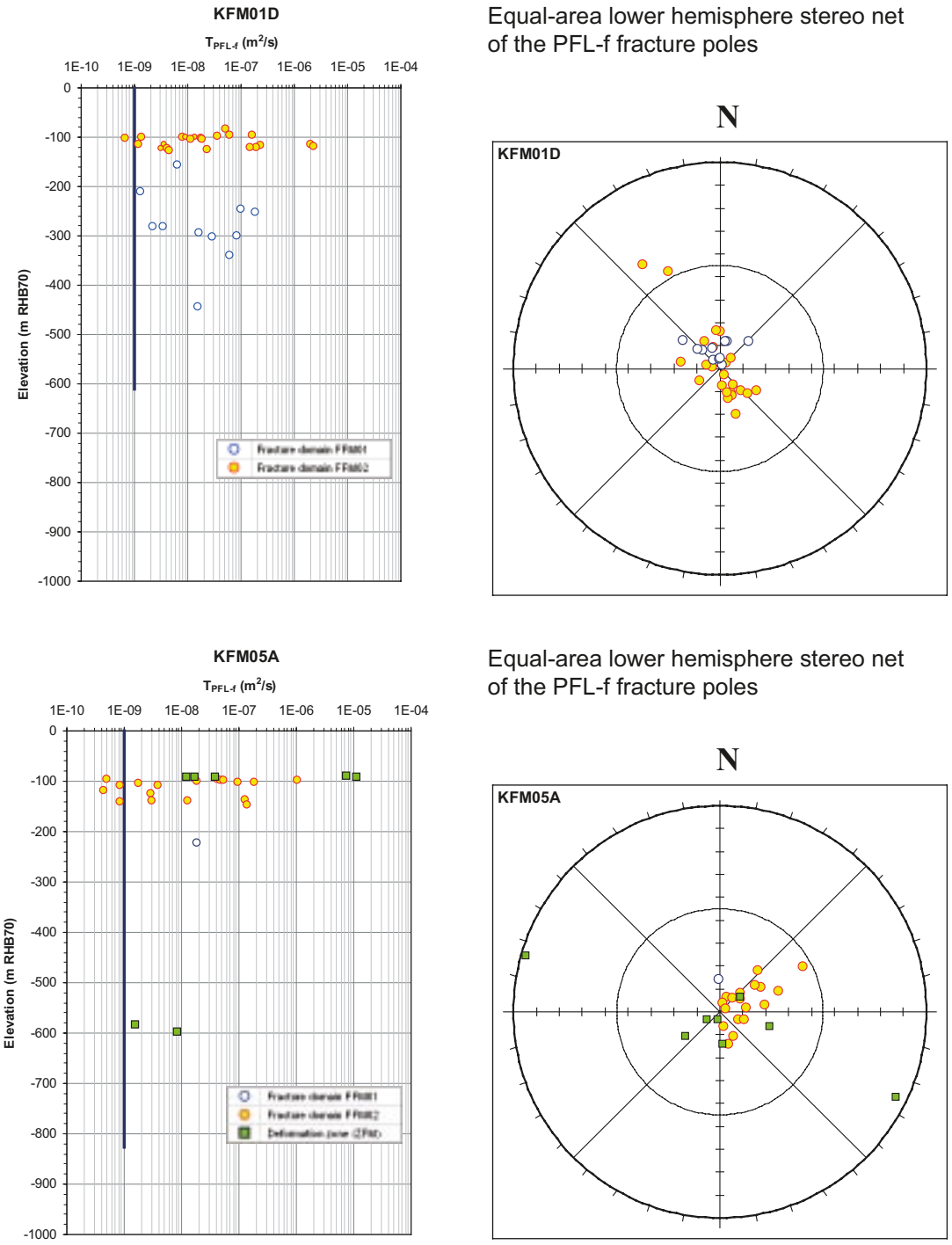

Figure 3-21. *There is one PFL-f transmissivity value close to repository depth in FFM01 in KFM01D but none in KFM05A. The blue lines indicate the typical lower transmissivity threshold of the PFL-f method at Forsmark (about $1 \cdot 10^{-9}$ m^2/s). Reproduced from /Follin et al. 2007b/.*

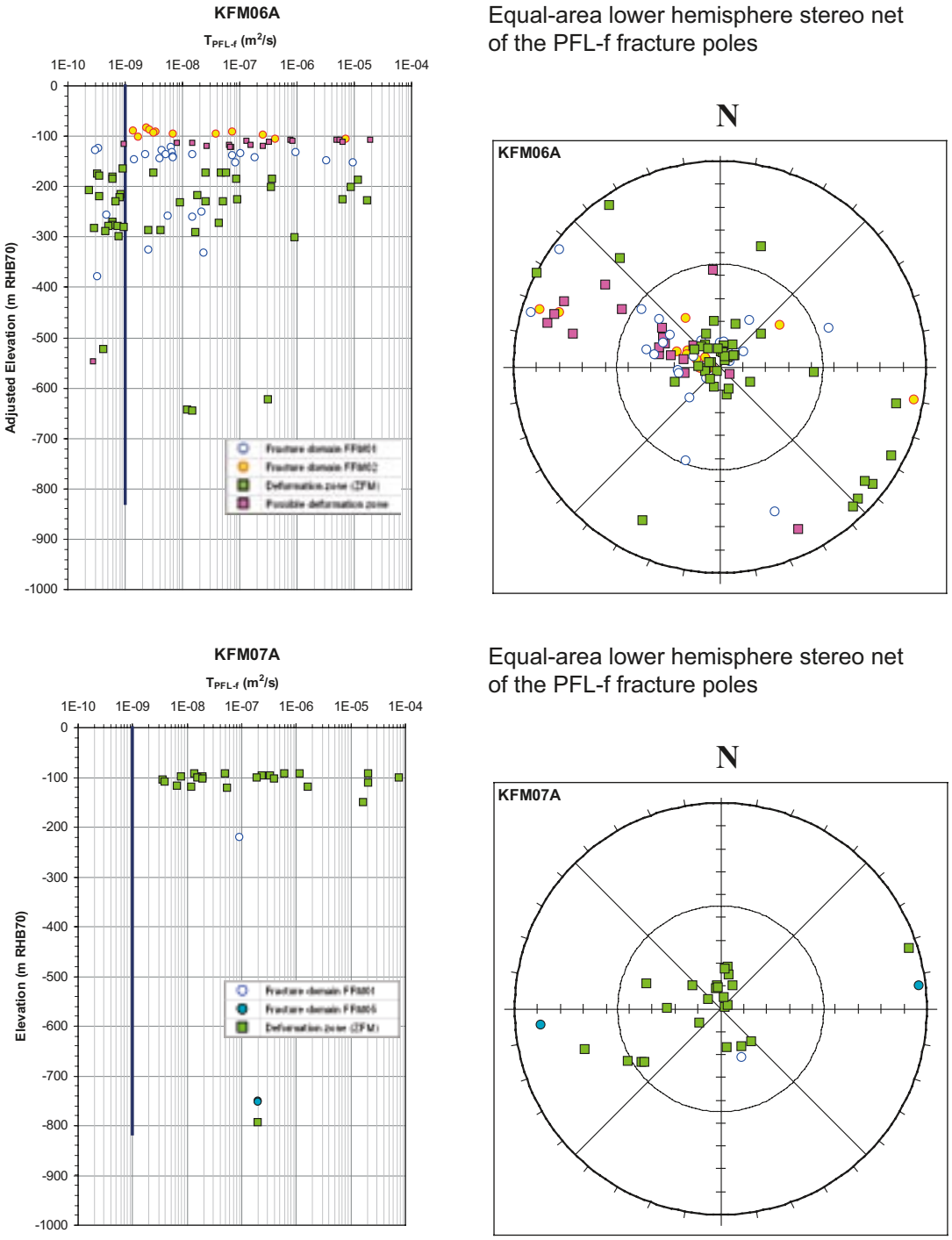

Figure 3-22. *There are no PFL-f transmissivities close to repository depth in FFM01 in KFM06A and KFM07A. The blue lines indicate the typical lower transmissivity threshold of the PFL-f method at Forsmark (about $1 \cdot 10^{-9}$ m²/s). Reproduced from /Follin et al. 2007b/.*

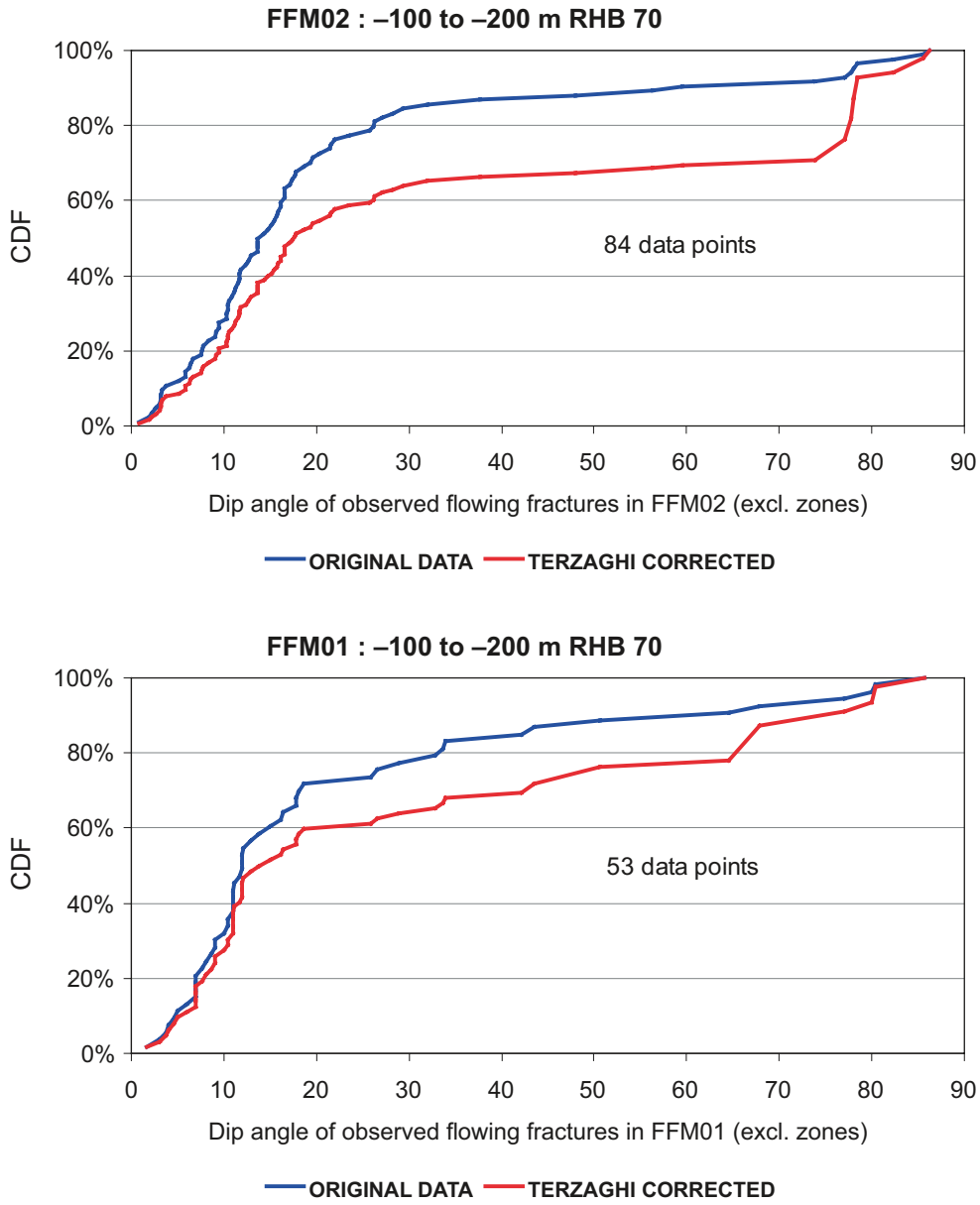

Figure 3-23. *Terzaghi corrected dip distributions between between 100 and 200 m depth in FFM02 and FFM01. Modified after /Follin et al. 2007c/.*

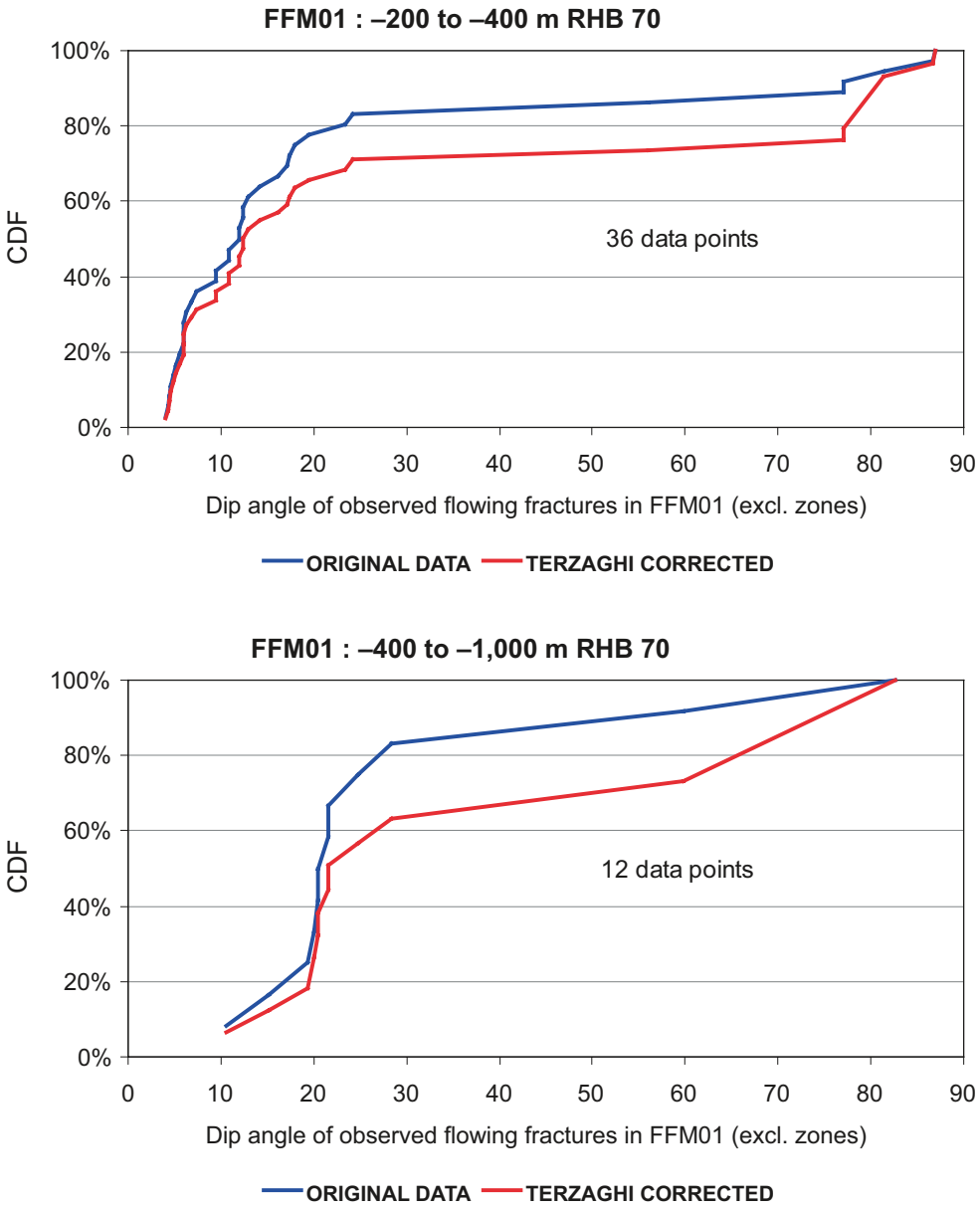

Figure 3-24. *Terzaghi corrected dip distributions between 200 and 400 m and between 400 and 1,000 m depth in FFM01. Ten of the twelve data points in lower plot were observed in KFM02A between zones A2 and F1, see Figure 3-8. Modified after /Follin et al. 2007c/.*

Table 3-4. Summary of Terzaghi corrected linear fracture intensities $P_{10,corr}$ by set of open fractures and PFL-f fractures within fracture domain FFM01 above 400 m depth and excluding deformation zones. Three fracture sets carry water: NS, NE and HZ. Reproduced from /Follin et al. 2007b/.

BH	$P_{10,o,corr}$ [1/m]					$P_{10,PFL,corr}$ [1/m]				
	NS	NE	NW	EW	HZ	NS	NE	NW	EW	HZ
KFM01A	0.195	0.790	0.119	0.066	0.824	0.000	0.033	0.000	0.000	0.053
KFM01D	0.116	0.004	0.185	0.010	0.404	0.000	0.000	0.000	0.000	0.040
KFM02A	–	–	–	–	–	–	–	–	–	–
KFM03A	–	–	–	–	–	–	–	–	–	–
KFM04A	–	–	–	–	–	–	–	–	–	–
KFM05A	0.097	0.177	0.154	0.055	0.120	0.000	0.000	0.000	0.000	0.006
KFM06A	0.071	0.291	0.085	0.053	0.508	0.025	0.042	0.000	0.000	0.123
KFM07A	0.107	0.409	0.051	0.086	0.148	0.000	0.000	0.000	0.000	0.005
KFM07C	0.020	0.443	0.067	0.037	0.238	0.000	0.035	0.000	0.000	0.035
KFM08A	0.208	0.473	0.188	0.166	0.466	0.014	0.021	0.000	0.000	0.107
KFM08C	0.135	0.281	0.106	0.151	0.277	0.006	0.000	0.000	0.000	0.017
KFM10A	0.707	0.580	0.526	0.600	2.841	0.000	0.000	0.000	0.000	0.000
All BH	0.125	0.339	0.126	0.083	0.374	0.006	0.015	0.000	0.000	0.049

Table 3-5. Summary of Terzaghi corrected linear fracture intensities $P_{10,corr}$ by set of open fractures and PFL-f fractures within fracture domain FFM01 below 400 m depth and excluding deformation zones. Two fracture sets carry water: NE and HZ. Reproduced from /Follin et al. 2007b/.

BH	$P_{10,o,corr}$ [1/m]					$P_{10,PFL,corr}$ [1/m]				
	NS	NE	NW	EW	HZ	NS	NE	NW	EW	HZ
KFM01A	0.089	0.072	0.026	0.000	0.150	0.000	0.000	0.000	0.000	0.000
KFM01D	0.087	0.034	0.178	0.026	0.080	0.000	0.000	0.000	0.000	0.006
KFM02A	0.099	0.094	0.104	0.005	0.040	0.000	0.016	0.000	0.000	0.021
KFM03A	–	–	–	–	–	–	–	–	–	–
KFM04A	0.109	0.094	0.198	0.022	0.273	0.000	0.000	0.000	0.000	0.002
KFM05A	0.127	0.270	0.127	0.013	0.174	0.000	0.000	0.000	0.000	0.000
KFM06A	0.110	0.426	0.062	0.112	0.134	0.000	0.000	0.000	0.000	0.000
KFM07A	0.030	0.133	0.057	0.016	0.024	0.000	0.000	0.000	0.000	0.000
KFM07C	0.168	0.953	0.000	0.128	0.222	0.000	0.000	0.000	0.000	0.000
KFM08A	0.077	0.078	0.108	0.055	0.142	0.000	0.000	0.000	0.000	0.000
KFM08C	0.088	0.180	0.056	0.138	0.163	0.000	0.000	0.000	0.000	0.000
KFM10A	–	–	–	–	–	–	–	–	–	–
All BH	0.094	0.163	0.098	0.039	0.141	0.000	0.002	0.000	0.000	0.003

Table 3-6. Summary of fracture statistics for fracture domains FFM01–03 subdivided by elevation. Terzaghi corrected values of the intensity of open and flowing fractures are shown for different elevation intervals. There are significant differences between the three fracture domains and a substantial decrease with depth of both open and flowing fractures. Values of the minimum and maximum fracture transmissivities (T) for the three fracture domains are also shown. Modified after /Follin et al. 2007b/.

Fracture Domain	FFM01			FFM02	FFM03	
Elevation, m RHB 70	–100 to –200	–200 to –400	–400 to –1,200	–100 to –200	–100 to –400	–400 to –1,200
Intensity of observed open fractures, m^{-1}	1.13	1.02	0.54	3.17	1.10	0.77
Intensity of observed flowing fractures, m^{-1}	0.15	0.04	< 0.01	0.33	0.09	0.05
T_{min}, m^2/s	$2.5 \cdot 10^{-10}$	$2.7 \cdot 10^{-10}$	$6.2 \cdot 10^{-10}$	$2.5 \cdot 10^{-10}$	$1.9 \cdot 10^{-9}$	$1.1 \cdot 10^{-9}$
T_{max}, m^2/s	$4.7 \cdot 10^{-5}$	$1.8 \cdot 10^{-7}$	$8.9 \cdot 10^{-8}$	$7.3 \cdot 10^{-6}$	$6.8 \cdot 10^{-7}$	$1.9 \cdot 10^{-7}$

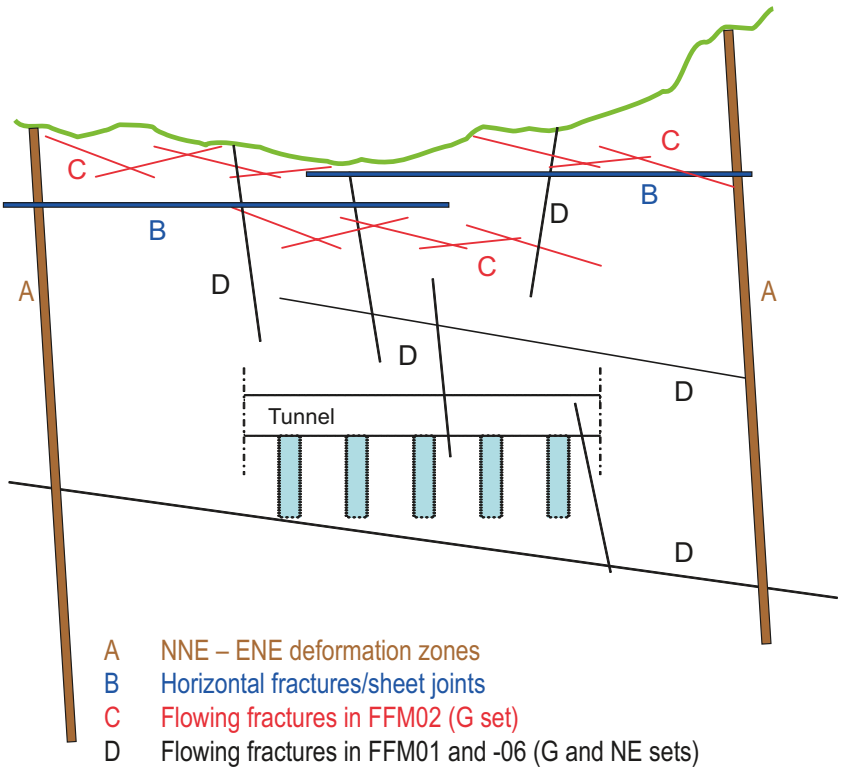

Figure 3-25. *Cross-section cartoon summarising the hydrogeological conceptual model of the bedrock within the target volume at Forsmark. The flow at repository depth in fracture domains FFM01 and FFM06 is probably channelised in the sparse network of connected fractures,* **D***, which consists of two fracture sets more or less, G and NE. The G fracture set is interpreted to be longer and probably more transmissive than the NE set.* **D** *connects to* **A** *and* **C***, where* **A** *represents the steeply dipping NNE-ENE deformation zones, which are abundant but hydraulically heterogeneous, and* **C** *represents the intensely fractured fracture domain FFM02, which lies on top of FFM01 and FFM06. The groundwater flow in FFM02 is dominated by the G fracture set, which occurs with a high frequency. More importantly, FFM02 is intersected by several extensive, horizontal fractures/sheet joints,* **B***, which can be very transmissive.* **B** *and* **C** *and the outcropping parts of* **A** *probably form a shallow network of flowing fractures. The network is interpreted to be highly anisotropic, structurally and hydraulically. Together with* **D***, which is close to the percolation threshold, the network create a hydrogeological situation that here is referred to as a shallow bedrock aquifer on top of a thicker bedrock segment with aquitard type properties.*

3.4 Hydraulic parameterisation

3.4.1 Quaternary deposits (HSD)

Table 3-7 and Table 3-8 show the preliminary values provided for groundwater flow modelling by the surface system group. Most of these values represent median values of the many hydraulic measurements carried out at Forsmark, see /Johansson 2008/.

Implementation of the Quaternary deposits in CONNECTFLOW

The modelling approach used in CONNECTFLOW implies a considerable simplification of the detailed geometrical description of the near-surface system. The thickness of the Quaternary deposits within the model area varies from less than a decimetre to over 25 m, not all layers exist everywhere, and the thickness of individual layers varies significantly. This complex stratigraphy was substituted by four element layers each of a constant 1 m thickness in order to relax the computational constraints in CONNECTFLOW. In operation, the same equivalent hydraulic conductivity tensor was specified for each vertical stack of four grid elements, but was varied horizontally from element-to-element, and was anisotropic between horizontal and vertical components. The horizontal component of the tensor was based on the arithmetic mean of the hydraulic properties of the original stratigraphy, whereas the vertical component was based on its harmonic mean. The resulting hydraulic conductivity distribution is illustrated in Figure 3-26.

Table 3-7. Values of the total porosity and the specific yield of the Quaternary deposits suggested for groundwater flow modelling in stage 2.2.

Layer	Total porosity [–] and specific yield [–] of layers with several types of Quaternary deposits					
	Fine till	Coarse till	Gyttja	Clay	Sand	Peat
L1	–	–	0.50/0.03	–	–	0.60/0.20
Z1	0.35/0.15	0.35/0.15	–	0.55/0.05	0.35/0.20	0.60/0.20
Z5	0.25/0.03	0.25/0.05	–	–	–	–
	Total porosity [–] and specific yield [–] of layers with one type of Quaternary deposits					
L2	0.35/0.20					
L3	0.45/0.03					
Z2	0.40/0.05					
Z3	0.35/0.20					
Z4	0.45/0.03					

Table 3-8. Values of the saturated hydraulic conductivity of the Quaternary deposits suggested for groundwater flow modelling in stage 2.2.

Layer	*K* [m/s] of layers with several types of Quaternary deposits					
	Fine till	Coarse till	Gyttja	Clay	Sand	Peat
L1	–	–	$3 \cdot 10^{-7}$	–	–	< 0.6 m: $1 \cdot 10^{-6}$
Z1	$3 \cdot 10^{-5}$	$3 \cdot 10^{-5}$	–	$1 \cdot 10^{-6}$	$1.5 \cdot 10^{-4}$	> 0.6 m: $1 \cdot 10^{-6}$
Z5	$1 \cdot 10^{-7}$	$1.5 \cdot 10^{-6}$	–	–	–	–
	K [m/s] of layers with one type of Quaternary deposits					
L2	$1.5 \cdot 10^{-4}$					
L3	< 0.6 m: $1 \cdot 10^{-6}$; > 0.6 m: $1.5 \cdot 10^{-8}$					
Z2	$3 \cdot 10^{-7}$					
Z3	$1.5 \cdot 10^{-4}$					
Z4	$1.5 \cdot 10^{-8}$					

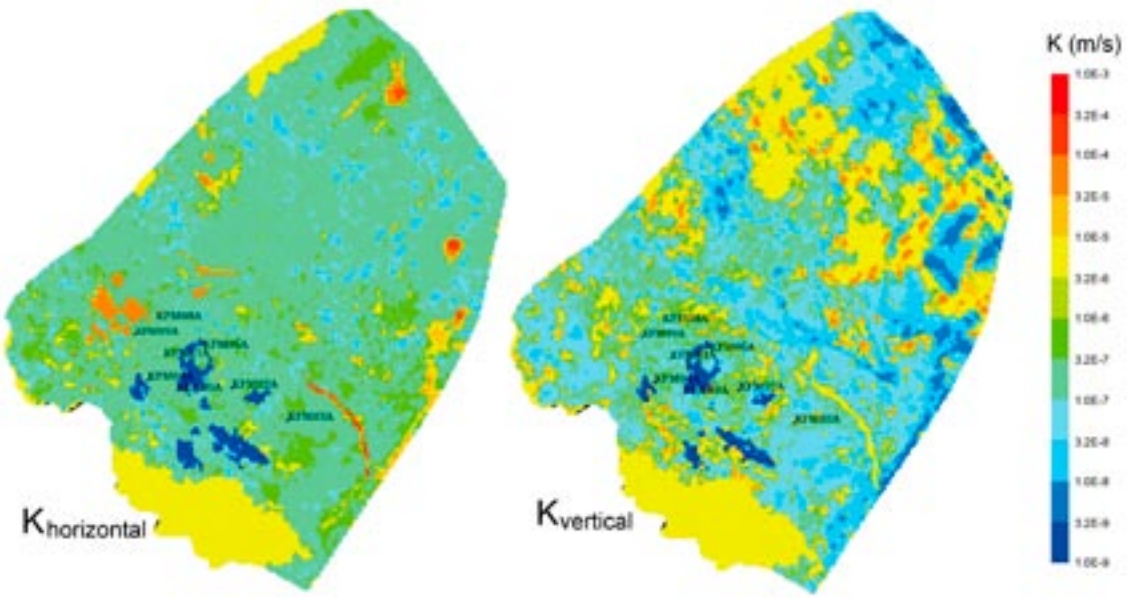

Figure 3-26. *Resulting effective hydraulic conductivity for HSD top layer based on QD layer thicknesses and hydraulic properties. Top: E-W horizontal component. Bottom: vertical component.*

3.4.2 Deterministically modelled deformation zones (HCD)

An exponential model for the depth dependency of the in-plane deformation zone transmissivity was suggested by /Follin et al. 2007b/ based on the data shown in Figure 3-14. The depth trend model may be written as:

$$T(z) = T(0)\ 10^{z/k} \qquad (3\text{-}1)$$

where T(z) is the in-plane deformation zone transmissivity, z is the elevation, $T(0)$ is the expected value of the transmissivity of the deformation zone at zero elevation and k is the depth interval that gives an order of magnitude decrease of the transmissivity. The value of $T(0)$ can be estimated by inserting a measured value [z', $T(z')$] in Equation (3-1), i.e.:

$$T(0) = T(z')\ 10^{-z'/k} \qquad (3\text{-}2)$$

In the case of several measurements at different locations in the same zone, the geometric mean of the calculated values of $T(0)$ is used as an effective value, $T_{eff}(0)$ in Equation (3-1).

Implementation of the deformation zones in CONNECTFLOW

The deformation zones shown in Figure 3-27 are coloured by the hydraulic conductivity within the zones and drawn as volumes to show their assigned hydraulic width. The effect of conditioning to a measurement was to extrapolate the conditioned value over the entire length of the deformation zone laterally, but not more than 100 m vertically. The geometrical and hydraulic properties of the zones were transferred to the computational grid using the implicit fracture zone (IFZ) approach /Marsic et al. 2001/.

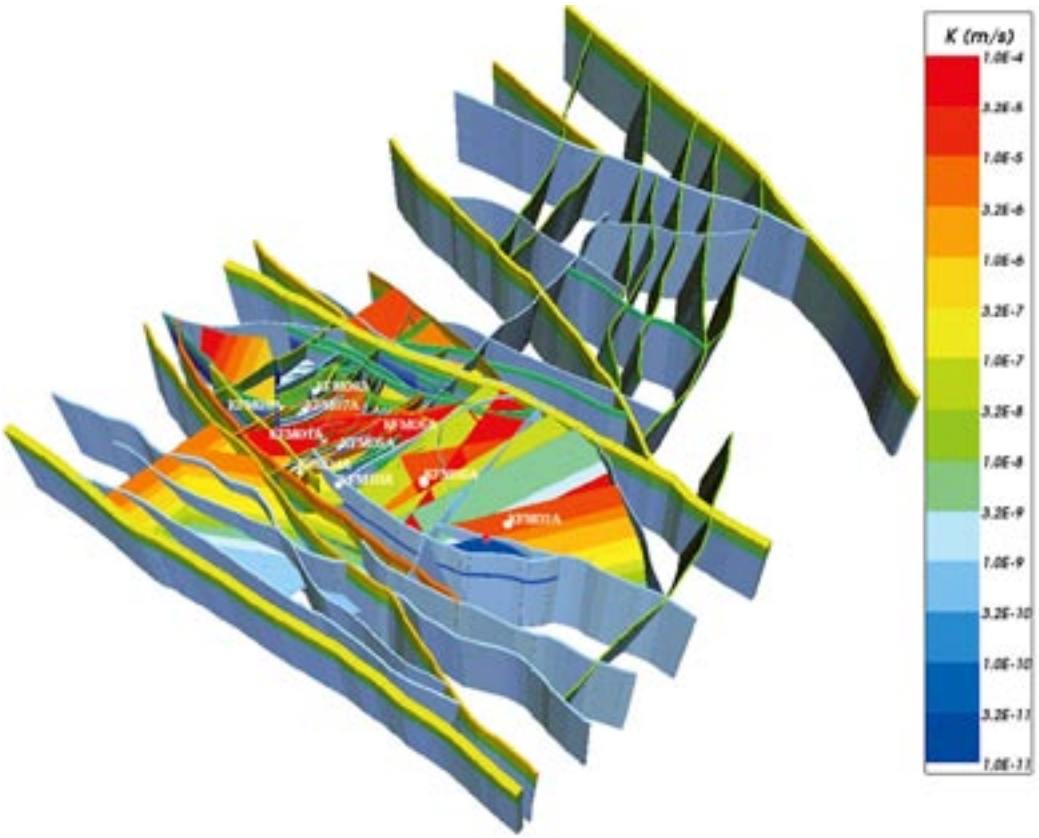

Figure 3-27. *The resulting property model using Equation (3-1). Here, the deformation zones are coloured by the hydraulic conductivity within the zones and drawn as volumes to show their assigned hydraulic width. The depth dependency is clearly apparent. The effect of conditioning to a measurement was to extrapolate the conditioned value over the entire length of the deformation zone laterally, but not more than 100 m vertically. Reproduced from /Follin et al. 2007c/.*

3.4.3 Fracture domains (HRD)

The hydrogeological DFN modelling analysed the statistics of *open* fractures and focussed on the geological DFN variant where the location parameter r_0 of the power-law fracture size distribution was fixed to equal the borehole radius. The shape parameter k_r of the power-law size distribution was tuned to simultaneously match the intensity of flowing (PFL-f) fracture in the boreholes (see /Follin et al. 2007b/ for details). Five of the fracture set orientations discussed in the geological DFN modelling was adopted for further analysis in the hydrogeological DFN modelling: NS, NE, NW, EW and HZ (horizontal). As shown in Table 3-4 and Table 3-5, the number of fracture sets that carry water is limited and varies with depth.

Figure 3-28 shows an example realisation of the regional Hydro-DFN. The realisation is shown as a NW-SE cross-section and as a horizontal trace plane at 500 m depth, cf. Figure 3-7. The images in the left column show the traces of *open fractures*. The images in the right column show the traces of the *connected open fractures*. The effect of the low connectivity of connected open fractures below 400 m depth is apparent. For the bedrock outside the mapped fracture domains, i.e. outside the tectonic lens, there is no fracture information available, and so a simplified property assignment must be used to specify homogeneous continuum porous medium (CPM) properties.

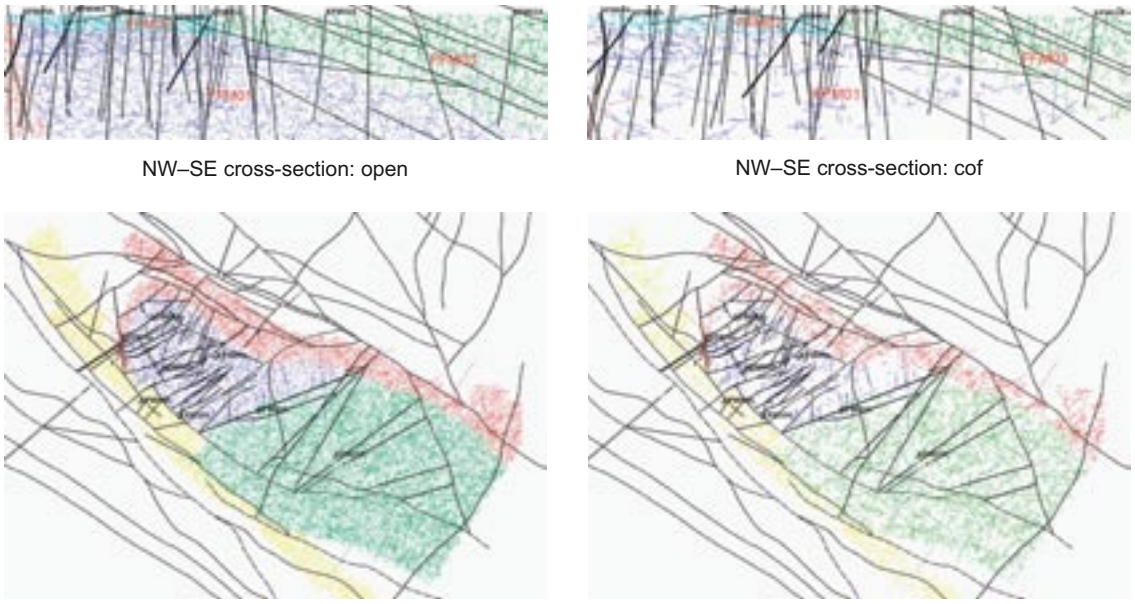

Figure 3-28. *An example of a fracture network realisation of the regional hydrogeological DFN. The realisation is shown as a NW-SE cross-section and a horizontal trace at 500 m depth. The depth extension of the cross-section is c. 1.2 km and the length is c. 5 km. The images in the left column show the traces of "open fractures". The images in the right column show the traces of the "connected open fractures" (cof). The DFN fracture traces are coloured by fracture domain: FFM01 and FFM06 are dark blue, FFM02 is light blue, FFM03 is green, FFM04 is yellow, and FFM05 is red. Slices through the deformation zones (local and regional models) at the same depths are superimposed in black. Here, the stochastic fractures are generated with radii between 5.64–564 m. Reproduced from /Follin et al. 2007c/.*

The methodology used to parameterise the fracture domains starts with a connectivity-sensitivity analysis of different DFN models and ends with flow simulations using the most reliable DFN model deduced in the connectivity analysis. Flow simulations were carried out using three different kinds of correlations between fracture transmissivity and fracture size, see Table 3-9.

Table 3-10 shows the resulting hydrogeological DFN parameterisation for a three-layer model of FFM01. The coefficients, exponents or standard deviations as appropriate to each transmissivity model reflect the rapid reduction in inflow magnitudes with depth. This trend is quantified in the comparison of measured and simulated total flow rates for each of the three transmissivity models tabulated in Table 3-9. The flow rates decrease by about two orders of magnitude below 200 m depth, then by about another order of magnitude below 400 m depth.

The resulting hydrogeological DFN parameterisations for fracture domains FFM02–06 are described in /Follin et al. 2007bc/. The groundwater flow simulations carried out in stage 2.2 utilised the semi-correlated transmissivity-size model, see Table 3-9. It should be noted that the hydrogeological DFN parameterisation was primarily developed for FFM01–03, which had abundant of hydrogeological information. This leaves the question of how to parameterise a hydrogeological DFN for FFM04–06 since they have very limited data. Based on the statistics available it was proposed in stage 2.2 that fracture domains FFM04 and FFM05 are assumed to have the same properties as inferred for FFM03. However, the hydraulic information about FFM06 was limited in data freeze 2.2. Based on the data observed in the neighbouring boreholes /Follin et al. 2007b/ assumed that the structural-hydraulic properties of FFM06 are identical to those observed in FFM01.

Table 3-9. Transmissivity parameters used for all sets when matching measured PFL-f flow distributions. Reproduced from /Follin et al. 2007c/.

Type	Description	Relationship	Parameters
Correlated	Power-law relationship	$\log(T) = \log(a\, r^{b})$	a, b
Semi-correlated	Log-normal distribution about a power-law correlated mean	$\log(T) = \log(a\, r^{b}) + \sigma_{\log(T)}\, \mathbf{N}[0,1]$	a, b, $\sigma_{\log(T)} = 1$
Uncorrelated	Log-normal distribution about a specified mean	$\log(T) = \mu_{\log(T)} + \sigma_{\log(T)}\, \mathbf{N}[0,1]$	$\mu_{\log(T)}$, $\sigma_{\log(T)}$

Table 3-10. Description of hydrogeological DFN parameters for the simulations of flow in open fractures in FFM01 with depth dependency above 200 m depth, between 200 and 400 m depth and below 400 m depth. Reproduced from /Follin et al. 2007c/.

Fracture domain (m RHB70)	Fracture set name	Orientation set pole: (trend, plunge), Fisher kappa	Size model, power-law (r_0, k_r)	Intensity (P_{32}) valid size interval: (r_0, 564 m)	Transmissivity model (Table 3-9)
			(m, –)	(m^2/m^3)	T (m^2s^{-1})
FFM01 above 200 m depth	NS	(292, 1) 17.8	(0.038, 2.50)	0.073	Semi-correlated: (a,b,$\sigma_{log(T)}$) ($6.3\cdot10^{-9}$, 1.3, 1.0); Correlated: (a,b) ($6.7\cdot10^{-9}$, 1.4); Uncorrelated: ($\mu_{log(T)}$, $\sigma_{log(T)}$) (–6.7, 1.2)
	NE	(326, 2) 14.3	(0.038, 2.70)	0.319	
	NW	(60, 6) 12.9	(0.038, 3.10)	0.107	
	EW	(15, 2) 14.0	(0.038, 3.10)	0.088	
	HZ	(5, 86) 15.2	(0.038, 2.38)	0.543	
FFM01 between 200 and 400 m depth	NS	As above	As above	0.142	Semi-correlated: (a,b,$\sigma_{log(T)}$) ($1.3\cdot10^{-9}$, 0.5, 1.0); Correlated: (a,b) ($1.6\cdot10^{-9}$, 0.8); Uncorrelated: ($\mu_{log(T)}$, $\sigma_{log(T)}$) (–7.5, 0.8)
	NE	As above	As above	0.345	
	NW	As above	As above	0.133	
	EW	As above	As above	0.081	
	HZ	As above	As above	0.316	
FFM01 below 400 m depth	NS	As above	As above	0.094	Semi-correlated: (a,b,$\sigma_{log(T)}$) ($5.3\cdot10^{-11}$, 0.5, 1.0); Correlated: (a,b) ($1.8\cdot10^{-10}$, 1.0); Uncorrelated: ($\mu_{log(T)}$, $\sigma_{log(T)}$) (–8.8, 1.0)
	NE	As above	As above	0.163	
	NW	As above	As above	0.098	
	EW	As above	As above	0.039	
	HZ	As above	As above	0.141	

3.4.4 Shallow bedrock aquifer

The transmissivity measurements corresponding to the crosses in Figure 3-20 are listed in Table 3-11. The measurements are grouped into three 50 m thick intervals to reflect the uncertainties involved in the mapping of the sheet joints. Furthermore, intervals with little or no flow are assigned a low transmissivity value of 10^{-7} m^2/s in the model order to reflect the uncertainty of the hydraulic test methods used, see /Follin et al. 2007bc/.

Table 3-11. Log transmissivities (log(T)) of single-hole hydraulic tests conducted in the uppermost c. 150 m of bedrock. The data are grouped into 50 m intervals for use in flow modelling of the shallow bedrock aquifer. Reproduced from /Follin et al. 2007c/.

Borehole name	log (T) (m^2s^{-1}) 0 to 50 m depth	log (T) (m^2s^{-1}) 50 to 100 m depth	log (T) (m^2s^{-1}) 100 to 150 m depth
HFM01	–4.30	–4.87	–7.00
HFM02	–3.23	–7.00	–7.00
HFM03	–3.37	–7.00	–7.00
HFM04	–7.00	–4.10	–7.00
HFM05	–7.00	–7.00	–3.40
HFM06	–3.99	–3.64	–7.00
HFM07	–7.00	–7.00	–7.00
HFM08	–7.00	–4.24	–2.92
HFM09	–3.43	–7.00	–7.00
HFM10	–7.00	–7.00	–3.51
HFM11	–4.65	–4.55	–7.00
HFM12	–7.00	–5.10	–7.00
HFM13	–7.00	–4.68	–3.54
HFM14	–3.46	–3.69	–7.00
HFM15	–3.66	–3.99	–7.00
HFM16	–3.93	–3.39	–7.00
HFM17	–4.41	–7.00	–7.00
HFM18	–3.79	–7.00	–7.00
HFM19	–7.00	–4.40	–3.53
HFM20	–4.24	–5.75	–4.99
HFM21	–3.87	–3.47	–3.68
HFM22	–4.70	–3.84	–7.00
HFM23	–7.00	–7.00	–7.00
HFM24	–3.96	–7.00	–7.00
HFM25	–7.00	–7.00	–7.00
HFM26	–7.00	–7.00	–7.00
HFM27	–4.44	–4.06	–7.00
HFM28	–7.00	–7.00	–7.00
HFM29	–7.00	–7.00	–7.00
HFM30	–7.00	–4.32	–4.06
HFM31	–7.00	–7.00	–7.00
HFM32	–3.02	–7.00	–7.00
KFM01C	–3.01	–3.61	–7.00
KFM01D	–7.00	–4.44	–4.90
KFM02A	–7.00	–3.08	–3.04
KFM03B	–4.65	–4.68	–7.00
KFM04A	–7.00	–4.43	–3.87
KFM05A	–7.00	–5.51	–5.75
KFM06A	–7.00	–4.10	–3.63
KFM06B	–3.22	–4.67	–7.00
KFM06C	–7.00	–4.66	–3.73
KFM07A	–7.00	–2.99	–4.26
KFM08A	–7.00	–5.20	–4.46
KFM08B	–4.41	–7.00	–7.00
KFM09A	–7.00	–7.00	–5.95
KFM09B	–4.37	–5.09	–7.00

Implementation of the shallow bedrock aquifer in CONNECTFLOW

The computational grid geometry implemented in CONNECTFLOW to represent the shallow bedrock aquifer was idealised into three 1 m thick parallel layers at approximately the mid-elevations of the three depth intervals shown in Table 3-11. The three layers were made parallel to the topographic surface to avoid outcropping on the top surface, see Figure 3-16. The horizontal extent of each layer was hypothesised based on Figure 3-20. The transmissivities of the three 1 m thick layers were based on the data shown in Table 3-11. For simplicity reasons, a nearest neighbour approach was chosen for the final model as this best preserved the varying scale of heterogeneity observed in the measurements while honouring the data at the measurement points. Figure 3-29 shows a cross-section that strike WNW-ESE through the target area.

3.5 Solute transport model

The solute transport model applied in the hydrogeological modelling of stage 2.2 is based on the ECPM approach. It should be noted that in safety assessment calculations such as SR-Can /Hartley et al. 2006/ and the upcoming SR-Site, the transport properties of the bedrock are calculated explicitly along migration pathways obtained from DFN flow simulations.

In the ECPM approach, the total connected pore-space available to solutes is divided between a mobile porosity, known as the *kinematic porosity*, in which both groundwater flow and solute transport takes place, and an immobile porosity, referred to as *diffusion accessible porosity*, in which only solute transport through diffusive exchange with the kinematic porosity is considered. For the sparsely fractured bedrock at Forsmark, the kinematic porosity may be interpreted as the open fracture channels that are connected and responsible for the circulation of groundwater, and the diffusion accessible porosity is the rest of the total connected porosity including inter-granular porosity and micro-fractures. The diffusion accessible porosity may

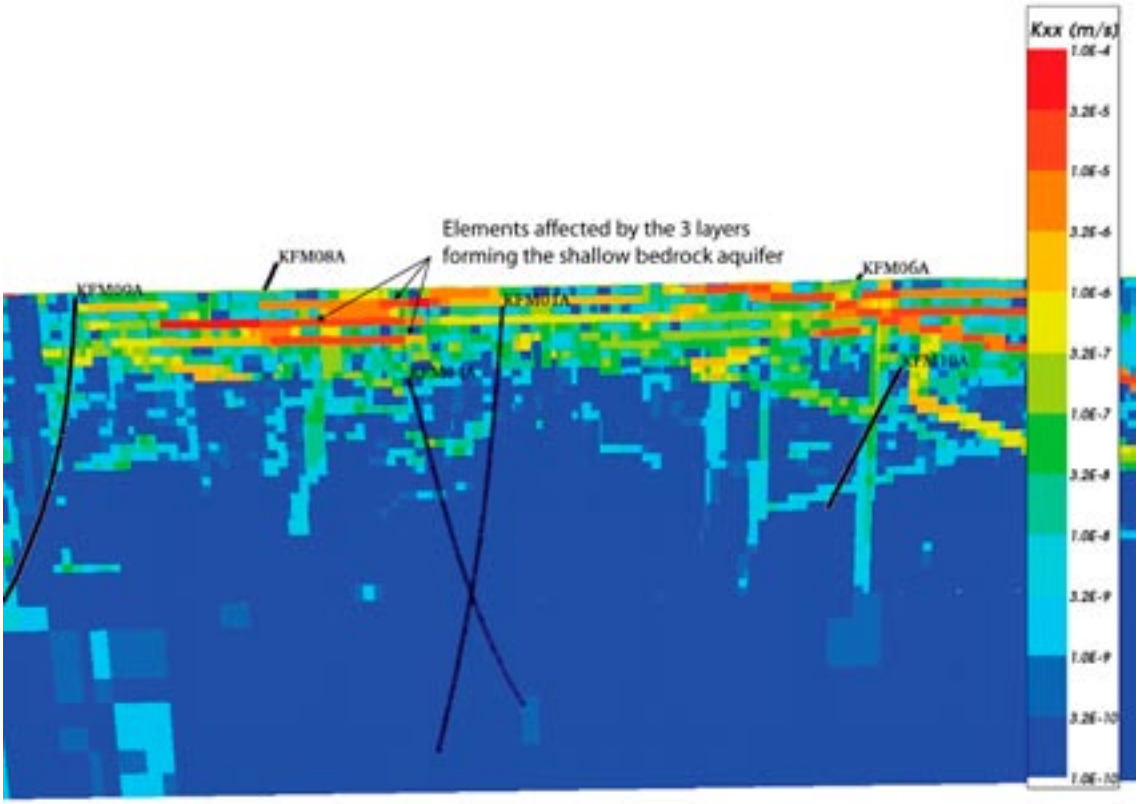

Figure 3-29. *A visualisation of the horizontal hydraulic conductivity in CONNECTFLOW on a WNW-ESE vertical slice through the target area. Note the effect of the three layers used to model the shallow bedrock aquifer. Modified after /Follin et al. 2007c/.*

also include contributions from fractures in which there is negligible flow and from regions of nearly immobile water in the larger fractures (resulting from constrictions in fracture aperture or the presence of gouge material). In practice, it may be difficult to estimate either type of porosity accurately by direct measurement, and hence one purpose of the solute transport modelling of natural tracers is to confirm the interpretation of transport properties.

In the mobile porosity, groundwater flow is modelled and solute transport takes place by advection, dispersion and diffusion through the kinematic porosity together with diffusion of solute between the groundwater in the kinematic porosity and immobile groundwater in the diffusion accessible porosity. The process of diffusion between groundwater in the kinematic porosity and the diffusion accessible porosity can lead to a significant retardation of solute migration relative to migration in the kinematic porosity alone. The rock matrix diffusion (RMD) model used in stage 2.2 represents the process in terms of a 1D model of diffusion between groundwater flowing in infinite, parallel, equidistant, constant-aperture, planar fractures and immobile groundwater in the intervening rock /Hoch an Jackson 2004/. The parameters used in the RMD model are:

- the effective (or intrinsic) diffusion coefficient (for diffusion in immobile water),
- the diffusion accessible porosity,
- the maximum distance available for diffusion into the diffusion accessible porosity,
- the flow-wetted fracture surface area per unit volume over which there may be diffusion between the groundwater flowing in the fractures and the diffusion accessible porosity, and
- the kinematic porosity.

Estimates of the effective diffusion coefficient and the diffusion accessible porosity are available for in diffusion experiments. Parameters relating to the fracture spacing can be derived from information about the hydraulic fracture network (hydrogeological DFN). This may be derived based on the frequency of water conducting fractures mapped using the PFL-f method. Because this frequency can be biased by the relative orientation of fractures to the borehole trajectory, it is more appropriate to estimate the 'true' fracture intensity, $P_{10,corr}$, rather than the intensity, P_{10}, measured in the borehole. The maximum distance available for diffusion into the diffusion accessible porosity can be based on the spacing of the fractures (if it is considered that all of the rock between the fractures is potentially accessible) or based on the dimensions of alteration halos around fractures (if it is considered that only the rock within a limited distance of fractures is accessible). Similarly, the flow-wetted surface per unit volume can be estimated from the unbiased fracture intensity, $P_{10,corr}$.

Measurement of the kinematic porosity is difficult, particularly in fractured rocks. In practice, it may be necessary to infer the kinematic porosity on the basis of DFN models of the flowing fractures. For the sake of the work reported here, the kinematic porosity, n_e, was derived based on the underlying Hydro-DFN calculated element-by-element as the total connected volume divided by the element volume. The fracture volume for an individual fracture was calculated as the fracture area within element multiplied by the transport aperture, and this is modelled based on Äspö Task Force 6c results /Dershowitz et al. 2003/, which assumes a direct correlation between the transport aperture e_t and the transmissivity T, such that:

$$e_t = a\, T^b \qquad (3\text{-}3)$$

The values suggested from Äspö Task Force 6c are $a = 0.46$ and $b = 0.5$. Although this approach provides a direct link between the assignment of kinematic porosity in the ECPM model and the underlying Hydro-DFN model, it relies on several approximations, including that the full fracture surface area contributes to advection and that the contribution to porosity of fractures below the truncation of fracture sizes in the regional DFN model is not significant[1].

[1] The size truncation applied in the regional Hydro-DFN modelling, $r_{min} = 5.64$ m, rendered a connected fracture porosity for FFM02 of $2 \cdot 10^{-5}$ compared with $6 \cdot 10^{-5}$, when $r_{min} = r_0 = 0.038$ m, i.e. a factor 3 too low.

Hence, the derived kinematic porosity was used as an initial guess to the calibration, and adjustments were made as part of the calibration to help inform the description of the fracture transport properties.

A list of the transport properties used is given in Table 3-12. The flow wetted fracture surface area per unit volume of rock, a_r, used to parameterise RMD of solutes in the palaeo-hydrogeological modelling task was derived from the Terzaghi corrected intensity of flowing features identified in PFL-f tests observed in boreholes and the approximation:

$$a_r = 2\, P_{10,PFL,corr} \qquad (3\text{-}4)$$

which in combination with the $P_{10,PFL}$ data reported by /Follin et al. 2007b/ results in the values given in Table 3-13. A minimum value of 0.15 m^2m^{-3} was used otherwise the 1D approximation of the solute profile in the matrix requires a prohibitively large number of terms in the numerical solution.

It should be noted that in safety assessment calculations, flow wetted fracture surface area per unit volume of rock is calculated explicitly along migration pathways obtained from DFN flow simulations implemented in CONNECTFLOW.

Table 3-12. Transport properties used in the HRD. Reproduced from /Follin et al. 2007c/.

Property	Value	Comment
Matrix porosity n_m	$3.7 \cdot 10^{-3}$	Based on /Hartley et al. 2006/
Dispersion lengths	Longitudinal a_L = 40 m on the regional-scale, 20 m on the local-scale, transverse a_T = 5 m	Minimal values for grid size
Flow wetted fracture surface area per unit volume of rock a_r ($m^2\,m^{-3}$)	See Table 3-13	Varies by fracture domain and depth according to $2\, P_{10,PFL,corr}$
RMD length, L_D	$1/a_r$	Assume can potentially diffuse into full matrix volume
Intrinsic diffusivity, D_i (m^2s^{-1})	$1 \cdot 10^{-13}$	Based on /Hartley et al. 2006/

Table 3-13. Alternative spatial variation of flow wetted fracture surface area per unit volume of rock based on Terzaghi corrected PFL-f intensities. Reproduced from /Follin et al. 2007c/.

HRD	Flow wetted fracture surface area per unit volume a_r (m^2m^{-3})
FFM01, FFM06	0.30 above –200 m RHB 70 0.15 < –200 m RHB 70
FFM02	0.60
FFM03, FFM04, FFM05	0.15
Outside FFM01–06	0.60 > –200 m RHB 70 0.30 < –200 m RHB 70

3.6 Initial conditions

The palaeohydrogeological simulations considered the evolution of groundwater flow and hydrochemistry from just after the melting of glacial ice sheets, 8000 BC, until the present-day. This involved setting an initial condition based on a conceptual model for the hydrochemical evolution at the surface and in groundwater. In the hydrochemical modelling it is suggested that the mixing of several so called *reference water* (*or end-members*) contribute to the groundwater composition in the Forsmark area /SKB 2005/. Conceptually, the different reference waters together reflect important aspects of the geological evolution, the changes in the palaeoclimate and the historic development of the hydrological conditions. Therefore, the specification of the initial condition is posed in terms of mixtures of defined reference waters as follows:

Deep Saline Water

Strong saline source → high chloride content (> 20,000 mg/L)

Non-marine origin → low magnesium content (< 20 mg/L)

Enriched $\delta^{18}O$

Holocene Glacial Melt Water

Non-saline source → low chloride content (< 8 mg/L)

Non-marine origin → low magnesium content (< 8 mg/L)

Significantly depleted $\delta^{18}O$

Littorina Sea Water

Brackish saline source → moderate chloride content (max. ~ 5,500 mg/L)

(The chloride content of the present-day *Baltic Sea Water* is ~ 3,000 mg/L).

Marine origin → high magnesium content (max. 250–350 mg/L)

Enriched $\delta^{18}O$ (> –10‰ SMOW)

Present-day Meteoric Water

Non-saline source → low chloride content (< 200 mg/L)

Non-marine origin → low magnesium content (< 50 mg/L)

Intermediate $\delta^{18}O$ (–12 to –11‰ SMOW)

Table 3-14 shows the major ion components and stable isotope compositions for the four reference water types.

For the *stage 2.2 base model simulation*, an initial condition at 8000 BC was assumed to be *Deep Saline Water* at depth, with the less saline groundwater above being a mixture of *Deep Saline Water*, *Old Meteoric-Glacial Waters and Holocene Glacial Melt Water*. By implication, this initial condition assumes that the flushing with *Holocene Glacial Melt Water* did not completely replace the pre-existing waters above the *Deep Saline Water*. This definition of the initial condition was introduced in stage 2.2 to improve the predictions of Oxygen and Hydrogen isotopes, and is referred to as the "Alternative Case model" in /Follin et al. 2007c/. Prior to stage 2.2, *Old Meteoric-Glacial Waters* were not considered in the initial conditions which lead to an over-prediction of *Holocene Glacial Melt Waters* or low $\delta^{18}O$ at depths around 400–1,000 m.

Table 3-14. Compilation of reference water composition for Forsmark in modelling stage 2.2 based on end-member data reported by /Laaksoharju et al. 2008/.

Reference water	Na mg/L	K mg/L	Ca mg/L	Mg mg/L	HCO_3 mg/L	Cl mg/L	SO_4 mg/L	Br mg/L	δ^2H ‰SMOW	$\delta^{18}O$ ‰SMOW
Deep Saline Water (DS)	8,200	45.5	19,300	2.12	14.1	47,200	10	323	–44.9	–8.9
Holocene Glacial Melt Water (HGM)	0.17	0.4	0.18	0.1	0.12	0.5	0.5	0	–158	–21
Littorina Sea Water (L)	3,674	134	151	448	92.5	6,500	890	22.2	–37.8	–4.7
Present-day Meteoric Water (PM)	274	5.6	41.1	7.5	466	181	85.1	0.6	–80.6	–11.1

To implement this new initial condition in CONNECTFLOW, *Old Meteoric-Glacial Waters* was introduced as an additional fifth reference water, which was assumed to have the same hydrochemical composition as the *Present-day Meteoric Water*, except that the levels of bicarbonate were reduced to those of the ancient *Deep Saline Water* in accordance with low bicarbonate levels measured at depths below about –200 m RHB 70. Figure 3-30 shows the definition of the hydrochemical initial condition for water in the fracture system in terms of fractions of 3 different reference waters (No *Littorina Sea Water* or *Present-day Meteoric Water* having entered the groundwater at this time).

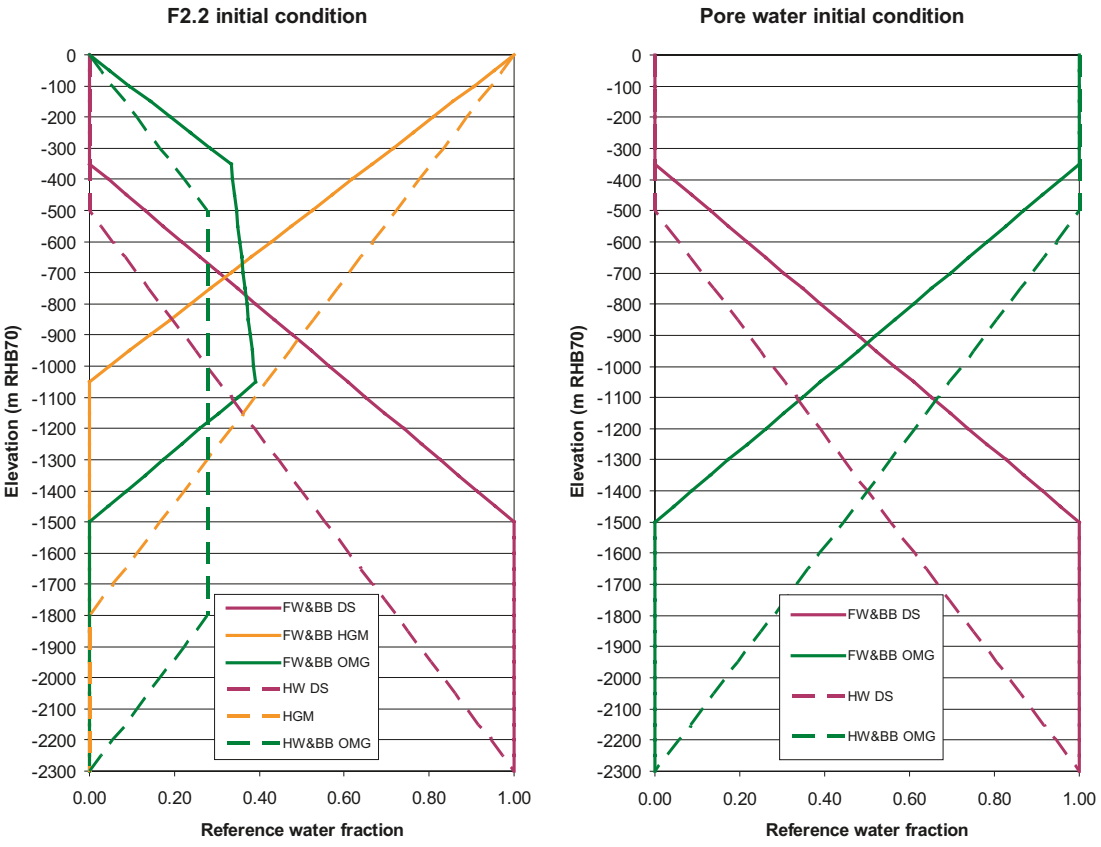

Figure 3-30. *Initial mixes of reference waters in the stage 2.2 base model simulation. Left: the fracture water chemistry at 8000 BC was assumed a mixture of Deep Saline Water (DS), Holocene Glacial Melt Water (HGM) and Old Meteoric-Glacial Water (OMG). Right: the initial pore water was assumed a mixture of Deep Saline Water (DS) and Old Meteoric-Glacial Waters. In both systems, different profiles were assumed for the footwall (FW) and border borehole (BB) regions of deformation zone A2 compared to the hanging wall (HW) bedrock of A2. Reproduced from /Follin et al. 2007c/.*

In the *stage 2.2 base model simulation*, a different initial condition was assumed for the pore water in the rock matrix. Based on differences between the hydrochemistry of the water samples form the fracture system and pore water it is hypothesised that there was insufficient time for significant in-diffusion of glacial water in to the pore water during the period that the fracture system may have been inundated with *Holocene Glacial Melt Water.* Therefore, the initial water in the matrix is assumed to be a mix of *Old Meteoric-Glacial Water* and *Deep Saline Water*, see the plot to the right in Figure 3-30.

3.6.1 Boundary conditions

The boundary conditions for palaeohydrogeological modelling are specified so as to represent the temporal changes of the hydraulic gradient and water composition at the upper surface, which vary mainly as a consequence of changes in shore-level displacement (Figure 3-31) and variations in the salinity of the Baltic Sea (Figure 3-32).

For groundwater flow, two types boundary conditions were applied:

- Below the shore level, a specified head type boundary condition is used, with head equal to the depth of the sea multiplied by the relative salinity of the Baltic Sea, and
- above the shore level, a specified flux (infiltration) type boundary condition is used, but the magnitude and direction of flux varies in time and space according to the relative elevations of ground surface and the water table.

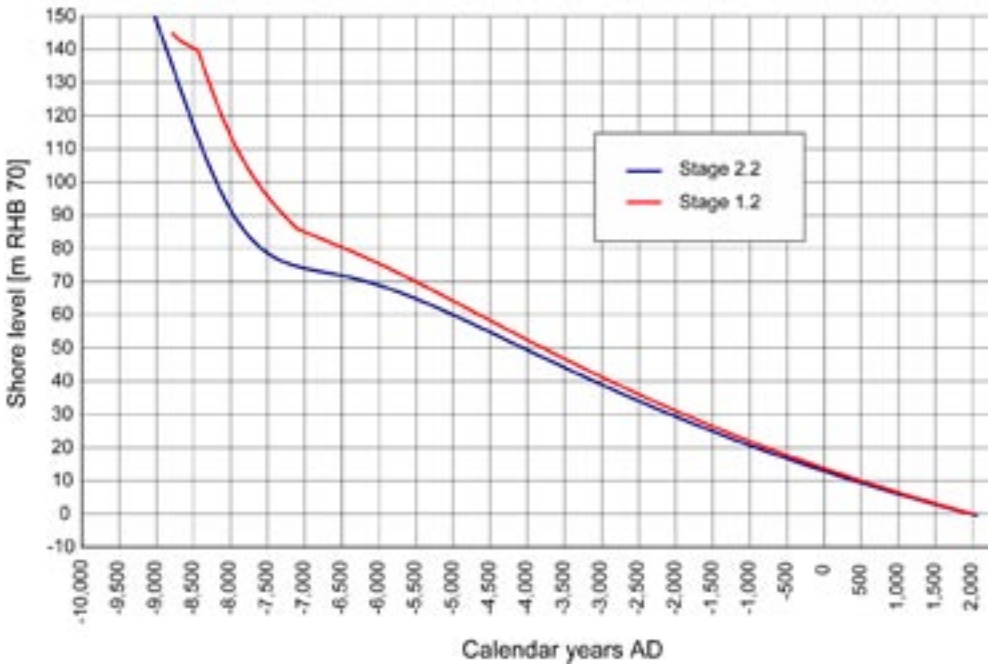

Figure 3-31. *Shore level displacement evolution specified for stage 2.2 and compared to the evolution used in stage 1.2. Based on /Påsse 1996, 1997, 2001/.*

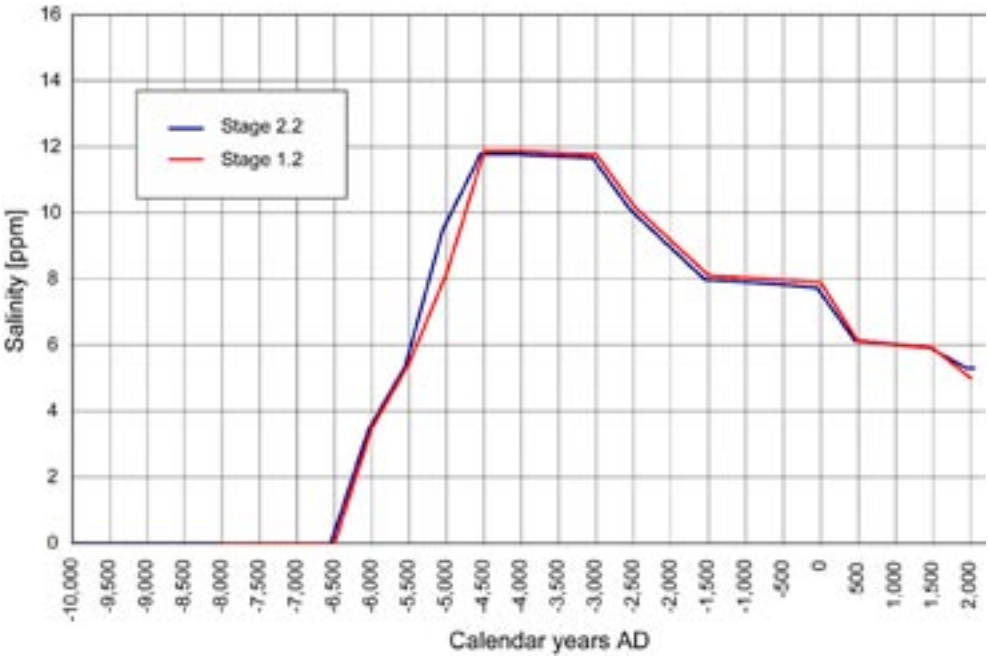

Figure 3-32. *Changes in the salinity of the aquatic systems in the Baltic basin specified for stage 2.2 and compared to the evolution used in Stage 1.2. Based on /Westman et al. 1999/.*

The standard approach in CONNECTFLOW for specifying an infiltration type condition is to define the recharge flux, R, into or out of the model as a function of the current head (groundwater level), h, in the model, the topographic surface height, z, and the maximum potential groundwater recharge, R_p. The maximum potential groundwater recharge is equal to the precipitation minus evapotranspiration (P–E) and surface run-off. Surface run-off is subtracted because we are only interested in the potential recharge to the sub-surface. Appropriate functions for the flux, R, must have certain characteristics. For recharge areas, the head, h, is below ground surface and so the recharge must be equal to the full recharge, R_p. R_p = 150 mm/year was used /Johansson 2008/. In discharge areas, the water table is just above ground surface, which can be achieved by taking a suitably large flux out of the model, i.e. a negative value of R, whenever the head goes above ground surface. The standard function used in CONNECTFLOW is:

$$R = \begin{cases} R_p & h \le z - \varepsilon \\ -R_p\,(h - z)/\varepsilon & h > z - \varepsilon \end{cases}, \qquad (3\text{-}5)$$

where ε is a small distance (2cm was used). This function implies that if the water table is more than ε below the topographic surface then recharge equals the full potential groundwater recharge. Above that, the recharge reduces until the water table is at the surface. If the water table is above the topographic surface, then recharge becomes negative, i.e. discharge, and an appropriate flux of groundwater is taken from the model to reduce the head until the water table is restored to the topographic height. Hence, this boundary condition is a non-linear equation (the flux depends on the free-variable head) that ensures a specified flux if the water table is low and a specified head where the water table is at or above ground surface. The topographic surface is not constant in time due to post-glacial rebound and marine transgressions, and hence $z = z(t)$ as given in Figure 3-31.

With the elevation changing in time the shore level changes, the above definition of the boundary conditions is used, but all groundwater levels and elevations are calculated relative to a sea-level datum that evolves in time. CONNECTFLOW uses residual pressure, P^R, as the independent flow variable which is related to total pressure, P^T, by

$$P^R = P^T + \rho_0 g (z - z_0) \tag{3-6}$$

where ρ_0 is the density of freshwater, g is acceleration due to gravity, and $(z - z_0)$ is the elevation of a point in the model relative to a datum. Hydraulic head scales with residual pressure as

$$h = P^R / \rho_0 g \tag{3-7}$$

In a similar way, the boundary conditions for solute transport have to account for evolution in the shore-level and in the mixture of different reference waters at the top surface. Two types of boundary condition are used: a time varying specified value hydrochemical boundary condition is used where there is an advective flow into the model (recharge area); or an outflow condition (flux type) where there is flow out (discharge). Because the flows are transient, the areas of recharge and discharge evolve in time, and hence it is important to have an automatic way of determining the recharge and discharge areas. The difficulty in achieving this is that it requires mixing a specified flux boundary condition on outflow and a specified concentration boundary condition on inflow; and since the recharge/discharge areas change in time, the type of boundary condition has to be changed in time. Our solution is to specify a flux of solute through the top surface that changes depending on the direction of flow across the surface. Where an inflow of groundwater at a specified input concentration is required, solute flux is equated to a penalty weight function based on the difference between solute concentration in the model and the required input concentration. Therefore, the flux of solute out of the model, F_c, is then given by the equation:

$$F_C = \begin{cases} (\boldsymbol{q} \cdot \boldsymbol{n})\, C & \boldsymbol{q} \cdot \boldsymbol{n} \geq 0 \\ (C - C_0)/\delta & \boldsymbol{q} \cdot \boldsymbol{n} < 0 \end{cases} \tag{3-8}$$

where $(\boldsymbol{q} \cdot \boldsymbol{n})$ is the magnitude of the advective flux of water out of the model, i.e. the groundwater flux, $\boldsymbol{q}$, in the direction parallel to the outward normal to the surface, $\boldsymbol{n}$, C is the solute concentration or mixing fraction, and δ is a small value (an inverse flow-rate, 10^{-4} s/m is used). For $(\boldsymbol{q} \cdot \boldsymbol{n}) \geq 0$, the flux corresponds to an outflow condition. For $(\boldsymbol{q} \cdot \boldsymbol{n}) < 0$, a specified value condition, $C = C_0$, is implemented as a penalty function such that solute is removed if $C > C_0$, and injected if $C < C_0$. This effectively ensures that $C \approx C_0$.

The mixture of reference waters at the top surface was calculated from the following rules:

- Below the shore level, $z < z_0(t)$,
  - Before 4500 BC, the water is a mixture of *Littorina Sea Water* and *Holocene Glacial Melt Water* according to the salinity given by Figure 3-32.
  - Else, the water is a mixture of *Littorina Sea Water* and *Present-day Meteoric Water* according to the salinity given by Figure 3-32.
- Above the shore level, $z < z_0(t)$, the water is *Present-day Meteoric Water*.

The hydrochemical boundary condition on the vertical sides of the model domain is assumed to be zero flux of solutes. On the base of the model at 1,200 m depth, the mixture of reference waters is held fixed (i.e. equal to the initial condition) since it is expected that groundwater is mostly *Deep Saline Water* subject to very little advective flow below this elevation.

3.7 Model calibration – outcome of Tasks B, C and D

The data presented above in section 3.4 through section 3.6 were use to define initial properties of the so called *stage 2.2 base model simulation*. Here, the term *base model simulation* implies a deterministic model of the HCD and HSD properties, and a single realisation of the HRD properties. The lessons learned during the calibration against the three tasks described in section 2.1.2 (Task B–D) are described in detail in /Follin et al. 2007c/. In the following, a summary of the calibrations process is shown.

It should be recalled that a primary idea of the term *confirmatory testing* in the SDM is that roughly the same groundwater flow and solute transport model can be used for each type of simulation to make it transparent that a single implementation of the conceptual model could be calibrated against all three types of field observations, although it may have been possible to improve the modelling of a particular data type by refining the model around a relevant observation borehole, for example.

3.7.1 Task B – Matching the interference test at HFM14 (2006)

The performance of the initial settings was assessed by comparing the measured and modelled drawdowns in each monitoring interval ordered according to their 3D distances from the abstraction borehole (HFM14), and by plotting the vertical distribution of drawdowns at appropriately selected times in boreholes where there are multiple monitoring intervals.

HFM14 intersects the high transmissivity gently dipping zone A2, so that the distribution of drawdowns against distance for monitoring points within about 500 m of HFM14 is dominated by the transmissivity of this zone. Further away, greater than about 600 m, the drawdown apparently depends on other structures such as steeply dipping deformation zones, sheet joints features and the boundary conditions that control recharge through the HSD. Hence, the drawdown versus distance plot is vital for guiding the properties and connections of the major hydraulic features and the hydraulic connection to the surface. Plots of drawdown profiles along the lengths of boreholes also help define the contrasts in hydraulic properties between HCD, the surrounding HRD, and HSD at the surface.

The key steps made in order to achieve an acceptable match to the HFM14 hydraulic interference test (*stage 2.2 base model simulation*) were:

- A low specific storage coefficient around 10^{-8} m^{-1} for the bedrock and 10^{-3} m^{-1} for the soil was required to obtain the rapid responses seen in monitoring intervals even those a kilometre or more from the HFM14.
- The transmissivity of A2 had to be increased to give $T = 2.8\ 10^{-4}$ m^2/s in the upper 100 m to give the correct drawdown of about 12 m in HFM14 and boreholes close to the abstraction.
- The hydraulic thicknesses of deformation zones A2, ENE0060, ENE0401 and A8 were reduced to 5 m. This made for a more discrete system with responses propagating rapidly along a smaller hydraulic volume associated with a few key deformation zones.
- The hydraulic conductivity of the hydraulic soil domains had to be reduced to decrease the recharge from the top surface.
- A reduction of the vertical hydraulic conductivity of the HRD to reproduce the very discrete propagation of the drawdown along deformation zones especially to deep intervals and to reduce the recharge to depth from ground surface via the background rock.

The level of match to the interference test that was achievable is demonstrated by Figure 3-33 and Figure 3-34. Figure 3-35 shows a comparison between measured and modelled drawdown away from the pumping plotted in a semi-logarithmic plot with distance from the pumping well on the logarithmic axis. A simple analytical model is applied to facilitate the evaluation of predictability.

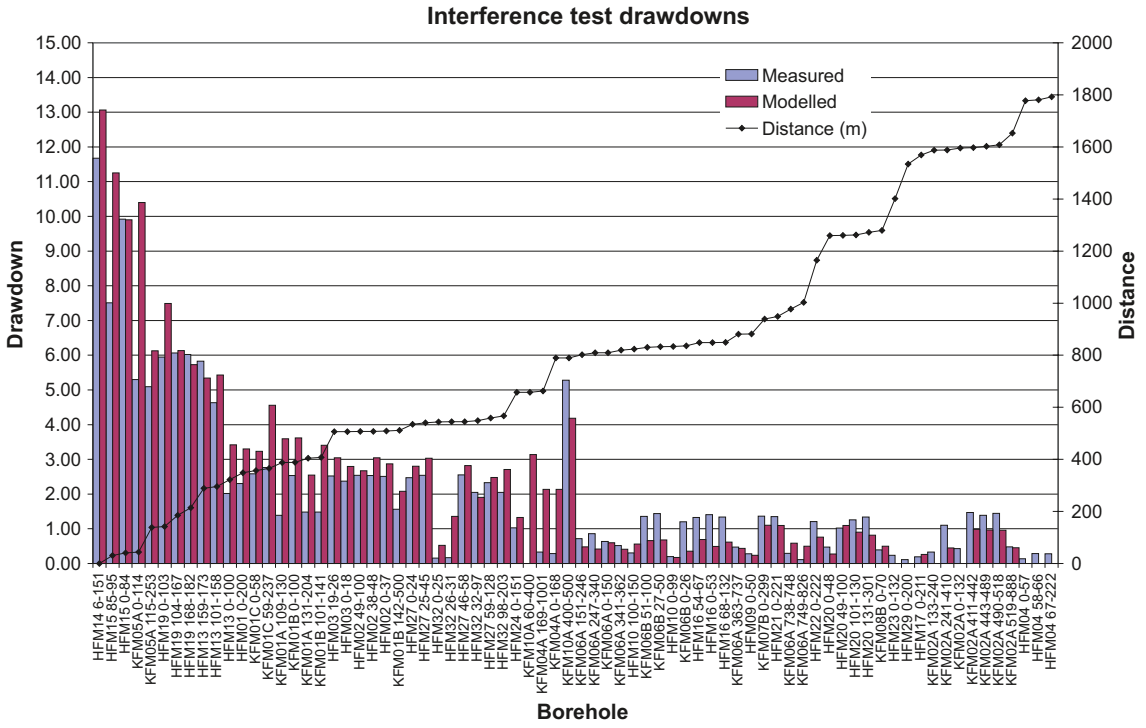

Figure 3-33. *Comparison of measured (blue) and modelled (red) drawdown at the end of pumping (21 days) for all monitored borehole intervals for the stage 2.2 base model simulation. The borehole intervals are ordered according to the three-dimensional distance (the right axis) of the monitoring intervals to the abstraction borehole HFM14. Reproduced from /Follin et al. 2007c/.*

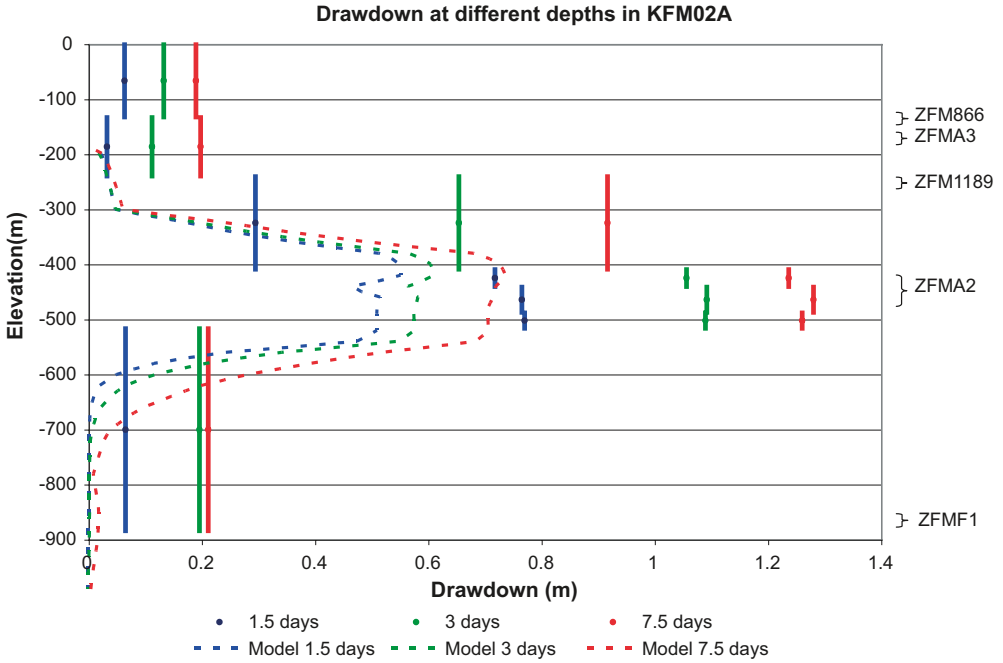

Figure 3-34. *Comparison of measured drawdown (solid) and simulated (dashed) using the stage 2.2 base model simulation at 3 different times for the KFM02A monitoring hole. For the data, a vertical line shows the extent of the monitoring section with the drawdown representing an average within the interval, while the simulated spatial variation in drawdown in the borehole is shown for the model. Reproduced from /Follin et al. 2007c/.*

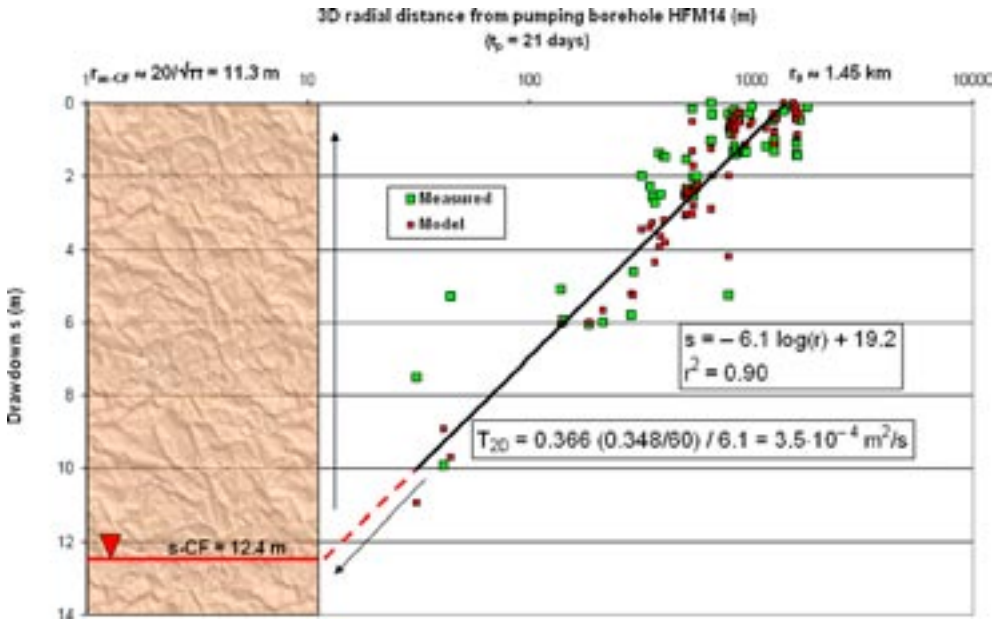

Figure 3-35. *Plot of measured drawdowns (green) and simulated (red) at the end of the 21-day log interference test in HFM14. The measured drawdown in HFM14 was 11.7 m and the simulated 12.4 m using the stage 2.2. base model simulation. The black line shows least-squares fit to the simulated drawdowns. The value of the correlation coefficient (r^2 = 0.90) indicates a less heterogeneous medium than does the regression of the measured data in the real system, cf. Figure 3-18. A 2D steady-state, radial flow approximation using the slope of the least-squares fit for an estimate of Δs (difference in drawdown per log cycle of distance) renders a large-scale equivalent transmissivity of $3.5 \cdot 10^{-4}$ m^2/s. This value is essentially a composite of the transmissivities assigned to zone A2, the sheet joints, and a bit of zone ENE0060. An extrapolation of the regression model to the edge of the pumped 20 m element matches the simulated drawdown in this cell, ($r_{w\text{-}CF} = 20/\sqrt{\pi} \approx 11.3$ m). Reproduced from /Follin et al. 2007c/.*

A short sensitivity study was performed as part of the numerical modelling mainly to illustrate why the above calibration steps were made. The sensitivity cases simulated included:

- HCD properties based on /Follin et al. 2007b/ without any calibration of zone A2, or changes to hydraulic thickness of A2, ENE0060 and ENE0401,
- increased transmissivity in zone ENE0401A,
- increased transmissivity in zone ENE0060A,
- removing the hydraulic cage features from HCD,
- more permeable Quaternary deposits beneath the lakes,
- more permeable Quaternary deposits in soil layers Z1 and Z5,
- more isotropic hydraulic fracturing based on the base model hydrogeological DFN fracture orientations defined in /Follin et al. 2007b/, and
- reduced vertical hydraulic conductivity in the HRD.

3.7.2 Task C – Matching the near-surface natural groundwater levels

The matching against the natural groundwater levels after matching against the interference test in HFM14 is shown in Figure 3-36 (upper bedrock , HFM boreholes) and in Figure 3-37 (Quaternary deposits, SFM boreholes). Lines indicating the elevation of the topographic surface and the elevation of the soil/bedrock contact are shown for reference. The boreholes are ordered by bedrock elevation.

The *stage 2.2 base model simulation* predicts a distribution of groundwater levels in reasonable agreement with the distribution in the data, i.e. groundwater levels are generally flat, and where they are more elevated or near to ground surface, this is reproduced. The groundwater level in the Quaternary deposits is higher than in the bedrock for almost all boreholes and is generally closer to topography, which suggests groundwater recharge is the prevalent situation for most of the candidate area. However, this case derived mainly from the interference test tends to over-predict the mean heads by nearly 1.6 m for the HFM boreholes and 1.4 m for the SFM boreholes. These discrepancies should be viewed relative to the size of the seasonal variations in the measurements, which is on the same order of magnitude, 1.26 m for HFM boreholes and 1.62 m for SFM boreholes, see Figure 3-38, and so some improvements should be sought.

The sensitivity cases from the interference test were considered together with a few additional cases to try to achieve a match to both types of data, see Table 3-15. The results show that increases in hydraulic conductivity of the HSD properties have the strongest control on the results. For one of the cases studied, the original errors were reduced by 37% to 1.0 m for the HFM boreholes and by 50% to 0.7 m for the SFM boreholes. This seeming contradiction prompted for an improved representation of the HSD properties in stage 2.3.

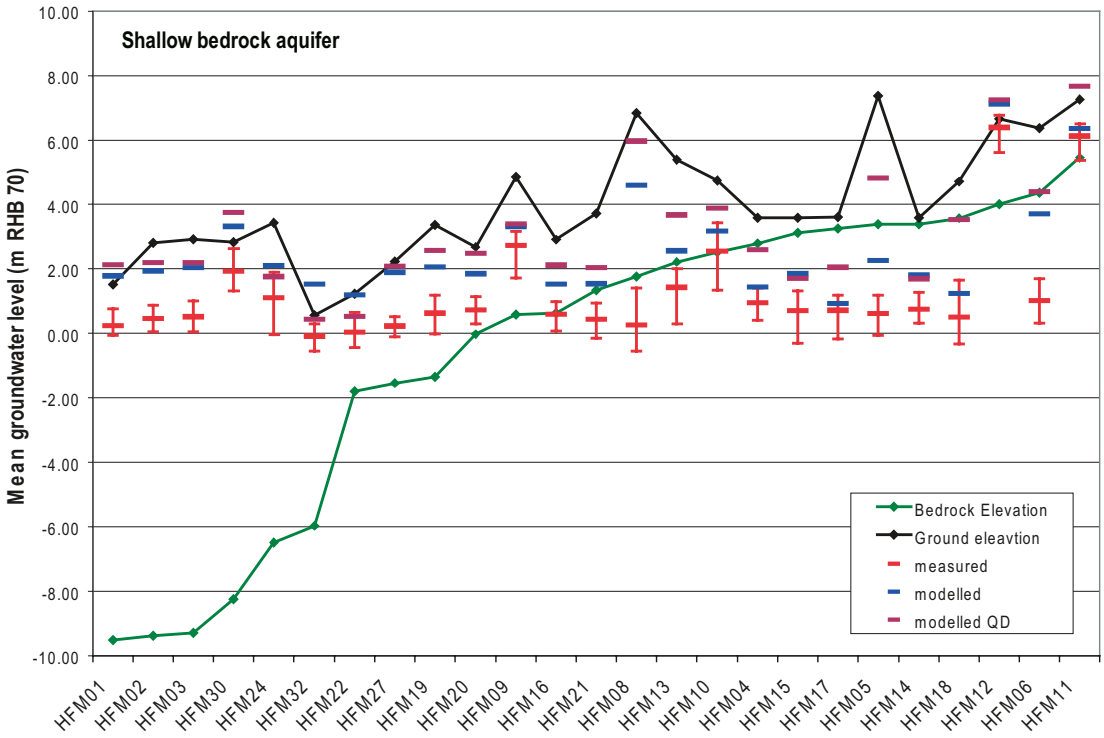

Figure 3-36. *Comparison of measured heads in HFM boreholes with the stage 2.2 base model simulation. For the model, values are given for the Quaternary deposits and as an average over the borehole section in the bedrock. The field data are plotted as mean groundwater levels in the bedrock with error bars to show the range of values over time. Reproduced from /Follin et al. 2007c/.*

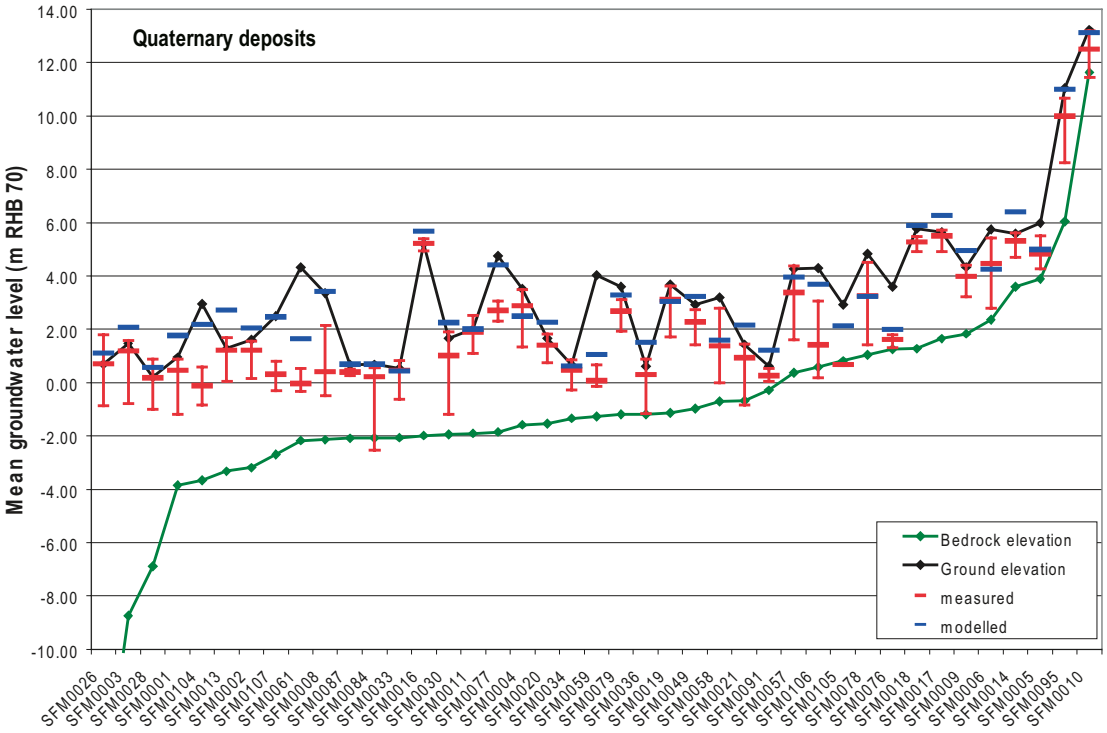

Figure 3-37. *Comparison of measured heads in SFM boreholes with the stage 2.2 base model simulation. For the model, values are given for the Quaternary deposits only. The field data are plotted as mean groundwater levels in the bedrock with error bars to show the range of values over time. Reproduced from /Follin et al. 2007c/.*

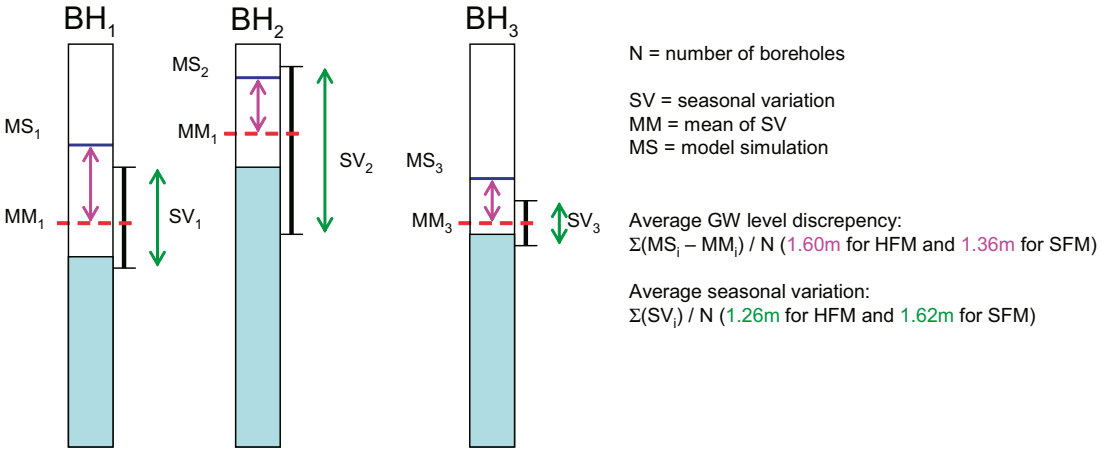

Figure 3-38. *Definition of average groundwater level discrepancy and average seasonal variation. In Figure 3-36 and Figure 3-37, the modelled groundwater level exceeds the topographic height at some locations. This highlights the issue of grid resolution. Depending on undulations in ground surface less than grid resolution, there are inevitably going to be discrepancies in the modelled groundwater levels in proportion to the magnitude of these local scale undulations.*

Table 3-15. Measures of the average differences between modelled groundwater level and mean measured groundwater level for HFM and SFM boreholes. The average variation in groundwater level between different times for the measurements is 1.26 m for HFM boreholes, and 1.62 m for SFM boreholes. T = transmissivity, K = hydraulic conductivity. Reproduced from /Follin et al. 2007c/.

Case	Mean difference in GW level for the HFM boreholes (m)	Mean difference in GW level for the SFM boreholes (m)
Average seasonal variation	*1.26*	*1.62*
Stage 2.2 base model simulation	*1.60*	*1.36*
Higher T in ENE0060	1.55	1.35
Higher T in ENE0401	1.59	1.36
Higher T in A8	1.63	1.36
No sheet joint	1.62	1.36
Higher K in Z1 and Z5	1.03	0.66
Higher K_h in Z1 and Z5	1.09	0.73
Higher K in Z1 and Z5 where topography > 2 m	1.26	0.86
Higher K for lake sediments	1.51	1.33
Version 1.2 DFN settings	1.75	1.37
No reduction in HRD K_v in top 400 m	1.76	1.37
10 times lower HRD K in top 400 m	1.69	1.35
100 times lower HRD K in top 400 m	1.67	1.35

3.7.3 Task D – Matching hydrochemical data in deep boreholes

An example of the hydrochemical matching for the *stage 2.2 base model simulation* is shown in Figure 3-39 for a few of the boreholes in the candidate area. Of the four chemical signatures used, Cl is used as an indicator of saline groundwater, Br/Cl is used to indicate the position of transition of the origin of this salinity from *Deep Saline Water* at depth to *Littorina Sea Water* above, $\delta^{18}O$ is used to indicate any remaining pockets of *Holocene Glacial Melt Water*, and HCO_3 indicates the penetration of *Present-day Meteoric Water*.

The steps taken in matching against hydrochemical profiles in deep boreholes followed many common themes with the calibration on hydraulic and hydrological data described above in sections 3.7.1 and 3.7.2 such as the importance of the deformation zones, the fracture orientations in the HRD and a reduction in the vertical hydraulic conductivity of HRD. However, other factors effecting solute transport had also to be considered, mainly the kinematic porosity, the flow wetted fracture surface area per unit volume of rock and the initial distribution of groundwater chemistry. These factors did not affect the calibration against the interference test in HFM14 (Task B) and the natural groundwater levels (Task C).

The steps taken in matching against hydrochemical profiles in deep boreholes followed many common themes with the hydraulic data like using the alternative DFN fracture orientations in the HRD and a reduction in the vertical hydraulic conductivity of the HRD. Factors specific to Task D were:

- to modify the initial hydrochemical conditions including different conditions for the fracture water and pore water,
- to increase the kinematic porosity by a factor of about 10, and
- to use low values of the flow wetted fracture surface area per unit volume of rock suggested by the PFL-f data.

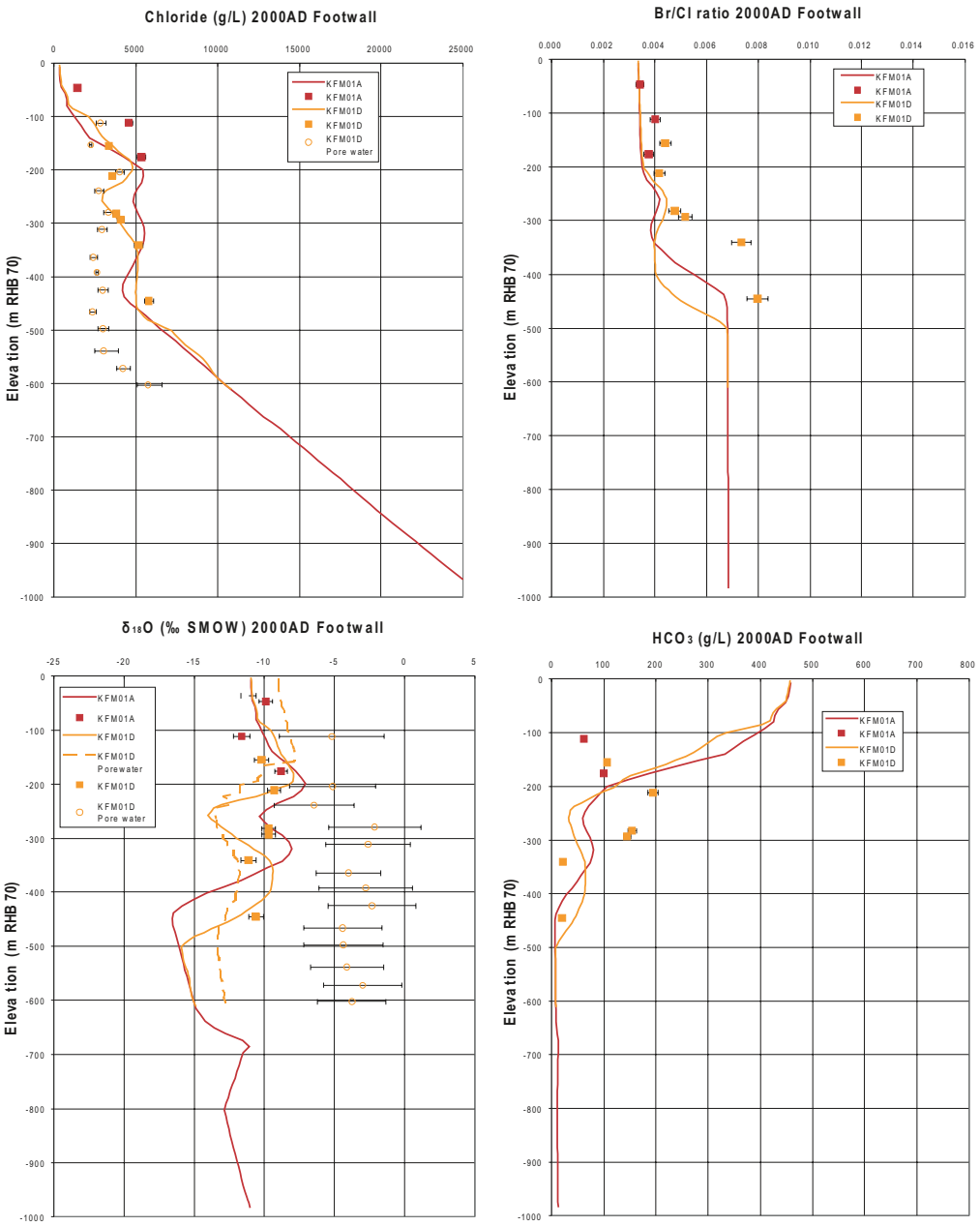

Figure 3-39. *Comparison of measured and modelled values of Cl, Br/Cl, $\delta^{18}O$ and HCO_3 in the fracture system for boreholes KFM01A and KFM01D using the stage 2.2 base model simulation. Both boreholes are located in the footwall of zone A2. Square symbols are used for the representative and less representative data. The error bars on the data only indicate the laboratory analytical error. The solid lines show the complete distribution in the borehole simulated in the fracture system, and the dashed lines show the specified compositions of reference waters. Modified after /Follin et al. 2007c/.*

The variations in predictions between boreholes within the candidate volume gives an estimate of the spatial variability, but since the *stage 2.2 base model simulation* is a single realisation it does not give an indication of the uncertainty in the predictions at an individual borehole. (This is quantified in the present work, see chapter 6.) Overall, the predictions of the *stage 2.2 base model simulation* are consistent with the various hydrochemical data considered. There are some boreholes with salinity occurring above 100 m depth that are not predicted by the model and the interface between *Littorina Sea Water* and *Deep Saline Water* also appears higher up. Hence, some improvements should be sought stage 2.3.

The sensitivities cases considered in stage 2.2 were again based on demonstrating the reasons for the steps taken in the calibration included:

- HCD properties based on /Follin et al. 2007b/ without any calibration of zone A2, or changes to hydraulic thickness of A2, ENE0060 and ENE0401,
- lower kinematic porosity,
- a uniform flow wetted fracture surface area per unit volume of rock of 0.17 m^2/m^3,
- four reference waters instead of five (excluding *Old Meteoric-Glacial Waters*), and
- using the same initial conditions for the fracture and matrix waters.

3.8 Conclusions

In the process of calibrating the numerical model to single-hole hydraulic tests, cross-hole tests, natural point-water head measurements and hydrochemistry samples, a number of lessons were learnt in terms of the key features, processes and parameters required to mimic the observed behaviour of the hydrogeological system. Sensitivities to various features and parameters had to be considered to find one or more ways to honour the field data. This prompted relatively few changes to the initial implementation of the conceptual model within the reasonable ranges of uncertainty on parameters. Among the lessons learnt in stage 2.2 we note in particular:

- *HCD model:* The description of the hydraulic properties and the depth dependency of deformation zones developed in the conceptual model appear to give simulation results consistent with the hydraulic and hydrochemistry measurements, although it is important to condition individual zones where data is available to the single-hole test data. It should be noted that the numerical modelling conducted in stage 2.2 did not honour the observed lateral heterogeneity in transmissivity. Further, deformation zones without hydraulic measurements were assumed to have different hydraulic properties depending on their orientation. The basis for this hypothesis is the large-scale anisotropy observed in the transmissivity data, at least in the upper c. 500 m of bedrock.
- *HRD model:* Using the Hydro-DFN fracture set orientation model derived from data freeze 2.2 rather than the model derived based on data freeze 1.2, improved the calibration of the flow and solute transport model, primarily by defining fractures in the sub-horizontal set to be more sub-parallel, which reduced the vertical connectivity and hence increased the hydraulic anisotropy. Further mechanisms for hydraulic anisotropy such as a lower transmissivity in the sub-vertical sets may also make the simulations correspond better to the observations, although this hypothesis was not tested here. It should be noted that fracture FFM04–FFM06 were not well covered by the field measurements carried out in stage 2.2. The numerical modelling conducted in stage 2.2 assumed that FFM04 and FFM05 have the same structural-hydraulic properties as fracture domain FFM03 and that FFM06 mimics FFM01.
- *HSD model:* The hydraulic properties of the simplistic HSD model used to represent the complex geometry and stratification of the regolith model suggested for stage 2.2 required considerable calibrations of the hydraulic properties to find consistency with the hydraulic interference test and point-water head measurements. The introduction of anisotropy (lower vertical hydraulic conductivity) in the Quaternary deposits being the key step. Further

mechanisms for anisotropy such as a lower transmissivity in the sub-vertical sets near the bedrock surface may also make the simulations correspond better to the observations, although this hypothesis was not tested here.

- *Solute transport model:* Changes to the initial ECPM bedrock transport parameters were necessary for the solute transport modelling of salt including (i) increasing the kinematic porosity about one order of magnitude from the initial empirical relationship used to relate fracture transport aperture to transmissivity, and (ii) increasing the flow wetted fracture surface area per unit volume of rock compared to the frequency of water bearing fractures measured by the PFL-f technique.
- *Initial conditions:* The Alternative Case hydrochemical initial condition suggested in stage 2.2 assumes a persistence of an interglacial groundwater composition over the Holocene. This hypothesis gave better predictions for both fracture and pore water samples than the Base Case hydrochemical initial condition used in model version 1.2. Such a model requires further consideration since it has implications for the description of the long term stability of hydrochemical conditions over glacial cycles.
- *Boundary conditions:* The simulations imply poor hydraulic contacts between the surface and upper bedrock within the target area, which raise questions about the locations of possible discharge areas. The importance of the local topography within the target area is likely to be less important due the hydraulic anisotropy in the uppermost c. 150 m of the bedrock, and hence hydraulic gradients in major deformation zones need to be considered as well as their contact to the sea.

In conclusion, the implementation of the hydrogeological conceptual model in a numerical model has been used to demonstrate its consistency with a wide range of field observations, and hence build confidence in its applicability to the Forsmark area. The calibration process has helped narrow uncertainties on some parameters and helped our understanding of the character of the hydrogeological system in the Forsmark area. It is emphasised that the results obtained from model stage 2.2 represent single realisations. Uncertainties relating to spatial variability in the geometrical and/or hydraulic properties will be quantified in model stage 2.3, e.g. sensitivity studies to spatial heterogeneity with deformation zones, and multiple Hydro-DFN realisations.

A vital characteristic of the Forsmark area is the hydrogeological conditions in the uppermost part of the bedrock. Besides outcropping deformation zones and a high frequency of single fractures in the near-surface rock masses between the zones, the percussion drilling and hydraulic testing have also identified a system of large, transmissive sub-horizontal fractures, which are interpreted to be sheet joints formed through stress release. Sheet joints commonly have their highest intensities near the bedrock surface and decrease rapidly with depth. Being related to the present surface, the sheet joints are recently-formed, especially compared with the ductile and brittle deformation zones and the discrete fracture networks in between the deformation zones.

Together, the three types of geological features (outcropping deformation zones, a high frequency of rock mass fractures and large, large sub-horizontal sheet joints) form a dense network of structures. Hydraulic diffusivity data from interference tests indicate that this network is highly connected laterally, if heterogeneously, and locally very transmissive. The network is presumably confined to within 150 m of the surface and largely parallels the undulations of the topography (horizontal anisotropy). It is noteworthy that the groundwater levels in the regolith (mainly Quaternary deposits) are found to be higher than the groundwater levels in the uppermost part of the bedrock below the regolith.

Hydraulic data suggest that the transmissive network of structures in the uppermost part of the bedrock may have a finite lateral extent. In the work reported here it is given the form of a triangle bounded to the northeast by the Singö deformation zone, (WNW0001), to the southeast by the NE0062A deformation zone, and to the west by the expression of the sheath fold structure in rock domains 32 and 44. This hypothesis will be tested hydraulically in model stage 2.3 by means of an interference test conducted at percussion-drilled borehole HFM33 located on the SFR peninsula.

The significant hydraulic diffusivity and horizontal anisotropy of the uppermost part of the bedrock reduce the hydraulic gradients across the deeper bedrock flow system in the target area below c. 150 m depth. In a way, the near-surface flow system acts like a "hydraulic cage phenomenon", though unlike a true hydraulic cage, the shallow network of transmissive structures only covers one side of the deeper bedrock flow system. It does not eliminate the hydraulic gradients entirely. Hence, a more appropriate hydrogeological analogue of the hydraulic phenomenon observed in the uppermost part of the bedrock is a shallow, anisotropic, bedrock "aquifer" on top of thicker segment of bedrock with "aquitard" type properties.

Since the sheet joints are not mapped to a very large detail in the site investigations, they are difficult to implement with a high degree of certainty due to uncertainties in their spatial extent and hydraulic heterogeneity. However, the chosen numerical approach to model the sheet joints in terms of three deterministic, hydraulically heterogeneous features, along with the interpreted deformation zones, communicates hydraulic disturbances across large distances in the numerical model that by and large are consistent with the field observations observed in the upper parts of the bedrock. In conclusion, the modelled extent and hydraulic properties of the shallow bedrock aquifer shortens the recharge from above and captures the discharge from below within the target area. The simulations carried out in stage 2.2 support the notion suggested in version 1.2 that the recharge area of the deeper flow system in the target area largely coincides with the topographic heights located in between the candidate area and the Forsmark deformation zone. The crest of these heights forms a regional water divide that clearly affects the runoff pattern of northern Uppland.

4 Verification of hypotheses

4.1 Three hypotheses in stage 2.2

Three of the hypotheses handled in stage 2.2 concerns:

I. The structural-hydraulic properties of deformation zones.

II. The structural-hydraulic properties of fracture domain FFM06.

III. The spatial extent of the shallow bedrock aquifer.

Hypothesis I: Figure 3-14 shows that, at each elevation, the gently dipping deformation zones that occur predominantly in the hanging wall bedrock of zones A2 and F1 are the most transmissive. The steeply dipping deformation zones that strike WNW and NW was hypothesised in stage 2.2 to come in second place as far as transmissivity is concerned. The steeply dipping deformation zones that strike ENE and NNE occur in the footwall bedrock mainly. These zones can occasionally also be fairly transmissive, but a main characteristic, as it appears from Figure 3-14, is that they are on the average the least transmissive but at the same time significantly more heterogeneous laterally than the other categories of deformation zones. The validity of this hypothesis may be constrained to the upper 400–500 m of bedrock, however.

The hypothesis was tested in stage 2.3 by means of single-hole hydraulic tests in the new boreholes the new boreholes KF08D, KFM11A, KFM12A, HFM34, HFM36 and HFM37 (see Appendix A, Figure A-1 and Figure A-2). These boreholes, except for KFM08D, intersect the regionally significant, ductile and brittle Singö and Forsmark deformation zones that border the tectonic lens and the candidate area. In contrast, KFM08D intersect a series of zones inside the target area that strike NNE-ENE.

Hypothesis II: Fracture domain FFM06 is one of three fracture domains within the so-called target area, the other being FFM01 and FFM02 (see section 3.2.3, Figure 3-9 and Figure 3-10). Due to lack of boreholes and hydraulic data in FFM06, it was hypothesised in stage 2.2 that this fracture domain has the same hydrogeological (structural-hydraulic) properties as inferred from the tests run in fracture domain FFM01. This hypothesis was tested in stage 2.3 by means of single-hole hydraulic tests in the new borehole KFM08D, see Figure 4-1 and Appendix A.

Based on the structural-hydraulic information gathered in neighbouring boreholes, a prediction of the number of PFL-f flow anomalies and their cumulative transmissivity value of each geological segment was made prior to the single-hole testing in KFM08D /SKB 2006b/. The predicted average hydraulic properties in KFM08D are shown in Table 4-1. In summary, the prediction forecasts in total a minimum of 31 flowing fractures in KFM08D, with a rapidly decreasing number with depth in the fracture domains, but not in the deformation zones. For fracture domains FFM01 and FFM06, a total of 23 flowing fractures were predicted with a maximum value of about 10^{-5} m^2/s and a minimum of about 10^{-9} m^2/s. 22 of the 23 flowing fractures were associated with FFM01. 14 of which were predicted to occur in the uppermost c. 170 m of the borehole. For the deformation a minimum of 8 flow anomalies were predicted with a maximum value of about 10^{-5} m^2/s and a minimum of about 10^{-9} m^2/s.

Hypothesis III: It was assumed in stage 2.2 that the sheet joints encountered in the target area follow the undulations of the bedrock surface, implying that some of them do not outcrop but stay below the bedrock surface as this dips under the Baltic Sea. The horizontal extent of the sheet joint was assumed to form a triangle bounded to the northeast by the Singö deformation zone, (WNW0001), to the southeast by the NE0062A deformation zone, and to the west by the expression of the sheath fold structure in rock domains 32 and 44. This hypothesis was tested hydraulically in stage 2.3 by means of an interference test conducted at the new percussion-drilled borehole HFM33 drilled on the peninsula close to the SFR buildings (see Appendix A, Figure A-1 and Figure A-2).

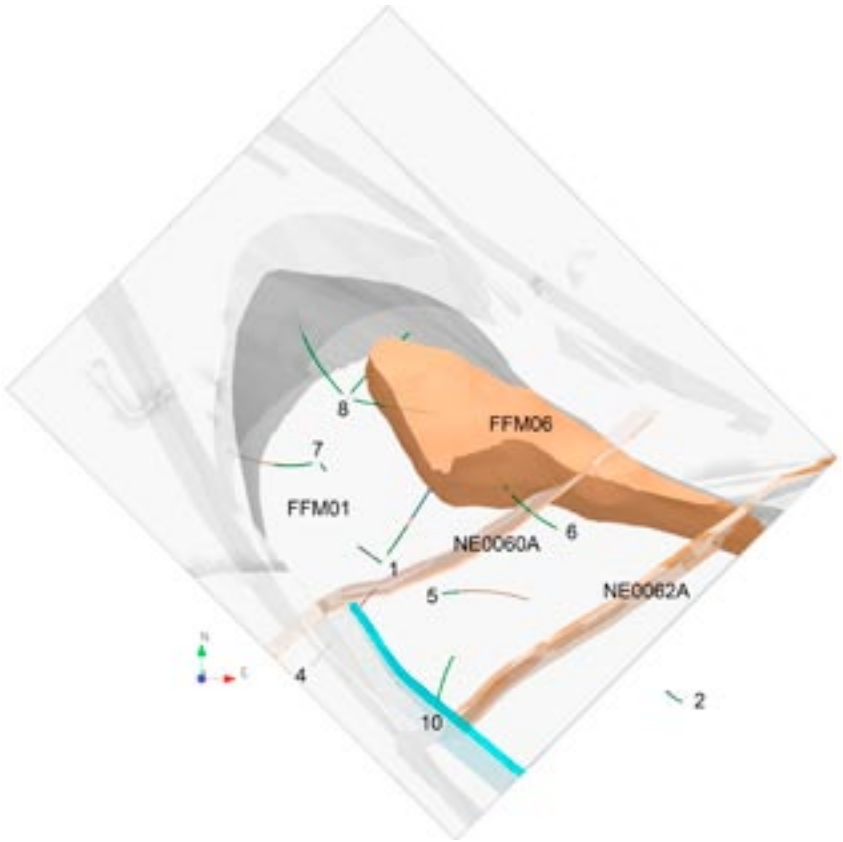

Figure 4-1. *A close-up view in X-ray mode of the cored boreholes drilled into the target area below c. 200 m depth. The boreholes shown are all hydraulically investigated with the PFL-f method. The labels represent drill site numbers (see Appendix A, Figure A-1 and Figure A-2), fracture domains and deformation zones. Here, fracture domain FFM01 is made transparent, whereas FFM06 has a brownish colour. NE0060A and -62A are two of the larger deformation zones with ENE strike that intersect the target volume. Data from borehole KFM08D was not available for modelling until stage 2.3.*

Table 4-1. Compilation of the structural-hydraulic predictions along the trajectory of KFM08D using the PFL-f method. The geological columns show rock domain (RFM), deformation zone (ZFM), fracture domain (FFM), borehole length [m] (Secup/Seclow) and elevation [m RHB 70] (Depthup/Depthlow). The hydraulic columns show the number of PFL-f data in each geological segment and the total transmissivity of the segments. Reproduced from /SKB 2006b/.

RFM	ZFM	FFM	Secup	Seclow	Depthup	Depthlow	No. PFL-f	Σ T PFL-f
29		FFM01	–	208	–	–168	14	1E–5
29	ENE2120		208	234	–168	–189	> 1	1E–5
29		FFM01	234	319	–189	–259	6	2E–8
29	ENE0159A		319	359	–259	–292	> 1	3E–8
29		FFM01	359	386	–292	–314	2	2E–8
29	ENE0159B		386	404	–314	–328	> 1	3E–8
45		FFM06	404	441	–327	–358	1	1.4E–9
45	NNE2309		441	456	–358	–371	> 1	3E–8
45		FFM06	456	617	–371	–503	0	Nil
45	NNE2308		617	639	–503	–521	> 1	1E–8
45		FFM06	639	685	–521	–559	0	Nil
45	NNE2320		685	760	–559	–620	> 1	3E–9
45	NNE2293		738	761	–602	–621	> 1	3E–8
45		FFM06	761	919	–621	–750	0	Nil
45	WNW2225		919	942+	–750	–782+	> 1	1E–9

4.2 Structural-hydraulic properties of deformation zones

The transmissivity data acquired from the investigations carried out i KFM08D, KFM11A, KFM12A, HFM34, HFM36 and HFM37 /Gustavsson et al. 2006, Harrström et al. 2007ab, Walger et al. 2007, Väisäsvaara and Pekkanen 2007/ were added to the transmissivity plot shown in Figure 3-14, see Figure 4-2.

- There are five transmissive, steeply dipping deformation zones in KFM08D, four of which having an ENE strike and one having a NNE strike.
- KFM11A and HFM34 penetrate the regional Singö deformation zone, which has strike WNW (WNW0001). The Singö deformation zones is fairly thick from a geological view point and very heterogeneous from a hydraulic viewpoint /Axelsson et al. 2002/.
- KFM12A, HFM36 and HFM37 are drilled into the regional Forsmark zone, which also strikes WNW strike (WNW0004). This zone is sub-parallel with the Singö deformation zone.

4.3 Structural-hydraulic properties of fracture domain FFM06

KFM08D was drilled with a slightly different orientation, but the differences are considered unimportant for the comparison made here. KFM08D intersects nine steeply dipping deformation zones, five of which strike ENE and four that strike NNE, see Figure 4-3.

The results from the single-hole testing in KFM08D is shown in Figure 4-4. There are in total 34 flowing fractures, with a rapidly decreasing with depth in the fracture domains, but not in the deformation zones. For fracture domains FFM01 and FFM06, a total of 17 flowing fractures were predicted with a maximum value of about 10^{-5} m^2/s and a minimum of about 10^{-9} m^2/s. All flowing fractures were associated with FFM01. and occurred in the uppermost c. 120 m of the borehole. 17 flowing fractures were associated with a maximum value of about $2 \cdot 10^{-7}$ m^2/s and a minimum of about 10^{-9} m^2/s. These numbers compare well with the predicted, see section 4.1 and Table 4-1.

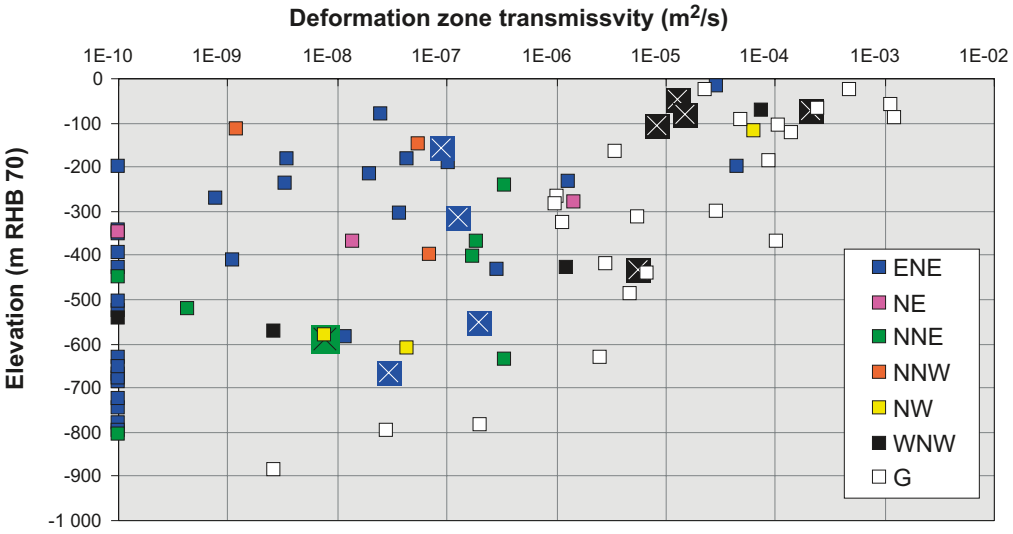

Figure 4-2. *Reproduction of the transmissivity plot shown in Figure 3-14. The new transmissivity data acquired from the investigations carried out i KFM08D, KFM11A, KFM12A, HFM34, HFM36 and HFM37 are added and denoted by* ☒.

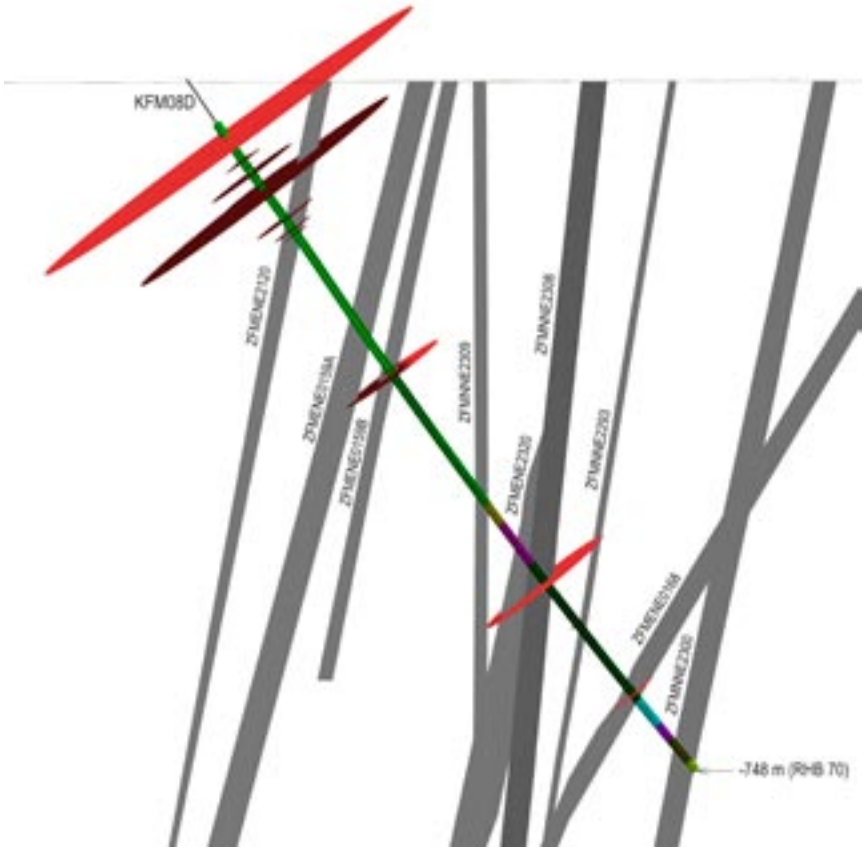

Figure 4-3. *Perspective view towards NNE showing the trajectory of KFM08A, its intersections with deterministically modelled deformation zones and the positions of the 34 PFL-f transmissivities observed (shown as circular discs). The PFL-f measurements did not cover the entire length of the borehole due to problems with drilling debris at the bottom. The measurement with the largest disc radius has a transmissivity of about $1.3 \cdot 10^{-5}$ m^2/s. The orientation of the discs are perpendicular to the borehole, hence do not reflect the orientations of the flowing fractures.*

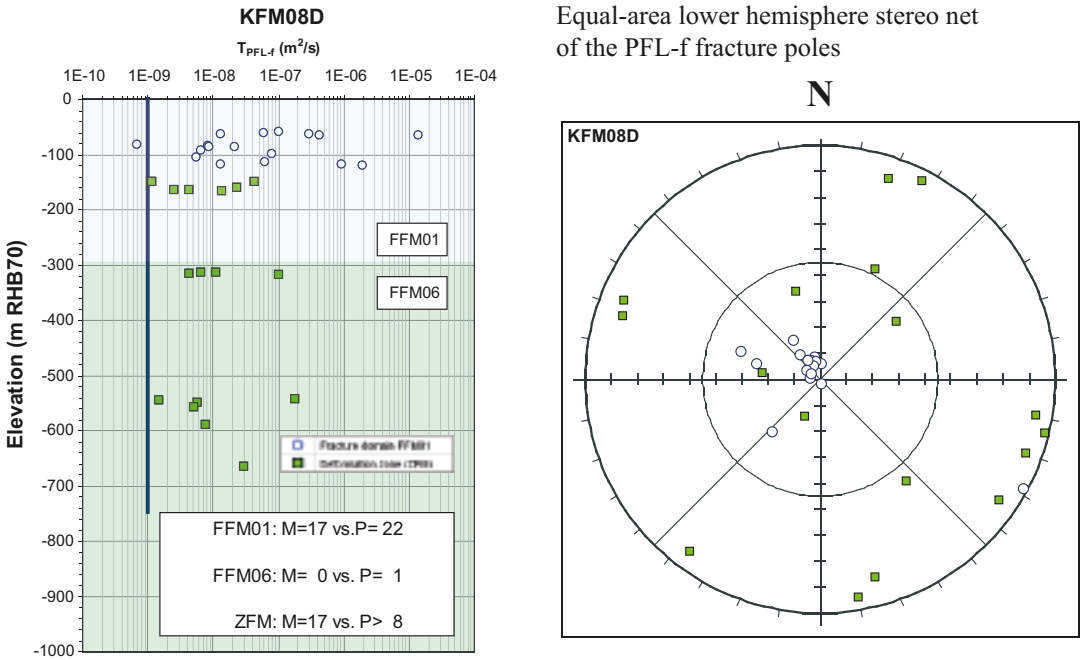

Figure 4-4. *Hydrogeological data in borehole KFM08D. There are 17 PFL-f transmissivities associated with single fractures and 17 associated with five deterministically modelled deformation zones (ZFM). The dark blue line indicates the elevation interval investigated. Fracture domain FFM06 (greenish area) begins at about –292 m RHB 70. M = measured number and P = predicted number of flowing fractures. The prediction is shown in Table 4-1.*

4.4 Spatial extent of the shallow bedrock aquifer

HFM33 is situated north of the candidate area close to drill site 11 on the peninsula where the SFR buildings are located (see Appendix A, Figure A1 and Figure A-2). The borehole is about 140 m long and inclined c. 59°. The single-hole hydraulic test conducted in May 2006 shows that the borehole is fairly dry except for a major water conducting horizontal fracture close to the bottom at c. 100 m depth. The interpreted fracture transmissivity is high, c. $5 \cdot 10^{-4}$ m^2/s /Gustavsson et al. 2006/. The natural groundwater level in HFM33 is c. –0.3 m RHB 70.

The pumping flow rate during the two-week long interference test conducted in HFM33 in November 2007 was on the average c. 232 L/min and resulted in a final drawdown in the pumping borehole of about 16 m /Gokall-Norman and Ludvigson 2007b/. These values indicate a specific capacity (~ transmissivity) of about $2 \cdot 10^{-4}$ m^2/s. Figure 4-5 shows a plan view of the monitoring network used during this test. In total, 148 observation sections in 40 observation boreholes were included. 22 of the 40 boreholes are core-drilled and have 103 sections included in the interference test. 18 boreholes are percussion-drilled with a total of 45 sections. Many monitoring sections were disturbed by sea level changes, tidal effects and precipitation but fairly clear test responses were observed in 62 monitoring sections in the candidate area. This means that the drawdown in the fracture at c. 100 m depth propagated below the Baltic Sea. The greatest distance of influence was about 2 km.

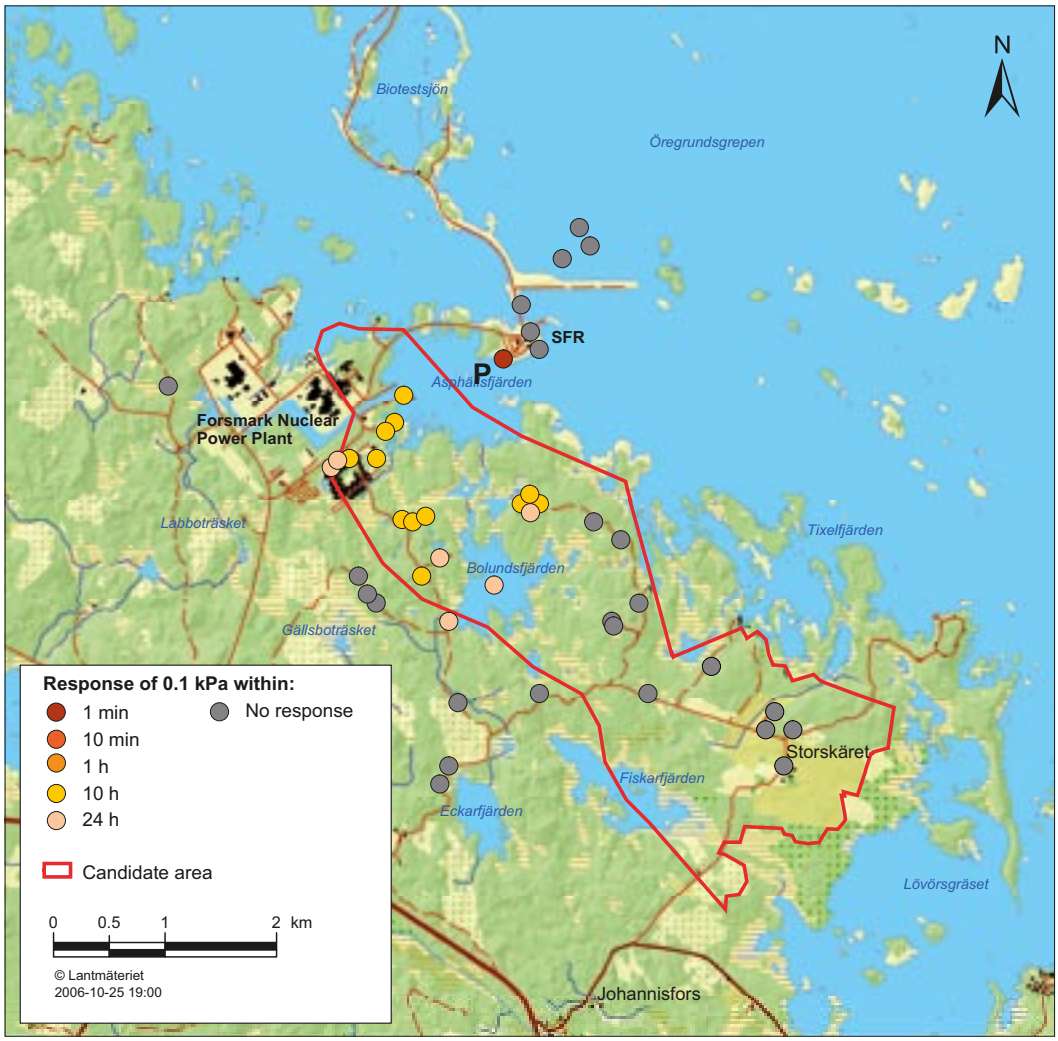

Figure 4-5. *Map showing response times in the bedrock to the two-week long interference conducted in HFM33 (P) during the fall of 2007. Many monitoring sections/boreholes were disturbed by sea level changes, tidal effects and precipitation but fairly clear test responses were observed in 62 out of a total of 148 monitoring sections. The radius of influence was about 2.2 km.*

4.5 Discussion and conclusions

4.5.1 Structural-hydraulic properties of deformation zones

The investigations carried out i KFM08D, KFM11A, KFM12A, HFM34, HFM36 and HFM37 constitutes a fairly small and shallow data set. However, since none of the new transmissivity values falsifies Hypothesis I, it cannot be rejected by this particular data set.

Transmissivity versus stress

The recommended in situ stress gradients versus depth at Forsmark is given in the work by /Glamheden et al. 2007/, see Table 4-2.

Table 4-2. Recommended horizontal and vertical stress magnitudes for the Forsmark target area, where the depth below surface is d in metres. A depth of 0 is approximately equal to an elevation of 0. Reproduced from /Glamheden et al. 2007/.

Depth (m)	Maximum horizontal stress σ_{1H} (MPa)	Trend (deg)	Minimum horizontal Stress σ_{2h} (MPa)	Trend (deg)	Vertical stress σ_{3v} (MPa)
0–150	19+0.008d ± 20%	145 ± 20	11+0.006d ± 25%	055	0.0265d ± 2%
150–400	9.1+0.074d ± 15%	145 ± 15	6.8+0.034d ± 25%	055	0.0265d ± 2%
400–600	29.5+0.023d ± 15%	145 ± 15	9.2+0.028d ± 20%	055	0.0265d ± 2%

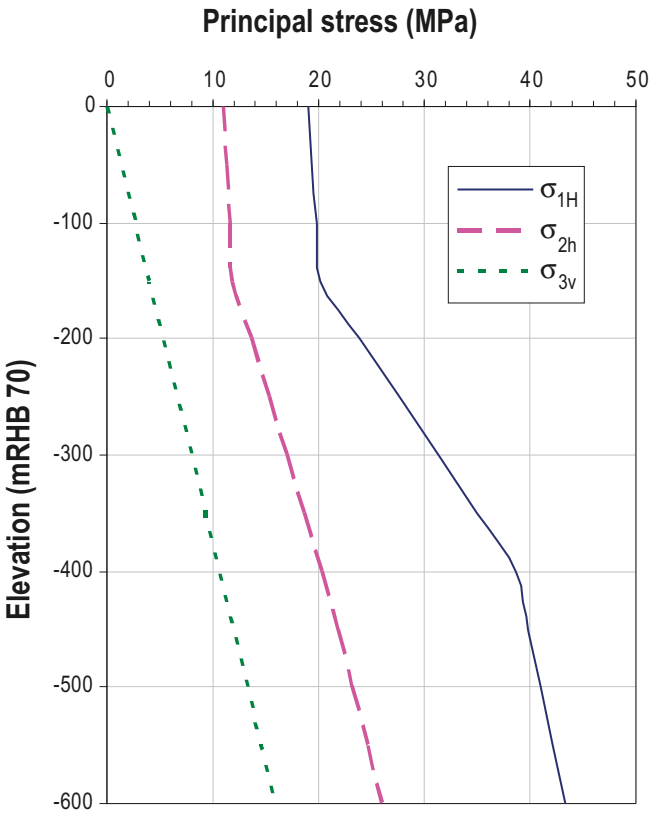

Figure 4-6. *Plot of the in situ stress gradients versus depth at Forsmark as given in the work by /Glamheden et al. 2007/. All principal stresses increase with depth.*

Table 4-2 implies that the very transmissive gently dipping deformation zones are at a high angle to the minimum principal stress (σ_{3v}) and at a low angle to the azimuths of both the first (σ_{1H}) and second principal stresses (σ_{2h}). This observation is supported by investigations carried at 200–250 m depth in the Juktan tunnel /Olsson 1979/.

Further, the deformation zones that strike WNW-NW are at low angle to the azimuth of σ_{1H}, whereas the opposite condition prevails for the deformation zones that strike NNE-ENE. The observation made in Figure 4-2 that the former set of zones are often more transmissive than the latter set, is supported by the underground observations carried out at 450 m depth in the Äspö HRL prototype repository /Rhén and Forsmark 2001/.

Laboratory tests have been used to establish relationships between flow (or transmissivity, T) along a discrete fracture and the normal stress (σ_n) applied to the fracture. As shown by /Raven and Gale 1985/ these relationships can be expressed as:

$$T = T_0 \sigma_n^{\alpha} \qquad (4\text{-}1)$$

where T_0 is the transmissivity at a normal stress of 1 MPa and α equals the slope of the relationship between log(T) versus log(σ_n). Equation (1-1) illustrates that in laboratory samples, the transmissivity decreases significantly as the confining stress increases, and according to /Indraratna et al. 1999/, when the confining stress exceeds 10 MPa, little or no decrease in transmissivity occurs, irrespective of the type of permeating fluid, air or water.

While this hypothesis is widely accepted and validated on laboratory samples, it is unknown if such relationships exist in situ or if these relationships can be scaled from the centimetre scale laboratory tests to the metre-scale of in situ fractures. /Martin and Follin 2008/ made an attempt to assess the relationship shown in Equation (4-1) for the PFL-f transmissivity data reported in the work by /Follin et al. 2007b/ and the stress state acting on the data using the in situ stress gradients given in the work by /Glamheden et al. 2007/, see Table 4-2.

/Martin and Follin 2008/ divided the PFL-f transmissivity database into the following categories:

1. All PFL-f data within the candidate area (ALL-PFL).
2. PFL-f data associated with fracture domains FFM01, FFM02, and FFM06 (FFM-PFL).
3. PFL-f data associated with the deterministically modelled deformation zones shown in Figure 3-14 (ZFM-PFL).

A systematic analysis of these data sets was carried out to explore possible relationships between the measured transmissivity values and the *normal stress* acting on the hydraulic feature. The main findings from these analyses are:

- No relationship was found between transmissivity and normal stress for the steeply dipping fractures/zones. The normal stress ranged from 10 to 40 MPa. /Indraratna et al. 1999/ noted that when the confining stress on laboratory samples exceeds 10 MPa, little or no decrease in transmissivity occurs.
- There is some evidence that the transmissivity of the gently dipping fractures/zones decreases with depth. However, because both the frequency of *open* gently dipping fractures/zones decreases with depth and the normal stress is also increasing with depth, it is not possible to sort out cause and effect for these gently dipping features.
- Comparison of the value of α for the empirical equation that links stress and transmissivity shows that shows that there is no agreement between the in situ values for α (–0.04 to –0.28) and the laboratory value (–1 to –2.145).

There does not appear to be sufficient evidence from these analyses to support the notion that the magnitude of the flow (transmissivity) along the fractures at Forsmark is solely controlled by the normal stress acting on the fracture/zone. This should not be surprising, because the majority of the fractures formed more than 1 billion years ago and the current stress state has only been active for the past 12 million years /Stephens et al. 2007/. This implies that

transmissivity versus *normal stress* relations cannot be explored on a site descriptive basis, hence the SDM needs to rely on measured data on fracture transmissivity. It is more likely that the fracture transmissivity values are controlled by fracture roughness, open channels within the fractures and fracture infilling material. The effect of mineral infilling may need to be explored further.

Figure 4-7 shows the comparison of the values of α for the three categories of data treated compared with the laboratory value. The values for T_0 have been normalised so that all the initial values for T_0 are 1. Figure 4-7 shows a significant difference between the stress-flow relationship established from the laboratory behaviour of a single joint, and the Forsmark in situ data.

4.5.2 Structural-hydraulic properties of fracture domain FFM06

The number of PFL-f data measured in KFM08D are in good agreement with the predictions, see Table 4-1 and Figure 4-4. This means that data from this new borehole do not falsify Hypothesis II. Thus, it cannot be rejected that FFM06 may have similar structural-hydraulic properties as FFM01.

4.5.3 Spatial extent of the shallow bedrock aquifer

The data from the interference test conducted in HFM33 do not falsify Hypothesis III. Thus, it cannot be rejected that the horizontal fractures/sheet joints observed in the target area follow the bedrock undulations below the Baltic Sea and connect to the Singö deformation zone.

The data acquired from the large-scale interference test performed during the summer of 2007 in HFM14 (~ 12 weeks) /Gokall-Norman and Ludvigson 2007a/ corroborate this conclusion. That is, while pumping in HFM14 hydraulic responses were observed in HFM33 and vice versa.

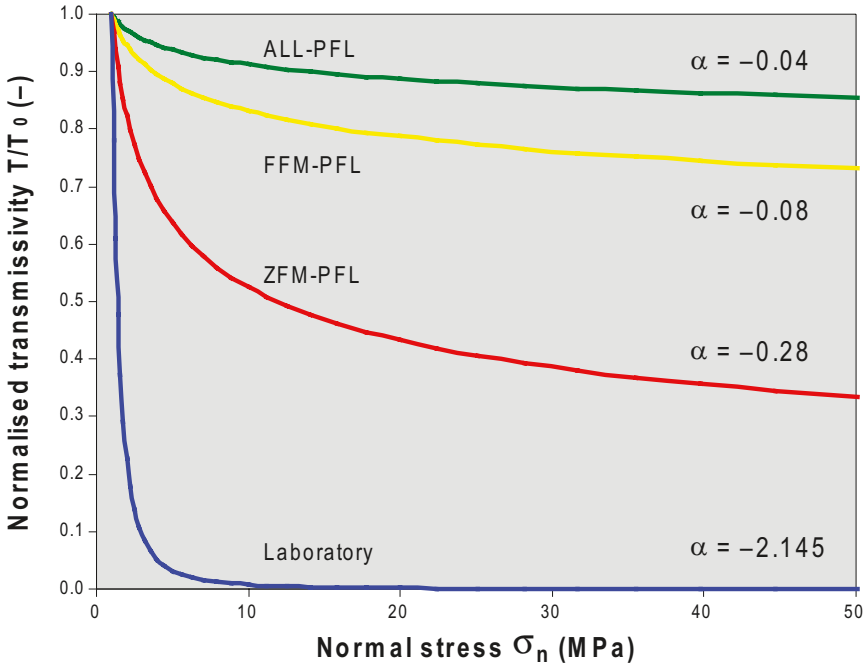

Figure 4-7. *Comparison of the trend lines used to establish a fit for Equation (4-1) to the three categories of PFL-f data analysed by /Martin and Follin 2008/.*

Pumping in the SFR repository

It should be noted that no responses were observed in the nearby boreholes on the other side of this zone, i.e. in KFM11A, HFM34 and HFM35, and no responses were observed in the SFR repository, while pumping in HFM33. This suggests that the particular horizontal fracture/sheet joint observed in HFM33 does not cut through this zone but "terminates" close to HFM33.
It should also be noted that the pumping of drainage water in the SFR repository (300–360 L/min) clearly affects the groundwater levels in a number of boreholes around the repository including HFM34 and HFM35 at drill site 11. For instance, the drawdown in deformation zone (ZFM)871 (or H2) located below the silo in the SFR repository (see Figure 3-5) is c. 24 m and the drawdown in HFM34 and HFM35 are c. 3–5 m /personal comm. with Jakob Levén, 2008/. Figure 4-8 shows the location of the boreholes with regard to the Singö deformation zone and the SFR repository. The bottom of the silo is at c 14 m depth.

Most of the hydraulic responses shown in Figure 4-5 represent boreholes in the shallow bedrock aquifer, i.e. the network of structures in the upper most c. 150 m of bedrock. Figure 4-9 shows the responses at repository depth from the two large-scale interference tests discussed above.

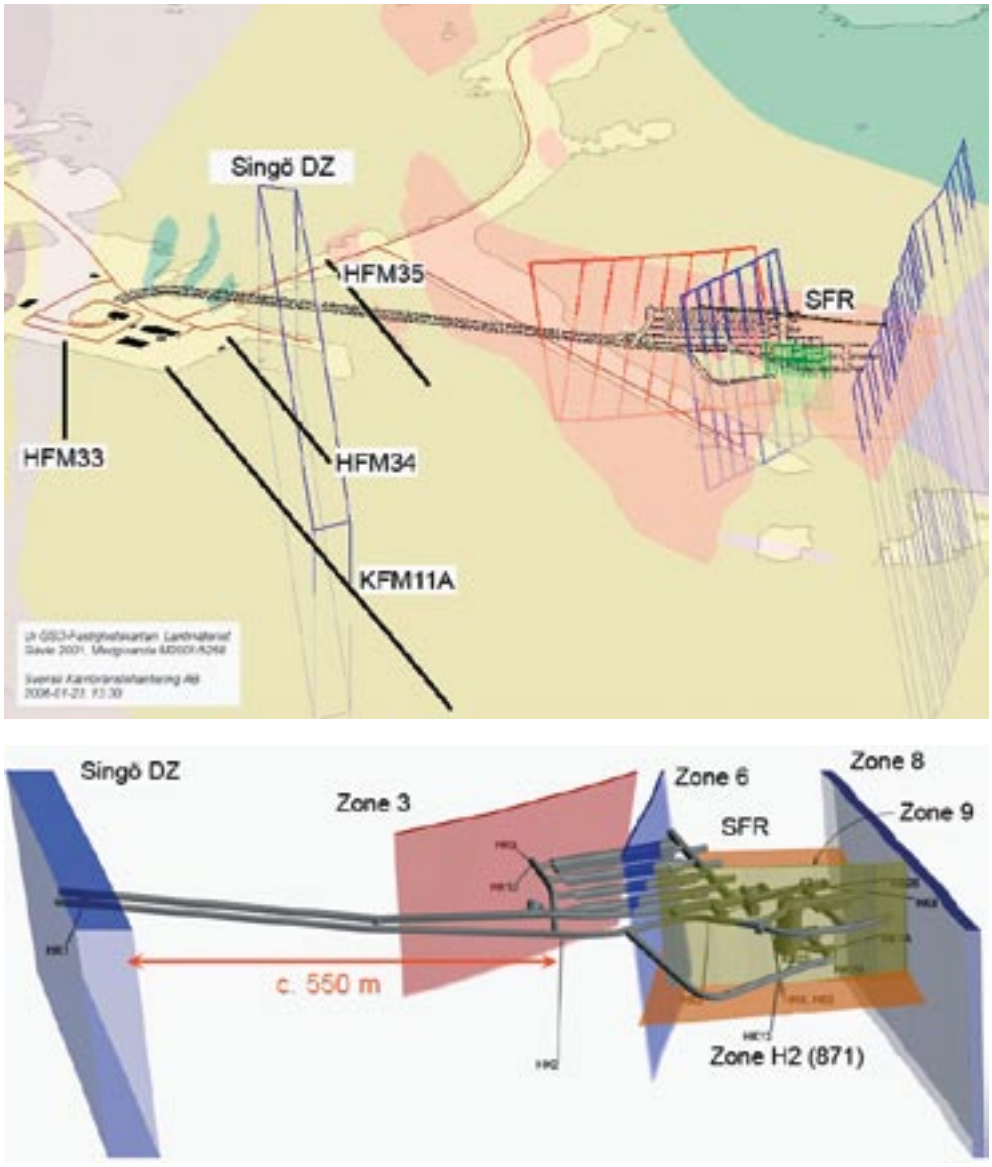

Figure 4-8. *Two views towards WNW showing the Singö deformation zone, the SFR repository and the boreholes close to the zone (top) and the repository (below).*

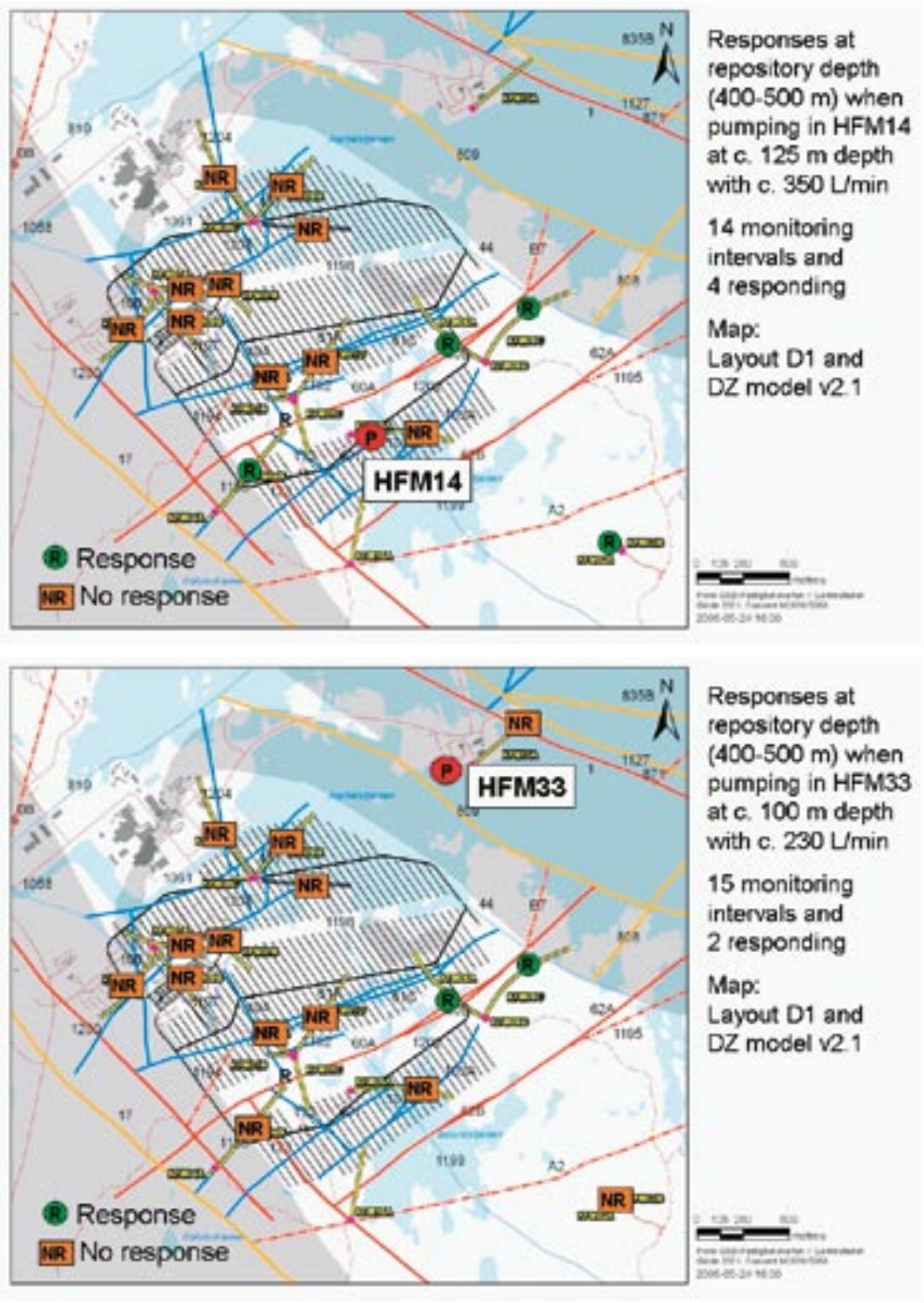

Figure 4-9. *Overview of hydraulic responses observed between 400 and 500 m depth during the twelve-week long pumping in HFM14 during the summer of 2007 (top) and during the two-week long pumping in HFM33 during November 2007 (bottom). Provided by /Jakob Levén 2008/.*

5 Stage 2.3 base model simulation

5.1 General

A comprehensive set of uncertainties have been quantified in stage 2.3 to each of the model elements: HCD, HRD and HSD as well as boundary conditions both in terms of their effects on the model calibration processes and in predictions of discharge areas for groundwater flow through the repository candidate volume. The importance of the handled uncertainties to model calibration and particle tracking is quantified as part of the uncertainty analysis presented in chapter 6.

It is noted that two changes were made to the CONNECTFLOW code in stage 2.3. These serve to: 1) improve the representation of the hydraulic properties of the regolith (HSD), and 2) improve the conditioning of transmissivity of the deformation zones (HCD) against single-hole hydraulic tests. The changes to the modelling of the HSD were made to improve the consistency with models made with the MIKE SHE code, which involved the introduction of spatial variability of the hydraulic properties within soil layers and horizontal versus vertical anisotropy in the hydraulic conductivity of soils. The changes to the HCD were in the methodology used to condition the HCD properties on single-hole hydraulic tests. It was necessary to modify this methodology so that conditioned stochastic realisations of spatial variability within each deformation zone could be generated in an automated way, rather than the manual conditioning process of stage 2.2.

Finally, as a reference point for the multiple realisations run in stage 2.3, as well as for a comparison to the *stage 2.2 base model simulation* described in chapter 4, a stage 2.3 *base model simulation* was defined based on a deterministic model of the HCD and HSD properties, and a single realisation of the HRD properties. As in stage 2.2, the HRD properties were based on upscaling of a particular realisation of the underling hydrogeological DFN model of the fracture domains. The derivation of the *stage 2.3 base model simulation* is presented in this chapter together with its calibration against Tasks B–D.

5.2 Changes to the stage 2.2 model set-up

5.2.1 Changes to the representation of hydraulic soil domains

The implementation of the HSD model was modified in three main respects:

- Lateral heterogeneity in the hydraulic properties was incorporated in Layers L1, Z1 and Z5 according to maps of soil type provided for each of these layers.
- Hydraulic properties were provided by /Bosson et al. 2008/ as two alternative HSD models, one ‘initial model’ and one ‘calibrated model’. The ‘initial model’ is shown in Table 5-1. It is slightly different than the model used in stage 2.2 (cf. Table 3-8). The properties of the ‘calibrated model’ is shown in Table 5-2. This model was deduced based on the modelling of diurnal groundwater level variations in the Quaternary deposits and bedrock with the MIKE SHE code.
- The sensitivity to horizontal versus vertical anisotropy was considered.

Table 5-1. Hydraulic conductivity specified by /Bosson et al. 2008/ for the *initial HSD model*. The figures in red colour denote changes made with regard to the model used in the *stage 2.2 base model simulation* (cf. Table 3-8).

Layer	*K* [m/s] of layers with several types of Quaternary deposits					
	Fine till	Coarse till	Gyttja	Clay	Sand	Peat
L1	–	–	$3{\cdot}10^{-7}$	–	–	$1{\cdot}10^{-6}$
Z1	$3{\cdot}10^{-5}$	$3{\cdot}10^{-5}$	–	$1{\cdot}10^{-6}$	$1.5{\cdot}10^{-4}$	$1{\cdot}10^{-6}$
Z5	$1 \cdot 10^{-7}$	$1.5 \cdot 10^{-6}$	–	–	–	–
Layer	***K* [m/s] of layers with one type of Quaternary deposits**					
L2	$1.5{\cdot}10^{-4}$					
L3	$1.5{\cdot}10^{-8}$					
Z2	$3{\cdot}10^{-7}$					
Z3	$1.5{\cdot}10^{-4}$					
Z4	$1.5{\cdot}10^{-8}$					

Table 5-2. Horizontal hydraulic conductivity specified by /Bosson et al. 2008/ for the *calibrated HSD model*. † $K_v = K_h/10$; K_h increased by an extra factor of 2 in Eckarfjärden catchment area. The figures in red colour denote changes made with regard to the 'initial HCD model' shown in Table 5-1.

Layer	*K* [m/s] of layers with several types of Quaternary deposits					
	Fine till	Coarse till	Gyttja	Clay	Sand	Peat
L1	–	–	$3{\cdot}10^{-7}$	–	–	$1{\cdot}10^{-6}$
Z1†	$1.5{\cdot}10^{-4}$	$1.5{\cdot}10^{-4}$	–	$5{\cdot}10^{-6}$	$7.5{\cdot}10^{-4}$	$5{\cdot}10^{-6}$
Z5†	$5{\cdot}10^{-7}$	$7.5{\cdot}10^{-6}$	–	–	–	–
Layer	***K* [m/s] of layers with one type of Quaternary deposits**					
L2	$1.5{\cdot}10^{-4}$					
L3	$1.5{\cdot}10^{-8}$					
Z2	$3{\cdot}10^{-7}$					
Z3	$1.5{\cdot}10^{-4}$					
Z4	$1.5{\cdot}10^{-8}$					

The same vertical soil layering (L1-L3 and Z1-Z5) and layer thicknesses were used as in stage 2.2. In layers L1, Z1 and Z5 the hydraulic properties varied according to an index provided for each layer:

- In L1, the soil types were either Gyttja or Peat whose distribution are shown in Figure 5-1.
- Layer Z1 is separated into soil types Fine Till, Coarse Till, Clay, Sand and Peat. The same hydraulic properties are specified for both types of Till, as is the case for Peat and Clay. Therefore, the soil types are grouped together according to their hydraulic properties in the illustration showed in Figure 5-2.
- Z5 is split into two soil types, Fine Till and Coarse Till.

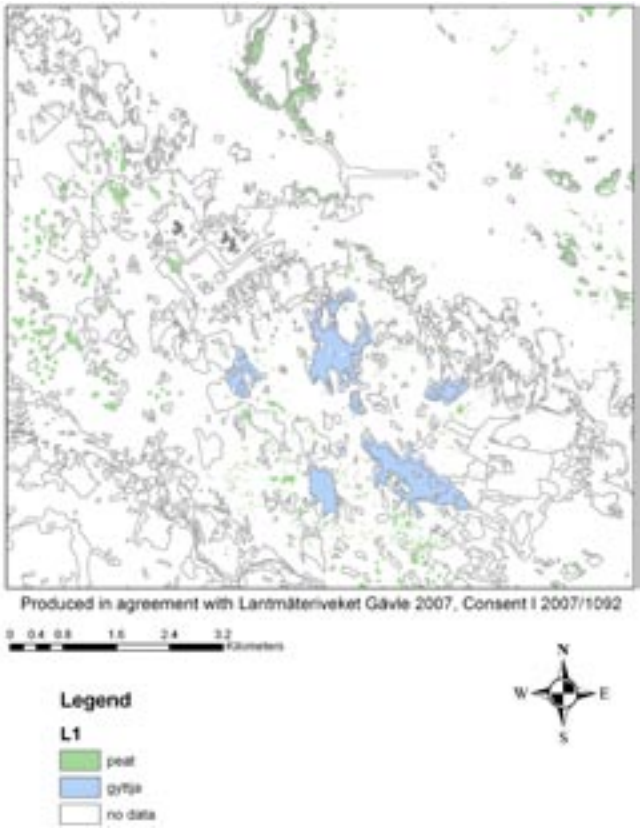

Figure 5-1. *Distribution of soil types defined within the L1 layer. The grey lines show the outline of surface water bodies.*

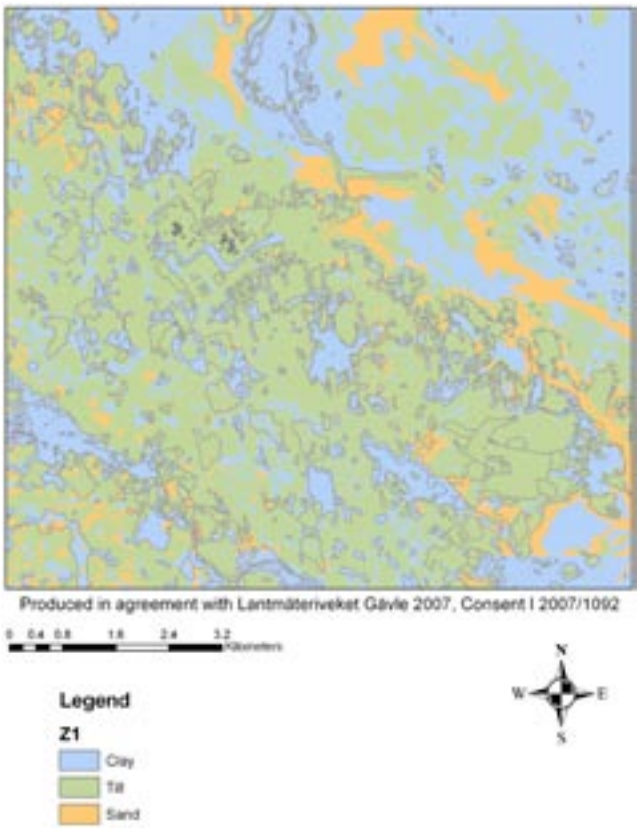

Figure 5-2. *Distribution of soil types defined within the Z1 layer. The grey lines show the outline of surface water bodies.*

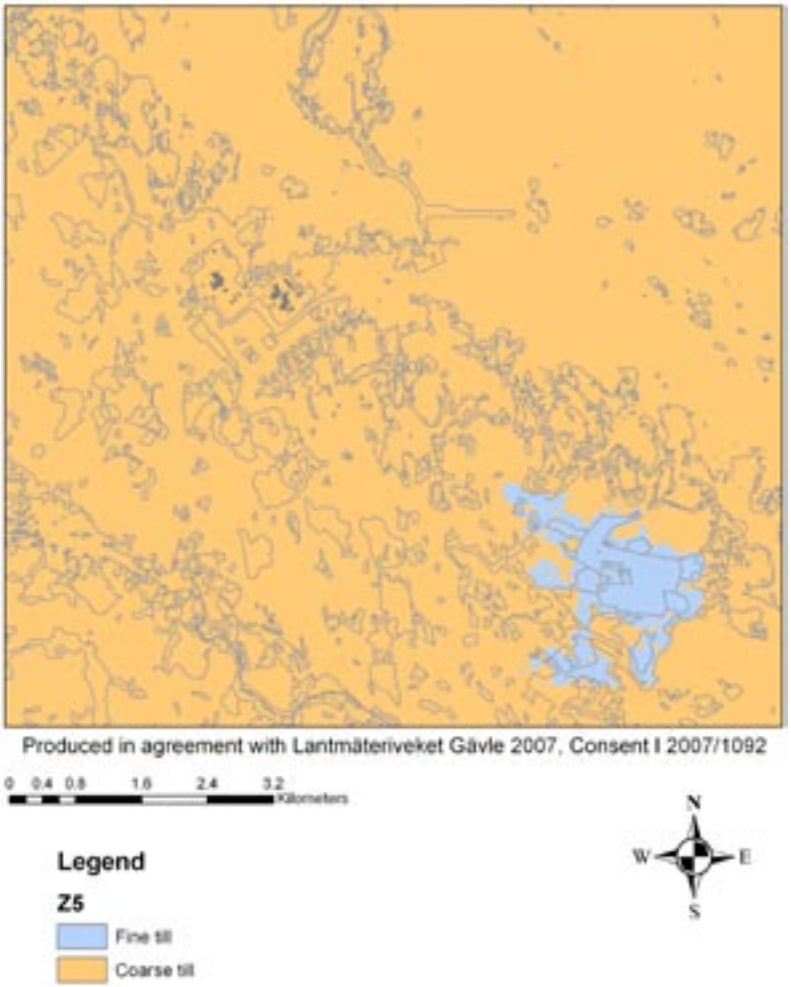

Figure 5-3. *Distribution of soil types defined within the Z5 layer. The grey lines show the outline of surface water bodies.*

The hydraulic properties described in Table 5-1 and Table 5-2 were used as a starting point for the hydrogeological calibration on the HFM14 interference test (Task B), natural groundwater levels (Task C) and hydrochemistry (Task C). In order to quantify the uncertainty associated with HSD each model, the above two models along with variants on K_h versus K_v anisotropy shown in Table 5-2 were considered.

Simulations of the spatial distribution of annual averaged groundwater levels in the Quaternary deposits and bedrock (Task C) confirmed the properties specified for the 'calibrated HSD model' given in Table 5-2 gave the best approximation to the groundwater levels, and both models gave a significant improvement on the match compared to the *stage 2.2 base model simulation*.

The calibration on the HFM14 interference test (Task B) motivated an increase in the anisotropy of the Quaternary deposits, i.e. a decrease in vertical hydraulic conductivity. A ratio of K_h:K_v of 100:1 was used in the most part. For consistency with the work of /Bosson et al. 2008/, it was decided to use the 'calibrated HSD model' properties (but with 100:1 anisotropy) in the *stage 2.3 base model simulation*, but then consider the 'initial HSD model' properties in the sensitivity cases described in chapter 7 along with different levels of anisotropy. The full set of HSD hydraulic conductivities used in the *stage 2.3 base model simulation* is given both horizontal and vertical directions in Table 5-3 and Table 5-4, respectively.

Table 5-3. Horizontal hydraulic conductivity of HSD used in the *stage 2.3 base model simulation*. † K_h increased by an extra factor 2 in Eckarfjärden catchment area.

Layer	K_h [m/s] Fine till	Coarse till	Gyttja	Clay	Sand	Peat	Default
L1	–	–	$3 \cdot 10^{-7}$	–	–	$1 \cdot 10^{-6}$	$3 \cdot 10^{-7}$
Z1†	$1.5 \cdot 10^{-4}$	$1.5 \cdot 10^{-4}$	–	$5 \cdot 10^{-6}$	$7.5 \cdot 10^{-4}$	$5 \cdot 10^{-6}$	$7.5 \cdot 10^{-4}$
Z5†	$5 \cdot 10^{-7}$	$7.5 \cdot 10^{-6}$	–	–	–	–	$5 \cdot 10^{-7}$
Layer	**K_h [m/s] of layers with one type of Quaternary deposits**						
L2	$1.5 \cdot 10^{-4}$						
L3	$1.5 \cdot 10^{-8}$						
Z2	$3 \cdot 10^{-7}$						
Z3	$1.5 \cdot 10^{-4}$						
Z4	$1.5 \cdot 10^{-8}$						

Table 5-4. Vertical hydraulic conductivity of HSD used in the *stage 2.3 base model simulation*.

Layer	K_v [m/s] Fine till	Coarse till	Gyttja	Clay	Sand	Peat	Default
L1	–	–	$3 \cdot 10^{-9}$	–	–	$1 \cdot 10^{-8}$	$3 \cdot 10^{-9}$
Z1	$1.5 \cdot 10^{-6}$	$1.5 \cdot 10^{-6}$	–	$5 \cdot 10^{-8}$	$7.5 \cdot 10^{-6}$	$5 \cdot 10^{-8}$	$7.5 \cdot 10^{-6}$
Z5	$7.5 \cdot 10^{-9}$	$7.5 \cdot 10^{-8}$	–	–	–	–	$5 \cdot 10^{-9}$
Layer	**K_v [m/s] of layers with one type of Quaternary deposits**						
L2	$1.5 \cdot 10^{-8}$						
L3	$1.5 \cdot 10^{-10}$						
Z2	$3 \cdot 10^{-8}$						
Z3	$1.5 \cdot 0^{-5}$						
Z4	$1.5 \cdot 10^{-9}$						

5.2.2 Changes to the representation of hydraulic conductor domains

Under stage 2.2, a deterministic model of the HCD hydraulic properties was developed based on /Follin et al. 2007b/. This defined the zone transmissivities to vary with depth piecewise using 100 m vertical sections according to a linear trend in Log(T), but without lateral heterogeneity. The linear depth trend was adjusted to fit single-hole hydraulic measurements. In deformation zones with more than 2 hydraulic measurements, if a measurement varied significantly from the linear depth trend for the zone, then the transmissivity of the corresponding 100 m vertical section was changed manually for that zone. With this approach, the effect of conditioning to a measurement was to extrapolate the conditioned value over the entire length of the deformation zone laterally, but not more than 100 m vertically.

For stage 2.3, a more automated method of conditioning to the single-hole hydraulic tests was required such that spatial variability in transmissivity within each zone could be simulated, but still honour measurement values in borehole test intervals. The approach used was to sub-divide each deformation zone geometry into sub-triangles of a specified size, Δ_g, and generate a transmissivity value according to a specified depth trend (with a possible stochastic variation) based on the coordinates of the elevation of the centre of the triangle. For stochastic cases, transmissivity is sampled for each triangle independently (i.e. a "nugget" approach) from a lognormal distribution with the geometric mean and standard deviation specified for each depth zone. Initially, the transmissivity values of the sub-triangles are unconditioned to the measured

data from individual hydraulic test intervals. The next step is to identify those triangles which should be conditioned by a measurement interval. A file defines the borehole depth intervals which intersect specified deformation zones. Using this, the borehole trajectory and a specified conditioning radius Δ_c, the location of the centre of the conditioning intervals, $\underline{x_c}$, is calculated, and the set of triangles to be conditioned is identified as any that have either a corner or centre point within $\Delta_c/2$ of the conditioning radius of $\underline{x_c}$. $\Delta_c/2$ was used otherwise a large number of surrounding triangles were also conditioned. The process of selecting sub-triangles to condition within a triangulated deformation zone is illustrated by the sketch shown in Figure 5-4. The list of conditioned transmissivities was provided as a list of two values for each interval: the measured value, T_c, and the lower detection limit for the test, T_l. These two values along with the unconditioned value of transmissivity sampled for the triangle, T_u, were used to determine the value used in the triangle according to the following rule:

- If $T_c \geq T_l$, use T_c;
- Else if $T_u < T_l$, use T_u;
- Else, use T_l.

The detection limit varies between different types of test, and sometimes we only know that the measurement was below the detection limit, and so in such cases the above rules ensure that stochastically sampled transmissivities do not exceed this limit. A list of the transmissivities used in the conditioning is given in Appendix C.

An example of the different approaches to transmissivity conditioning of HCD is shown on ZFMENE0060A in Figure 5-5. In stage 2.2, a conditioning value was manually used to adjust the transmissivity of all triangles within a 100 m lateral band. In stage 2.3, the transmissivity is changed only in the triangles around the borehole intercept.

In summary, lateral heterogeneity was simulated in stage 2.3 by adding a log-normal random deviate to the exponent in Equation (3-1), i.e.:

$$T(x, y, z) = T(0)\ 10^{z/k + \sigma_{\log(T)}\,\mathbf{N}[0,1]} \qquad (5\text{-}1)$$

where $\sigma_{\log(T)} = 0.632$. This value of $\sigma_{\log(T)}$ implies that 95% of the lateral spread in $\log(T)$ is assumed to be within 2.5 orders of magnitude. It should be noted that the *stage 2.3 base model simulation* assumes that $\sigma_{\log(T)} = 0$.

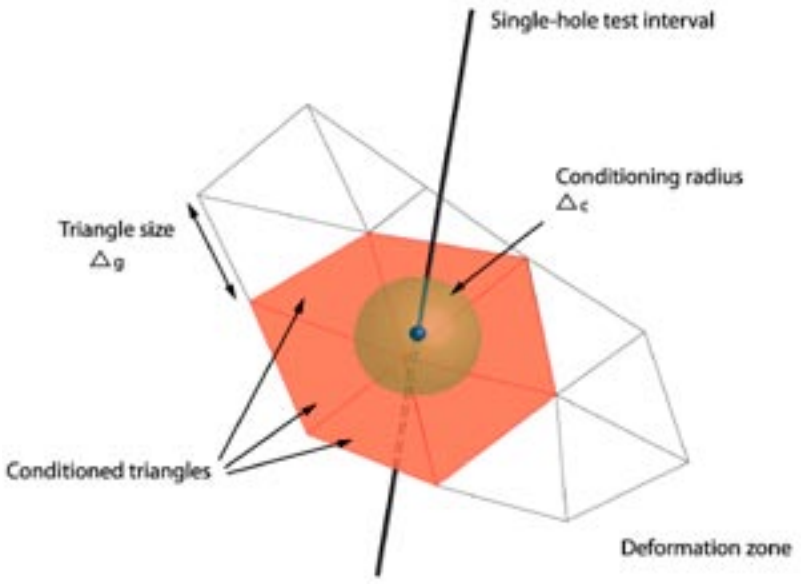

Figure 5-4. *Schematic of approach to automated conditioning of deformation zone transmissivity used in stage 2.3. The selected triangles on which the transmissivity is conditioned are coloured orange here.*

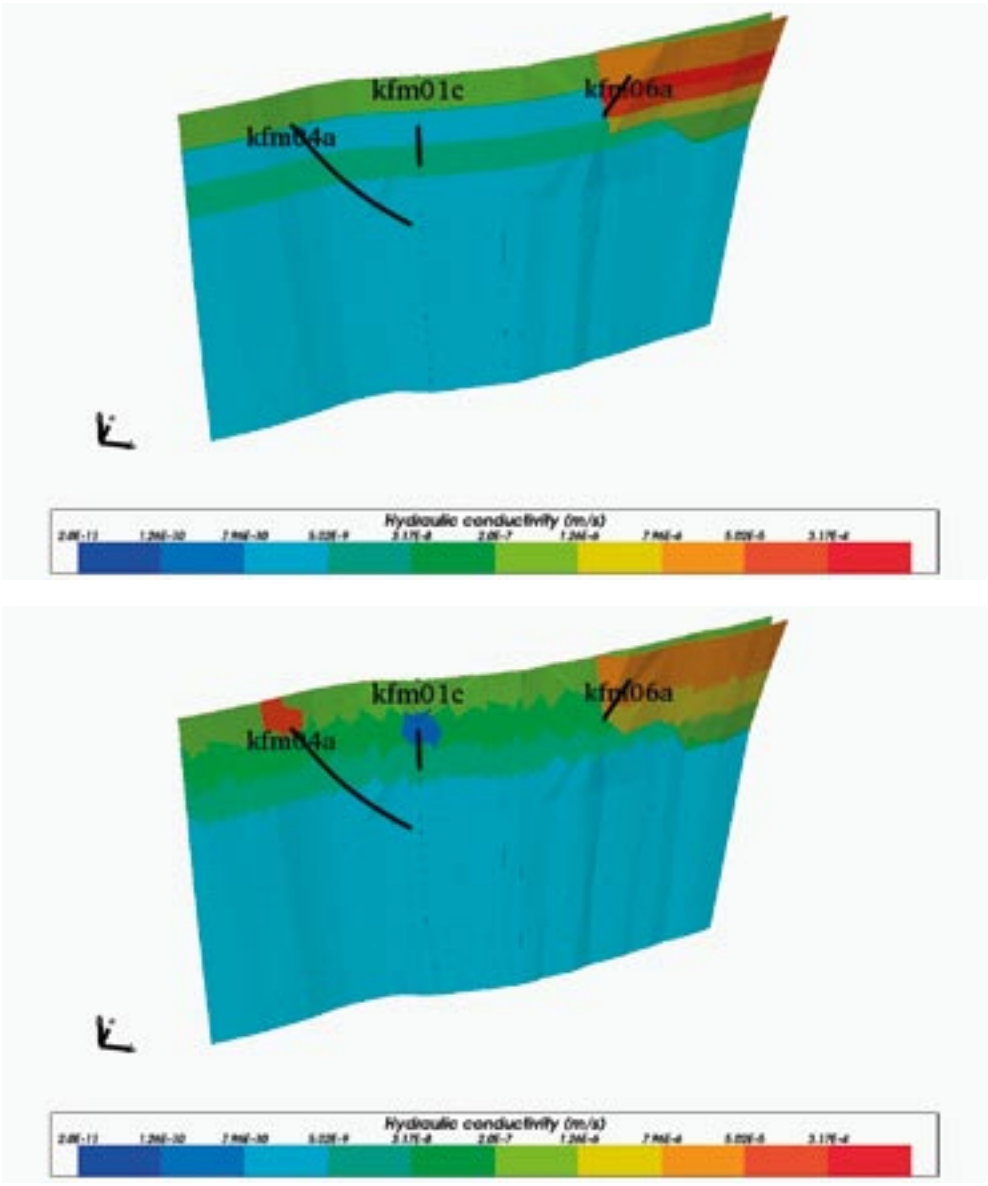

Figure 5-5. *Example of change in transmissivity conditioning methodology used for deformation zones between stage 2.2 (top) and stage 2.3 (bottom). Here, ENE0060 is shown with 3 conditioning intervals in KFM01C, KFM04A and KFM06A. Note: the zone has a splay to the NE around KFM06A.*

5.3 Calibration of the stage 2.3 base model simulation

The calibrated *stage 2.3 base model simulation* is shown in this section. The display of the results allow for comparisons with for the *stage 2.2 base model simulation* shown in section 3.7.

5.3.1 Task B – Matching the interference test at HFM14 (2006)

The localised conditioning of the HCD transmissivities was again found to be the key step in obtaining a match to the interference test results. The comparison of predicted and measured drawdown after 21 days is shown in Figure 5-6. The quality of match is similar to that for the *stage 2.2 base model simulation* as shown in Figure 3-33. Examples of comparisons of the variation in drawdown along the length of boreholes and at different times are shown in Figure 5-7 to Figure 5-12. Again, these are similar to the stage 2.2 results.

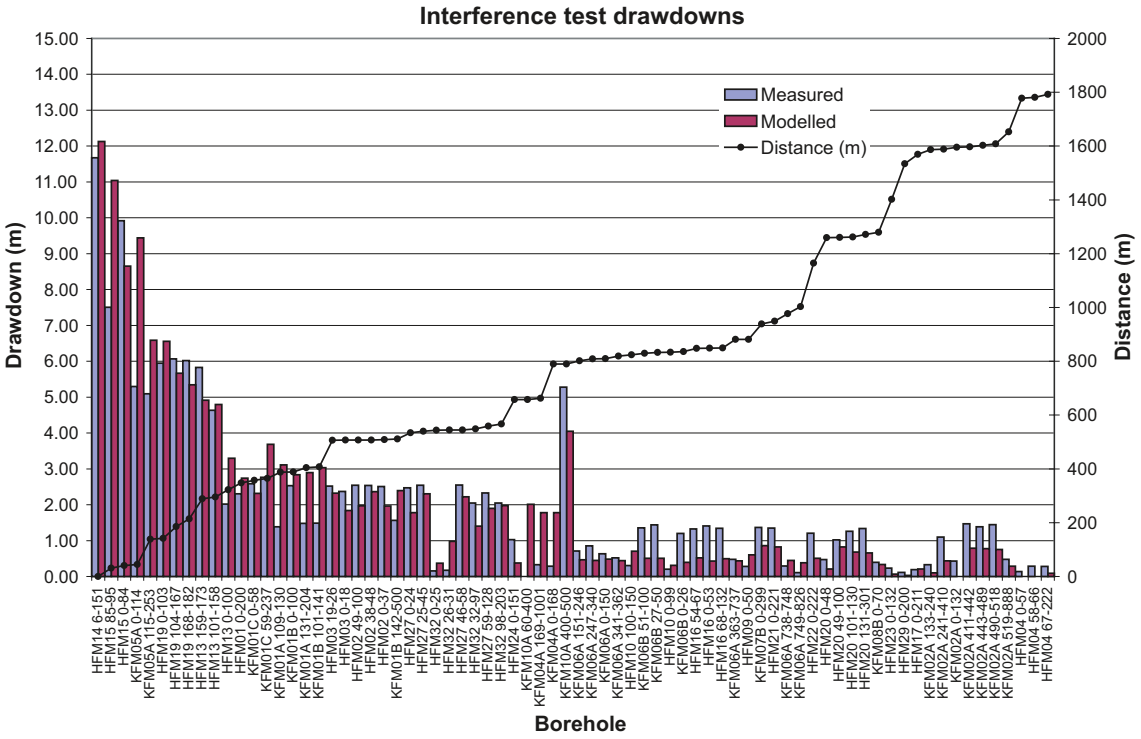

Figure 5-6. *Comparison of measured (blue) and modelled (red) drawdown at the end of pumping (21 days) for all monitored borehole intervals for the stage 2.3 base model simulation. The borehole intervals are ordered according to the 3-dimensional distance (the right axis) of the monitoring intervals to the abstraction at HFM14.*

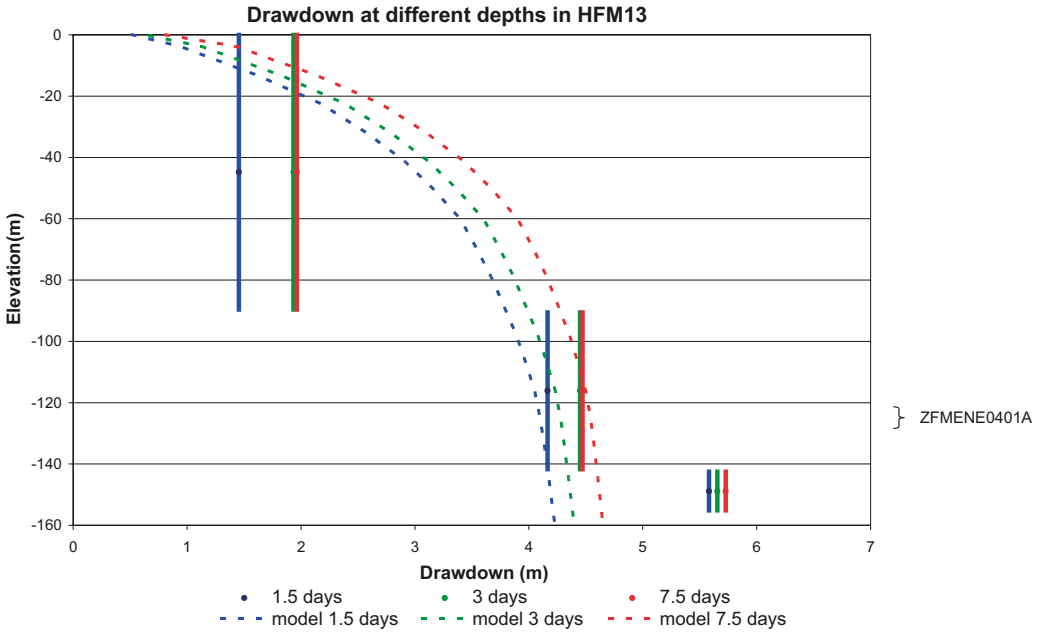

Figure 5-7. *Comparison of measured (solid) and stage 2.3 base model simulation (dashed) drawdown at 3 times for the HFM13 monitoring hole. For the data, a vertical line shows the extent of the monitoring section with the drawdown representing an average within the interval, while the simulated spatial variation in drawdown in the borehole is shown for the model.*

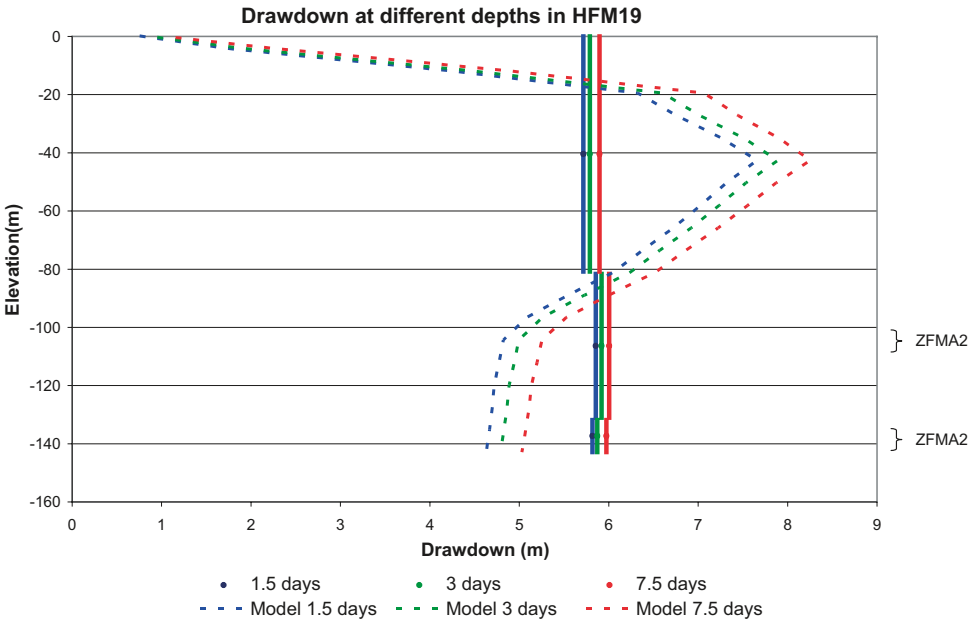

Figure 5-8. *Comparison of measured (solid) and stage 2.3 base model simulation (dashed) drawdown at 3 times for the HFM19 monitoring hole. For the data, a vertical line shows the extent of the monitoring section with the drawdown representing an average within the interval, while the simulated spatial variation in drawdown in the borehole is shown for the model.*

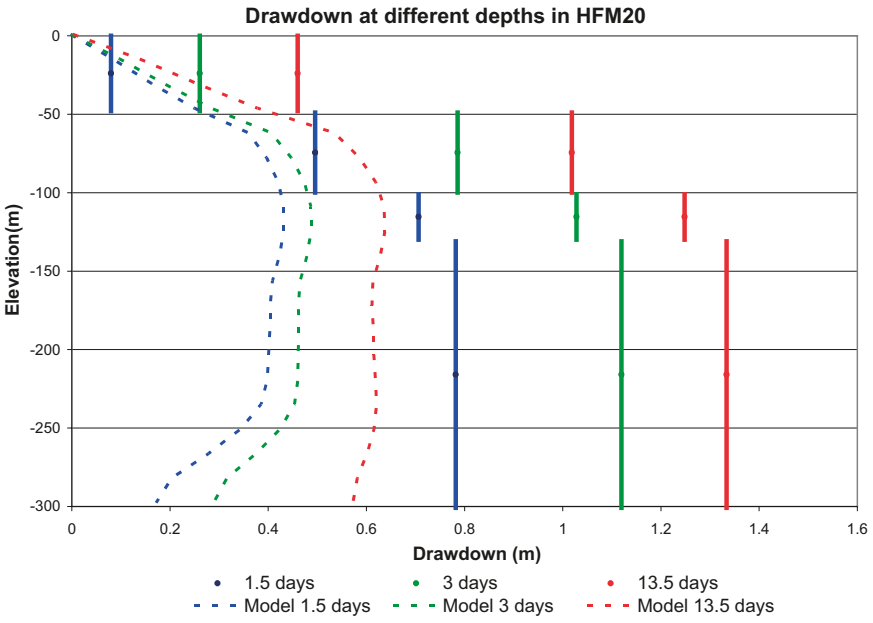

Figure 5-9. *Comparison of measured (solid) and stage 2.3 base model simulation (dashed) drawdown at 3 times for the HFM20 monitoring hole. For the data, a vertical line shows the extent of the monitoring section with the drawdown representing an average within the interval, while the simulated spatial variation in drawdown in the borehole is shown for the model.*

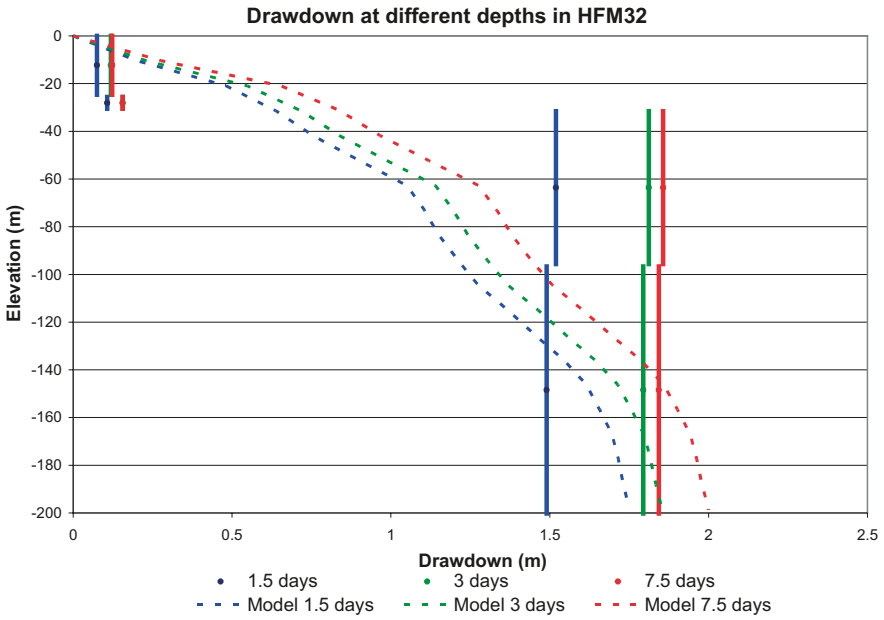

Figure 5-10. *Comparison of measured (solid) and stage 2.3 base model simulation (dashed) drawdown at 3 times for the HFM32 monitoring hole. For the data, a vertical line shows the extent of the monitoring section with the drawdown representing an average within the interval, while the simulated spatial variation in drawdown in the borehole is shown for the model.*

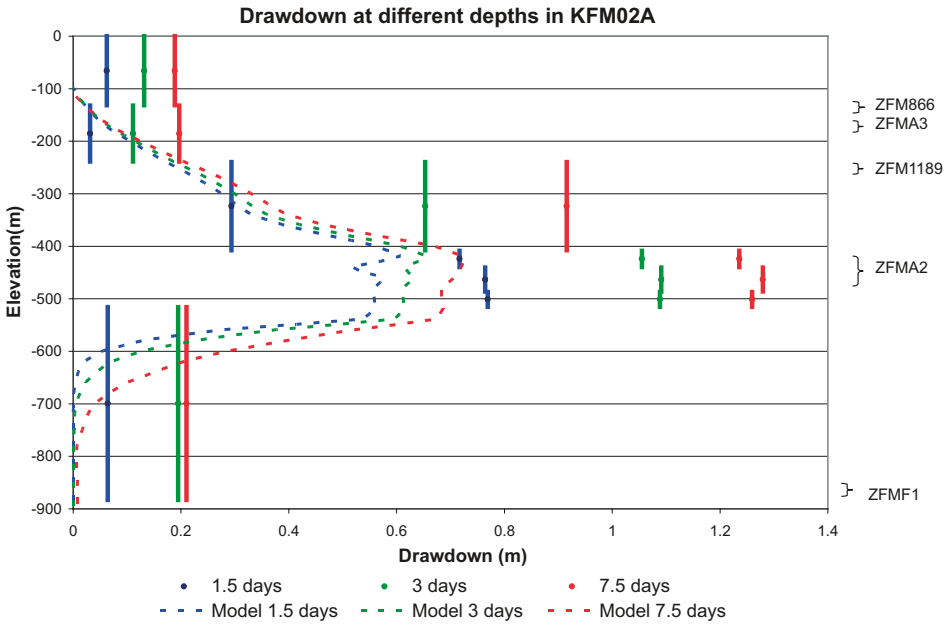

Figure 5-11. *Comparison of measured (solid) and stage 2.3 base model simulation (dashed) drawdown at 3 times for the KFM02A monitoring hole. For the data, a vertical line shows the extent of the monitoring section with the drawdown representing an average within the interval, while the simulated spatial variation in drawdown in the borehole is shown for the model.*

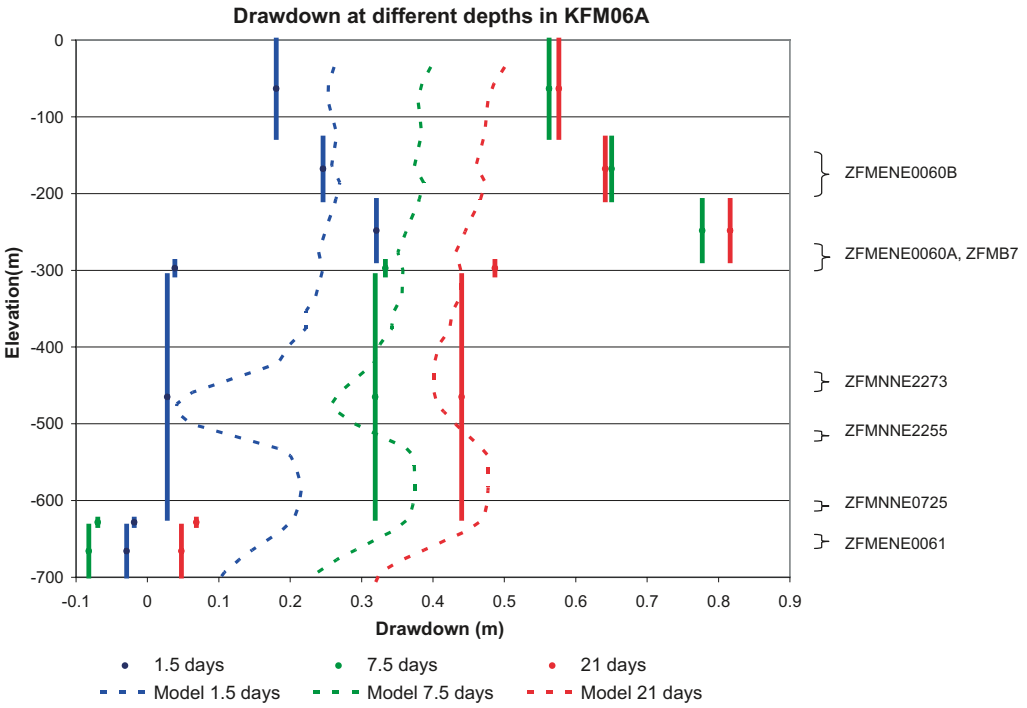

Figure 5-12. *Comparison of measured (solid) and stage 2.3 base model simulation (dashed) drawdown at 3 times for the KFM06A monitoring hole. For the data, a vertical line shows the extent of the monitoring section with the drawdown representing an average within the interval, while the simulated spatial variation in drawdown in the borehole is shown for the model.*

Both model predictions and data consistently show that:

- The hydraulic disturbance propagates predominantly along transmissive, low storage discrete structures in the sub-surface and have a poor hydraulic connection to the surface.
- The hydraulic disturbance propagates in one or more deep intervals more rapidly than in the shallowest packer interval. (The exceptions are KFM06A which intersects the steeply dipping zone ENE0060, and HFM19 which intersects the gently dipping A2 close to its outcrop.).

5.3.2 Task C – Matching the near-surface natural groundwater levels

The changes made to the model of the Quaternary deposits had a significant effect on the simulation of natural groundwater levels. Generally, these changes implied a higher horizontal hydraulic conductivity and lower vertical hydraulic conductivity in the HSD. The average discrepancy in modelled head versus measured in the HFM boreholes fell to 0.9 m, and 0.7 m for the SFM boreholes. This is approximately half that reported in section 3.7.2 for the *stage 2.2 base model simulation*. The discrepancies are nearly all an over-prediction of the measured head. Significantly, the four HFM boreholes (HFM05, HFM06, HFM08 and HFM30) with the largest discrepancies are outside the candidate area around drill-sites 2 and 3 to the south-east. This may be an indication that either the transmissivities assigned to the gently dipping deformation zones to the east of the candidate area are a bit low, or there are additional cage features in the portion of the tectonic lens to the south-east. The average discrepancy in modelled head is 0.7 m for HFM boreholes within the candidate area. This magnitude of discrepancy is considered acceptable for comparing steady-state model predictions with seasonally averaged head data that fluctuates by about 1.3–1.6 m over recordings made at different dates. The comparison with HFM and SFM data is illustrated by Figure 5-13 and Figure 5-14, respectively, and can be compared to Figure 3-36 and Figure 3-37 for stage 2.2. Figure 5-13 shows that head is generally higher in the Quaternary deposits than the bedrock indicating recharge conditions over much of the investigation area.

An analysis of sensitivities with respect to soil properties and infiltration rates is given in chapter 7.

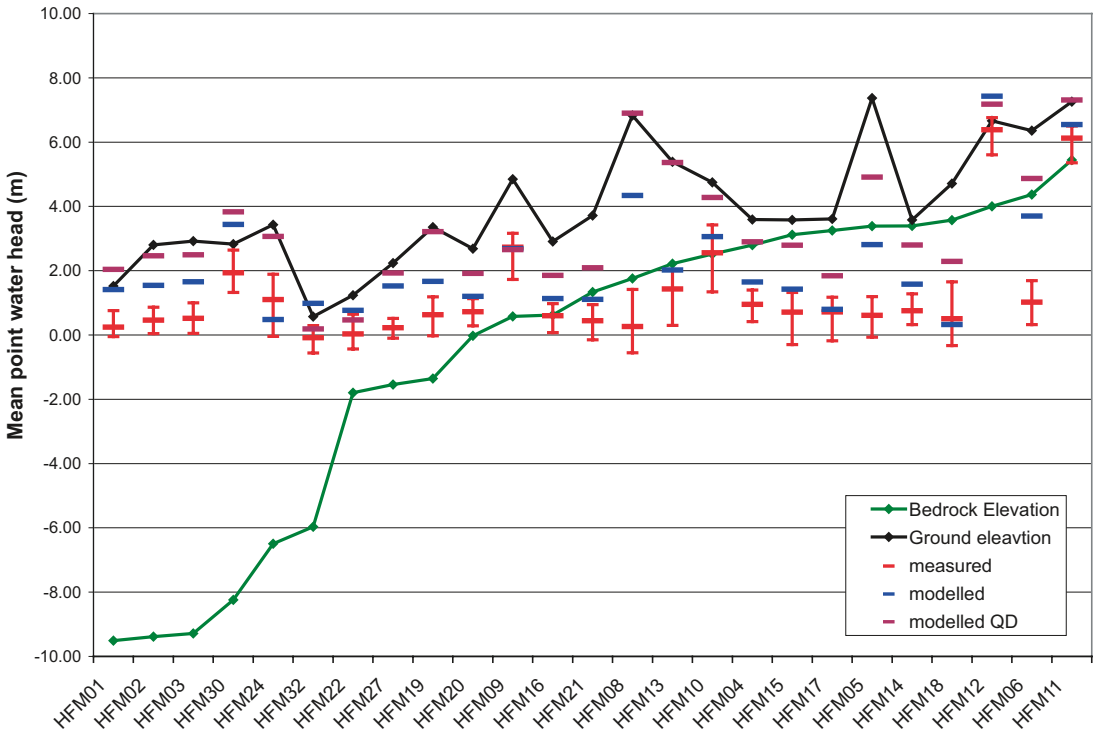

Figure 5-13. *Comparison of measured heads in percussion drilled boreholes (HFM) with the stage 2.3 base model simulation. For the model, values are given for the Quaternary deposits and as an average over the borehole section in the bedrock. The field data is plotted as mean groundwater levels in the bedrock with error bars to show the range of values at different times. The boreholes are ordered by bedrock elevation.*

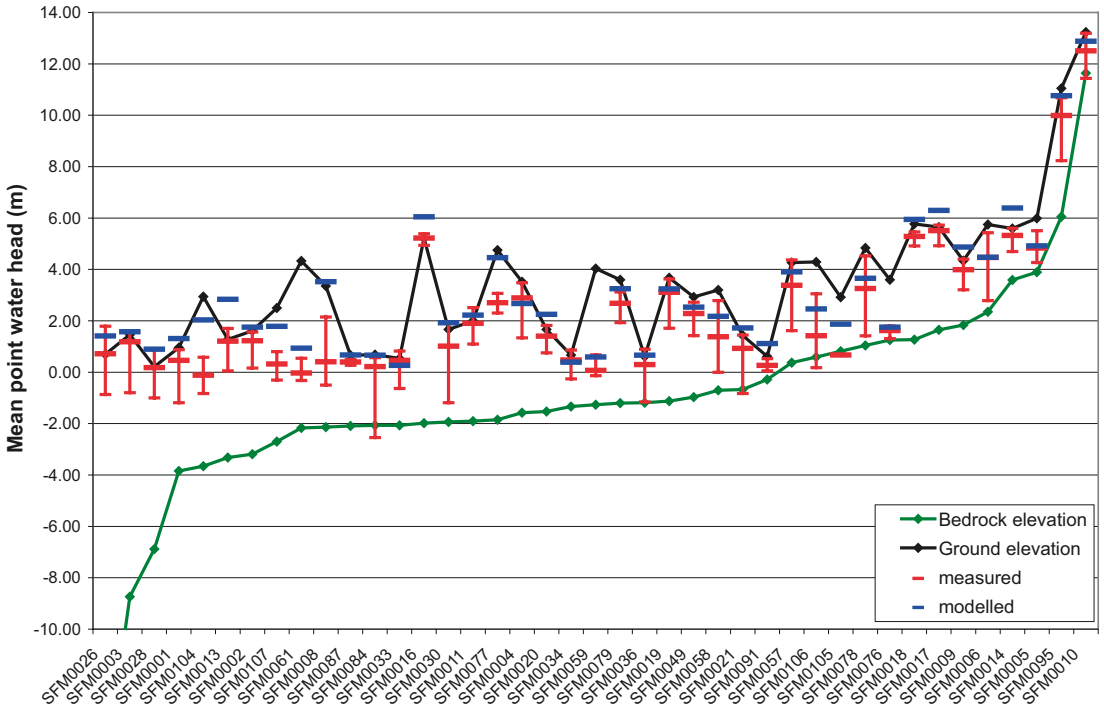

Figure 5-14. *Comparison of measured heads in SFM boreholes with the stage 2.3 base model simulation. For the model, values are given for the Quaternary deposits only. The field data are plotted as mean groundwater levels in the bedrock with error bars to show the range of values over time. The boreholes are ordered by bedrock elevation.*

5.3.3 Task D – Matching hydrochemical data in deep boreholes

A comparison of the predicted hydrochemistry profiles and groundwater samples from deep boreholes for the *stage 2.3 base model simulation* is presented in Figure 5-15 to Figure 5-19. Profiles of salinity for boreholes in the candidate volume corresponding to the footwall of zone A2 are shown in Figure 5-15, along with borehole sections in the hanging wall to the east. The performance of the model in predicting salinity is generally improved from stage 2.2, mainly due to the changes in conditioning the transmissivity of the HCD. For instance, the updated model in stage 2.3 more correctly predicts salinity is encountered at shallower depths in KFM01A and KFM01D than in stage 2.2. The high salinity at c. 100 m depth observed in KFM05A is not quite predicted, although many other boreholes have salinity > 5g/L at this elevation. The predictions of salinity in the hanging have also improved compared to stage 2.2.

Figure 5-16 and Figure 5-17 show the four main hydrochemical indicators used in the calibration: Cl, Br/Cl, $\delta^{18}O$ and HCO_3 (see section 3.7.3) for a series of boreholes. Figure 5-16 indicates the predictions of transitions from *Littorina Sea Water* to *Deep Saline Water* shown by Br/Cl, and *Present-day Meteoric Water* to *Littorina Sea Water* shown by HCO_3 are both at the correct depths. Similarly good results are obtained for the series of boreholes in the footwall of zone A2. There is notable variability between boreholes in the predictions of Br/Cl and $\delta^{18}O$. This Whether this is simply due to spatial variability is explored in the sensitivity analyses reported in chapter 7.

The predictions of Cl in the pore water compared to the fracture system is shown for KFM01D and KFM06A in Figure 5-18. The model predicts the observed higher salinity in the fracture system relative to the pore water.

For completeness, predicted profiles of other major ions, Na, Ca, Mg and SO_4 are shown in Figure 5-19 for the first series of boreholes in the footwall of zone A2. These are also in reasonable agreement despite the model only modelling mixing and not non-conservative processes such as cat-ion exchange. Considering the depths at which Mg was detected rather than the absolute magnitudes of concentration measured, Mg confirms that Littorina Sea Water has penetrated only the top 300–400 m of bedrock, as correctly predicted by the model.

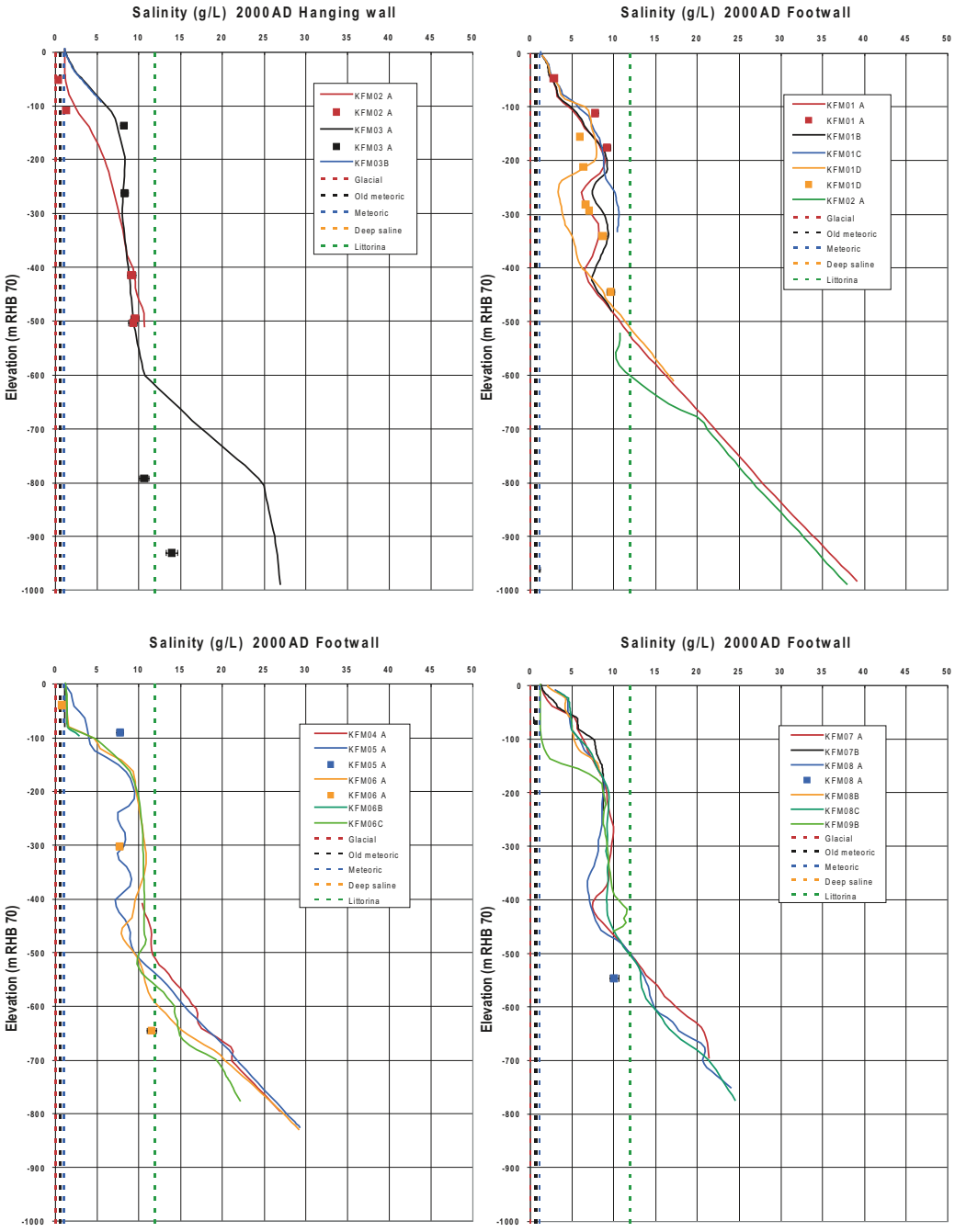

Figure 5-15. *Comparison between the deterministic base model simulation (solid lines) and measured salinity concentrations (TDS) in the fracture system (filled squares) for different groups of calibration boreholes. The error bars on the measured data indicate the laboratory analytical error. The dashed lines show the specified concentration of TDS in the reference waters.*

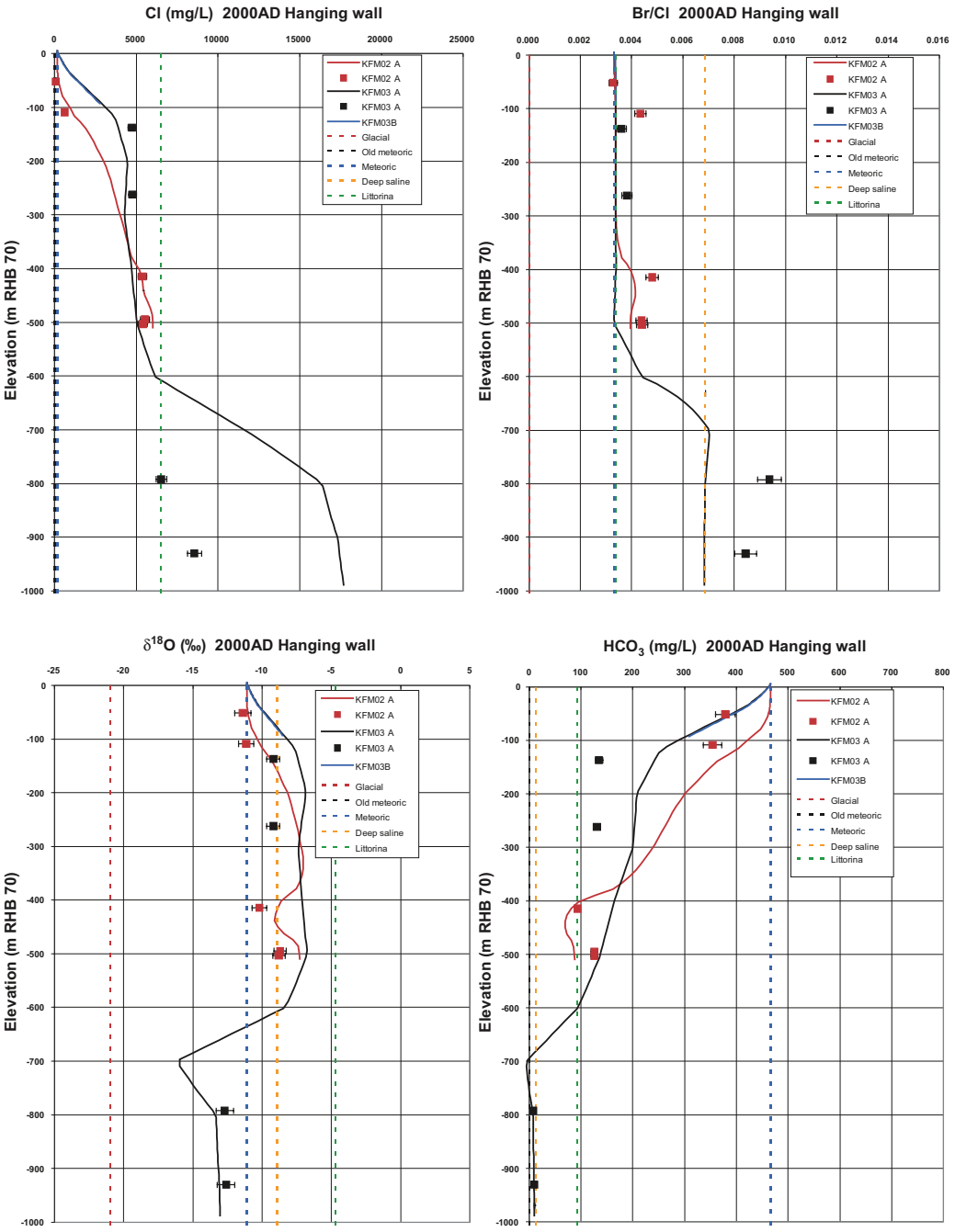

Figure 5-16. *Comparison between the deterministic base model simulation (solid lines) and measured concentrations of Cl, Br/Cl, $\delta^{18}O$ and HCO_3 in the fracture system (filled squares) for boreholes in the hanging wall of A2. The error bars on the measured data indicate the laboratory analytical error. The dashed lines show the specified concentration of Cl, Br/Cl, $\delta^{18}O$ and HCO_3 in the reference waters.*

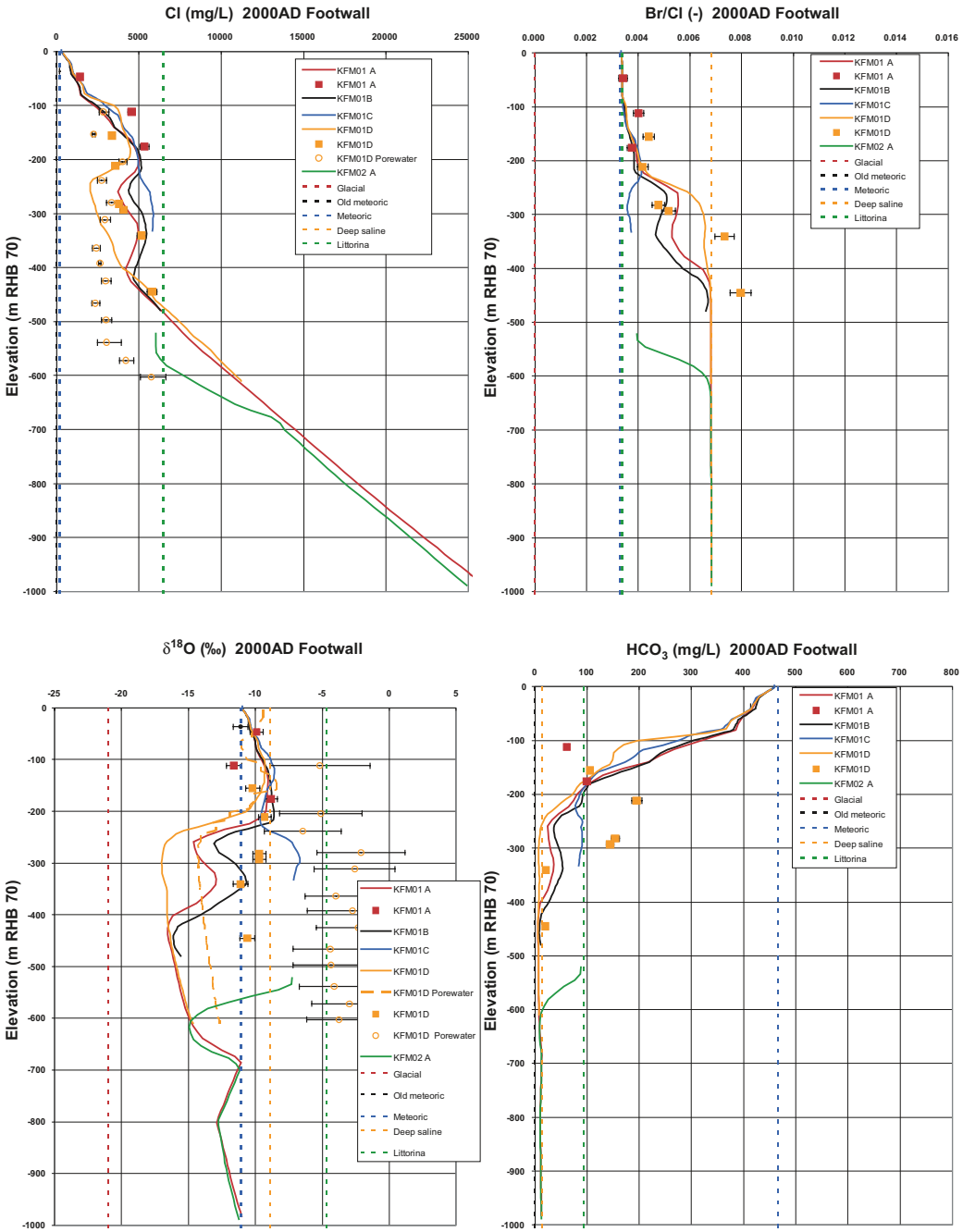

Figure 5-17. *Comparison between the deterministic base model simulation (solid lines) and measured concentrations of Cl, Br/Cl, $\delta^{18}O$ and HCO_3 in the fracture system (filled squares) for the first set of boreholes in the footwall of A2. The error bars on the measured data indicate the laboratory analytical error. The dashed lines show the specified concentration of Cl, Br/Cl, $\delta^{18}O$ and HCO_3 in the reference waters.*

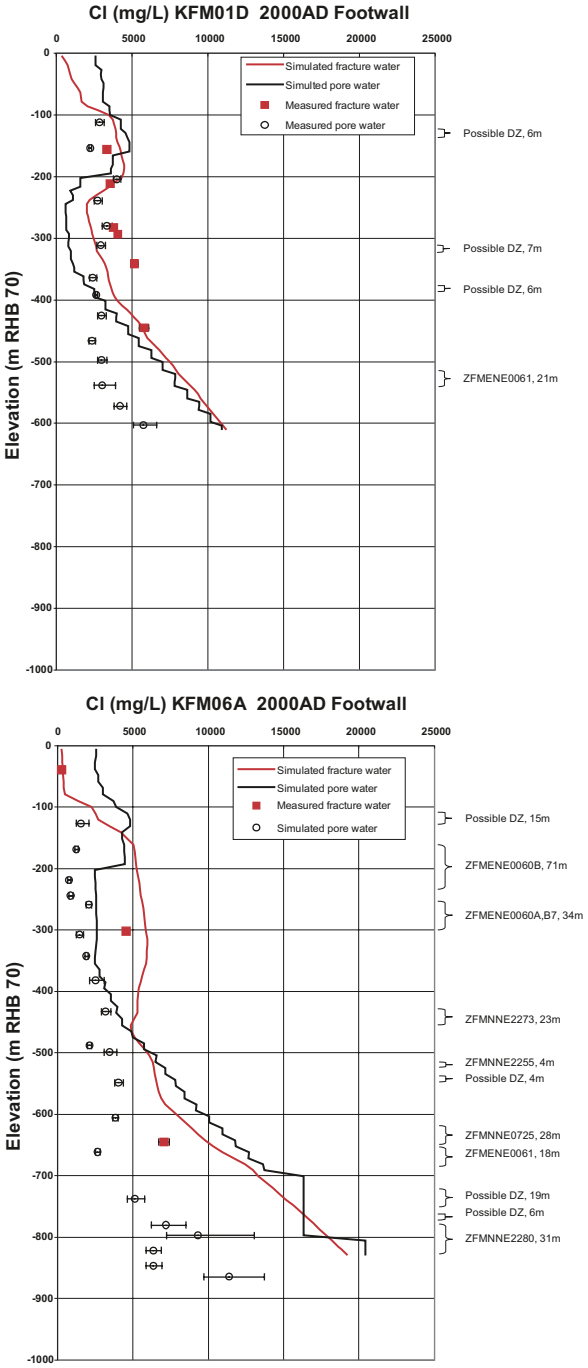

Figure 5-18. *Comparison between the stage 2.3 base model simulation and measured concentrations of Cl in the fracture water and pore water for boreholes KFM01D and KFM06A. The fracture water data are plotted as filled squares and the pore water data are plotted as open circles. The error bars on the fracture data only indicate the laboratory analytical error, while in the pore water they also reflect the uncertainty in the porosity of the rock sample. The red lines show the simulated values in the fracture system, and the black lines show the simulated values in the matrix blocks.*

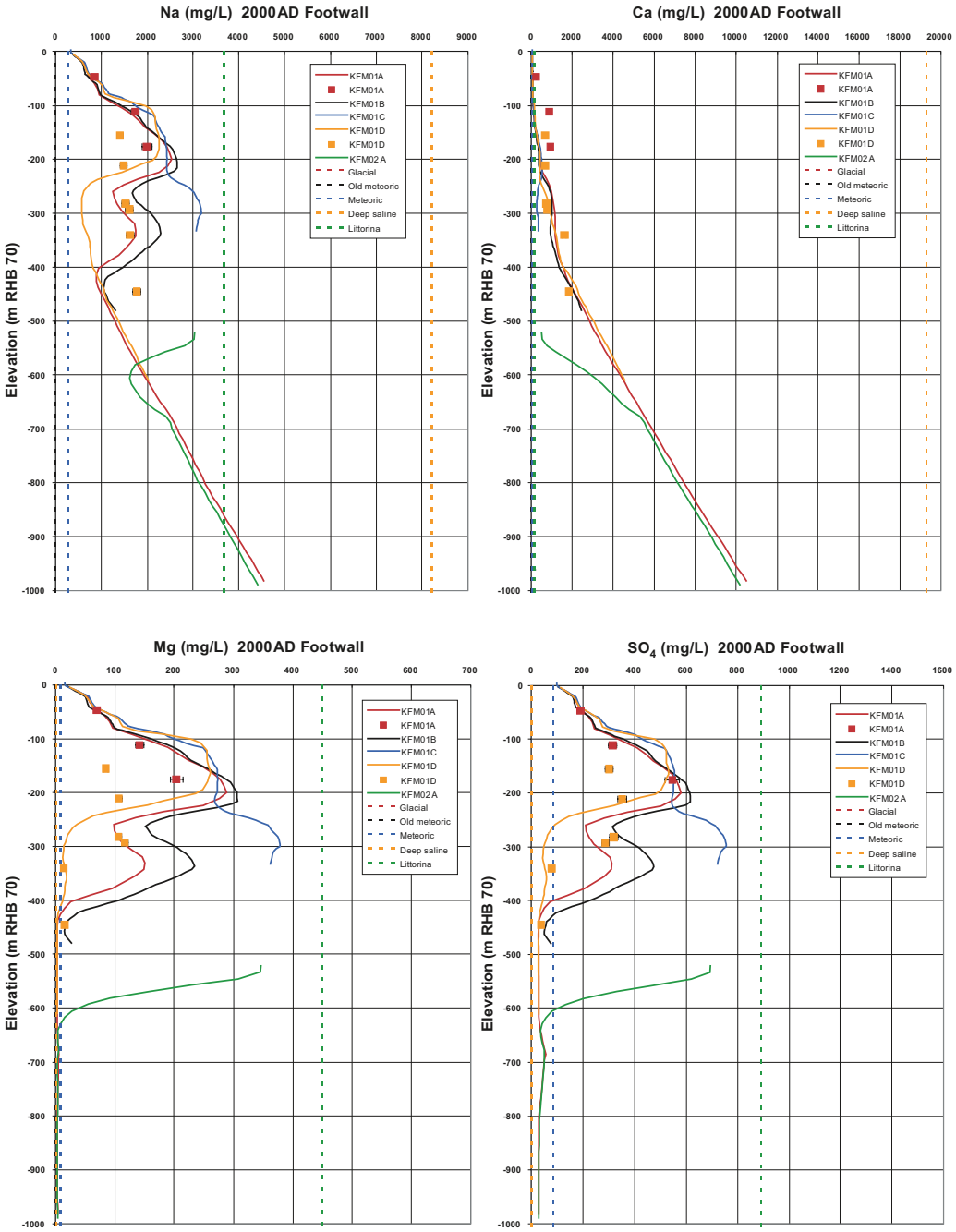

Figure 5-19. *Comparison between the deterministic base model simulation (solid lines) and measured concentrations of Na, Ca, Mg and SO_4 in the fracture system (filled squares) for the first set of boreholes in the footwall of A2. The error bars on the measured data indicate the laboratory analytical error. The dashed lines show the specified concentration of Na, Ca, Mg and SO_4 in the reference waters.*

5.4 Conclusions

The stage 2.3 base model simulation represents a refinement of the stage 2.2 base model simulation defined in /Follin et al. 2007c/ to improve the representation of the Quaternary deposits and the conditioning of transmissivity in HCD against single-hole hydraulic tests. The changes to the modelling of the Quaternary deposits changes were made to improve the consistency with the near-surface hydrological and hydrogeological modelling made with the MIKE SHE code /Bosson et al. 2008/, which involved the introduction of spatial variability within soil layers and horizontal versus vertical anisotropy in the hydraulic conductivity of soils. For the HCD, the same prescription for assigning transmissivities given in /Follin et al. 2007b/ was followed for both stages 2.2 and 2.3, but the approach to conditioning the transmissivity in the vicinity of where a transmissivity had been interpreted from single-hole tests was automated in stage 2.3. It should be noted that the *stage 2.3 base model simulation* assumes that $\sigma_{\log(T)} = 0$.

The consequence of these changes to the calibration of the base model simulation are:

- Results for the interference test in HFM14 are very similar to those for stage 2.2 and the match is of equal quality.
- Simulations of the natural point-water heads are in much better agreement for stage 2.3 with the average discrepancy in head reduced by about half to 0.9 m for HFM holes and 0.7 for soil pipes. This is mainly a result of the changes to the implementation of the HSD model and their properties. The largest discrepancies are outside the candidate area. This magnitude of difference is considered acceptable given the simulations are simplified steady-state simulations of seasonal transient conditions where the measurements vary in time by a larger margin.
- Results of matching profiles of hydrochemistry in boreholes based on simulations of the palaeo-hydrogeology have also improved slightly for the stage 2.3 model. Predictions are generally in good agreement for the variety of major ions, environmental isotopes and pore water chemistry considered in the calibration.

6 Exploration simulations

6.1 Identification of discharge areas using particle tracking

Particle tracks were calculated for a release within a tentative repository layout (D1, /SKB 2006a/) and shown in Figure 6-1. Particles were started on a 100 m spacing at a depth of 500 m. There are two distinct types of paths followed, one short toward the shoreline of the Baltic Sea to the north, and a set of longer that move downwards before returning to the Baltic Sea to the east.

The short paths are generally associated with the western side of the release area and travel upward until they encounter the sheet joint features in the shallow bedrock aquifer, then track along these until they discharge around the intersect with the Singö deformation zone. Some of which cross the zone and discharge in the sea floor around the SFR repository. These particle-tracking results highlight the importance of the property assignment of the Singö deformation zone in influencing the discharge areas. It should be noted that pumping in the SFR repository was not implemented in this application of the *stage 2.3 base model simulation*.

Particles starting in the eastern side of the release area tend to move horizontally or downward, as shown in Figure 6-2, until they encounter the deformation zones that slope gently south-east. The implications of this divergence of pathways on solute transport should be a subject for analysis within the SR-Site safety assessment project. The pattern of discharge areas is broadly similar to that for the *stage 2.2 base model simulation*, see Figure 6-2. A larger number of particles appear to go beyond the Singö deformation zone for the stage 2.3 base case.

As a way of comparing the two base model simulations, the mean difference in the location of the exit points for the same start point is calculated as:

$$\sum_{i=1}^{n} \left| \underline{x}_i^{b2.3} - \underline{x}_i^{b2.2} \right| \Big/ n \qquad (6\text{-}1)$$

where $\underline{x}_i^{b2.3}$ is the location of the final position of the i^{th} particle for the *stage 2.3 base model simulation*, $\underline{x}_i^{b2.2}$ is the location of the final position of the i^{th} particle for the *stage 2.2 base model simulation* , and n is the number of particles released. The expression in (6-1) implies a mean difference in exit location between stage 2.3 and stage 2.2 of 930 m. This size of difference is not unexpected for particle tracking as it tends to be a very sensitive to changes in the parameterisation of heterogeneous systems. For comparison, /Follin et al. 2005/ report a mean difference of around 600 m when slightly different HCD models were used in the Stage 1.2 modelling. The sensitivity of particle exit locations is studied further in the context of heterogeneity in chapter 7.

In order to give some measure of which deformation are most important to transport from the repository target area, the percentage of particles that enter each individual HCD is plotted in Figure 6-3. The zones are shown in order of which see the most particles, and so for example, zone WNW0001 (Singö deformation zone) sees 75% of the released particles and the lower sheet joint feature (–150 m to –100 m RHB 70) sees just over 50% of particles. These 2 features account for the later stages of transport pathways near to discharge. Other zones probably have greater importance to flows close to the repository volume.

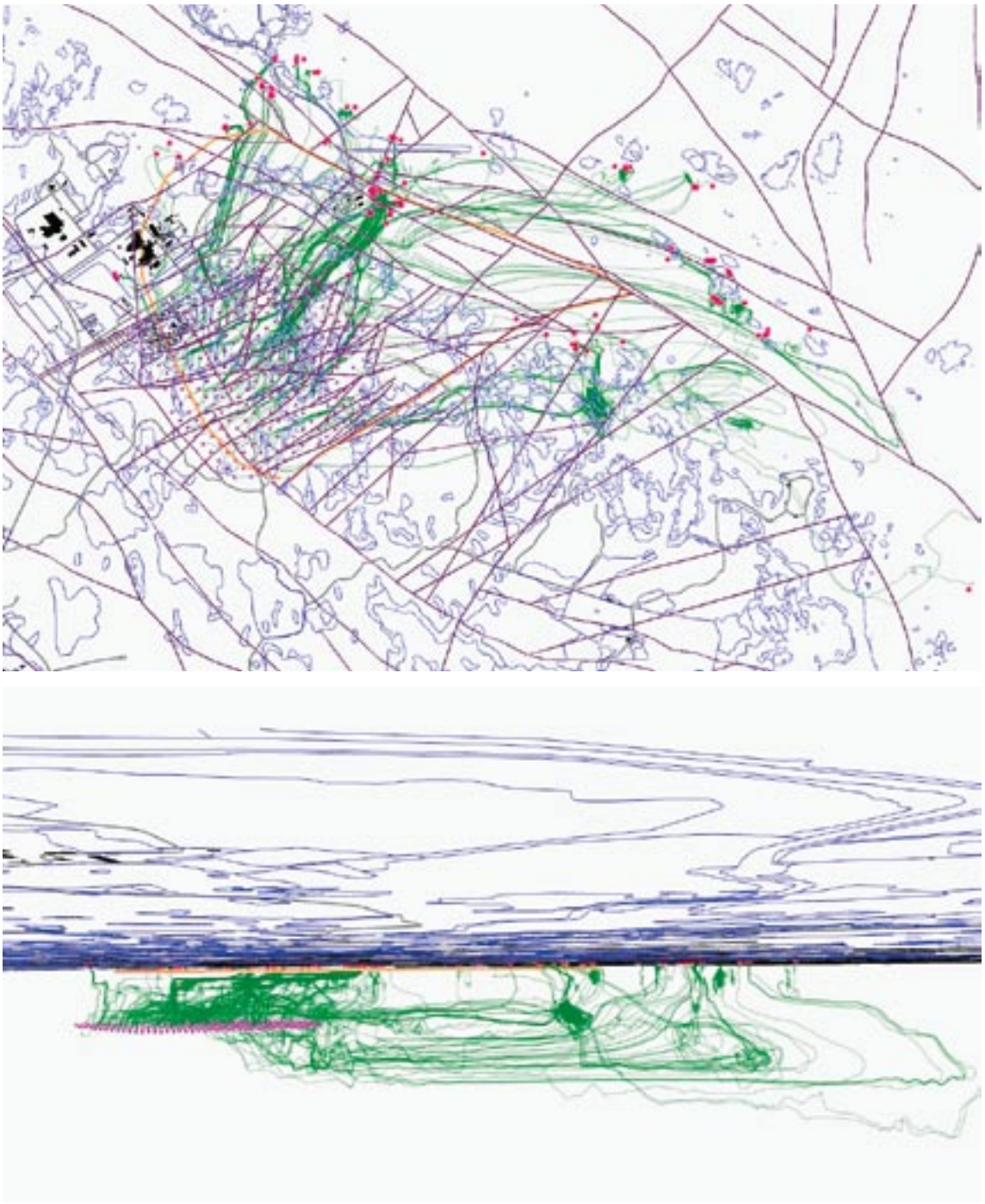

Figure 6-1. *Top: Plan view of the target area with predicted flow paths and exit locations at the surface (red dots) of c. 300 particles using the stage 2.3 base model simulation. The particles were released in a 100 m by 100 m mesh at –500 m RHB 70 using an approximation of the D1 repository layout. Below: A perspective view towards northwest showing flow paths of c. 300 particles using the "stage 2.2 base model simulation". The particles were released in a 100 m by 100 m mesh at –500 m RHB 70 using an approximation of the D1 repository layout. Particles that exit at the surface are indicated by a red dot.*

Figure 6-2. *Top: Plan view of the target area with predicted flow paths and exit locations at the surface (red dots) of c. 300 particles using the stage 2.2 base model simulation. The particles were released in a 100 m by 100 m mesh at –500 m RHB 70 using an approximation of the D1 repository layout. Below: A perspective view towards northwest showing flow paths of c. 300 particles using the "stage 2.2 base model simulation". The particles were released in a 100 m by 100 m mesh at –500 m RHB 70 using an approximation of the D1 repository layout. Particles that exit at the surface are indicated by a red dot.*

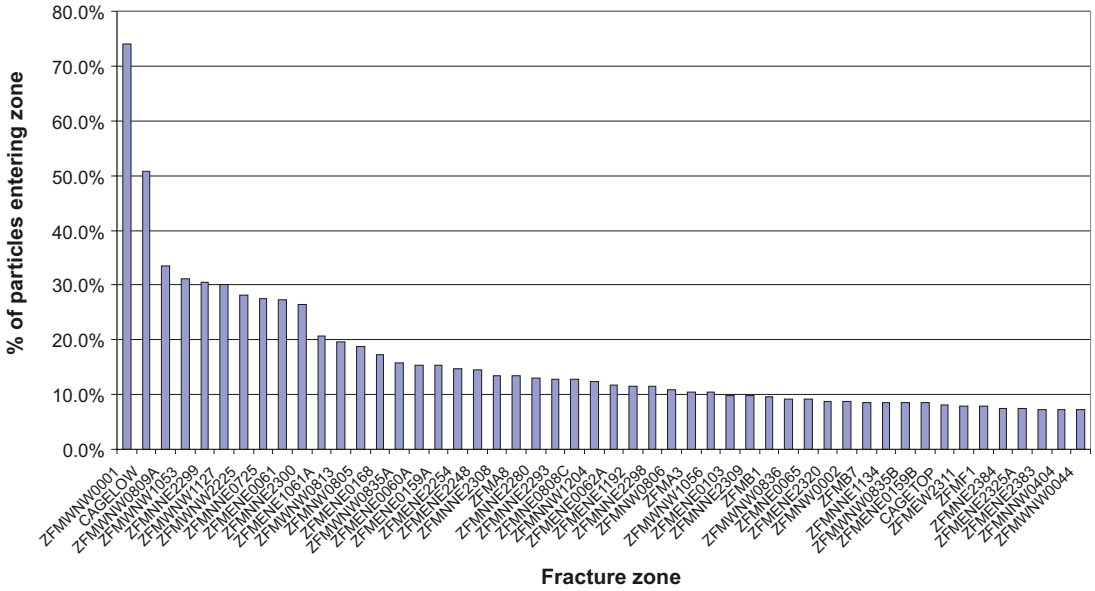

Figure 6-3. *An indication of the relative importance of individual HCD to transport. The percentage of particles that enter each zone is plotted and used to order the HCD according to which zones see the most particles. The particles were released in a 100 m by 100 m mesh at –500 m RHB 70 using an approximation of the D1 repository layout.*

6.2 Comparison between modelled and measured gradients

Particle tracking is a useful tool for calculation of solute transport flow path properties. Figure 6-4 shows another picture of particle tracks for the *stage 2.3 base model simulation* at 2000 AD. Here, 447 particles were released at 450 m depth within a subarea located in the centre of the target volume, with one particle starting every 40 m on a regular mesh. Here, one of the particle tracks, #228, is coloured red and the trajectory of this flow path is shown in a perspective view in Figure 6-5, where the different colours represent the structural elements that the particle encounters on its way to the exit point, i.e. fracture domains, deformation zones and sheet joint features. In these two figures, the blue line denotes the shoreline and the greenish polygon the candidate area.

Figure 6-6 shows the hydraulic gradients in the ECPM model along the flow path of particle #228. The gradients are coloured with regard to the structural elements shown in Figure 6-5. Figure 6-7 shows a scatter plot of the hydraulic gradient for particle #228 versus the geometric mean hydraulic conductivity. The dots in the scatter plot are coloured with regard to elevation (m RHB 70).

Figure 6-6 and Figure 6-7 show that the hydraulic gradients along the visualised flow path are low ($2 \cdot 10^{-5}$ to $7 \cdot 10^{-3}$ m/m). The highest values of the hydraulic gradient are found in the proximity of the release position in fracture domain FFM01, where the ECPM hydraulic conductivity is low (~ 10^{-11} m/s). The lowest values of the hydraulic gradient are found in the proximity of the sheet joint features, where the ECPM hydraulic conductivity is high (~ 10^{-4} m/s). The correlation between hydraulic gradients and hydraulic conductivity, with decreasing gradient with increasing hydraulic conductivity is expected because, for a given flow path with a given flow, low-conductive parts require a higher gradient drop than high-conductive parts. However, it is emphasised that Figure 6-6 and Figure 6-7 show results for a single particle only. /Crawford 2008/ discuss the representativeness of the calculated F-factor and the advective residence time for particle #228 in relation to the transport properties of the ensemble of particles shown in Figure 6-4.

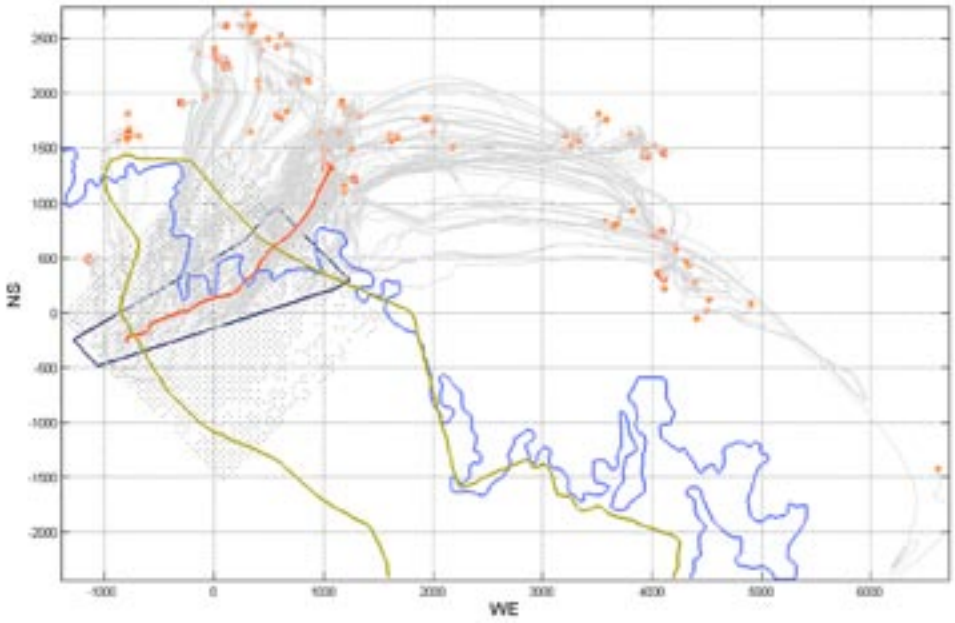

Figure 6-4. *Visualisation of 447 particles released at 450 m depth within a sub area located in the centre of the target volume with one particle starting every 40 m on a regular mesh. One of the particle tracks, #228, is coloured red and the trajectory of this flow path is shown in a perspective view in Figure 6-5.*

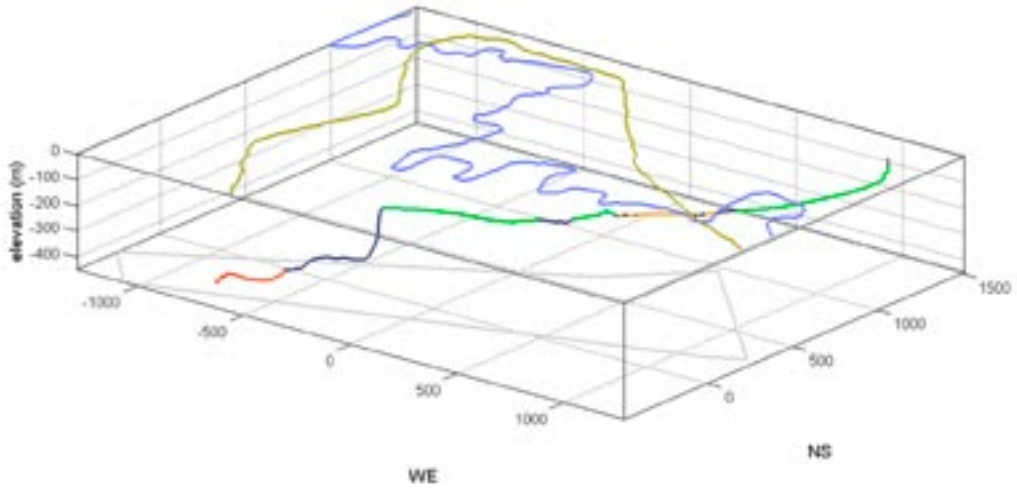

Figure 6-5. *The flow path of particle #228 shown in Figure 6-4 is here coloured with regard to the structural elements that the particle encounters on its way to the exit point, i.e. red for fracture domain FFM01 and yellow for FFM06, blue for various deformation zones, green for different sheet joint features and brown for the Quaternary deposits.*

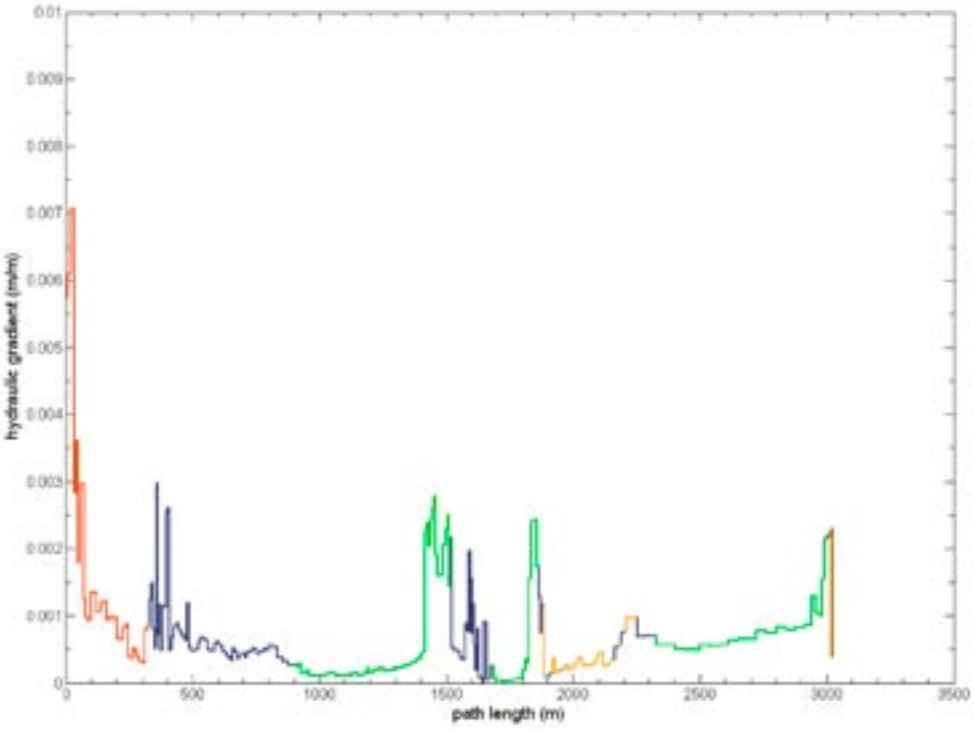

Figure 6-6. *A plot of the hydraulic gradients along the flow path of particle #228 in the ECPM model. The gradients are coloured with regard to the structural elements that the particle encounters on its way to the exit point, cf. Figure 6-5.*

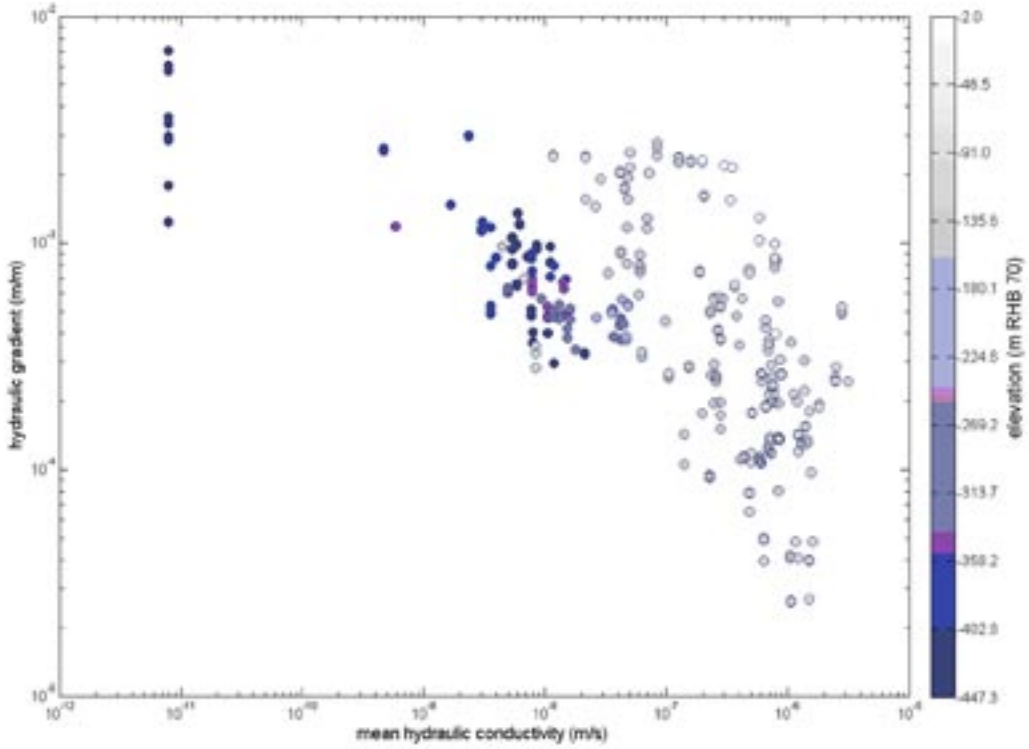

Figure 6-7. *A scatter plot of the hydraulic gradient for particle #228 versus the geometric mean hydraulic conductivity for particle #228. The dots are coloured with regard to elevation (m RHB 70).*

Figure 6-8 shows groundwater flow vs. mid-section elevation for dilution measurements in Forsmark and Figure 6-9 shows the interpreted hydraulic gradients versus mid-section elevation for the same dilution measurements. There is an overall impression that the magnitudes of the calculated hydraulic gradient tend to be too high relative to reasonable topographically-based estimates of the regional hydraulic gradient, which is of the order of c. 1%. This viewpoint is supported by gradients obtained in the numerical simulations; see Figure 6-6 for an example.

/Nordqvist et al. 2008/ provides an examination of possible sources of error for the gradient estimation. They conclude that it is likely that gradients tend to be over-estimated. This because the flow convergence correction factor probably often is larger than the commonly assumed value of 2, due to fracture orientation and artificially increased hydraulic conductivity (negative skin) around the borehole (cf. Figure 4-8 in /Follin et al. 2007b/). Of particular importance is the transmissivity values used for estimation of hydraulic gradients and this may be the largest source of error. The transmissivity values used are obtained from different hydraulic test methods (PFL-f, PSS or HTHB). Further, independent of methods, transmissivity values are obtained during a different flow regime (radial flow) than what prevails during the tracer experiments. Reported data are often based on preliminary transmissivity estimates from then available measurements. One may argue that the relatively long-term PFL-f measurements provide more representative transmissivity estimates for the connected flowing path, and some support for this may also be found in available data (cf. Figure 7-2 in /Nordqvist et al. 2008/). In order to improve the hydraulic gradient estimates, the used transmissivity data should be updated using final transmissivity estimates, and preferably from PFL-f measurements if available.

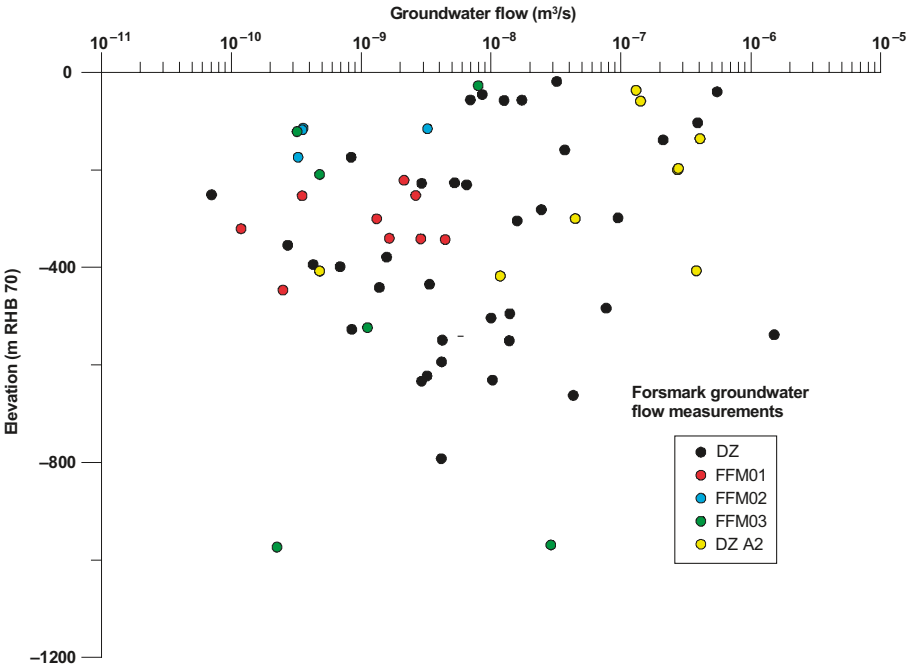

Figure 6-8. *Groundwater flow versus mid-section elevation for dilution measurements in Forsmark. Plotted points are classified into deformation zones and fracture domains. Modified after /Nordqvist et al. 2008/.*

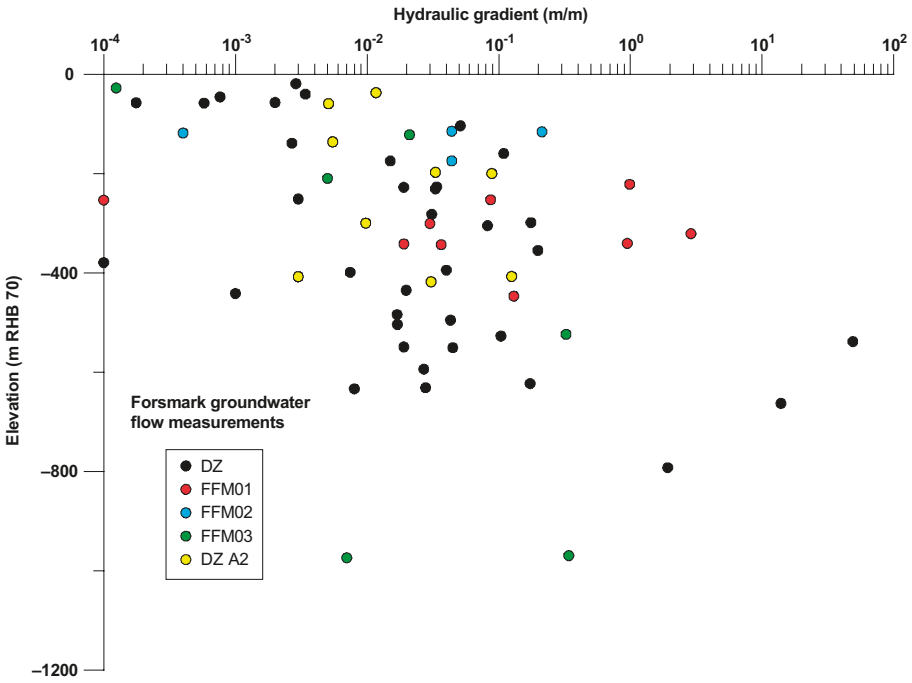

Figure 6-9. *Interpreted hydraulic gradient versus mid-section elevation for dilution measurements in Forsmark. Plotted points are classified into deformation zones and fracture domains. Modified after /Nordqvist et al. 2008/.*

6.3 Visualisation for the interpretation of hydrochemistry

Figure 6-10 shows a 2D cross section parallel to the shoreline with contoured chloride concentrations for the *stage 2.3 base model simulation*. The blue line is a regional water divide, which is used as the upstream flow boundary. The black arrows indicate the directions of the resultant Darcy fluxes in the plane of the cross section. (The discretisation is finer within the local model domain.) The directions of the Darcy fluxes vary, but the mean direction is essentially perpendicular to the cross section pointing towards the shoreline, i.e. parallel with the topographic gradient. The red lines indicate flow paths of 100 particles that cross the sloping intersection between the 2D cross section and zone A2 (grey shade). The majority of these crossings recharge at different places downstream the regional water divide. The flow paths that cross the sloping intersection between 150 and 550 m depth stay close to zone A2, whereas the flow paths that cross above c. 150 m depth follow the "sheet joint features". In summary, Figure 6-10 supports the conclusion that the groundwater flow system at Forsmark is highly heterogeneous and to a large extent structure-controlled. Detailed interpretations of hydrochemical data using 2D cross sections must therefore be handled with care.

Figure 6-11 shows simulated concentrations of Cl and $\delta^{18}O$ in the plane of the 2D cross-section shown in Figure 6-10. The obvious differences between the footwall and the hanging wall to zone A2 are due to the structural-hydraulic differences between the bedrock segments and to the differences these cause regarding the initial conditions at 8000 BC. It is noted that the results shown in Figure 6-11 represent the *stage 2.3 base model simulation*.

The flat topography of the Forsmark area and the recent withdrawal of the Baltic Sea are examples of important factors in determining the surface and near-surface hydrochemistry. Marine remnants in the Quaternary deposits, as well as modern sea water transgressions, are strongly influencing the hydrochemistry, especially in areas at low altitude close to the coast. However, hydrological and chemical observations in the surface water and the shallow groundwater indicate that there is probably little ongoing discharge of deep saline waters into the superficial freshwater system located above the horizontal sheet joints within the area modelled as a

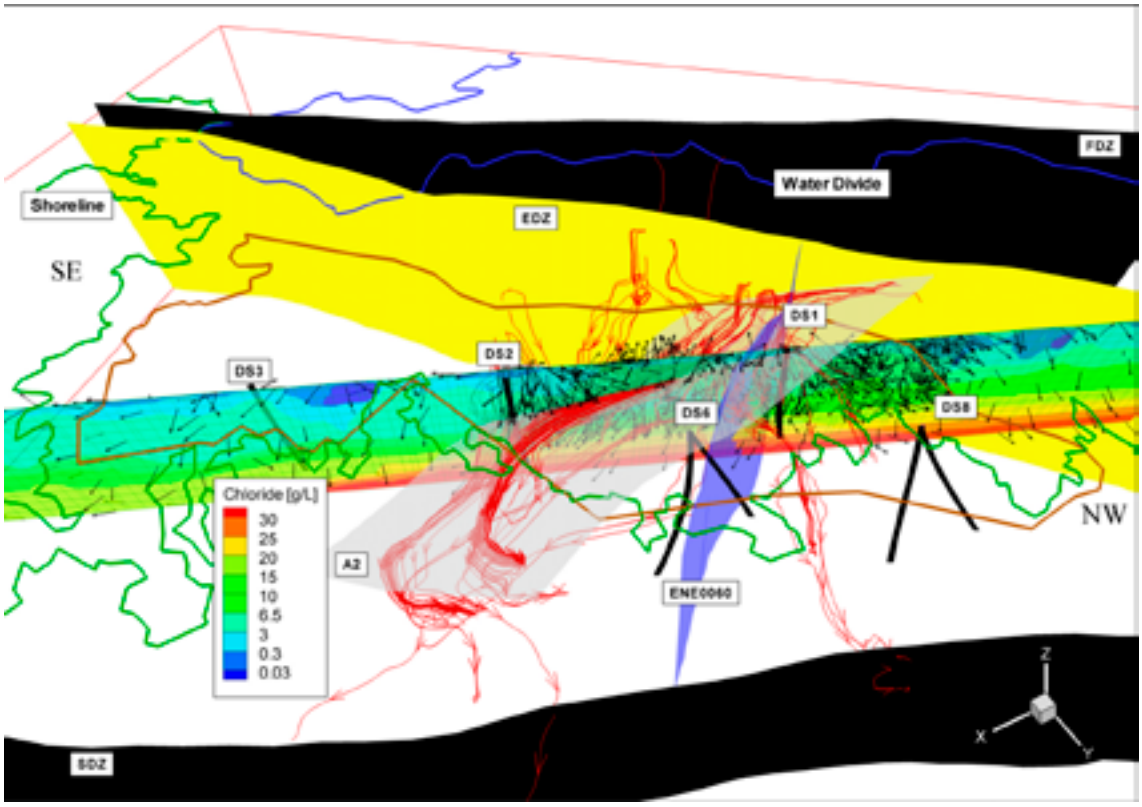

Figure 6-10. *A 1,200 m deep 2D cross section parallel to the shoreline (green line) showing chloride concentrations for the stage 2.3 base model simulation. Black arrows indicate the directions of the Darcy flux along the plane of the cross section. Red lines indicate backward (recharge) and forward (discharge) flow paths for 100 particles that cross the sloping intersection between the 2D cross section and zone A2. The solid blue line is the upstream boundary of the model domain, which coincides with a regional water divide.*

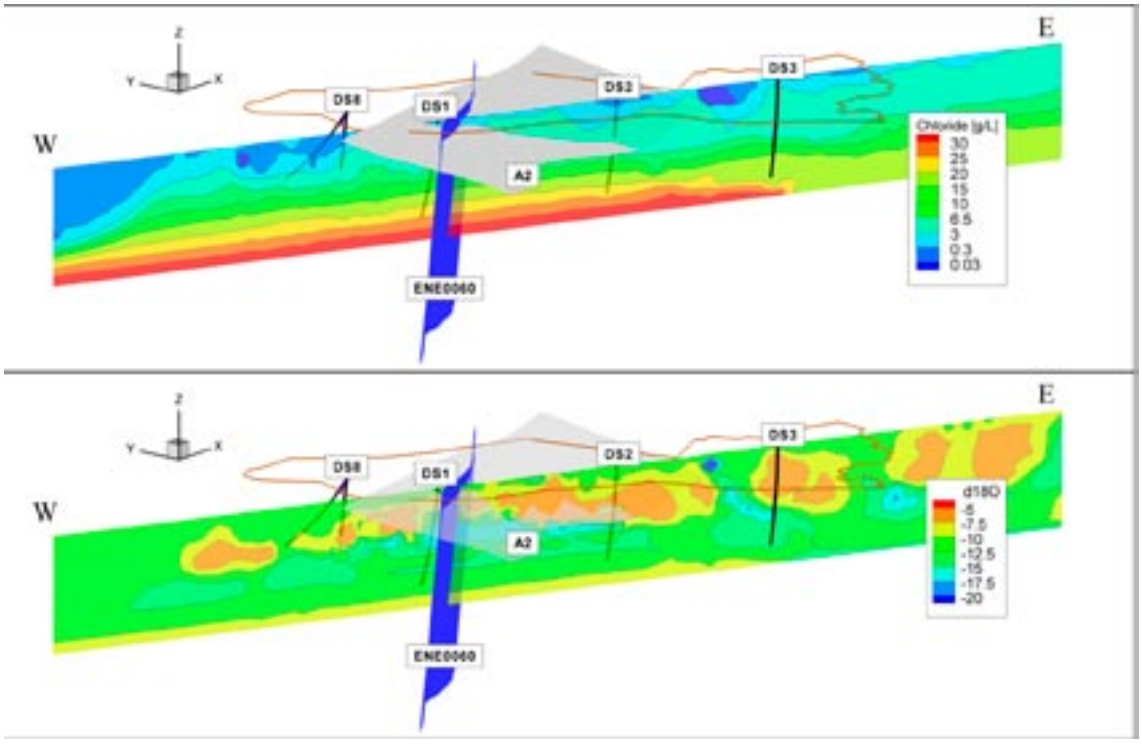

Figure 6-11. *Perspective view towards NE showing simulated concentrations of Cl and $\delta^{18}O$ in the plane of the 1,200 m deep 2D cross-section shown in Figure 6-10.*

shallow bedrock aquifer. However, outside this area there are examples of observations that possibly indicate deep saline signatures in the groundwater at relatively shallow depths in the Quaternary deposits One such area is Lake Gällsboträsket, which coincides with a depression along the trace line of the Eckarfjärden deformation zone. Here, the concentration of chloride in the discharging brook indicates an influence from deep groundwater of older origin than the Littorina Sea Water /Tröjbom et al. 2007, Follin et al. 2007c, Johansson 2008/.

Figure 6-12 and Figure 6-13 shows the predicted present-day spatial distribution of chloride at the surface and at 50 m depth, respectively. Table 6-1 shows the magnitudes of the predicted concentrations together with the ranges of the measured concentrations measured in the till.

The predictions shown in Figure 6-12, Figure 6-13 are calculated with the *stage 2.2 base model simulation* using a grid size of 20 m. The magnitude of discrepancies in relation to the measured data shown in Table 6-1 are considered acceptable for comparing a single realisation of the flow model without uncertainties with borehole hydrochemical data that fluctuates in space and over recordings made at different dates.

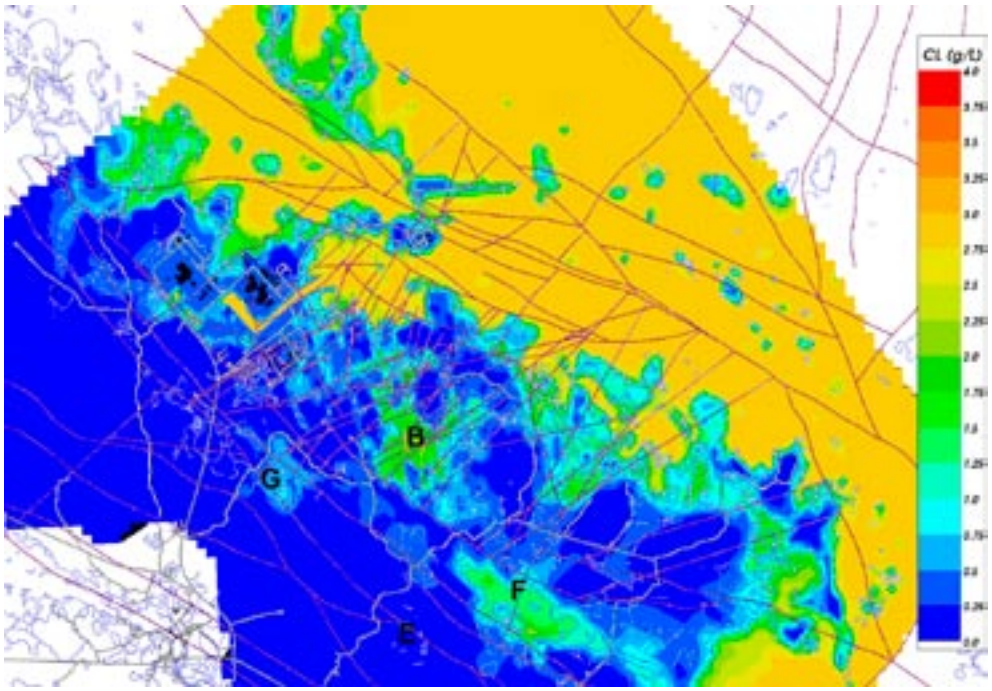

Figure 6-12. *Predicted spatial distribution of chloride at the surface using the stage 2.2 base model simulation. B = Lake Bolundsfjärden, F = Lake Fiskarfjärden, E = Lake Eckarfjärden, G = Lake Gällsboträsket. Reproduced from /Follin et al. 2007c/.*

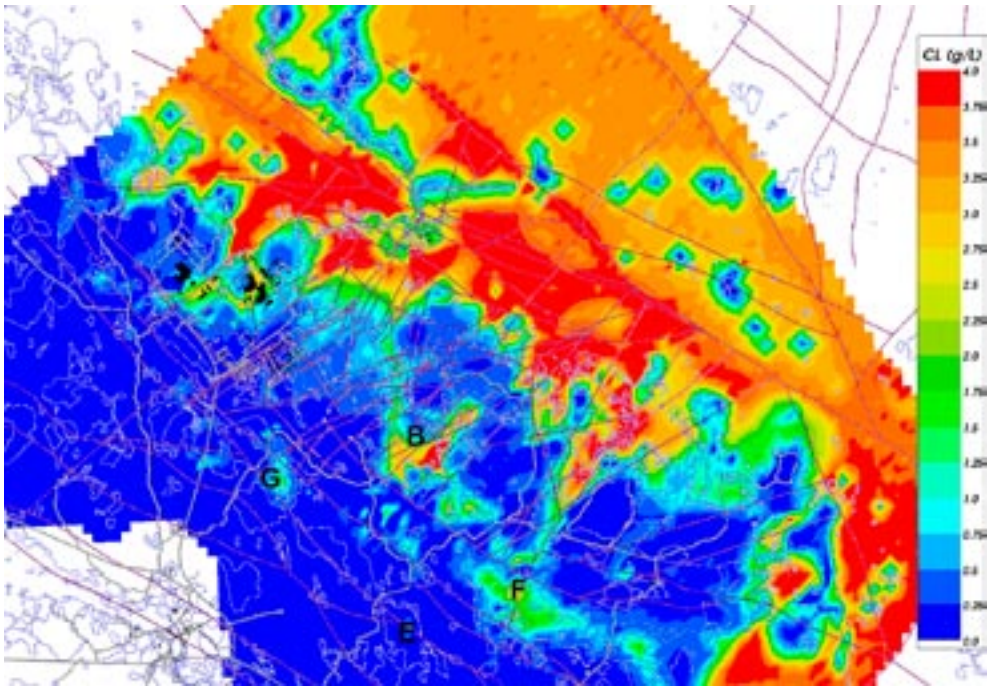

Figure 6-13. *Predicted spatial distribution of chloride at 50 m depth using the stage 2.2 base model simulation in B = Lake Bolundsfjärden, F = Lake Fiskarfjärden, E = Lake Eckarfjärden, G = Lake Gällsboträsket. Data from hydraulic tests and analyses of water compositions in the till below the lakes indicate that the waters sampled below B and F are probably stagnant and of a marine origin (Littorina Sea Water). In contrast, the outflow rate of chloride in the brook that discharges from G suggests an influence of deep saline groundwater. This observation is supported by the chemical signature of the groundwater sampled in the monitoring well SFM0057 located at the edge of the Gällsboträsket. Reproduced from /Follin et al. 2007c/.*

Table 6-1. Predicted and measured chloride concentrations (mg/L) in the till layer below the lake sediments in Lake Bolundsfjärden, Lake Fiskarfjärden, Lake Eckarfjärden, Lake Gällsboträsket and the Baltic Sea. Predicted concentrations at 50 m depth below these water bodies are also shown. The predicted concentrations represent the *stage 2.2 base model simulation*.

Object	Predicted maximum value of Cl in the till and at 50 m depth	Range of the Cl data in the till	Monitoring well
B ; L. Bolundsfjärden	2,250/4,000+	3,520–4,340	SFM0023
F ; L. Fiskarfjärden	2,250/2,750	947–1,300	SFM0022
E ; L. Eckarfjärden	250/250	277–375	SFM0015
G ; L. Gällsboträsket	1,000/1,750	2,160–2,340	SFM0012
Baltic Sea	3,000/4,000+	690–3,940	SFM0024, -25, -65, -81

6.4 Groundwater levels in the shallow bedrock aquifer

The CONNECTFLOW model uses a simplistic representation of the near-surface hydrogeological system and aims at matching the average groundwater levels of time series data in different boreholes with a steady-state flow model. Although, the magnitude and direction of the modelled gradient between the Quaternary deposits and the uppermost bedrock in the CONNECTFLOW model are in accordance with the monitoring data, the absolute values of the simulated average groundwater levels are a too high, c. +0.7 m of mean difference for both the percussion-drilled boreholes and the monitoring wells *within* the target area. In comparison, the results reported from the MIKE SHE model /Bosson et al. 2008/, which uses a detailed representation of the near-surface hydrogeological system and models the time series data on a diurnal basis, suggest that the low groundwater levels measured in the uppermost part of the bedrock cannot be matched unless there is a continuous sink somewhere in the bedrock. That is, without a continuous sink in the bedrock, the downward hydraulic gradients between the Quaternary deposits and the uppermost bedrock are not as pronounced in the MIKE SHE model as they are in the field measurements (and in the CONNECTFLOW model). In fact, the simulated hydraulic gradients locally points upwards in the MIKE SHE model unless there is a continuous sink in the bedrock. If this is the case or not cannot be readily checked because there are no known continuous sinks within the target area. (It is noted that the simulated groundwater levels in the Quaternary deposits in the MIKE SHE model are independent of whether or not there is a sink in the bedrock.)

There are two examples of sinks in the uppermost bedrock not far form the target area, none of which that can be turned off, however. The stronger of these sinks is the abstraction of drainage water in the SFR repository, cf. section 4.5.3. The SFR repository is located below the Baltic Sea and is reached by two tunnels, which cross the Singö deformation zone, see Figure 4-8. The drainage water is abstracted at two pump stations. The first pump station is located after the crossing of the Singö deformation zone (88 m depth; 1.2 L/s) and the other is located below the bottom of the SFR repository (140 m depth; 4.8 L/s).

The other example of a sink is the lowering of the groundwater level beneath the three nuclear power reactors, which are located northwest of the target area (Appendix A, Figure A-1). The pumping under the reactors is not continuous (c. 20 m depth; c. 1–2 L/s of intermittent pumping).

The simulations carried out with the MIKE SHE model suggest that a continuous abstraction of drainage water in the SFR repository affects the on-shore groundwater levels in the uppermost part of the bedrock within the target volume. It is noted that the calibrated MIKE SHE model is based on the CONNECTFLOW model with two main exceptions: 1) the horizontal hydraulic conductivity, K_h,was increased ten times in the part of the model describing the sheet joints only (Figure 3-20), and 2) the vertical hydraulic conductivity, K_v, was decreased ten times in the uppermost 200 m of bedrock throughout the entire model domain.

The results obtained from the single-hole geological interpretation and hydraulic testing of borehole KFM11A, which investigates the Singö deformation zone, together with the interference test data obtained from the interference test at borehole HFM33 during the fall of 2007, suggest that the Singö deformation zone is hydraulically heterogeneous and has a very low transverse transmissivity in the surroundings of the SFR buildings, i.e. there are no hydraulic responses observed in boreholes HFM34, HFM35 and KFM11A while pumping in borehole HFM33, see Figure 4-5 and Figure 4-8. The crossing of the two SFR tunnels could provide a possibility for a hydraulic interference through the Singö deformation zone, but the tunnels cross through the zone in close proximity to borehole HFM34, which did not respond to the pumping in borehole HFM33.

In conclusion, the prevailing situation, with quite low groundwater levels in the shallow bedrock within the target area, may partly be caused by the pumping in the SFR repository. However, no definite conclusions on this issue can be made based on existing data. The CONNECTFLOW model assumes that the Singö deformation zone is heterogeneous, but the model is not calibrated for a scenario where there is a continuous sink in the bedrock in the SFR repository. However, exploration simulations, with the pumping in the SFR repository included in the calibrated CONNECTFLOW model, see section 6.4.1, confirm that the hydraulic properties of the shallow bedrock aquifer system used in the *stage 2.3 base model simulation* are credible and adequate for further modelling, because the differences between measured and simulated groundwater levels decrease when the pumping in the SFR repository is incorporated. That is, even if the abstraction of drainage water in the SFR repository is an uncertain boundary condition that may affect the natural groundwater levels, the hydraulic stresses (drawdowns) induced by the cross-hole tests run in the target area apparently are sufficiently strong to allow for a fair calibration of the hydraulic properties.

6.4.1 Preliminary modelling of inflows to the SFR facility

The inflows to the SFR facility provide an additional hydraulic interference test and give indications of the connections between the SFR deformation zones, the Singö deformation zone, and the shallow bedrock aquifer that is centred on the target area and extend out beneath the shore-line (Figure 3-20). During dry summer periods, drawdowns of a few decimetres have been observed within parts of the candidate area, such as around HFM32, suggesting a hydraulic connection between the SFR deformation zones and the horizontal sheet joints (Appendix J in /Follin et al. 2007c/).

In order to investigate whether the *stage 2.3 base model simulation* had such hydraulic connections, a transient simulation of the drawdown due to pumping at SFR was performed. The boundary conditions for this simulation were:

- an abstraction of 6 L/s at coordinate (1632766, 6701708 RT 90) and between –100 m to –200 m RHB 70, and
- a low infiltration rate on the top surface, nominally 1 mm/year, to mimic dry summer period conditions.

Using the calculated drawdown after 21 days, the region of hydraulic influence for SFR is illustrated in Figure 6-14 by drawing the 1 decimetre contour of drawdown at 100 m depth. The simulation shows a “finger” of drawdown extending south around HFM32 and no drawdown around HFM19.

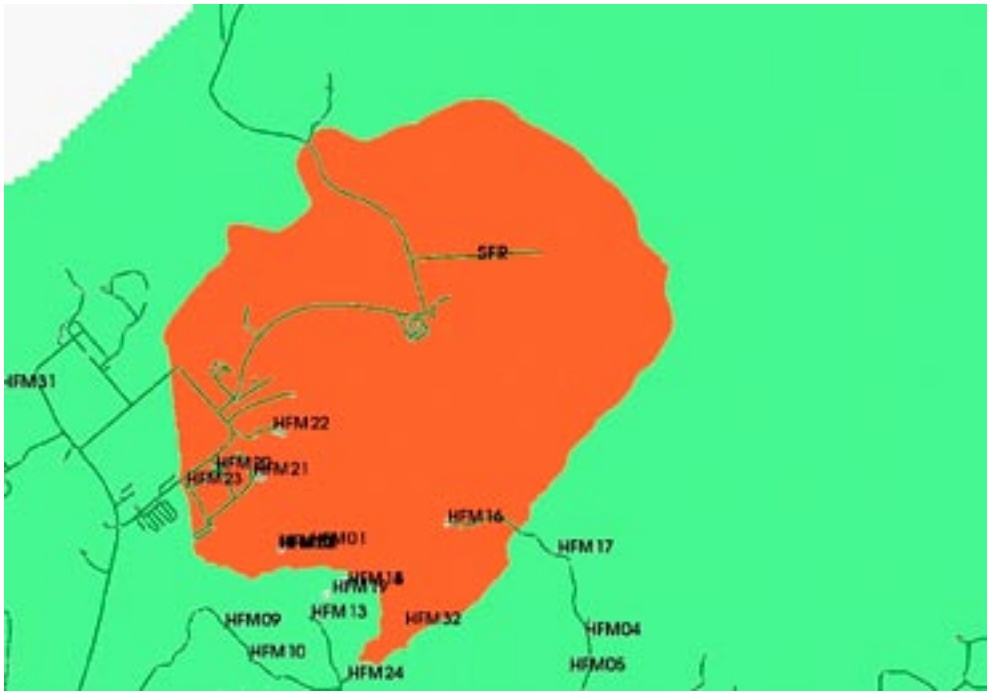

Figure 6-14. *Simulated hydraulic zone of influence of the abstraction of drainage water in the SFR repository during dry periods at an elevation of –100 m RHB 70. The area coloured orange has a simulated drawdown of more than 0.1 m.*

7 Model uncertainties

As part of the numerical modelling in stage 2.2, a number of uncertainties were analysed by performing variant cases to illustrate the sensitivity of the model calibration to alternative concepts and parameters (see section 3.7 and /Follin et al. 2007c/). A more comprehensive uncertainty analysis was performed under stage 2.3. In this section, we explain what uncertainties that were considered, how they were quantified numerically in terms of sensitivity cases, and the results in terms of impact on the model calibration measures and particle tracking where appropriate. A full list of the sensitivity cases considered is given in Table 7-2 as a summary in section 7.4, but are first described more fully in sections 7.1 to 7.3. The results of this uncertainty analysis follow in 7.5 and 7.6.

7.1 Spatial variability

A major theme in the uncertainty analysis is the influence of spatial variability (heterogeneity) in both the HCD and the HRD.

7.1.1 Spatial variability within HCD

The analysis of transmissivity measurements described in /Follin et al. 2007b; section 9.4/ concluded a clear trend with depth, but also considered a significant lateral heterogeneity between measurements made at the same depth. Assuming a log-normal distribution of transmissivity, a standard deviation of 0.632 in log(T) was interpreted. This implies a 95% confidence interval variability of about two and half orders of magnitude. A length scale for the variability was not suggested in /Follin et al. 2007b/. However, there are several measurements in zone A2 in boreholes HFM14, HFM15 and KFM05A that are spaced about 40 m apart and show spatial variability in log(T) of about one order of magnitude. This length scale of the spatial variability in log(T) in zone A2 is also seen at repository depth in borehole KFM02B that was drilled adjacent to borehole KFM02A in stage 2.3. In comparison, studies at the Äspö hard rock laboratory have suggested lengths scales of 100–200 m appropriate for a log-normal distribution of log(T) /Winberg 1994/. Therefore, 50–200 m would seem an appropriate range of length scales for considering the spatial heterogeneity in HCD.

The methodology for generating stochastic realisations of the log(T) distribution with each zone is described in Section 5.2.2. Briefly, each zone was triangulated to a specified scale, Δ_g . log(T) of each triangle was sampled independently from a normal distribution, and the values were conditioned where hydraulic tests have been performed. The conditioning radius, Δ_c, was set to 100 m for the 2.3 base model simulation. In conclusion, four variants were considered: $\Delta_c = \Delta_g$ = 50 m, 100 m, 150 m and 200 m. For each variant, ten realisation of log(T) were generated, i.e. 40 realisations in total.

7.1.2 Spatial variability within HRD

The properties of the rock mass are based on upscaling a probabilistic hydrogeological DFN model. The positions and properties of fractures change between realisations, and therefore, the upscaled ECPM vary accordingly. Here, ten realisations of the regional hydrogeological DFN model were generated and upscaled to give ten corresponding realisations of the ECPM properties for the HRD. In order to keep the number of variants tractable, the 10 realisations of HCD were combined with the 10 realisations of the HRD (i.e. realisation #1 of the HCD was combined with realisation #1 of the HRD) to give a set of 40 realisations that quantify the effect of spatial heterogeneity overall.

7.2 Uncertainties in hydraulic conductor domains

In addition to spatial heterogeneity, uncertainties in the HCD were also considered to the existence of partially detected deformation zones, and the importance of particular deformation zones to the model calibration and discharge areas.

7.2.1 Additional possible deformation zones

Additional 43 *possible deformation zones* (PDZ) were identified in the single-hole geological interpretations of the cored boreholes that could not be linked to deterministically modelled deformation zones (cf. section 3.2.2). Hence, there is an uncertainty as to the presence of additional minor deformation zones (cf. Table 3-2).

Although there are about 43 borehole intervals demarked as PDZ, /Follin et al. 2007b/ established that only ten of these corresponded with a hydraulic test above the detection limit. Of these, six were gently dipping zones in the top 150 m of bedrock and considered to be near-surface sheet joints, leaving four PDZs above the hydraulic detection limit at or close to repository depth. Hence, sensitivity cases were constructed with these four additional PDZs added to the HCD model.

The properties used for the four PDZs are given in Table 7-1. The PDZs were modelled as rectangular planes centred on the intersect with borehole intervals, oriented according to their interpreted trend and plunge (all were assumed to be sub-vertical), and extended until they met an existing sub-vertical HCD, see Figure 7-1. The PDZ were triangulated and ascribed a stochastic field of log(T) values in the same way as geologically modelled HCD described in Section 5.2.2. Three realisations of the PDZ properties were calculated and combined with the first three HCD realisations to quantify the effect of the PDZ on model calibration and particle tracking.

7.2.2 The importance of particular deformation zones

Additional sensitivity cases were perfumed to address the following 3 issues:

- How sensitive is the model calibration to the HCD?
- Which HCD are most important to the model calibration?
- How much does the Singö deformation zone control the discharge area for the candidate volume?

Table 7-1. Properties used in constructing the additional HCD based on the identification of possible hydraulic deformation zones (see /Follin et al. 2007b; Table 7-2/).

Possible DZ	Borehole	Elevation	Trend	Plunge	Length	Transmissivity
PDZ24	KFM04A	–762	71.3	16.8	500 m	$1.3\ 10^{-9}$ m²/s
PDZ26	KFM06A	–549	159.4	9.7	500 m	$2.7\ 10^{-10}$ m²/s
PDZ30	KFM06C	–520	152.4	26.2	1,200 m	$9.3\ 10^{-8}$ m²/s
PDZ36	KFM08A	–543	167.7	27.0	1,100 m	$1.4\ 10^{-6}$ m²/s

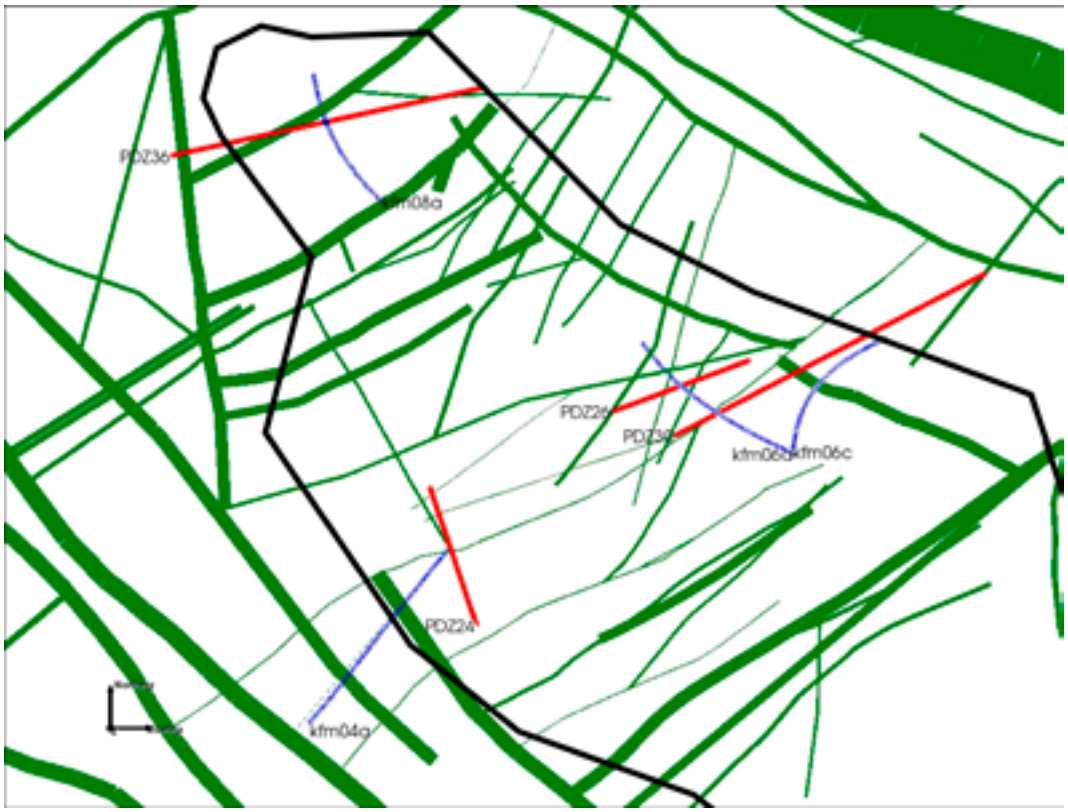

Figure 7-1. *A horizontal slice through the target volume in the north-western part of the candidate area at 600 m depth. The deterministically modelled deformation zones are shown in green, the four possible deformation zones added are shown in red and the supporting boreholes with hydraulic data are shown in blue.*

The first two of these issues were assessed by considering appropriate increases or decreases in the transmissivity of particular HCD as detailed below relative to the Stage 2.3 base case simulation:

- an order of magnitude higher transmissivity in zone A2,
- an order of magnitude lower transmissivity in zone A2,
- an order of magnitude higher transmissivity in zone ENE0060, and
- an order of magnitude higher transmissivity in all other HCD.

On the last issue, variants were considered to the hydraulic description of the Singö deformation zone. The interference test in HFM33 suggested a poor hydraulic communication across the Singö deformation zone (cf. section 4.4), while there is evidence that the inflow pumping from SFR yields a detectable drawdown at some HFM boreholes within the candidate area during dry periods. This seemingly contrary information may be a result of heterogeneity in the Singö deformation zone and gently dipping hydraulic features around SFR. That is, the Singö deformation may be tight in places breaking the hydraulic continuity of the near-surface sheet joints, while in other areas there are hydraulic features that cross the Singö zone giving a discrete and erratic pattern to flow in this area, which is likely to have important effects on discharge locations for particle tracking. Part of the issue of the Singö deformation zone's influence on discharge can be assessed by the sensitivity cases considering heterogeneity in HCD, one of which is the Singö zone. Two other sensitivity cases specific to the Singö zone considered the transverse hydraulic conductivity of Singö zone to be either one or two orders of magnitude lower than the longitudinal hydraulic conductivity to consider the Singö zone acting progressively more as barrier to transverse flow.

7.3 Uncertainties in hydraulic soil domains

As mentioned in section 5, the Quaternary deposits have an effect on the calibration against both the HFM14 interference test and natural groundwater levels. To quantify these sensitivities, the following variants were considered:

- soil properties set according to the initial case properties used by /Bosson et al. 2008/ in the near-surface modelling with MIKE SHE, see Table 5-1, but with a modified anisotropy, $K_v = K_h/100$,
- soil properties set according to the calibrated case properties used by /Bosson et al. 2008/ in the near-surface modelling with MIKE SHE, see Table 5-2, but with a modified anisotropy, $K_v = K_h/10$, and
- soil properties set according to the calibrated case properties used by /Bosson et al. 2008/ in the near-surface modelling with MIKE SHE, see Table 5-2, but with a modified anisotropy, $K_v = K_h/1{,}000$.

The base case simulations of natural point-water heads and hydro-chemistry used a seasonal average maximum potential infiltration to the saturated zone of 150 mm/year /Johansson et al. 2008/. As a variant, a maximum infiltration of 70 mm/year was considered to quantify how sensitive the assumed distribution of steady-state levels are to this boundary condition parameter.

7.4 Summary of variants

Table 7-2 summarises the full set of sensitivity cases used to quantify uncertainties. Sensitivities were measured in terms of their effect on one or more of the three calibration targets – the HF14 interference test, the natural groundwater levels and the hydrochemical data in deep boreholes. For some of the sensitivity cases, the particle tracking discharge locations were also evaluated. The number of sensitivity measures was restricted appropriately to reflect only the key sensitivities of the system.

7.5 Sensitivities of model calibration

The first uncertainty assessment focuses on how sensitive are the simulations of the different calibration targets to uncertainties in model features and parameters. Essentially this quantifies whether the field data is useful in constraining particular aspects of the hydrogeological model.

7.5.1 Interference test data

The role of spatial heterogeneity in determining the distribution of drawdown resulting from the HFM14 interference test was assessed by 10 realisations of the spatial variability both with the HCD and HRD. Figure 7-2 shows the variation in predicted drawdown across the 10 realisation in the form of a bar and whisker plot to indicate the median, 25/75 percentiles, minimum and maximum for each monitoring interval. For boreholes with about 300 m of HFM14 the drawdowns vary by about 2–4 m, and about 1 m with about 800 m of HFM14. These variations are likely to result primarily from the spatial variability with zone A2. Further than 800 m, the effect of the boundary condition at the Baltic has strong control, and variation are only a few decimetres at most.

These results do not suggest that spatial variability within HCD or HRD would lead to significantly different conclusions during the model calibration of either the *stage 2.2 or stage 2.3 base model simulations*. For many of the monitored intervals at distance less than 800 m, the measured drawdown falls within the simulated variations, which may indicate that heterogeneity within A2 and other zones is the cause the variations in drawdown distribution. Further away, spatial variability is less important, and improved simulation results may require consideration of issues such as the connections between deformation zones and boundary conditions.

Table 7-2. A list of sensitivity cases considered in the stage 2.3 study with an indication of the measures of sensitivity considered to either the calibration and/or particle tracking.

Sensitivity case	Interference test	Groundwater level	Hydro-chemistry	Particle tracking
HCD + HRD realisation 1	✓	✓	✓	✓
HCD + HRD realisation 2	✓	✓	✓	✓
HCD + HRD realisation 3	✓	✓	✓	✓
HCD + HRD realisation 4	✓	✓	✓	✓
HCD + HRD realisation 5	✓	✓	✓	✓
HCD + HRD realisation 6	✓	✓	✓	✓
HCD + HRD realisation 7	✓	✓	✓	✓
HCD + HRD realisation 8	✓	✓	✓	✓
HCD + HRD realisation 9	✓	✓	✓	✓
HCD + HRD realisation 10	✓	✓	✓	✓
HCD + HRD + PDZ realisation 1	✓			✓
HCD + HRD + PDZ realisation 2	✓			✓
HCD + HRD + PDZ realisation 3	✓			✓
Base case + HCD 50 m Log(*T*) conditioning scale	✓			
Base case + HCD 150 m Log(T) conditioning scale	✓			
Base case + HCD 200 m Log(*T*) conditioning scale	✓			
Base case + higher T in A2	✓			
Base case + lower T in A2	✓			
Base case + higher T in ENE0060	✓			
Base case + higher T in other DZ	✓			
Base case + 1/10 transverse K in Singö zone				✓
Base case + 1/100 transverse K in Singö zone				✓
Base case + Surface system's initial case HSD properties ($K_v = K_h/100$)	✓	✓		
Base case + Surface system's calibrated case HSD properties ($K_v = K_h/10$)	✓	✓		
Base case + Surface system's calibrated case HSD properties ($K_v = K_h/1{,}000$)	✓	✓		
Base case + lower infiltration (70 mm/year)		✓		

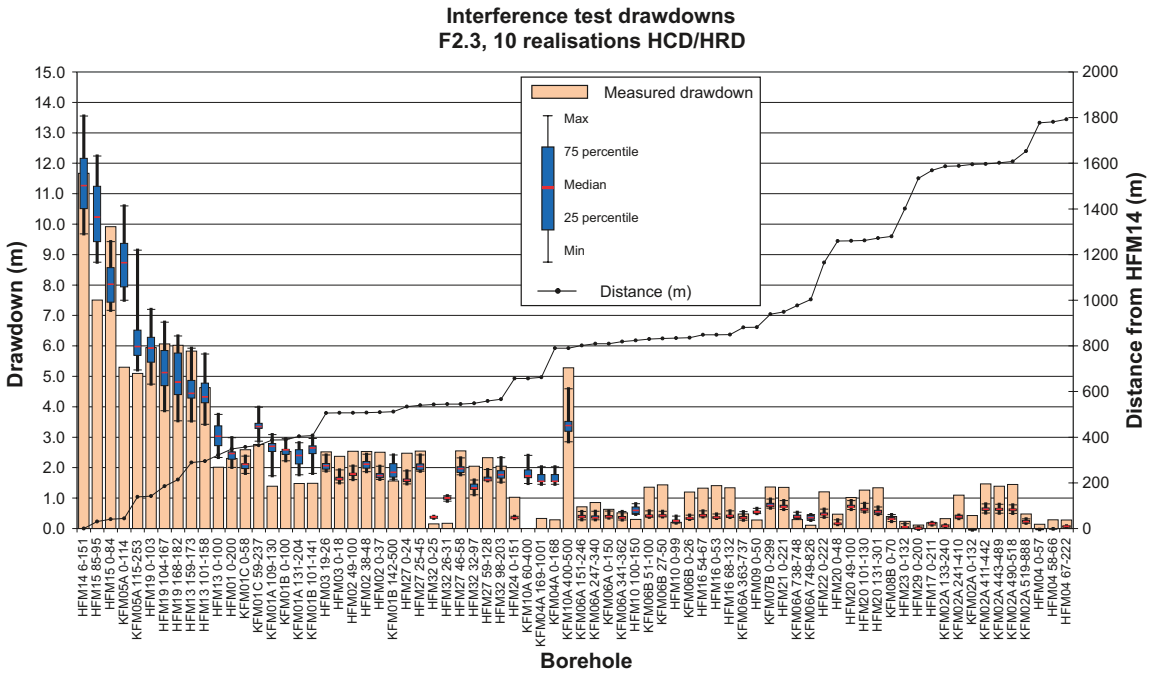

Figure 7-2. *A bar and whisker plot comparing the predictions of drawdown for the HFM14 interference test for 10 realisations of spatial variability in the HCD and HRD. The red line indicates the median drawdown over the 10 realisations, the blue bar indicates the 25/75 percentile, and the whiskers indicate the minimum and maximum simulated drawdown. The brown vertical bars represent the measured drawdown after 21 days of pumping.*

Introducing the additional three possible deformation zones (PDZ) into the HCD model had a similar magnitude of effect as shown in Figure 7-3. These PDZs do not effect the model calibration against the HFM14 interference test, although realisation 3 shows an improvement in the predictions for KFM01A, for example.

In the *stage 2.3 base model simulation*, and stochastic HCD variants, a decision was made to use a 100 m conditioning radius for conditioning the properties of HCD around a measurement point. Figure 7-4 shows the sensitivity of the interference test results to this choice. The conditioning radius only really affects the results at monitoring intervals within about 300 m of HFM14. Using a larger conditioning radius, 150–200 m resulted in a 10–20% reduction in drawdown, while a 50 m conditioning radius made relatively little difference, though possibly a small improvement. Therefore, 50–100 m seems an appropriate scale for the heterogeneity of transmissivity within zones.

Figure 7-5 shows the results of the sensitivity tests to quantify the relative importance of individual zones. The changes to the properties of zone A2, 10 times higher or 10 times lower T, had the greatest effect. (Note: Local conditioning was still applied at the measurement points when the overall value of T within a zone was changed.) Increasing the transmissivity of zone A2 by a factor 10, reduced drawdowns by about 4 m close to HFM14, and increased them by about 4 m when T was decreased. Changing T in zone A2 improved the results in some monitoring points, again suggesting some spatial heterogeneity in zone A2 may be the cause for some of the difference between the stage 2.3 base model predictions and the measurements, and this is true even for some distant monitoring hols such as KFM07B, HFM20 and HFM21. Increasing T in zone ENE0060 made only small difference to the predicted drawdown. Again, to confirm the importance of zone A2 to the HFM14 interference test, increasing the T in all other zones by a factor 10 had a smaller effect than changing zone A2. The other zones only changed the drawdown by 1–2 m. These results underline that the HFM14 interference test has primarily helped confirm the dominance and properties of zone A2 and its connection, to the sheet joint features and the surface boundary conditions.

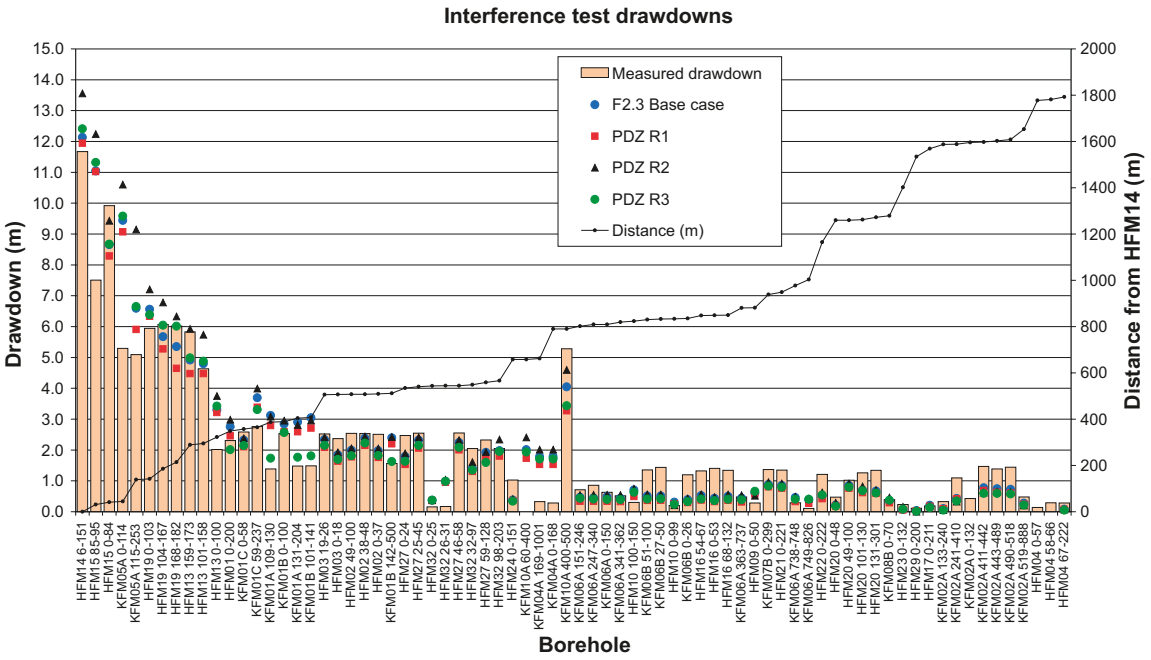

Figure 7-3. *Sensitivities of the drawdown for the HFM14 interference test for three realisations of the potential deformation zones (PDZ) and compared to the stage 2.3 base model simulation. The simulations are shown as dots and the data as vertical bars.*

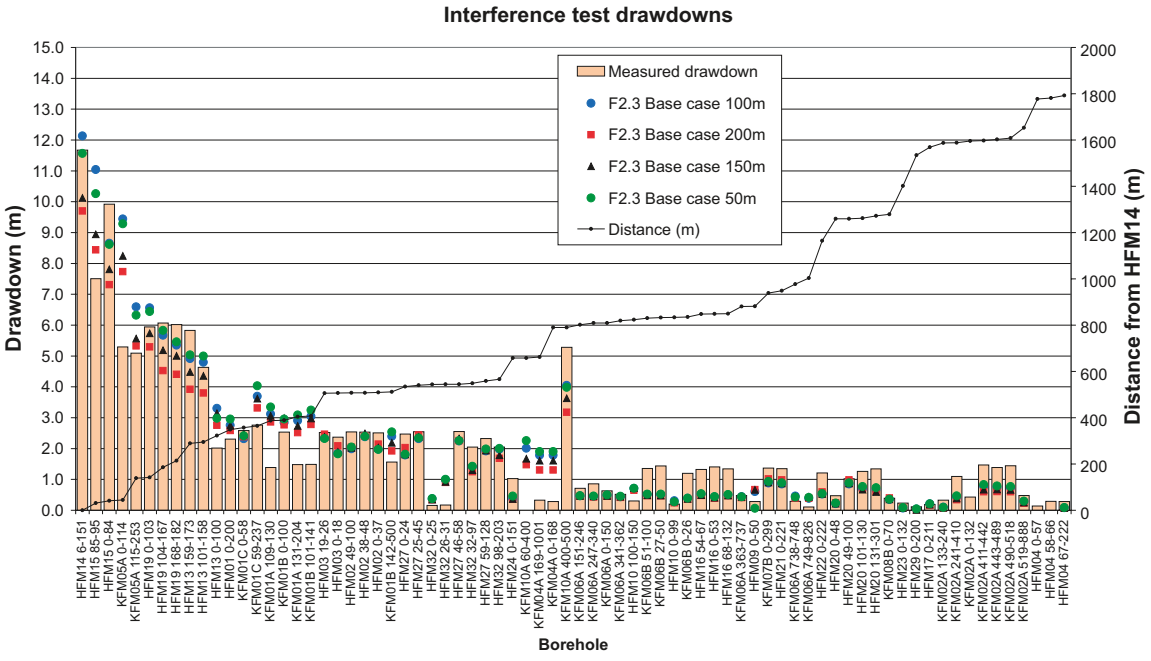

Figure 7-4. *Sensitivities of the drawdown for the HFM14 interference test resulting from changes in the conditioning radius, Δ_c, used in the HCD in comparison to the 2.3 base model simulation. The simulations are shown as dots and the data as vertical bars.*

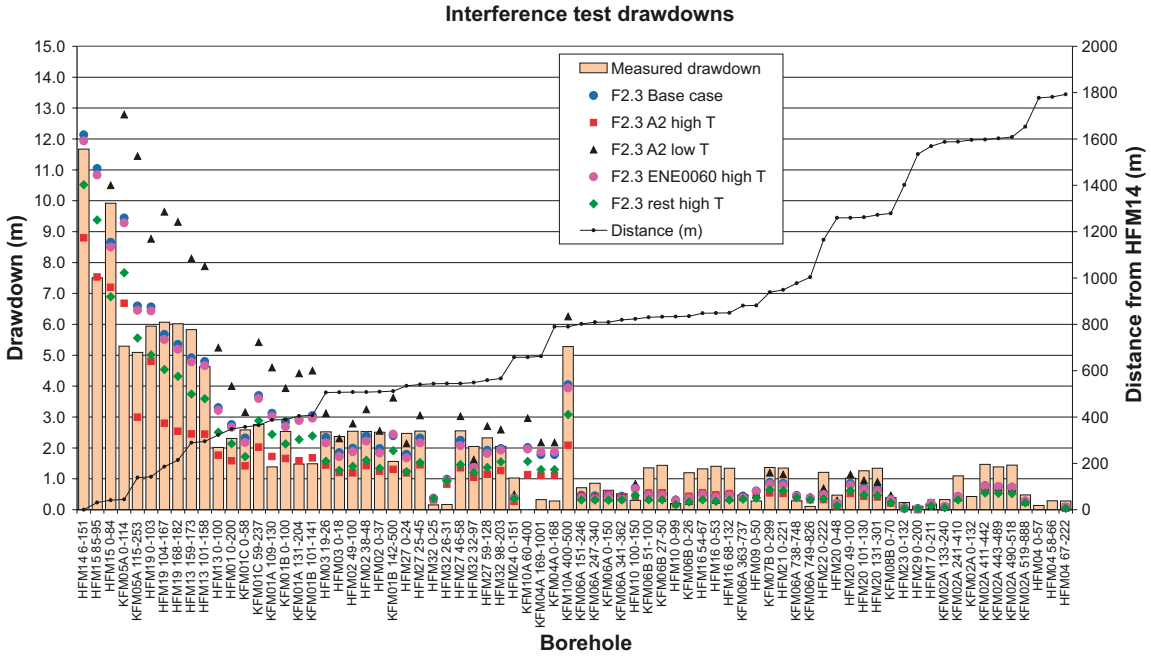

Figure 7-5. *Sensitivities of the drawdown for the HFM14 interference test resulting from changes in the transmissivity of particular zones in comparison to the 2.3 base model simulation. The simulations are shown as dots and the data as vertical bars.*

The sensitivity of the HFM14 interference test to the HSD properties is quantified in Figure 7-6. Using the initial case HSD properties (i.e. $K_h/5$) with a 100:1 anisotropy gives results similar to the *stage 2.3 base model simulation*, but with slightly higher drawdowns. Reducing the anisotropy to 10:1 for the calibrated HSD model lowered the drawdowns significantly and results in a poor calibration to the measured data > 800 m from HFM14. This was the reason for using a high anisotropy of 100:1. Using 1,000:1 makes a slight improvement to the predictions far from HFM14. Therefore, the HFM14 interference test is mainly sensitive to the vertical hydraulic conductivity of the soil and suggests that there should be strong anisotropy.

7.5.2 Groundwater levels

The distribution of natural groundwater levels showed very little sensitivity to heterogeneity of the HCD and HRD as demonstrated by Figure 7-7. The blue bars show the median, minimum and maximum. The variations are typically only a few decimetres. It suggests that the distribution of groundwater levels is mainly governed by the top surface boundary conditions and the properties of the HSD controlling the amount of infiltration through the top surface. Hence, sensitivity cases focussed on variants of the amount of potential infiltration available to recharge the saturated zone and hydraulic properties of the HSD.

The *stage 2.3 base model simulation* assumed an maximum potential infiltration to the saturated zone of 150 mm/year based the results reported by /Johansson 2008/. Results of sensitivity cases with a reduced potential infiltration are presented in Table 7-3. Reducing the maximum potential infiltration form 150 to 70 mm/year reduces the average discrepancy in head from 0.91 to 0.71 m in HFM boreholes and from 0.71 to 0.41 m in SFM boreholes. The groundwater level in the HFM boreholes is not as sensitive as the SFM boreholes because of the strong hydraulic anisotropy introduced into the HSD properties making it a semi-confining layer.

The results of varying the HSD properties are given in Table 7-4. When the initial case HSD properties were used (i.e. $K_h/5$), but anisotropy of 100:1 was retained, then the discrepancy increased significantly toward higher groundwater levels. Using the calibrated HSD properties, the match to the measurements improved as the degree of anisotropy was increased. The best results were obtained with 1,000:1 anisotropy. This is consistent with the HFM14 interference test, and confirms that the near-surface hydrology is best understood in terms of strong anisotropy in the Quaternary deposits and upper bedrock.

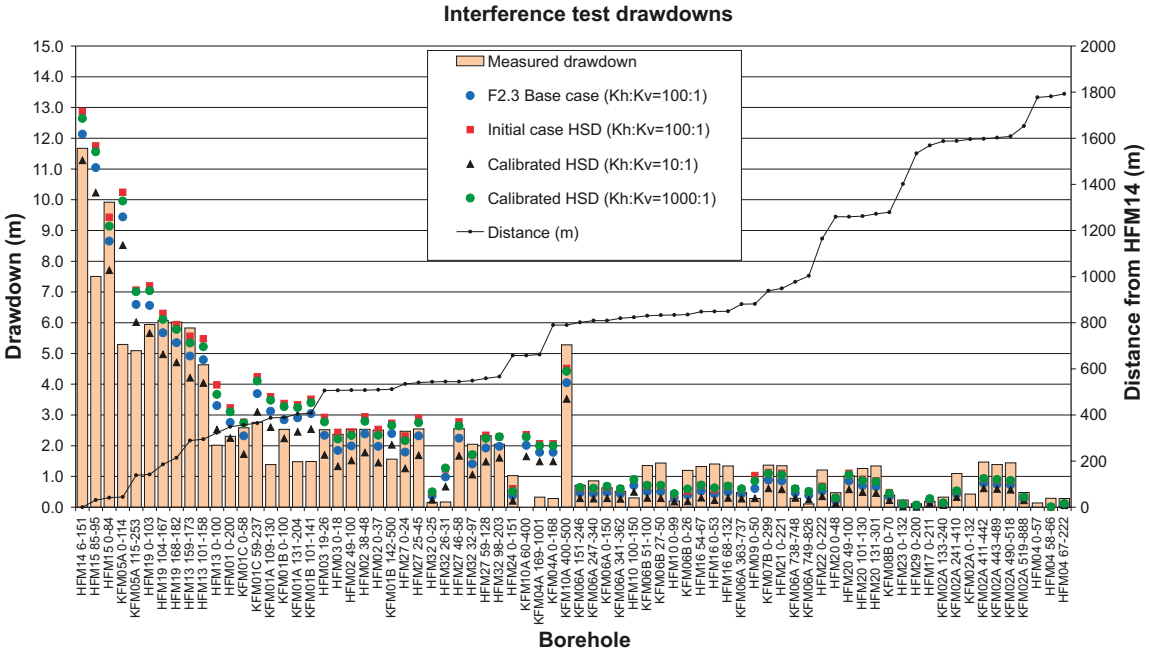

Figure 7-6. *Sensitivities of the drawdown for the HFM14 interference test to the properties of the HSD in comparison to the 2.3 base model simulation. The simulations are shown as dots and the data as vertical bars.*

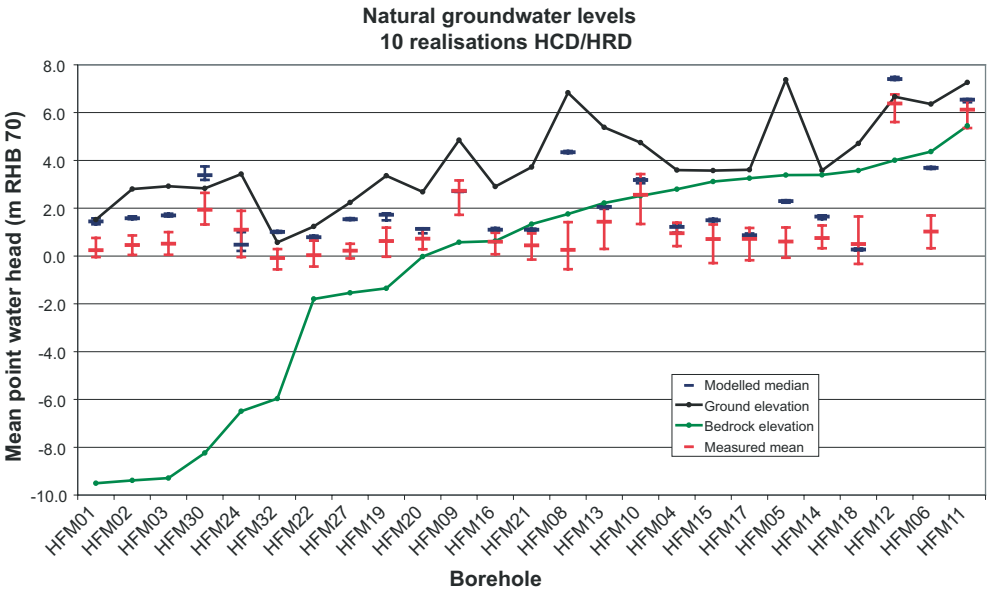

Figure 7-7. *Sensitivities of the natural groundwater levels to 10 realisations of spatial variability in the HCD and HRD. The simulations are shown as blues bars (median, minimum and maximum) and the data as red bars(average, minimum and maximum from different measurement times).*

Table 7-3. The performance of the model in predicting natural groundwater level as a function of maximum potential infiltration to the saturated zone. The average difference in head between the models minus the measurement is calculated over: all HFM boreholes, the HFM boles within the candidate area, and the SFM holes in the Quaternary deposits.

Maximum potential infiltration (mm/year)	Average head difference in HFM holes (m)	Average head difference in HFM holes within candidate area (m)	Average head difference in SFM holes (m)
150 (Base model simulation)	0.91	0.71	0.71
120	0.86	0.67	0.64
100	0.81	0.64	0.56
70	0.71	0.56	0.41

Table 7-4. A comparison of steady-state predictions of average natural groundwater levels for alternative HSD properties suggested by /Bosson et al. 2008/, and different levels of hydraulic anisotropy. The average difference in head between the models minus the measurement is calculated over: all HFM boreholes, the HFM boreholes within the target area, and the SFM boreholes in the Quaternary deposits.

Case	Average head difference in HFM holes (m)	Average head difference in HFM boreholes within target area (m)	Average head difference in SFM boreholes (m)
Calibrated case HSD, $K_v = K_h/100$ (Base model)	0.91	0.71	0.71
Initial case HSD, $K_v = K_h/100$	1.32	1.12	1.12
Calibrated case HSD, $K_v = K_h/10$	1.03	0.88	0.72
Calibrated case HSD, $K_v = K_h/1{,}000$	0.64	0.37	0.56

7.5.3 Hydrochemistry profiles

The effects of spatial variability on predictions of the main hydrochemical species considered are estimated in Figure 7-8 and Figure 7-9. Here, the simulations of palaeo-hydrogeology for 10 realisations of the HCD and HRD properties are shown in red for Cl, Br/Cl, $\delta^{18}O$ and HCO_3 with a solid line to show the mean, and dashed lines to show the minimum and maximum prediction at each depth over the realisations. Each of these 10 realisations is stochastic, with spatial variability within each HCD. They are compared with the *stage 2.3 base model simulation*, which has deterministic HCD properties, and measured data for KFM01D and KFM06A, which each have samples from both the fracture water and pore water. In a sense, these plots indicate the margin to which we should expect any individual simulation, such as the *stage 2.3 base model simulation*, to predict the measured data. The prediction of Cl and HCO_3 are relatively stable between realisations, suggesting models should be expected to give quite close approximation to the data from these species, whereas Br/Cl and $\delta^{18}O$ vary more between realisations, especially for KFM01D. It is interesting that the *stage 2.3 base model simulation* over-predicted glacial water in KFM01D, while a number of the stochastic realisation give a much better prediction. Overall, the envelope of realisation captures much of the sampled data and shows that the few shortcomings in the stage 2.3 base model predictions may be explained by heterogeneity. Potentially, one could use the hydrochemistry results to identify simulations that give further improvements to the matching.

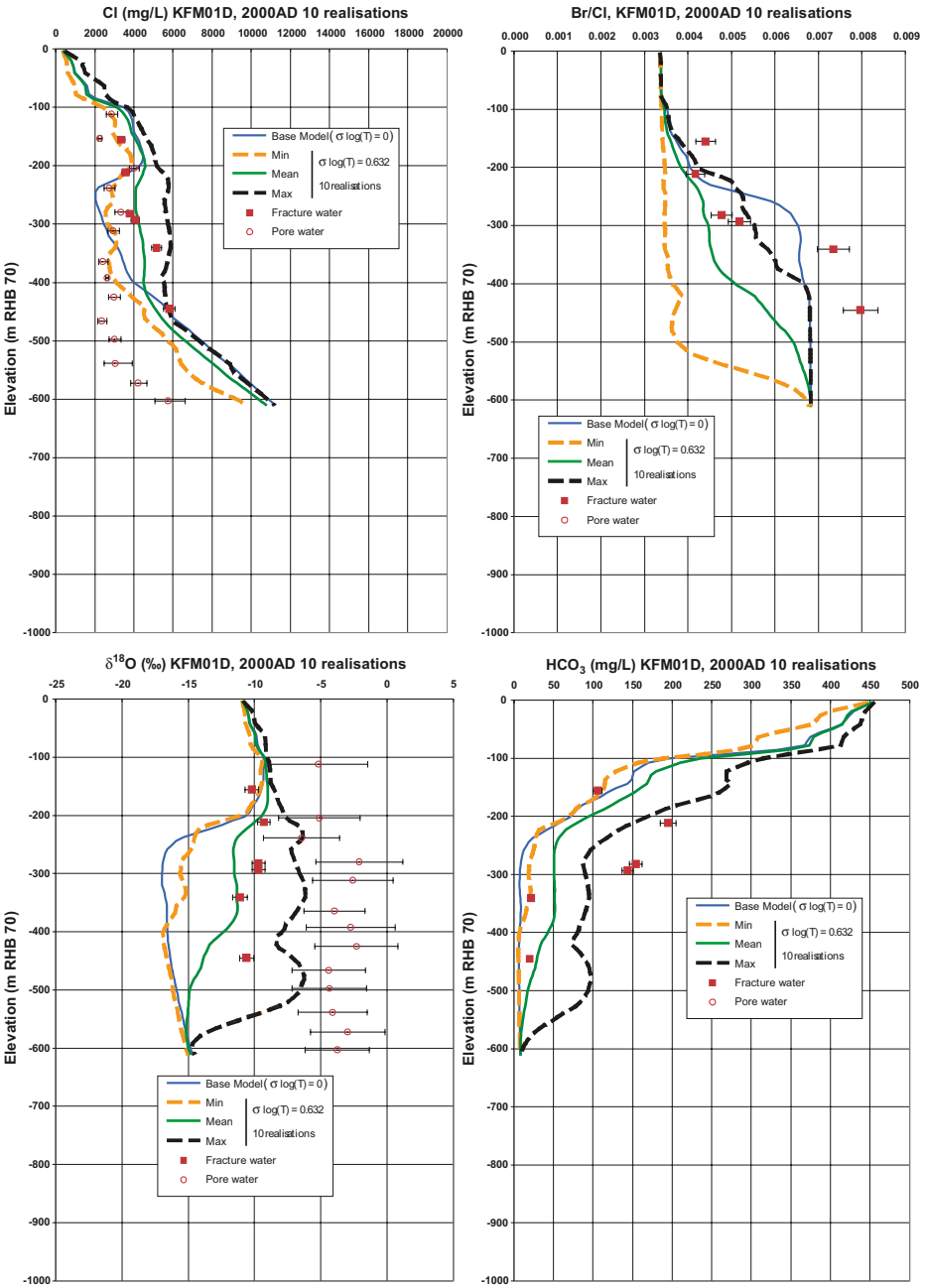

Figure 7-8. *An indication of the uncertainty in predictions of different hydrochemical components in KFM06A associated with heterogeneity in transmissivity. The blue line shows the result for the stage 2.3 base model simulation. The red line represent the mean of 10 realisations of varying transmissivity in the HCD and the HRD. The dashed lines show the minimum and maximum in these realisations. The field data are shown by points.*

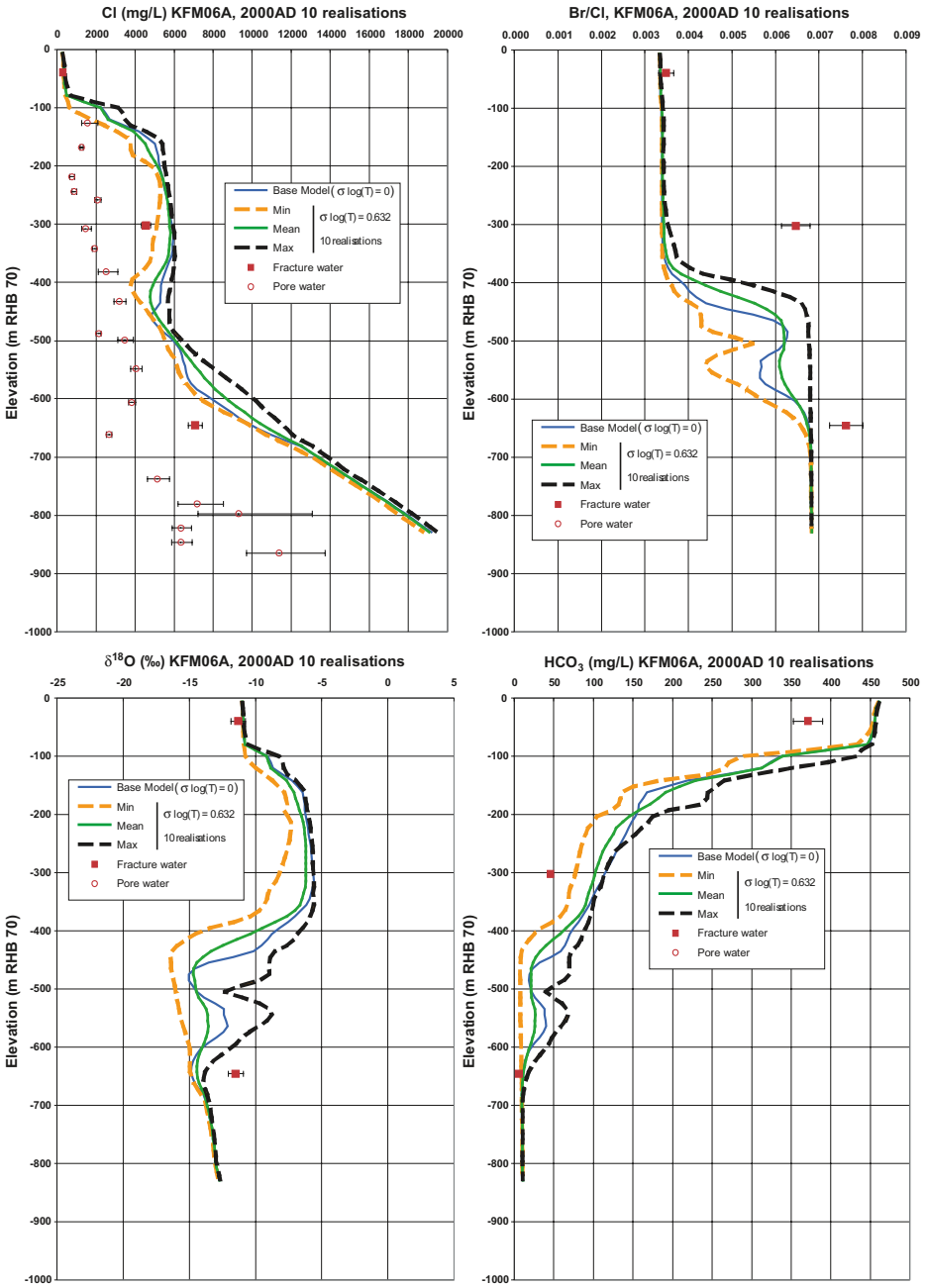

Figure 7-9. *An indication of the uncertainty in predictions of different hydrochemical components in KFM06A associated with heterogeneity in transmissivity. The blue line shows the result for the stage 2.3 base model simulation. The red line represent the mean of 10 realisations of varying transmissivity in the HCD and the HRD. The dashed lines show the minimum and maximum in these realisations. The field data are shown by points.*

7.6 Sensitivities of particle tracking

Two main questions were considered with regards to particle tracking for a release from an approximation of the D1 repository layout:

- How sensitive are the exit locations to spatial heterogeneity in the HCD and HRD and are the exit locations predicted by the *stage 2.3 base model simulation* representative?
- How much do the properties of the Singö zone effect the discharge area, for example making it less conductive or a barrier to flow?

The first of these issues was addressed by comparing the set of exit locations predicted by the 10 stochastic sensitivity cases which have spatial heterogeneity within the HCD and are based on different realisations of the Hydro-DFN model used to derive the spatially varying HRD properties. Around 300 particle tracks were calculated for each of the 10 realisations to give an ensemble of exit locations which is compared with the exit locations for the *stage 2.3 base model simulation* in Figure 7-10. This confirms that the *stage 2.3 base model simulation*, which uses deterministic HCD properties, gives a consistent prediction of the main discharge areas, which is not unexpected since the exit locations are largely controlled by the deterministically modelled geological structures, i.e. HCD. Heterogeneity does not disperse the exit locations to any radical degree.

In terms of individual exit locations, the average variation in particle exit location for the same start point between the stochastic realisations and the *stage 2.3 base model simulation* is 1.2 km. Therefore, heterogeneity can have a significant effect on the fate of an individual particle, but the numbers and positions of key discharge areas is quite stable.

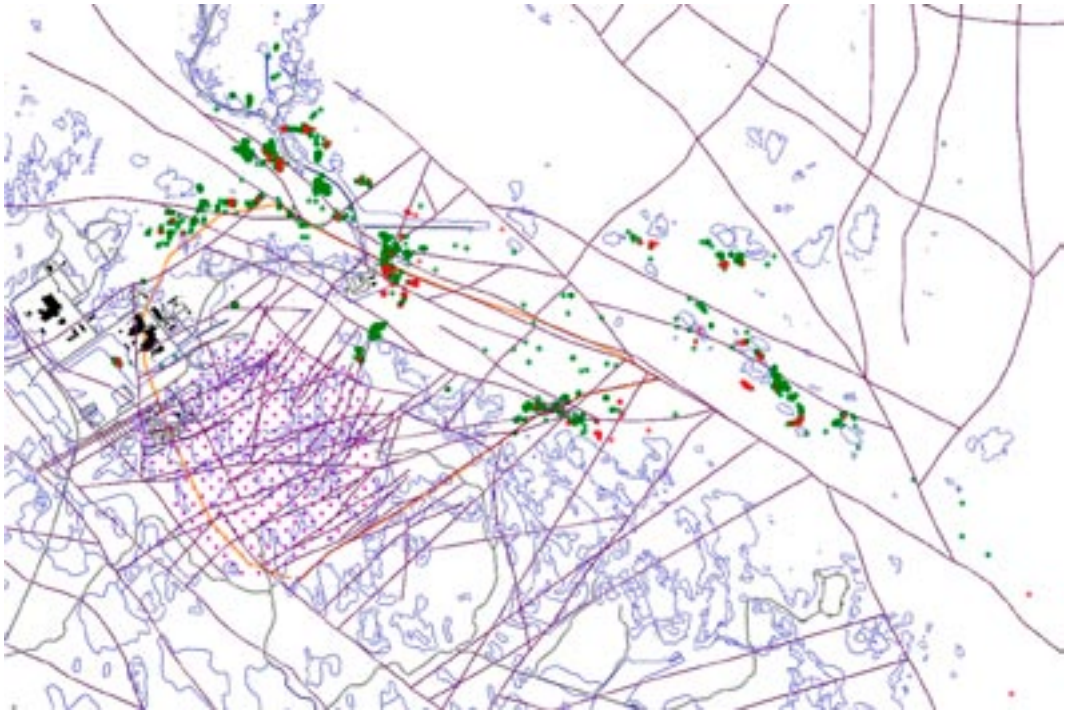

Figure 7-10. *Plan view of the target area with predicted flow paths and exit locations of c. 300 particles for the stage 2.3 base model simulation (red dots) and from the ensemble of 10 realisations of spatial heterogeneity in HCD and HRD (green dots). The particles were released in a 100 m by 100 m mesh at –500 m RHB 70 using an approximation of the D1 repository layout.*

Figure 7-10 confirms the importance of the Singö deformation zone to discharge locations around the peninsula where the SFR buildings are located, as already indicated in Figure 6-3. Two variants were made with a reduced transverse hydraulic conductivity through the Singö deformation zone to act as a partial barrier to flow beyond the zone. However, in doing this there was also the consideration of what property to use at the intersect between the WNW Singö deformation zone and other steeply dipping ENE deformation zones or sub-horizontal sheet joint features. Since evidence of the drawdown from the SFR repository has thought to have been witnessed in the part of the target area, it was decided to have the sheet joints features penetrate the Singö deformation zone. This means that particles could still pass through the Singö deformation zone in some localised areas. Figure 7-11 shows the results of reducing the transverse conductivity of Singö by a factor 1/10 and 1/100. Interestingly, 1/10 decrease reduced the length of particle tracks to the east, but had less effect around the SFR repository. A reduction of 1/100 shorten the paths more dramatically with most particles discharging around the outcrop of Singö or the immediate area around the SFR repository.

7.7 Conclusions

A comprehensive set of uncertainties have been quantified to each of the model elements: HCD, HRD and HSD as well as boundary conditions both in terms of their effects on the model calibration processes used in deriving the *stage 2.3 base model simulation*, and in predictions of discharge areas for groundwater flow through the repository target area.

Sensitivity studies confirm that the HFM14 interference test has primarily helped inform the large-scale hydraulic properties of the major A2 deformation zone, as well as its connection to the sheet joint features and the top surface boundary conditions. Other results from the HFM14 interference test are that heterogeneity may account for some of the variability in the magnitude of drawdowns for boreholes < 800 m away from HFM14, 50–100 m is an appropriate scale for heterogeneity, and the HSD and/or uppermost bedrock is very anisotropic, 100:1 or 1,000:1 for $K_h : K_v$.

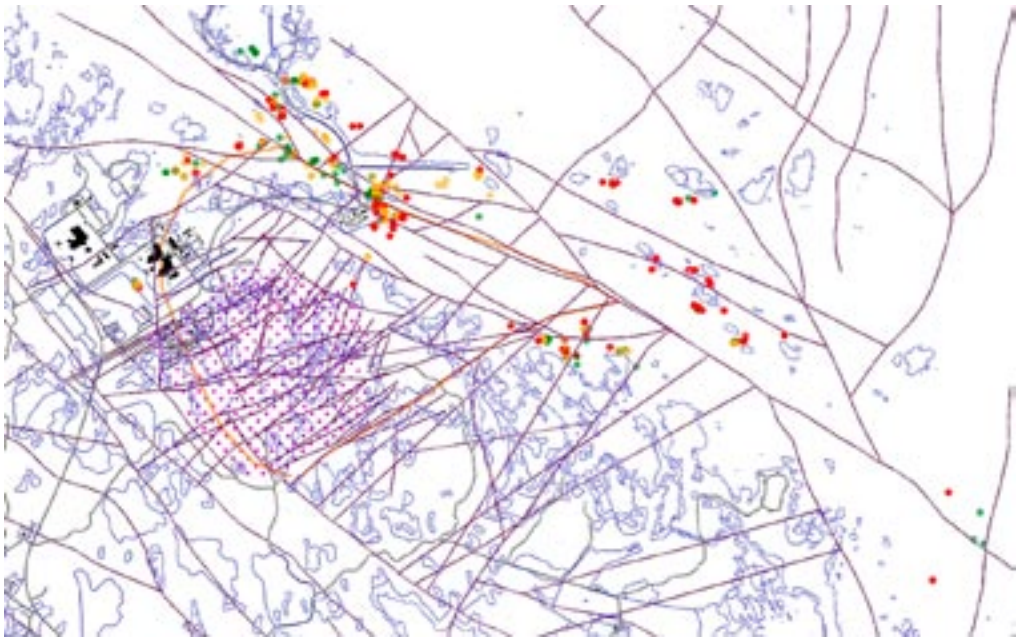

Figure 7-11. *Plan view of the target area with predicted flow paths and exit locations of c. 300 particles for the stage 2.3 base model simulation (red dots), for the sensitivity case with a 1/10 transverse hydraulic conductivity through the Singö zone (orange), and for the sensitivity case with a 1/100 transverse hydraulic conductivity through the Singö zone (green). The particles were released in a 100 m by 100 m mesh at 500 m depth using an approximation of the D1 repository layout.*

The natural groundwater levels are relatively insensitive to heterogeneity and bedrock properties in general. Rather they are governed by the top surface boundary conditions, i.e. amount of potential infiltration, and the hydraulic properties of the HSD. Generally, the results are improved as the horizontal hydraulic conductivity of HSD is increased, or vertical hydraulic conductivity is decreased, confirming that high degrees of anisotropy in the HSD and/or uppermost bedrock is very anisotropic seem to characterise the site.

Sensitivities of the predictions of hydrochemistry simulations to heterogeneity demonstrate that prediction of Cl and HCO_3 are relatively stable between realisations and so these species should be matched to a relatively high degree, as is the case for the stage 2.3 base case. There is a higher degree of variability in the predictions of Br/Cl and $\delta^{18}O$ between realisations, which varies between boreholes. Overall, the envelope of realisation captures much of the sampled data and shows that the few shortcomings in the stage 2.3 base case predictions may be explained by heterogeneity. Potentially, one could use the hydrochemistry results to identify simulations that give further improvements to the matching.

Sensitivities studies considering the role of spatial heterogeneity on discharge locations for the repository target area corroborate that the *stage 2.3 base model simulation* gives a consistent prediction of the main discharge areas, confirming the deterministically modelled geological structures are the dominant control on groundwater pathways, and that hydraulic heterogeneity does not disperse the exit locations to any radical degree. Exploratory simulations considering the Singö deformation zone as potential barrier to flow emphasise the importance of this zone for controlling the ultimate fate of any release.

8 Conclusions

8.1 Conceptual modelling

The conceptual modelling in stage 2.2 invoked three important hypotheses that were addressed in stage 2.3 by means of complementary field investigations (hydraulic tests).

Hypothesis I: The field investigations carried out suggest that the gently dipping deformation zones that occur predominantly in the hanging wall bedrock of zones A2 and F1 are the most transmissive at each elevation. The steeply dipping deformation zones that strike WNW and NW was hypothesised in stage 2.2 to come in second place as far as transmissivity is concerned. The steeply dipping deformation zones that strike ENE and NNE occur in the footwall bedrock mainly. These zones can occasionally also be fairly transmissive, but a main characteristic, as it appears from data, is that they are on the average the least transmissive but at the same time significantly more heterogeneous laterally than the other categories of deformation zones. The validity of this hypothesis may be constrained to the upper 400–500 m of bedrock, however.

The hypothesis was tested in stage 2.3 by means of single-hole hydraulic tests in the new boreholes the new boreholes KF08D, KFM11A, KFM12A, HFM34, HFM36 and HFM37 (see Appendix A, Figure A-1 and Figure A-2). These boreholes, except for KFM08D, intersect the regionally significant, ductile and brittle Singö and Forsmark deformation zones that border the tectonic lens and the candidate area. In contrast, KFM08D intersect a series of zones inside the target area that strike NNE-ENE.

Hypothesis II: Fracture domain FFM06 is one of three fracture domains within the so-called target area, the other being FFM01 and FFM02. Due to lack of boreholes and hydraulic data in FFM06, it was hypothesised in stage 2.2 that this fracture domain has the same hydrogeological (structural-hydraulic) properties as inferred from the tests run in fracture domain FFM01. This hypothesis was tested in stage 2.3 by means of single-hole hydraulic tests in the new borehole KFM08D.

Hypothesis III: It was assumed in stage 2.2 that the sheet joints encountered in the target area follow the undulations of the bedrock surface, implying that some of them do not outcrop but stay below the bedrock surface as this dips under the Baltic Sea. The horizontal extent of the sheet joint was assumed to form a triangle bounded to the northeast by the Singö deformation zone, (WNW0001), to the southeast by the NE0062A deformation zone, and to the west by the expression of the sheath fold structure in rock domains 32 and 44. This hypothesis was tested hydraulically in stage 2.3 by means of an interference test conducted at the new percussion-drilled borehole HFM33 drilled on the peninsula close to the SFR buildings.

The results from the hydraulic tests carried out in stage 2.3 do not falsify or contradict any of these hypotheses, hence none of them should be rejected. In fact, the hypotheses are all supported by new evidence, which strengthens the overall credibility in the conceptual model developed in stage 2.2.

8.2 Numerical modelling

The primary objective of the numerical modelling carried out in stage 2.3 is to address the sensitivity of the calibrated groundwater flow and solute transport model developed in stage 2.2 to parameter uncertainty. A comprehensive set of uncertainties have been quantified to each of the model elements: HCD, HRD and HSD as well as boundary conditions both in terms of their effects on the model calibration processes and in predictions of discharge areas for groundwater flow through the repository candidate volume. The results from the numerical modelling and the sensitivity tests carried out may be summarised as follows:

Transient, large-scale cross-hole (interference) tests

Sensitivity studies confirm that the large-scale cross-hole (interference) test carried out in stage 2.2 – 21 days of pumping in borehole HFM14 – has primarily helped inform the large-scale hydraulic properties of the major A2 deformation zone as well as its connection to the sheet joints (called cage features in the numerical model), and the top surface boundary conditions. Other important results from the HFM14 interference test are that heterogeneity in the hydraulic properties of the HCD and the cage features may account for some of the variability in the magnitude of drawdowns for bedrock boreholes less than c. 800 m away from HFM14, that 50–100 m is an appropriate integral scale for this heterogeneity, and that the HSD and/or uppermost bedrock is very anisotropic; the transient simulations reported here indicate 100:1 or 1,000:1 for $K_h : K_v$.

Natural groundwater levels

The steady-state model of the natural groundwater level (point-water head) measurements in the uppermost part of the bedrock are relatively insensitive to structural-hydraulic heterogeneity and bedrock properties in general. Rather they are governed by the top surface boundary conditions, i.e. amount of potential infiltration, and the hydraulic properties of the HSD. Generally, the results are improved as the horizontal hydraulic conductivity of HSD is increased, or vertical hydraulic conductivity is decreased, confirming that high degrees of anisotropy in the HSD and/or uppermost bedrock seem to characterise the site.

Hydrochemical data in deep boreholes

Sensitivities of the predictions of the hydrochemical conditions at depth to heterogeneity in the structural-hydraulic properties demonstrate that prediction of Cl and HCO_3 are relatively stable between realisations and so these species should be matched to a relatively high degree, as is the case for the *stage 2.3 base model simulation* (a single realisation of the HRD and no lateral heterogeneity in the hydraulic properties of the HCD). There is a higher degree of variability in the predictions of Br/Cl and $\delta^{18}O$ between realisations, which varies between boreholes. Overall, the envelope of realisations captures much of the sampled data and shows that the few shortcomings in the predictions of the *stage 2.3 base model simulation* may be explained heterogeneity in the structural-hydraulic properties. Potentially, one could use the hydrochemical results to identify simulations that give further improvements to the matching.

Particle tracking

Sensitivities studies considering the role of structural-hydraulic heterogeneity on discharge locations for the repository target volume corroborate that the *stage 2.3 base model simulation* gives a consistent prediction of the main discharge areas, confirming that the deterministically modelled geological structures are the dominant control on groundwater pathways, and that hydraulic heterogeneity does not disperse the exit locations to any radical degree. Exploratory simulations considering the Singö deformation zone as potential barrier to flow emphasise the importance of this zone for controlling the ultimate fate of any release.

8.3 Confidence and remaining uncertainties

Model calibration is non-unique in that different combinations of parameter settings may achieve equally good and plausible matches to the test data. In the process of calibrating the numerical model against single-hole hydraulic tests, cross-hole tests, natural point-water head measurements and hydrochemical data samples, a number of lessons were learnt in terms of the key features, processes and parameters required to mimic the observed behaviour of the hydrogeological system. Sensitivities to various features and parameters had to be considered to find one or more ways to honour the field data. This prompted relatively few changes to the initial implementation of the conceptual model within the reasonable ranges of parameter uncertainty. In conclusion, there is a good understanding of the overall hydrogeology inside the target volume and the confidence in the developed models is high. The remaining uncertainties concern predominantly the structural hydraulic conditions outside this volume. These are identified and described in /SKB 2008/. Three uncertainties that affect the modelling of the hydrogeological conditions inside the target volume are described below in sections 6.4 through 8.3.3.

8.3.1 Groundwater levels in the shallow bedrock aquifer

The CONNECTFLOW model uses a simplistic representation of the near-surface hydrogeological system and aims at matching the average groundwater levels of time series data in different boreholes with a steady-state flow model. Although, the magnitude and direction of the modelled gradient between the Quaternary deposits and the uppermost bedrock in the CONNECTFLOW model is in accordance with the monitoring data, the absolute values of the simulated average groundwater levels are a too high, c. +0.7 m of mean difference for both the percussion-drilled boreholes and the monitoring wells *within* the target volume. In comparison, the results reported from the MIKE SHE model, which uses a detailed representation of the near-surface hydrogeological system and models the time series data on a diurnal basis, suggest that the low groundwater levels measured in the uppermost part of the bedrock cannot be matched unless there is a continuous sink somewhere in the bedrock. That is, without a continuous sink in the bedrock, the downward hydraulic gradients between the Quaternary deposits and the uppermost bedrock are not as pronounced in the MIKE SHE model as they are in the field measurements (and in the CONNECTFLOW model). In fact, the simulated hydraulic gradients locally points upwards in the MIKE SHE model unless there is a continuous sink in the bedrock. If this is the case or not cannot be readily checked because there are no known continuous sinks within the target area. (It is noted that the simulated groundwater levels in the Quaternary deposits in the MIKE SHE model are independent of whether or not there is a sink in the bedrock.)

There are two examples of sinks in the uppermost bedrock not far form the target area, none of which that can be turned off, however. The stronger of the these sinks is the abstraction of drainage water in the SFR repository. The SFR repository is located below the Baltic Sea and is reached by two tunnels, which cross the Singö deformation zone. The drainage water is abstracted at two pump stations. The first pump station is located after the crossing of the Singö deformation zone (88 m depth; 1.2 L/s) and the other is located below the bottom of the SFR repository (140 m depth; 4.8 L/s). The other example of a sink is the lowering of the groundwater level beneath the three nuclear power reactors, which are located northwest of the target area. The pumping under the reactors is not continuous (c. 20 m depth; c. 1–2 L/s of intermittent pumping).

The simulations carried out with the MIKE SHE model suggest that a continuous abstraction of drainage water in the SFR repository affects the on-shore groundwater levels in the uppermost part of the bedrock within the target volume. It is noted that the calibrated MIKE SHE model is based on the CONNECTFLOW model with two main exceptions: 1) the horizontal hydraulic conductivity, K_h,was increased ten times in the part of the model describing the sheet joints only (Figure 3-20), and 2) the vertical hydraulic conductivity, K_v, was decreased ten times in the uppermost 200 m of bedrock throughout the entire model domain.

The results obtained from the single-hole geological interpretation and hydraulic testing of borehole KFM11A, which investigates the Singö deformation zone, together with the interference test data obtained from the interference test at borehole HFM33 during the fall of 2007, suggest that the Singö deformation zone is hydraulically heterogeneous and has a very low transverse transmissivity in the surroundings of the SFR buildings, i.e. there are no hydraulic responses observed in boreholes HFM34, HFM35 and KFM11A while pumping in borehole HFM33. The crossing of the two SFR tunnels could provide a possibility for a hydraulic interference through the Singö deformation zone, but the tunnels cross through the zone in close proximity to borehole HFM34, which did not respond to the pumping in borehole HFM33.

In conclusion, the prevailing situation, with quite low groundwater levels in the shallow bedrock within the target area, may partly be caused by the pumping in the SFR repository. However, no definite conclusions on this issue can be made based on existing data. The CONNECTFLOW model assumes that the Singö deformation zone is heterogeneous, but the model is not calibrated for a scenario where there is a continuous sink in the bedrock in the SFR repository. However, exploration simulations, with the pumping in the SFR repository included in the calibrated CONNECTFLOW model, confirm that the hydraulic properties of the shallow bedrock aquifer system reported in the SDM are credible and adequate for further modelling, because the differences between measured and simulated groundwater levels decrease when the pumping in the SFR repository is incorporated. That is, even if the abstraction of drainage water in the SFR repository is an uncertain boundary condition that may affect the natural groundwater levels, the hydraulic stresses (drawdowns) induced by the cross-hole tests run in the target area apparently are sufficiently strong to allow for a fair calibration of the hydraulic properties.

8.3.2 Compartmentalised fracture networks at repository depth

The hydraulic description of the less fractured bedrock between the deformation zones is focussed on the conductive fracture frequency (CFF) of continuously flowing fractures. This means that the connected fracture network situations were regarded as more important for the hydrogeological DFN modelling and the groundwater flow modelling in the site description than disconnected (compartmentalised) network situations. The role of compartmentalised networks, if any, needs to be addressed in the safety assessment.

8.3.3 Evaluation of PFL-f transmissivity data

It is important to recollect what is actually measured with the PFL-f tests. For each PFL-f transmissivity value identified, the change in flux (inflow) and head (drawdown) after several days of pumping relative to conditions prior to pumping are calculated. A transmissivity value is interpreted for each PFL-f test based on Thiem's equation /Thiem 1906/ and an assumed value of the radius of influence to borehole radius ratio (R_0 / r_w) = 500. The choice of 500 reflects that tests are performed over several days, and hence should represent an effective transmissivity of the whole fracture intersected, and possibly adjoining parts of the network, but the choice of 500 is otherwise arbitrary. Consequently, the interpreted values of transmissivity should not be viewed as necessarily the transmissivity of individual fractures, or the transmissivity of the fracture local to the borehole intersect. They are more indicative of the effective transmissivity over a larger scale. This remark influences the way the PFL-f data are used in the hydrogeological DFN modelling as explained in the present report, see section 3.4.3.

References

Andersson J, Ström A, Almén K-E, Ericsson LO, 2000. Vilka krav ställer djupförvaret på berget? Geovetenskapliga lämplighetsindikationer och kriterier för lokalisering och platsutvärdering. SKB R-00-15, Svensk Kärnbränslehantering AB.

Axelsson C-L, Ekstav A, Lindblad Påssé A, 2002. SFR – Utvärdering av hydrogeologi. SKB R-02-14, Svensk Kärnbränslehantering AB.

Berggren M, 1998. Hydraulic conductivity in Swedish bedrock estimated by means of geostatistics, Thesis Report Series 1998:9, Royal Institute of Technology, Stockholm.

Bosson E, Berglund S, 2006. Near-surface hydrogeological model of Forsmark. Open repository and solute transport applications – Forsmark 1.2. SKB R-06-52, Svensk Kärnbränslehantering AB.

Bosson E, Gustafsson L-Å, Sassner M, 2008. Numerical modelling of surface hydrology and near-surface hydrogeology at Forsmark. Site descriptive modelling, SDM-Site Forsmark. SKB R-08-09, Svensk Kärnbränslehantering AB.

Crawford J, 2008. Bedrock transport properties Forsmark. Site descriptive modelling, SDM-Site Forsmark. SKB R-08-48, Svensk Kärnbränslehantering AB.

Dershowitz W, Winberg A, Hermanson J, Byegård J, Tullborg E-L, Andersson P, Mazurek M, 2003. Äspö Task Force on modelling of groundwater flow and transport of solutes. Task 6c. A semi synthetic model of block scale conductive structures at the Äspö HRL. Äspö Hard Rock Laboratory, International Progress Report IPR-03-13, Svensk Kärnbränslehantering AB.

DHI, 2004. MIKE SHE. An integrated hydrological modelling system. Users guide. DHI Water & Environment, Hørsholm, Denmark.

Follin S, Stigsson M and Svensson U, 2005. Regional hydrogeological simulations for Forsmark - numerical modelling using DarcyTools. Preliminary site description Forsmark area – version 1.2. SKB R-05-60, Svensk Kärnbränslehantering AB.

Follin S, Johansson P-O, Levén J, Hartley L, Holton D, McCarthy R, Roberts D, 2007a. Updated strategy and test of new concepts for groundwater flow modelling in Forsmark in preparation of site descriptive stage 2.2. SKB R-07-20, Svensk Kärnbränslehantering AB.

Follin S, Levén J, Hartley L, Jackson P, Joyce S, Roberts D, Swift B, 2007b. Hydrogeological characterisation and modelling of deformation zones and fracture domains, Forsmark modelling stage 2.2. SKB R-07-48, Svensk Kärnbränslehantering AB.

Follin S, Johansson P-O, Hartley L, Jackson P, Roberts D, Marsic N, 2007c. Hydrogeological conceptual model development and numerical modelling using CONNECTFLOW, Forsmark modelling stage 2.2. SKB R-07-49, Svensk Kärnbränslehantering AB.

Fox A, La Pointe P, Hermanson J, Öhman J, 2007. Statistical geological discrete fracture network model for the Forsmark site, stage 2.2. Forsmark stage 2.2. SKB R-07-46, Svensk Kärnbränslehantering AB.

Glamheden R, Fredriksson A, Persson L, Röshoff K, Karlsson J, Bohlin H, Lindberg U, Hakami H, Hakami E, Johansson M, 2007. Rock mechanics Forsmark, Site descriptive modelling Forsmark stage 2.2. SKB R-07-31, Svensk Kärnbränslehantering AB.

Gokall-Norman K, Ludvigson J-E, 2007a. Large-scale interference test with borehole HFM14 used as pmping borehole, 2007. Forsmark site investigation. Forsmark site investigation. SKB P-07-228, Svensk Kärnbränslehantering AB.

Gokall-Norman K, Ludvigson J-E, 2007b. Hydraulic interference test with borehole HFM33 used as pumping borehole, November of 2007. Forsmark site investigation. SKB P-07-229, Svensk Kärnbränslehantering AB.

Gustavsson E, Jönsson S, Ludvigson J-E, 2006. Pumping tests and flow logging. Boreholes HFM33, HFM34 and HFM35. Forsmark site investigation. SKB P-06-193, Svensk Kärnbränslehantering AB.

Harrström J, Svensson T, Ludvigson J-E, 2007a. Single-hole hydraulic tests in borehole KFM11A. Forsmark site investigation. SKB P-07-177, Svensk Kärnbränslehantering AB.

Harrström J, Svensson T, Ludvigson J-E, 2007b. Single-hole injection tests in borehole KFM12A. Forsmark site investigation. SKB P-07-121, Svensk Kärnbränslehantering AB.

Hartley L J, Holton D, 2004. CONNECTFLOW (Release 8.0). Technical summary document, Serco Assurance Report SA/ERRA C/TSD02V1.

Hartley L J, Hoch A R, Cliffe K A, Jackson C P, Holton D, 2004a. NAMMU (Release 8.0). Technical summary document, Serco Assurance Report SA/ENV/0626.

Hartley L J, Holton D, Hoch A R, 2004b. NAPSAC (Release 8.0). Technical summary document, Serco Assurance Report SA/ERRA-N/TSD02V1.

Hartley L J, Cox I, Hunter F, Jackson C P, Joyce S, Swift B, Gylling B, Marsic N, 2005. Regional hydrogeological simulations for Forsmark – numerical modelling using CONNECTFLOW, Preliminary site description Forsmark area – stage 1.2. SKB R-05-32, Svensk Kärnbränslehantering AB.

Hartley L J, Hoch A, Jackson C P, Joyce S, McCarthy R, Rodwell W, and Marsic N, 2006. Groundwater flow and transport modelling during the temperate period for the SR-Can assessment – Forsmark subarea – version 1.2, SKB R-06-98, Svensk Kärnbränslehantering AB.

Hedenström A, Sohlenius G, Strömgren M, Brydsten L, Nyman H, 2008. Depth and stratigraphy of regolith at Forsmark. Site descriptive modelling, SDM-Site Forsmark. SKB R-08-07, Svensk Kärnbränslehantering AB.

Hoch A R, Jackson C P, 2004. Rock-matrix Diffusion in Transport of Salinity. Implementation in CONNECTFLOW. SKB R-04-78, Svensk Kärnbränslehantering AB.

Indraratna B, Ranjith P G, Gale, W, 1999. Single phase water flow through rock fractures. Geotechnical and Geological Engineering, 17, 211–240.

Johansson P-O, Werner K, Bosson E, Berglund S, Juston J, 2005. Description of climate, surface hydrology, and near-surface hydrogeology. Forsmark 1.2. SKB R-05-06. Svensk Kärnbränslehantering AB.

Johansson P-O, Juston J, 2007. Monitoring of brook levels, water electrical conductivities, temperatures and discharges from April 2004 until March 2007. Forsmark site investigation. SKB P-07-135, Svensk Kärnbränslehantering AB.

Johansson P-O, 2008. Description of surface hydrology and near-surface hydrogeology at Forsmark. Site descriptive modelling, SDM-Site Forsmark. SKB R-08-08, Svensk Kärnbränslehantering AB.

Juston J, Johansson P-O, 2005. Analysis of meteorological data, surface water level data, and groundwater level data. Forsmark site investigation. SKB P-05-152, Svensk Kärnbränslehantering AB.

Juston J, Johansson P-O, Levén J, Tröjbom M, Follin S, 2007. Analysis of meteorological, hydrological and hydrogeological monitoring data. SKB R-06-49, Svensk Kärnbränslehantering AB.

Laaksoharju M, Smellie J, Tullborg E-L, Gimeno M, Hallbäck L, Molinero J, Waber N, 2008a. Bedrock hydrogeochemistry Forsmark. Site descriptive modelling, SDM-Site Forsmark. SKB R-08-47, Svensk Kärnbränslehantering AB.

Marsic N, Hartley L, Jackson P, Poole M, 2001. Development of hydrogeological modelling tools based on NAMMU. SKB R-01-49, Svensk Kärnbränslehantering AB.

Martin C D, Follin S, 2008. Review of possible correlations between in-situ stress and transmissivity of PFL-f data at Forsmark. SKB R-08-69, Svensk Kärnbränslehantering AB.

Nordqvist R, Gustafsson E, Andersson P, Thur P, 2008. Groundwater flow and hydraulic gradients in fractures and fracture zones at Forsmark and Oskarshamn. SKB R-08-103, Svensk Kärnbränslehantering AB.

Olofsson I, Simeonov A, Stephens M, Follin S, Nilsson A-C, Röshoff K, Lindberg U, Lanaro F, Fredriksson A, Persson L, 2007. Site descriptive modelling Forsmark, stage 2.2: Presentation of a fracture domain concept as a basis for the statistical modelling of fractures and minor deformation zones, and interdisciplinary coordination. SKB R-07-15, Svensk Kärnbränslehantering AB.

Olsson T, 1979. Hydraulic properties and groundwater balance in a soil-rock aquifer system in the Juktan area, northern Sweden. Striae 12, 72 pp. Uppsala.

Påsse T, 1996. A mathematical model of the shore level displacement in Fennoscandia. SKB TR 96-24, Svensk Kärnbränslehantering AB.

Påsse T, 1997. A mathematical model of past, present and future shore level displacement in Fennoscandia. SKB TR-97-28, Svensk Kärnbränslehantering AB.

Påsse T, 2001. An empirical model of glacio-isostatic movements and shore-level displacement in Fennoscandia. SKB R-01-41, Svensk Kärnbränslehantering AB.

Raven K G, Gale J E, 1985. Water flow in a natural rock fracture as a function of stress and sample size. Int. J. Rock. Mech. Min. Sci. & Geomech Abstr. 22, 251–261.

Rhén I, Forsmark T, 2001. Äspö Hard Rock Laboratory. Prototype Repository. Hydrogeology. Summary report of investigations before the operation phase. SKB IPR-01-65, Svensk Kärnbränslehanetring AB.

Rhén I, Follin S, Hermanson J, 2003. Hydrological Site Descriptive Model – a strategy for its development during Site Investigations. SKB R-03-08, Svensk Kärnbränslehantering AB.

SKB 2005. Hydrogeochemical evaluation for Forsmark version 1.2. Preliminary site description of the Forsmark area. SKB-R-05-17. Svensk Kärnbränslehantering AB.

SKB 2006a. Site descriptive modelling Forsmark stage 2.1 – Feedback for completion of the site investigation including from safety assessment and repository engineering. SKB R-06-38, Svensk Kärnbränslehantering AB.

SKB 2006b. Prediction of hydraulic properties in KFM08D. Documentum 1071524, Svensk Kärnbränslehantering AB.

SKB 2008. Confidence assessment Forsmark, Site descriptive modelling, SDM-Site Forsmark. SKB R-08-82, Svensk Kärnbränslehantering AB.

Stephens M B, Fox A, La Pointe P R, Isaksson H, Simeonov A, Hermanson J, Öhman J, 2007. Geology – Site descriptive modelling Forsmark stage 2.2. SKB R-07-45, Svensk Kärnbränslehantering AB.

Thiem G, 1906. Hydrologische Methoden, J M Gebhardt, Leipsig.

Tröjbom M, Söderbäck B, Johansson P-O, 2007. Hydrochemistry in surface water and shallow groundwater Site descriptive modelling SDM-Site Forsmark. SKB R-07-55, Svensk Kärnbränslehantering AB.

Väisäsvaara J, Pekkanen J, 2007. Difference flow logging in borehole KFM11A. Forsmark site investigation. SKB P-07-85, Svensk Kärnbränslehantering AB.

Walger E, Jönsson S, Ludvigson J-E, 2007. Pumping tests and flow logging. Boreholes HFM36, HFM37 and HFM38. Forsmark site investigation. SKB P-07-22, Svensk Kärnbränslehantering AB.

Werner K, Bosson E, Berglund S, 2006. Analysis of Water Flow Paths: Methodology and Example Calculations for a Potential Repository in Sweden, Ambio, 35(8), 425-434, Royal Swedish Academy of Science.

Werner K, Johansson P-O, Brydsten L, Bosson E, Berglund S, Tröjbom M, Nyman H, 2007. Recharge and discharge of near-surface groundwater in Forsmark. Comparison of classification methods. SKB R-07-08, Svensk Kärnbränslehantering AB.

Winberg A, 1994. Geostatistical analysis of transmissivity data from fracture zones at Äspö. Compilation of data, experimental variography and interference of hard-soft data relationships. Swedish Nuclear Fuel and Waste Management Company. Äspö Hard Rock Laboratory Progress Report SKB PR 25-94-17, Svensk Kärnbärnslehantering AB.

Drill sites and boreholes

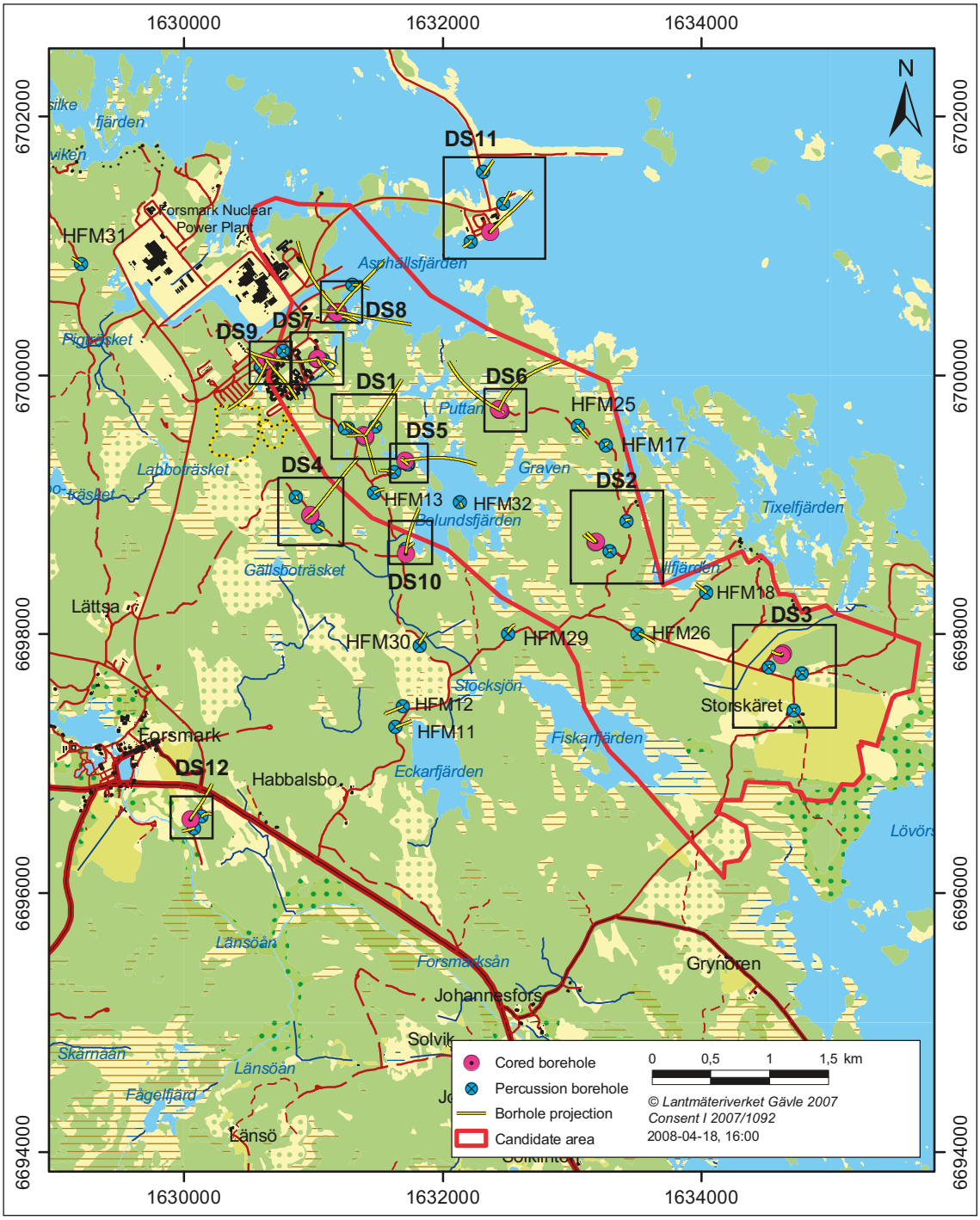

Figure A-1. *Map showing all telescopic, conventionally core-drilled and percussion-drilled boreholes produced during the site investigation at Forsmark 2002–2007. The projection on the ground surface of inclined boreholes is also illustrated.*

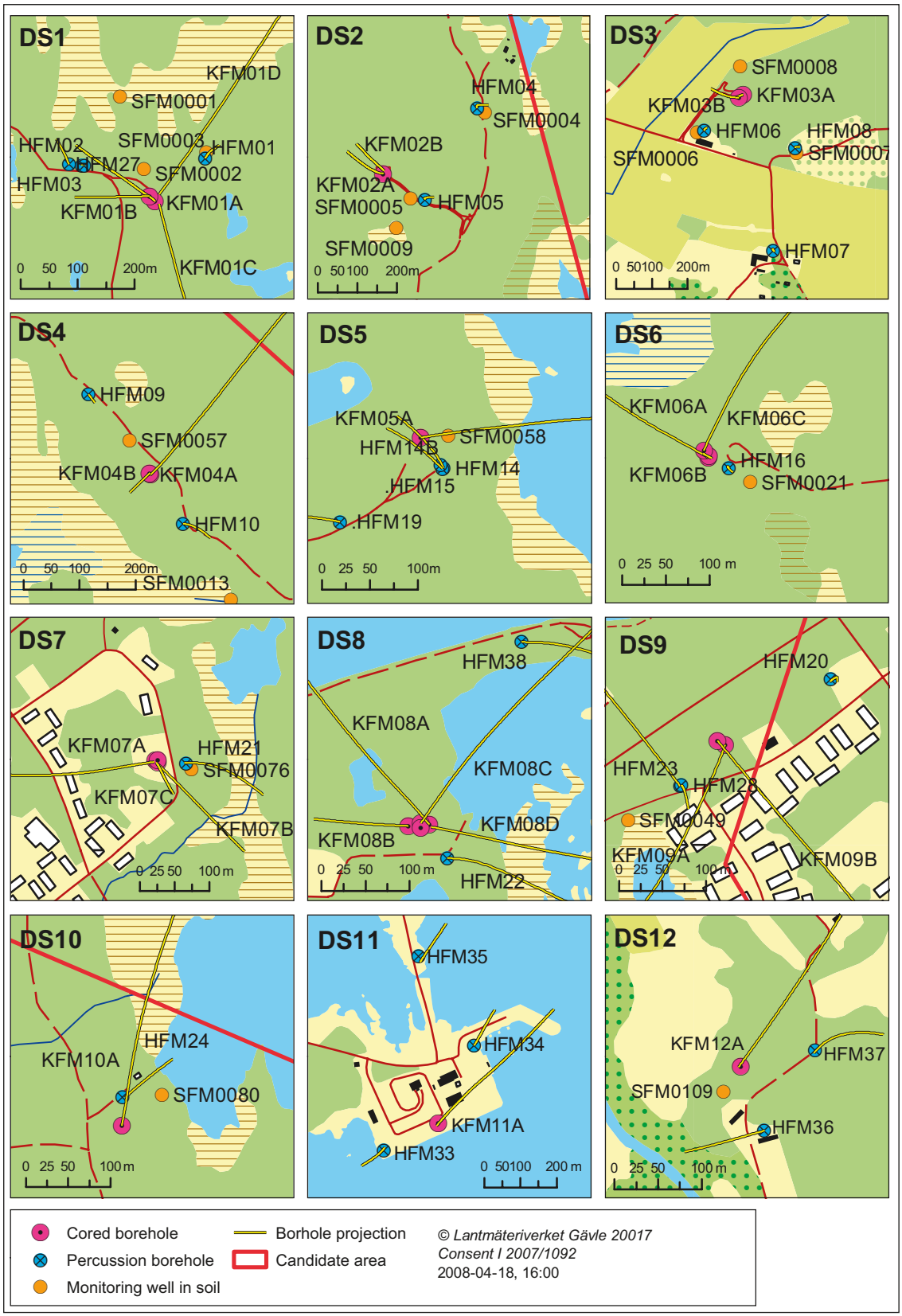

Figure A-2. *Detailed maps of the twelve drill sites for deep telescopic and conventionally core drilled boreholes at Forsmark. Also percussion drilled holes and monitoring wells in soil at or close to the respective drill sites are shown.*

Rock domains model

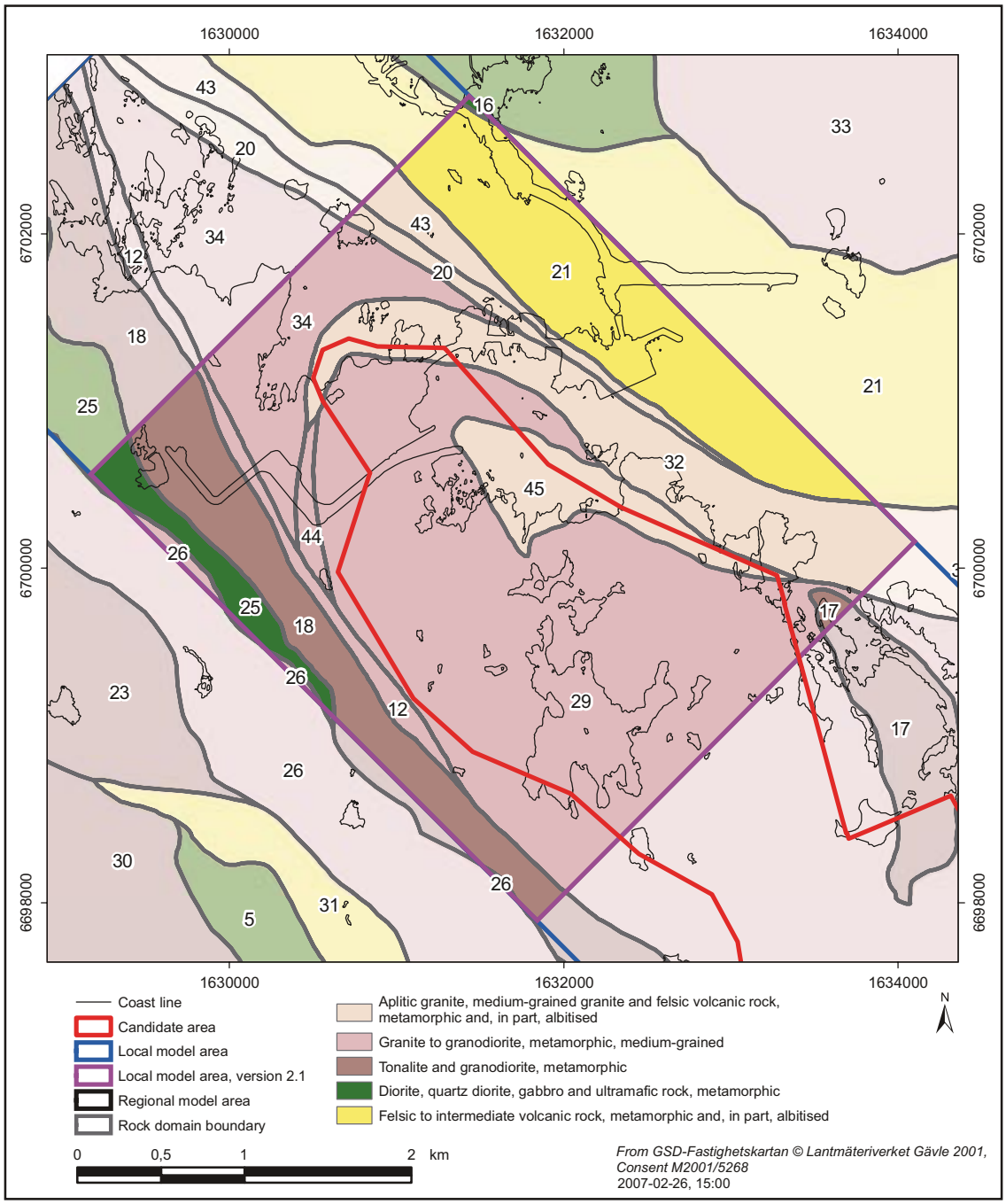

Figure B-1. *Horizontal slice at the surface for rock domains inside and immediately around the local model area in Forsmark. Reproduced from /Stephens et al. 2007/.*

Appendix C

Conditioning properties for deformation zones

The deformation zone transmissivities were conditioned according to the measurement intervals listed in Table C-1. T_c is the conditioning value, T_l is the detection limit.

Table C-1. Conditioning values on transmissivity for single-hole hydraulic tests in intervals intercepting mapped deformation zones.

Borehole	Identified zone name	Top (elev.)	Bottom (elev.)	T_c (m^2/s)	T_l (m^2/s)
HFM01	ZFMA2	–33	–41	$4.50\ 10^{-5}$	10^{-6}
HFM02	ZFM1203	–39	–44	$5.90\ 10^{-4}$	10^{-6}
HFM04	ZFMA3	–177	–181	0.00	10^{-6}
HFM04	ZFM866	–57	–60	$7.87\ 10^{-5}$	10^{-6}
HFM05	ZFM866	–144	–145	$3.96\ 10^{-4}$	10^{-6}
HFM06	ZFMA5	–54	–64	$2.29\ 10^{-4}$	10^{-6}
HFM07	ZFMA6-e	–48	–60	$1.00\ 10^{-6}$	10^{-6}
HFM07	ZFMA6-w	–48	–60	$1.00\ 10^{-6}$	10^{-6}
HFM08	ZFMA5	–128	–133	$1.20\ 10^{-3}$	10^{-6}
HFM09	ZFMENE0060A	–12	–21	$3.26\ 10^{-4}$	10^{-6}
HFM10	Possible DZ (S-ENE)	–96	–104	$3.11\ 10^{-4}$	10^{-6}
HFM10	Possible DZ (S-ENE)	–56	–60	0.00	10^{-6}
HFM11	ZFMNW0003	–53	–105	$2.80\ 10^{-5}$	10^{-6}
HFM12	ZFMNW0003	–60	–118	$7.87\ 10^{-6}$	10^{-6}
HFM13	ZFMENE0401A	–135	–147	$2.91\ 10^{-4}$	10^{-6}
HFM14	ZFMA2	–77	–87	$4.98\ 10^{-4}$	10^{-6}
HFM14	ZFMA2	–56	–63	$1.64\ 10^{-4}$	10^{-6}
HFM15	ZFMA2	–56	–63	$1.02\ 10^{-4}$	10^{-6}
HFM16	ZFMA8	–9	–68	$5.26\ 10^{-4}$	10^{-6}
HFM18	ZFMA7	–94	–117	0.00	10^{-6}
HFM18	ZFMA4	–25	–36	$1.62\ 10^{-4}$	10^{-6}
HFM18	Possible DZ (G)	–3	–4	$2.73\ 10^{-5}$	10^{-6}
HFM23	Possible DZ (S-ENE)	–77	–77	$1.00\ 10^{-6}$	10^{-6}
HFM23	ZFMNNW0100	–56	–62	$1.00\ 10^{-6}$	10^{-6}
HFM24	ZFMWNW0123	–54	–86	0.00	10^{-6}
HFM24	ZFMWNW0123	–32	–50	$7.99\ 10^{-5}$	10^{-6}
HFM24	ZFMWNW0123	–12	–24	$3.01\ 10^{-5}$	10^{-6}
HFM25	ZFMENE0062A	–122	–134	$1.00\ 10^{-6}$	10^{-6}
HFM25	ZFMENE0062A	–105	–113	$1.00\ 10^{-6}$	10^{-6}
HFM25	Possible DZ (S-ENE)	–61	–70	$1.00\ 10^{-6}$	10^{-6}
HFM25	Possible DZ (S-ENE)	–31	–41	$1.00\ 10^{-6}$	10^{-6}
HFM25	Possible DZ (S-ENE)	–4	–26	$1.00\ 10^{-6}$	10^{-6}
HFM26	ZFMNE0065	–116	–144	$1.00\ 10^{-6}$	10^{-6}
HFM26	ZFMA4	–44	–70	$1.00\ 10^{-6}$	10^{-6}
HFM26	ZFMA4	–7	–33	$1.00\ 10^{-6}$	10^{-6}
HFM27	Possible DZ (G)	–105	–111	$6.70\ 10^{-6}$	10^{-6}
HFM27	ZFM1203	–39	–56	$4.00\ 10^{-5}$	10^{-6}
HFM27	ZFMA2	–22	–25	$2.30\ 10^{-5}$	10^{-6}
HFM28	ZFMENE1208A	–8	–60	$1.00\ 10^{-6}$	10^{-6}
HFM29	ZFMWNW0123	–127	–131	$1.00\ 10^{-6}$	10^{-6}
HFM29	ZFMWNW0123	–50	–67	$1.00\ 10^{-6}$	10^{-6}
HFM29	ZFMWNW0123	–12	–17	$1.00\ 10^{-6}$	10^{-6}
HFM30	ZFMNW0017	–63	–170	$1.28\ 10^{-4}$	10^{-6}

Table C-1 (continued). Conditioning values on transmissivity for single-hole hydraulic tests in intervals intercepting mapped deformation zones.

Borehole	Identified zone name	Top (elev.)	Bottom (elev.)	T_c (m^2/s)	T_l (m^2/s)
KFM01A	ZFMENE2254	–630	–674	0.00	10^{-9}
KFM01A	ZFMENE1192	–380	–406	0.00	10^{-9}
KFM01A	ZFMENE1192	–262	–280	$7.79\ 10^{-10}$	10^{-9}
KFM01A	Possible (G)	–212	–220	0.00	10^{-9}
KFM01C	ZFMENE0060C	–227	–245	$3.37\ 10^{-9}$	10^{-9}
KFM01C	ZFMENE0060A	–175	–187	$3.48\ 10^{-9}$	10^{-9}
KFM01C	ZFMA2	–44	–72	$1.13\ 10^{-3}$	10^{-9}
KFM01C	ZFMA2	–15	–34	$4.82\ 10^{-4}$	10^{-9}
KFM01D	Possible DZ (S-ENE)	–589	–591	0.00	10^{-9}
KFM01D	ZFMENE0061	–517	–538	0.00	10^{-9}
KFM01D	Possible DZ (S-NNW)	–383	–389	0.00	10^{-9}
KFM01D	Possible DZ (S-NNW)	–325	–332	0.00	10^{-9}
KFM01D	Possible DZ (S-NNW)	–141	–147	0.00	10^{-9}
KFM02A	Possible DZ (G)	–963	–969	0.00	10^{-9}
KFM02A	Possible DZ (G)	–909	–912	0.00	10^{-9}
KFM02A	ZFMB4	–881	–892	2.62 10–9	10^{-9}
KFM02A	Possible DZ (G)	–511	–590	0.00	10^{-9}
KFM02A	ZFMF1	–467	–511	$4.66\ 10^{-6}$	10^{-9}
KFM02A	ZFMA2	–408	–433	$2.85\ 10^{-6}$	10^{-9}
KFM02A	ZFM1189	–232	–302	$1.03\ 10^{-6}$	10^{-9}
KFM02A	ZFMA3	–152	–176	$3.46\ 10^{-6}$	10^{-9}
KFM02A	ZFM866	–102	–114	$1.07\ 10^{-4}$	10^{-9}
KFM03A	Possible DZ (G)	–929	–936	$3.46\ 10^{-7}$	10^{-9}
KFM03A	ZFMA3	–791	–804	$2.86\ 10^{-8}$	10^{-9}
KFM03A	ZFMB1	–627	–635	$2.50\ 10^{-6}$	10^{-9}
KFM03A	ZFMA7	–438	–445	$6.72\ 10^{-6}$	10^{-9}
KFM03A	ZFMA4	–347	–390	$1.01\ 10^{-4}$	10^{-9}
KFM03B	Possible DZ (G)	–53	–58	$1.01\ 10^{-5}$	10^{-9}
KFM03B	ZFMA5	–15	–33	$2.32\ 10^{-5}$	10^{-9}
KFM04A	Possible DZ (S-NNW)	–761	–763	$1.29\ 10^{-9}$	10^{-9}
KFM04A	ZFMWNW0123	–541	–546	0.00	10^{-9}
KFM04A	ZFMNE1188	–348	–389	$1.38\ 10^{-8}$	10^{-9}
KFM04A	ZFMNE1188	–245	–313	$1.46\ 10^{-6}$	10^{-9}
KFM04A	ZFMA2	–169	–204	$8.79\ 10^{-5}$	10^{-9}
KFM04A	ZFMNW1200	–88	–146	$6.48\ 10^{-5}$	10^{-9}
KFM05A	ZFMENE2383	–773	–818	0.00	10^{-9}
KFM05A	ZFMENE0103	–738	–757	0.00	10^{-9}
KFM05A	ZFMENE0401A	–570	–598	$1.20\ 10^{-8}$	10^{-9}
KFM05A	ZFMENE0401B	–492	–514	0.00	10^{-9}
KFM05A	ZFMNE2282	–333	–366	0.00	10^{-9}
KFM06A	ZFMNNE2280	–789	–820	0.00	10^{-9}
KFM06A	Possible DZ (S-NNE)	–769	–775	0.00	10^{-9}
KFM06A	Possible DZ (S-NNE)	–734	–753	0.00	10^{-9}
KFM06A	ZFMENE0061	–659	–677	0.00	10^{-9}
KFM06A	ZFMNNE0725	–620	–648	$3.40\ 10^{-7}$	10^{-9}
KFM06A	Possible DZ (S-NNE)	–547	–551	$2.74\ 10^{-10}$	10^{-9}
KFM06A	ZFMNNE2255	–520	–524	$4.26\ 10^{-10}$	10^{-9}
KFM06A	ZFMNNE2273	–436	–459	0.00	10^{-9}
KFM06A	ZFMENE0060A	–269	–303	$9.79\ 10^{-7}$	10^{-9}
KFM06A	ZFMENE0060B	–164	–235	$4.54\ 10^{-5}$	10^{-9}
KFM06A	Possible DZ (G)	–107	–122	$3.90\ 10^{-5}$	10^{-9}
KFM06B	ZFMA8	–51	–88	$2.42\ 10^{-4}$	10^{-9}
KFM06C	ZFMNNE2008	–234	–253	$3.40\ 10^{-7}$	10^{-9}
KFM06C	ZFMB7	–296	–328	$5.67\ 10^{-6}$	10^{-9}
KFM06C	ZFMNNE2263	–340	–397	$1.84\ 10^{-7}$	10^{-9}
KFM06C	ZFMWNW0044	–407	–448	$1.22\ 10^{-6}$	10^{-9}
KFM06C	Possible DZ (S-NNE/WNW)	–500	–540	$9.33\ 10^{-8}$	10^{-9}
KFM06C	Possible DZ	–83	–140	$8.74\ 10^{-5}$	10^{-9}

Table C-1 (continued). Conditioning values on transmissivity for single-hole hydraulic tests in intervals intercepting mapped deformation zones.

Borehole	Identified zone name	Top (elev.)	Bottom (elev.)	T_c (m^2/s)	T_l (m^2/s)
KFM07A	Possible DZ (G)	–165	–173	0.00	10^{-9}
KFM07A	ZFMENE0159A	–351	–355	0.00	10^{-9}
KFM07A	ZFMENE1208B	–665	–694	0.00	10^{-9}
KFM07A	ZFMENE1208A	–708	–739	0.00	10^{-9}
KFM07A	ZFMB8	–756	–815	$2.00\ 10^{-7}$	10^{-9}
KFM07A	ZFM1203	–90	–156	$1.41\ 10^{-4}$	10^{-9}
KFM07B	ZFMENE2320	–175	–190	$4.36\ 10^{-8}$	10^{-9}
KFM07B	Possible DZ (G)	–38	–43	0.00	10^{-9}
KFM07B	ZFM1203	–71	–78	0.00	10^{-9}
KFM07B	Possible DZ (G)	–92	–104	0.00	10^{-9}
KFM07C	ZFMENE2320	–303	–383	0.00	10^{-9}
KFM07C	ZFMENE2320	–424	–434	0.00	10^{-9}
KFM07C	ZFM1203	–88	–99	$4.81\ 10^{-5}$	10^{-9}
KFM08A	ZFMENE1061A	–204	–262	$1.31\ 10^{-6}$	10^{-9}
KFM08A	ZFMNNW1204	–392	–405	$6.93\ 10^{-8}$	10^{-9}
KFM08A	Possible DZ (S-NNE)	–430	–451	0.00	10^{-9}
KFM08A	Possible DZ (S-NNW)	–500	–501	0.00	10^{-9}
KFM08A	Possible DZ (S-WNW)	–536	–551	$1.41\ 10^{-6}$	10^{-9}
KFM08A	ZFMENE2248	–608	–654	0.00	10^{-9}
KFM08A	Possible DZ (S-WNW)	–700	–719	0.00	10^{-9}
KFM08A	Possible DZ (S-WNW)	–732	–738	0.00	10^{-9}
KFM08B	ZFMNNW1205	–111	–117	$1.22\ 10^{-9}$	10^{-9}
KFM08B	ZFMNNW1205	–139	–154	$5.60\ 10^{-8}$	10^{-9}
KFM08C	Possible DZ (S-NNE)	–137	–162	$6.68\ 10^{-9}$	10^{-9}
KFM08C	ZFMNNE2312	–353	–454	$1.76\ 10^{-7}$	10^{-9}
KFM08C	ZFMWNW2225	–561	–586	$2.61\ 10^{-9}$	10^{-9}
KFM08C	ZFMENE1061A	–685	–687	0.00	10^{-9}
KFM08C	ZFMENE1061A	–777	–779	0.00	10^{-9}
KFM09A	ZFMENE0159A	–179	–200	$1.03\ 10^{-7}$	10^{-9}
KFM09A	ZFMENE0159A	–200	–232	$1.96\ 10^{-8}$	10^{-9}
KFM09A	Possible (NNW)	–531	–531	0.00	10^{-9}
KFM09A	ZFMNW1200	–570	–591	$7.74\ 10^{-9}$	10^{-9}
KFM09A	ZFMNW1200	–602	–615	$4.37\ 10^{-8}$	10^{-9}
KFM09A	ZFMENE1208B	–69	–95	$2.50\ 10^{-8}$	10^{-9}
KFM09A	ZFMENE1208A	–9	–30	0.00	10^{-9}
KFM09B	Possible (S-ENE)	–223	–223	$3.22\ 10^{-10}$	10^{-9}
KFM09B	Possible (S-ENE)	–242	–266	0.00	10^{-9}
KFM09B	ZFMENE2320	–284	–322	$3.76\ 10^{-8}$	10^{-9}
KFM09B	ZFMENE1208A	–3	–31	$2.92\ 10^{-5}$	10^{-9}
KFM09B	ZFMENE2325A	–399	–420	$1.10\ 10^{-9}$	10^{-9}
KFM09B	ZFMENE2325B	–428	–437	$2.86\ 10^{-7}$	10^{-9}
KFM09B	ZFMENE1208B	–44	–59	$1.01\ 10^{-5}$	10^{-9}
KFM09B	ZFMENE0159A	–82	–103	$3.57\ 10^{-6}$	10^{-9}
KFM10A	ZFMENE2403	–196	–202	0.00E	10^{-9}
KFM10A	ZFMA2	–296	–307	$2.92\ 10^{-5}$	10^{-9}
KFM10A	ZFMA2	–324	–331	$1.15\ 10^{-6}$	10^{-9}
KFM10A	ZFMWNW0123	–43	–105	$7.47\ 10^{-5}$	10^{-9}